

Development of Hybrid GPCR Ligands:
Photochromic and Butyrylcholinesterase Inhibiting Human
Cannabinoid Receptor 2 Agonists

Dissertation

zur Erlangung des naturwissenschaftlichen Doktorgrades der
Julius-Maximilians-Universität Würzburg



vorgelegt von

Dominik Dolles

aus Amberg

Würzburg, 2018

Eingereicht bei der Fakultät für Chemie und Pharmazie am

Gutachter der schriftlichen Arbeit

1. Gutachter: _____

2. Gutachter: _____

Prüfer des öffentlichen Promotionskolloquiums

1. Prüfer: _____

2. Prüfer: _____

3. Prüfer: _____

Datum des öffentlichen Promotionskolloquiums

Doktorurkunde ausgehändigt am

The presented work has been carried out under the supervision of Professor Dr. Michael Decker at the Chair of Pharmaceutical and Medicinal Chemistry at the Institute of Pharmacy and Food Chemistry of the Julius Maximilian University Würzburg between August 2014 and March 2018.

Meinen Eltern

List of Publications

Dolles, D.; Nimczick, M.; Scheiner, M.; Ramler, J.; Stadtmüller, P.; Sawatzky, E.; Drakopoulos, A.; Sotriffer, C.; Wittmann, H.-J.; Strasser, A.; Decker, M. Aminobenzimidazoles and Structural Isomers as Templates for Dual-Acting Butyrylcholinesterase Inhibitors and *h*CB₂R Ligands to Combat Neurodegenerative Disorders. *ChemMedChem* **2016**, *11*, 1270 – 1283.

Dolles, D.; Decker, M. Dual-acting compounds acting as receptor ligands and enzyme inhibitors. In *Design of Hybrid Molecules for Drug Development*; Decker, M.; Ed.; Elsevier: Oxford, 2017; pp. 137 – 165.

Dolles, D.; Hoffmann, M.; Gunesch, S.; Marinelli, O.; Möller, J.; Santoni, G.; Chatonnet, A.; Lohse, M. J.; Wittmann, H.-J.; Strasser, A.; Nabissi, M.; Maurice, T.; Decker, M. Structure-Activity Relationships and Computational Investigations into the Development of Potent and Balanced Dual-Acting Butyrylcholinesterase Inhibitors and Human Cannabinoid Receptor 2 Ligands with Pro-Cognitive *in vivo* Profiles. *J. Med. Chem.* **2018**, *61*, 1646 – 1663.

Dolles, D.; Strasser, A.; Wittmann, H.-J.; Marinelli, O.; Nabissi, M.; Pertwee, R. G.; Decker, M. The First Photochromic Affinity Switch for the Human Cannabinoid Receptor 2. *Adv. Therap.* **2018**, DOI: 10.1002/adtp.201700032.

Other scientific contributions:

Dolles, D.; Nimczick, M.; Scheiner, M.; Ramler, J.; Stadtmüller, P.; Sawatzky, E.; Drakopoulos, A.; Sotriffer, C.; Wittmann, H.-J.; Strasser, A.; Decker, M. Aminobenzimidazoles and Structural Isomers as Templates for Dual-Acting Butyrylcholinesterase Inhibitors and *h*CB₂R Ligands to Combat Neurodegenerative Disorders. *ChemMedChem* **2016**, Cover Picture.

Dolles, D.; Gunesch, S.; Decker, M. Development of benzimidazole-based photoswitchable compounds: physico-chemical and biological evaluation as BChE inhibitors / CB₂ ligands. International Symposium on Photopharmacology, Groningen (Netherlands), February 16th 2017 (Poster).

Dolles, D.; Sawatzky, E.; Chatonnet, A.; Möller, J.; Lohse, M.; Drakopoulos, A.; Strasser, A.; Wittmann, H.-J.; Maurice, T.; Decker, M. Design, Synthesis, Pharmacological Evaluation and Computational Studies of Novel Dual-Acting BChE Inhibitors and *h*CB₂R Ligands for the Treatment of Alzheimer's Disease. 253rd American Chemical Society National Meeting and Exposition, San Francisco (USA), April 2nd – 6th 2017 (Poster).

Dolles, D.; Hoffmann, M.; Gunesch, S.; Chatonnet, A.; Möller, J.; Lohse, M.; Strasser, A.; Wittmann, H.-J.; Maurice, T.; Decker, M. Design, Synthesis, Pharmacological Evaluation and Computational Studies of Novel Dual-Acting BChE Inhibitors and *h*CB₂R Ligands for the Treatment of Alzheimer's Disease. Hybrid Molecules and Polypharmacology in Drug Discovery and Development, Würzburg (Germany), November 10th – 11th 2017 (Poster).

Copyrights

Parts of this work have been published previously and are reproduced, adapted and/or modified with the permission of:

Dolles, D.; Nimczick, M.; Scheiner, M.; Ramler, J.; Stadtmüller, P.; Sawatzky, E.; Drakopoulos, A.; Sotriffer, C.; Wittmann, H.-J.; Strasser, A.; Decker, M. Aminobenzimidazoles and Structural Isomers as Templates for Dual-Acting Butyrylcholinesterase Inhibitors and *hCB₂R* Ligands to Combat Neurodegenerative Disorders. *ChemMedChem* **2016**, *11*, 1270 – 1283.

Copyright (2016) Wiley-VCH Verlag GmbH & Co. KGaA, Weinheim. Reproduced with permission.

<http://onlinelibrary.wiley.com/doi/10.1002/cmdc.201500418/abstract>

Dolles, D.; Decker, M. Dual-acting compounds acting as receptor ligands and enzyme inhibitors. In *Design of Hybrid Molecules for Drug Development*; Decker, M.; Ed.; Elsevier: Oxford, 2017; pp. 137 – 165.

Copyright (2018), with permission from Elsevier.

<https://www.sciencedirect.com/science/article/pii/B9780081010112000052>

Dolles, D.; Hoffmann, M.; Gunesch, S.; Marinelli, O.; Möller, J.; Santoni, G.; Chatonnet, A.; Lohse, M. J.; Wittmann, H.-J.; Strasser, A.; Nabissi, M.; Maurice, T.; Decker, M. Structure-Activity Relationships and Computational Investigations into the Development of Potent and Balanced Dual-Acting Butyrylcholinesterase Inhibitors and Human Cannabinoid Receptor 2 Ligands with Pro-Cognitive *in vivo* Profiles. *J. Med. Chem.* **2018**, *61*, 1646 – 1663.

Copyright (2018) American Chemical Society.

<https://pubs.acs.org/doi/abs/10.1021%2Facs.jmedchem.7b01760>

Dolles, D.; Strasser, A.; Wittmann, H.-J.; Marinelli, O.; Nabissi, M.; Pertwee, R. G.; Decker, M. The First Photochromic Affinity Switch for the Human Cannabinoid Receptor 2. *Adv. Therap.* **2018**, DOI: 10.1002/adtp.201700032.

Copyright (2018) Wiley-VCH Verlag GmbH & Co. KGaA, Weinheim. Reproduced with permission.

<http://onlinelibrary.wiley.com/doi/10.1002/adtp.201700032/abstract>

Documentation of Authorship

All individual contributions for each author to the publications reprinted in this thesis are listed below:

Dolles, D.(1); Nimczick, M.(2); Scheiner, M.(3); Ramler, J.(4); Stadtmüller, P.(5); Sawatzky, E.(6); Drakopoulos, A.(7); Sotriffer, C.(8); Wittmann, H.-J.(9); Strasser, A.(10); Decker, M.(11) Aminobenzimidazoles and Structural Isomers as Templates for Dual-Acting Butyrylcholinesterase Inhibitors and <i>hCB₂R</i> Ligands to Combat Neurodegenerative Disorders. <i>ChemMedChem</i> 2016 , <i>11</i> , 1270 – 1283.											
	1	2	3	4	5	6	7	8	9	10	11
Design and Development of Target Compounds	X	X									X
Synthesis of Target Compounds	X	X	X	X							
Analytical Characterization	X	X	X	X							
Radioligand Binding Studies at <i>hCB₁R</i> / <i>hCB₂R</i>	X				X						
Determination of IC ₅₀ values at <i>eeAChE</i> / <i>eqBChE</i>						X					
Computational Studies at <i>hCB₂R</i>									X	X	
Computational Studies at <i>hBChE</i>							X	X			
Writing and Correction of the Paper	X										X
Supervision of D. Dolles											X

Dolles, D.(1); Decker, M.(2) Dual-acting compounds acting as receptor ligands and enzyme inhibitors. In <i>Design of Hybrid Molecules for Drug Development</i> ; Decker, M.; Ed.; Elsevier: Oxford, 2017; pp. 137 – 165.		
	1	2
Literature Research	X	
Writing and correction of the Manuscript	X	X
Supervision of D. Dolles		X

Dolles, D.(1); Hoffmann, M.(2); Gunesch, S.(3); Marinelli, O.(4); Möller, J.(5); Santoni, G.(6); Chatonnet, A.(7); Lohse, M. J.(8); Wittmann, H.-J.(9); Strasser, A.(10); Nabissi, M.(11); Maurice, T.(12); Decker, M.(13) Structure-Activity Relationships and Computational Investigations into the Development of Potent and Balanced Dual-Acting Butyrylcholinesterase Inhibitors and Human Cannabinoid Receptor 2 Ligands with Pro-Cognitive *in vivo* Profiles. *J. Med. Chem.* **2018**, *61*, 1646 – 1663.

	1	2	3	4	5	6	7	8	9	10	11	12	13
Design and Development of Target Compounds	X												X
Synthesis of Target Compounds	X												
Analytical Characterization	X												
Radioligand Binding Studies at <i>hCB₁R</i> / <i>hCB₂R</i>	X												
Determination of IC ₅₀ values at <i>hAChE</i> / <i>hBChE</i>		X	X										
Computational Studies at <i>hCB₂R</i>									X	X			
Radioligand Binding Studies at <i>hMOP</i> receptor					X			X					
Determination of Efficacy				X		X					X		
<i>In vivo</i> Studies							X					X	
Writing and Correction of the Paper	X												X
Supervision of D. Dolles													X

Dolles, D.(1); Strasser, A.(2); Wittmann, H.-J.(3); Marinelli, O.(4); Nabissi, M.(5); Pertwee, R. G.(6); Decker, M.(7) The First Photochromic Affinity Switch for the Human Cannabinoid Receptor 2. *Adv. Therap.* **2018**, DOI: 10.1002/adtp.201700032.

	1	2	3	4	5	6	7
Design and Development of Target Compounds	X						X
Synthesis of Target Compounds	X						
Analytical Characterization	X						
Determination of Photophysical Properties	X						
Radioligand Binding Studies at <i>hCB₁R</i> / <i>hCB₂R</i>	X						
Computational Studies at <i>hCB₂R</i>		X	X				
Determination of Efficacy (cAMP assay/ gene expression experiment)				X	X		
Determination of Efficacy (GTPγS assay)						X	
Writing and Correction of the Paper		X					X
Supervision of D. Dolles							X

Acknowledgements

The present work would not have been possible without the experience and dedication of my colleagues and cooperation partners. It is a great example of European team work.

Therefore, I would like to thank all scientists that contributed to the projects (in arbitrary order): Massimo Nabissi and Co-Workers from the University of Camerino for the determination of efficacy by cAMP assays and gene expression experiments; Tangui Maurice and Arnaud Chatonnet from the University of Montpellier for *in vivo* experiments; Roger G. Pertwee and Co-Workers from the University of Aberdeen for performing GTP γ S assays; Andrea Strasser and Hans-Joachim Wittmann from the University of Regensburg for computational studies at *hCB₂R*; Antonios Drakopoulos and Christoph Sotriffer from the University of Würzburg for computational studies at *hBChE*; Jan Möller from the University of Würzburg for radioligand binding studies at μ -opioid receptor; Matthias Hoffmann, Sandra Gunesch and Edgar Sawatzky from the University of Würzburg for determination of AChE and BChE inhibition; my bachelor and practical students Matthias Scheiner, Jacqueline Ramler, Jan Kraus, Alexander Fritz and Patrick Offenegger; Sonja Kachler and Karl-Norbert Klotz for providing workspace for radioligand binding assays and technical assistance.

Furthermore, I would like to thank my supervisor Prof. Dr. Michael Decker for the opportunity to work in his group and for his support and motivation during the projects.

I would also like to thank the whole working group and my long-time lab partner Dr. Xinyu Chen for a pleasant time in- and outside the lab and numerous vivid discussion.

Special thanks go to the Alzheimer Forschung Initiative e.V. for supporting me with a travel grant for the ACS Meeting in San Francisco.

Lastly, I would like to thank my parents for supporting me in every possible situation.

Table of Contents

List of Publications.....	I
Copyrights	III
Documentation of Authorship.....	V
Acknowledgements	VII
1. Introduction.....	1
2. Scope and Objective	6
3. Dual-Acting Compounds Acting as Receptor Ligands and Enzyme Inhibitors	7
4. Aminobenzimidazoles and Structural Isomers as Templates for Dual-Acting Butyrylcholinesterase Inhibitors and <i>hCB₂R</i> Ligands To Combat Neurodegenerative Disorders	10
4.1 Design and Development.....	12
4.2 Pharmacological Evaluation and SARs.....	15
4.3 Computational Studies at <i>hCB₂R</i> and <i>hBChE</i>	18
4.4 Conclusions	20
5. Structure-Activity Relationships and Computational Investigations into the Development of Potent and Balanced Dual-Acting Butyrylcholinesterase Inhibitors and Human Cannabinoid Receptor 2 Ligands with Pro-Cognitive <i>in vivo</i> Profiles	21
5.1 Structure Optimization	22
5.2 Pharmacological Evaluation and SARs.....	24
5.3 Computational Studies.....	29
5.4 <i>In vivo</i> Studies	30
5.5 Conclusions	32
6. The First Photochromic Affinity Switch for the Human Cannabinoid Receptor 2	34
6.1 Introduction	35
6.2 Design and Development.....	37
6.3 Pharmacological Evaluation	38
6.4 Computational Studies.....	39
7. Summary and Outlook	42
8. Zusammenfassung und Ausblick	45
9. References.....	48
10. Abbreviations	56
11. Appendix	58

1. Introduction

Protocol from the dialogue between the German psychologist Alois Alzheimer and his patient Auguste Deter (29th November 1901):¹

„Alzheimer: Wie heißen Sie?

Deter: Auguste.

Alzheimer: Familienname?

Deter: Auguste.

Alzheimer: Wie heißt Ihr Mann?

Deter: Auguste...glaube ich.

Alzheimer: Ihr Mann?

Deter: Achso...

Alzheimer: Sind Sie verheiratet?

Deter: Mit Auguste.

Alzheimer: Mit Frau Deter?

Deter: Ja, genau...Auguste Deter.

(...)

Ich zeige ihr einen Schlüssel, einen Stift und ein Buch. Sie benennt sie korrekt.

Alzheimer: Was habe ich Ihnen gezeigt?

Deter: Ich weiß es nicht, ich weiß es nicht.

Alzheimer: Ist es sehr schwierig?

Deter: Ich habe Angst, so sehr Angst.“

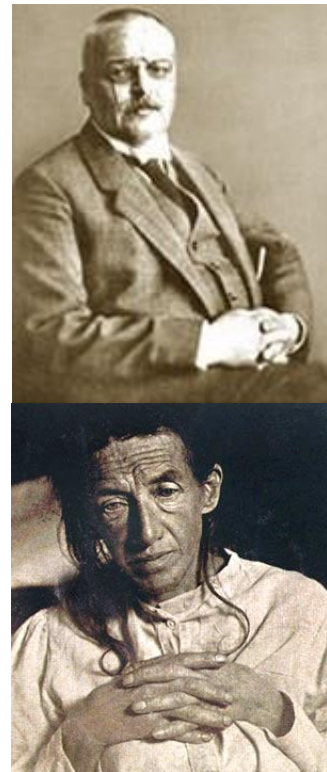


Figure 1.1. Alois Alzheimer (top) and Auguste Deter (bottom).¹

When Auguste Deter was asked to write down “Frau Auguste Deter”, she just wrote “Frau...” and forgot about the rest. Instead, she repeated the words “Ich habe mich selbst verloren...”.¹

Auguste Deter was the first patient ever recorded suffering from Alzheimer's disease (AD). Alois Alzheimer was the first one to describe her memory loss in combination with other psychiatric symptoms including mood changes (anxiety) and disorientation.² After her death in 1906 *post mortem* studies were carried out on Auguste Deter's brain, where Alzheimer found the *miliary foci*, which are now known as senile plaques, a deposition of an insoluble substance in the cerebral cortex.^{1,2}

Today, AD represents the most common form of dementia (50% – 75% of all types of dementia) with 47 million cases worldwide.³ Since AD is mainly linked to aging,⁴ the disease becomes more relevant with regard to an increased life expectancy and demographic change. Although there have been immense efforts from academic and industrial research there is still no cure for this disease. Today's medication is limited to four approved drugs: three cholinesterase inhibitors (rivastigmine **1**, donepezil **2** and galantamine **3**) and one *N*-methyl-D-aspartate receptor antagonist (memantine **4**) (**figure 1.2**). A fifth drug, the acetylcholinesterase (AChE) inhibitor tacrine **5**, was withdrawn from the market because of hepatotoxic side effects.⁵

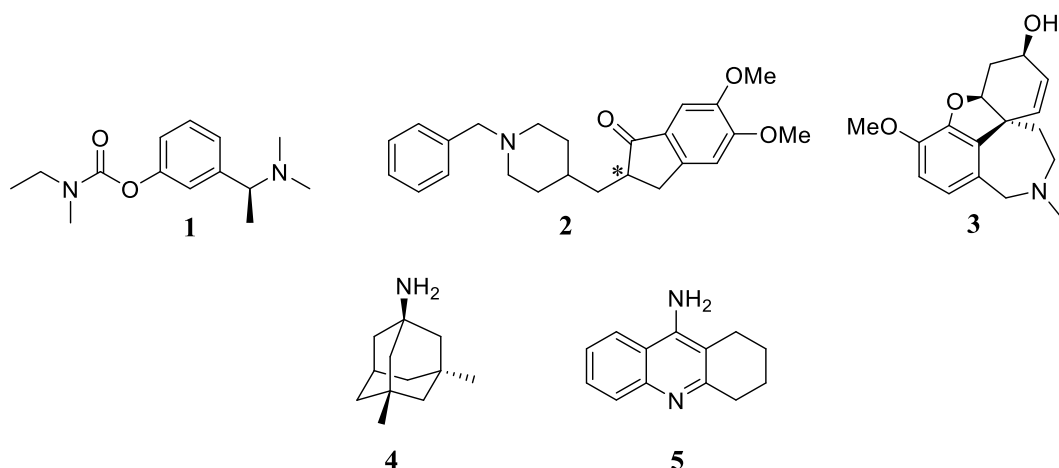


Figure 1.2. Approved drugs for AD (**1-4**) and tacrine **5**, which was withdrawn from the market.

Unfortunately, these drugs are only effective in early stages of the disease, and they only act symptomatically, but do not slow down the progression of AD or even cure it.⁶ One of the main problems in finding an effective treatment for AD is its complexity. AD is characterized as a multifactorial disease, which means that there's not only one cause, but a complex combination of multiple factors. Still, all causes as well as their interactions among each other are not yet elucidated.

Pathobiologically, AD is characterized by the formation of senile plaques, which was already found by Alois Alzheimer in 1906.² Senile plaques consist of the insoluble peptide (40-42 amino acids) amyloid β ($A\beta$). $A\beta$ originates from the amyloid precursor protein (APP), a transmembrane glycoprotein, which undergoes proteolytic cleavage triggered by the enzymes β - and γ -secretase. In healthy tissue, APP is cleaved by α - and γ -secretase resulting in soluble nonamyloidogenic peptides.⁷ According to the amyloid cascade hypothesis,^{8,9} $A\beta$ aggregates and thus triggers neuroinflammation characterized by activated microglia and astrocytes.¹⁰ Subsequently, pro-inflammatory chemokines, cytokines and neurotoxins are produced ultimately leading to neurodegeneration and thus AD.¹¹ Besides the amyloid cascade hypothesis, other hallmarks of AD are the formation of neurofibrillary tangles (consisting of hyperphosphorylated τ protein aggregates), the formation of reactive oxygen species and the irreversible loss of (cholinergic) neurons.^{12,13}

Since the discovery of Δ^9 -tetrahydrocannabinol (Δ^9 -THC) and its analogues by Mechoulam and Gaoni,¹⁴ the endocannabinoid system consisting of its two representative G-protein coupled receptors (GPCRs): human cannabinoid receptor subtype 1 and 2 (hCB_1R and hCB_2R), their endogenous ligands (endocannabinoids, e.g. *N*-arachidonylethanolamine and 2-arachidonoylglycerol) and the involved enzymes, attracted more and more interest as targets for potential therapeutics. Its involvement in numerous processes in the brain made it an interesting focus with regard to neurodegenerative diseases. hCB_1R is the most abundant GPCR in the central nervous system (CNS)¹⁵ and is mainly expressed in the basal ganglia nuclei, hippocampus, cortex and cerebellum. It is mainly linked to the control of memory, cognition and motoric functions.^{16,17} In contrast, hCB_2R is mainly expressed in the peripheral immune system, where it modulates immune cell migration and cytokine release, and to a lesser extent in the CNS, especially in microglia cells.¹⁸ Because of its high level of distribution and therefore involvement in the CNS, hCB_1R was initially targeted by numerous drug development approaches based on structure-activity relationships (SARs) from Sanofi's drug rimonabant.¹⁹ The hCB_1R -selective inverse agonist rimonabant (SR141,716) was a promising anorectic drug for the treatment of obesity. Yet, due to psychiatric side-effects such as depression, rimonabant was withdrawn from the market in 2008. In the past few years, hCB_2R has regained more attention due to its immunomodulatory role and its lack of psychoactive side effect. Especially, in diseased tissue, several studies could demonstrate the importance of hCB_2Rs as potential drug target. As a counter measurement of the body, hCB_2Rs are overexpressed in inflamed human brain tissue, especially in activated microglia cells and astrocytes that are surrounded by neuritic plaques.²⁰⁻²³ The expression level of hCB_2Rs correlates with the formation of $A\beta$,

which is one key building block of neuritic plaques.²⁴ Furthermore, fatty acid amide hydrolase (FAAH), which metabolizes the endocannabinoid *N*-arachidonylethanolamine, is overexpressed during neuroinflammatory processes. In contrast, expression levels of *hCB₁R* do not change in the course of AD.²² The theory that an up-regulation of *hCB₂R* signaling has beneficial effects by reducing inflammatory processes, was substantiated in several *in vitro* and *in vivo* studies: the selective *hCB₂R* agonists JWH-015 and JWH-133 induced protection of neuronal cells against A β -induced neurotoxicity.^{25,26} Rats that were pretreated with A β ₁₋₄₀ (intracerebral injection) showed improved cognition with the treatment of the *hCB₂R* agonist MDA7. Examination of the brain slices furthermore showed an increased promotion of A β clearance and decreased secretion of pro-inflammatory mediators.²⁷ Transgenic AD-mice that were continuously treated with the agonist JWH-133 showed afterwards a reduction of activated microglia cells surrounded by A β -plaques as well as the level of cytokines going along with cognitive improvement.²⁸ Besides neurodegenerative diseases such as AD, Parkinson's and Huntington's diseases,²⁹ *hCB₂R*s also play a role in the development of anti-cancer drugs³⁰ as well as in the treatment of pain³¹.

As previously mentioned, the approved drugs on the market mainly consist of AChE inhibitors (**figure 1.2**). This goes back to the oldest and most prominent theory regarding AD: the cholinergic hypothesis, which indicates a loss of the neurotransmitter acetylcholine (ACh) in the course of AD.^{32,33} In early stages of AD, it is possible to prevent this loss of ACh and thus slow down progression of the disease by the administration of an AChE inhibitor. As AD further progresses, the concentration of AChE in the brain decreases up to 90%, which makes the application of AChE inhibitors ineffective.³⁴ As the concentration of AChE decreases, the amount of its isoenzyme butyrylcholinesterase (BChE) increases.^{35,36} BChE is less selective, but also capable of hydrolyzing ACh into choline and acetate. An inhibition of BChE may open a new field of drugs that can be applied at later stages of AD.³⁷ Furthermore, BChE is found to be co-localized and overexpresses in glia cells and correlates with the formation of senile plaques and the transformation of non-fibrillar to fibrillary A β plaques.^{35,38,39} Beneficial effects addressing BChE have already been investigated *in vivo*: Maurice *et al.*⁴⁰ compared normal mice to BChE knockout mice. Those mice lack of BChE showed enhanced learning abilities in memory tests compared to their normal fellows. While knockout mice appeared less affected by learning and memory deficits and oxidative stress, the average mice suffered from AD symptoms. In one of the very few *in vivo* studies, where selective nanomolar BChE inhibitors were applied, Kosak *et al.*⁴¹ demonstrated improved learning and memory abilities in several

in vivo test systems (passive avoidance test and Morris water maze). Adverse cholinergic effects were not observed.

The development of a compound aiming for activation of *hCB₂R* and inhibition BChE is not randomly chosen. In glia cells both *hCB₂R* and BChE are colocalized. Activated glia cells play an important role in the (over-)expression of BChE and are a target of potential *hCB₂R* agonists. Addressing activated glia cells may also block the overproduction of BChE and therefore positively affect hydrolysis of ACh.^{35,42}

Taken together, a multitarget / dual-active *hCB₂R* agonist and BChE inhibitor might play a key role in the combat against AD. Although, a cure of AD appears currently to be far away, it is still beneficial to develop a real medication, which addresses AD especially at later stages. Patients and their families will not only benefit from a slowdown of the disease, but also from a remaining life with reduced symptoms and restrictions.

2. Scope and Objective

Regarding the multifactorial character of AD and the relevance of BChE and *hCB₂R* in its course (as described in chapter 1), there is a huge interest in the development of multifunctional drugs that act as both a BChE inhibitor and *hCB₂R* agonist.

The first part of the thesis gives a general overview on multitarget compounds and highlights their development as well as the design strategies involved.

The second part focusses on classical drug development and deals with the design and development of a set of dual-active compounds that acts as both a BChE inhibitor and *hCB₂R* agonist:

- In the initial project, both pharmacological properties were combined by merging pharmacophores into one single molecule. A library of different heterocycles was designed, synthesized and analyzed to investigate SARs. Using these data, binding mode and interactions at both targets of selected compounds were analyzed in computational studies.
- In the follow-up project, the compound library was extended and optimized. Further *in vitro* assays confirmed agonism and helped to avoid affinities towards unwanted off-targets. Based on a novel *hCB₁R* crystal structure, a homology model for the *hCB₂R* was developed and used for molecular dynamics studies to further investigate binding modes. First positive *in vivo* results with short- and long-term memory improvement were obtained

The third part of the thesis is set apart from the classical drug development and deals with the development of photochromic tool compounds to investigate the receptor itself and ligand binding. The first photochromic ligands for the *hCB₂R* were designed, synthesized and evaluated.

3. Dual-Acting Compounds Acting as Receptor Ligands and Enzyme Inhibitors⁴³



Dual-Acting Compounds Acting as Receptor Ligands and Enzyme Inhibitors

Dominik Dolles, Michael Decker

JULIUS MAXIMILIAN UNIVERSITY OF WÜRZBURG, WÜRZBURG, GERMANY

Author contributions:

D. Dolles (under the supervision of Prof. Dr. M. Decker) was responsible for the preparation and correction of the manuscript (Julius Maximilian University Würzburg).

As discussed in chapter 1, AD belongs to the class of multifactorial diseases. The classical approach to treat such a disease with the “one disease – one target” paradigm is therefore not constructive, if not invalid. A multitarget drug that aims for different targets at the same time would be the perfect tool to address multifactorial diseases. There are two common structural approaches when it comes to the development of multitarget drugs: a hybrid or a merged ligand. In case of a hybrid, two drug entities are connected by a linker. A merged ligand consists of one small molecule, in which pharmacophores for both targets are “fused” (**figure 3.1**).^{43, 44}

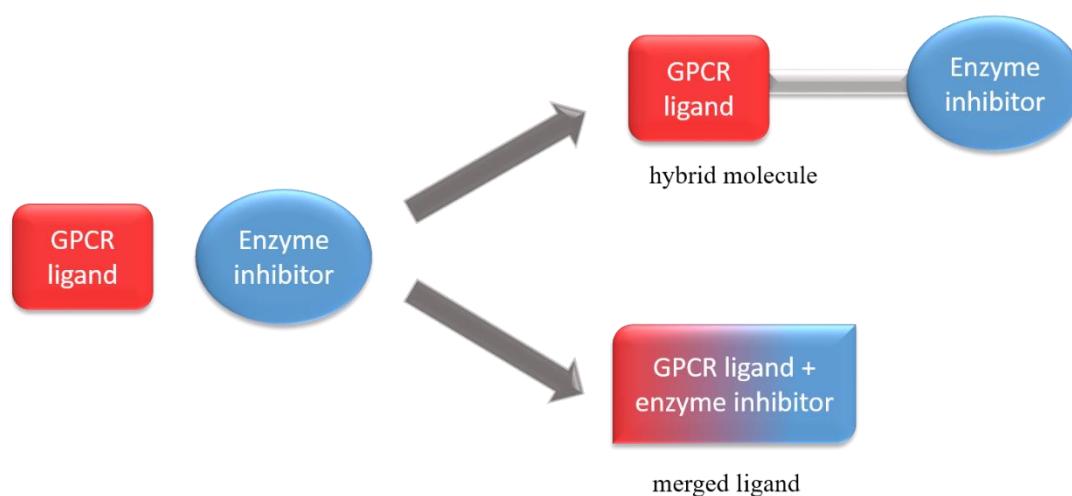


Figure 3.1. Schematic concept of the two possible approaches for the development of multitarget compounds: hybrid and merged ligand.⁴³

For the hybrid-approach, drug molecules don't have to be (dramatically) altered, which makes the development far easier as compared to merged ligands, but then their main disadvantage is their high molecular mass, which goes not along with Lipinski's rule of five.⁴⁵ Despite their disadvantages, hybrids have been successfully developed for a variety of different targets⁴⁶ (for review see reference 47). In contrast, development of merged ligands is very laborious. Pharmacophores have to be “fused”, which goes mostly along with a dramatic change of the overall chemical structure. It can be depicted as a pair of scales: if affinity at one target is increased, it is very likely that the affinity for the other target decreases.⁴³ The advantage is their low molecular weight, which remains mostly the same as it is the case for “single-target” drugs and is therefore in accordance with Lipinski's rule of five.⁴⁵ In the literature, there are three common design approaches for multitarget compounds: designing in, designing out and balancing.⁴³ Designing in represents the most prominent approach, where two highly active chemical scaffolds (from two different drug molecules) are fused. The resulting multitarget

compound then incorporates high affinities for both targets. The designing out approach assumes that there's a chemical scaffold that already shows affinity for two desired targets, but also for an unwanted off-target. In this case, it is necessary to cut out those off-target affinity, but to keep affinity for the desired targets. In the third case, a compound only shows affinity for two desired targets, but acts at different concentration ranges. In this case, a balancing of the affinities is necessary.^{43,44} Despite these difficulties, several multitarget compounds based on the merged ligand approach have been developed for different target combinations: μ -opioid (MOP) receptor agonists / neuronal nitric oxide synthase inhibitors,⁴⁸ adenosine A_{2A} receptor antagonists / monoamine oxidase B inhibitors,⁴⁹ histamine H₃ receptor antagonists / AChE inhibitors⁵⁰ and several more (for full review see reference 43, cf. appendix I).

4. Aminobenzimidazoles and Structural Isomers as Templates for Dual-Acting Butyrylcholinesterase Inhibitors and *h*CB₂R Ligands To Combat Neurodegenerative Disorders⁵¹

CHEMMEDCHEM
CHEMISTRY ENABLING DRUG DISCOVERY

12/2016

Front Cover Picture:
Michael Decker et al.
Aminobenzimidazoles and Structural Isomers as Templates
for Dual-Acting Butyrylcholinesterase Inhibitors and *h*CB₂R Ligands
To Combat Neurodegenerative Disorders

Special Issue
Polypharmacology & Multitarget Drugs
Guest Editors:
Maria Laura Bolognesi and
Andrea Cavalli

A Journal of
ChemPubSoc
Europe

WILEY-VCH

www.chemmedchem.org



Aminobenzimidazoles and Structural Isomers as Templates for Dual-Acting Butyrylcholinesterase Inhibitors and *hCB*₂R Ligands To Combat Neurodegenerative Disorders

Dominik Dolles,^[a] Martin Nimczick,^[a] Matthias Scheiner,^[a] Jacqueline Ramler,^[a] Patricia Stadtmüller,^[a] Edgar Sawatzky,^[a] Antonios Drakopoulos,^[a] Christoph Sotriffer,^[a] Hans-Joachim Wittmann,^[b] Andrea Strasser,^[b] and Michael Decker^{*[a]}

Dedicated to Professor John L. Neumeyer on the occasion of his 85th birthday.

A pharmacophore model for butyrylcholinesterase (BChE) inhibitors was applied to a human cannabinoid subtype 2 receptor (*hCB*₂R) agonist and verified it as a first-generation lead for respective dual-acting compounds. The design, synthesis, and pharmacological evaluation of various derivatives led to the identification of aminobenzimidazoles as second-generation leads with micro- or sub-micromolar activities at both targets and excellent selectivity over *hCB*₁ and AChE, respectively. Computational studies of the first- and second-generation lead

structures by applying molecular dynamics (MD) on the active *hCB*₂R model, along with docking and MD on *hBChE*, has enabled an explanation of their binding profiles at the protein levels and opened the way for further optimization. Dual-acting compounds with “balanced” affinities and excellent selectivities could be obtained that represent leads for treatment of both cognitive and pathophysiological impairment occurring in neurodegenerative disorders.

Author contributions:

D. Dolles and M. Nimczick (under the supervision of Prof. Dr. M. Decker), performed design and the synthesis of the test compounds (Julius Maximilian University Würzburg).

As bachelor thesis, M. Scheiner and J. Ramler (under the supervision of D. Dolles and Prof. Dr. M. Decker) helped synthesizing test compounds (Julius Maximilian University Würzburg).

D. Dolles and P. Stadtmüller performed biological evaluation of test compounds on *hCB*₁R / *hCB*₂R by radioligand binding studies (Julius Maximilian University Würzburg).

E. Sawatzky performed biological evaluation of test compounds on BChE / AChE by Ellmann’s assay (Julius Maximilian University Würzburg).

Computational studies were performed at BChE by A. Drakopoulos (under the supervision of Prof. Dr. C. Sotriffer) (Julius Maximilian University Würzburg) and at *hCB*₂R by H.-J. Wittman and A. Strasser (University of Regensburg).

4.1 Design and Development

As starting point, a potent and selective *hCB*₂R agonist **1** developed by AstraZeneca's drug development program was used.⁵² Based on the previous work by Darras *et al.*⁵⁰ on the development of quinazoline-based BChE inhibitors / histamine H₃ antagonists **3** and by Gonzalez-Naranjo *et al.*⁵³ on dual-acting compounds addressing *hCB*₂R and BChE **2** as well, several similarities and structural requirements for an inhibition of BChE were observed (**figure 3.1**): a condensed basic heterocycle (blue), a substituted aromatic ring (green) and aromatic and/or hydrophobic moieties (yellow/red). The structural characteristics were also apparent in AstraZeneca's ligand **1**, which was therefore tested for BChE inhibition. In fact, ligand **1** showed a moderate and selective inhibition of *eqBChE*.⁵¹

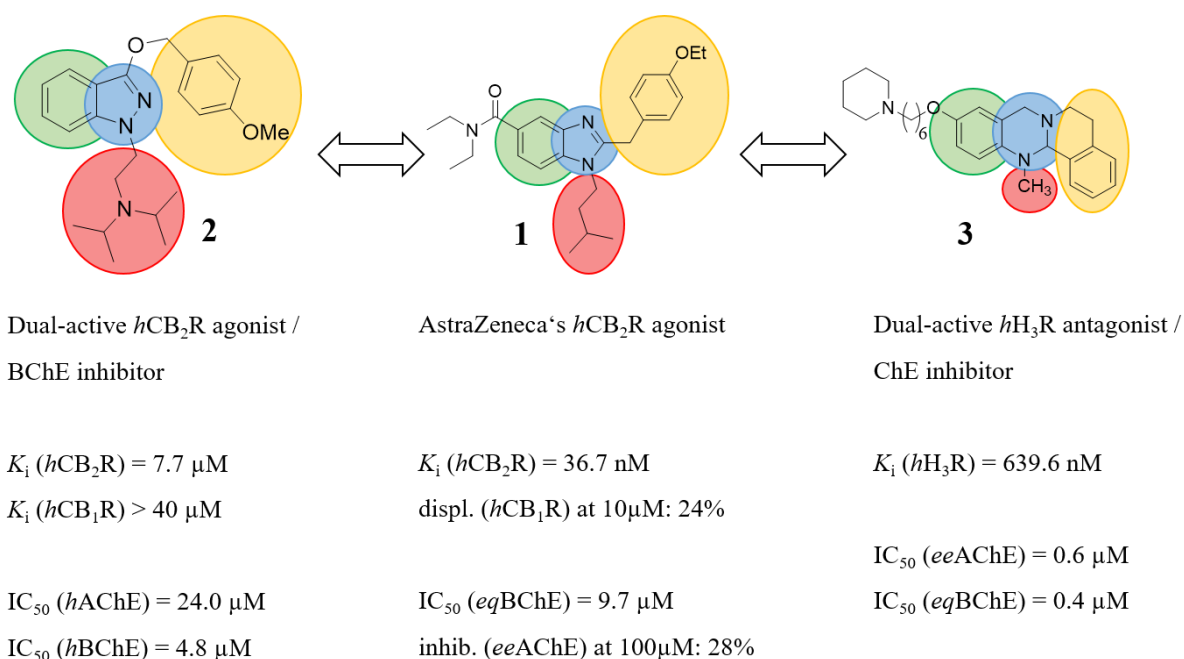


Figure 3.1. Structural similarities between AstraZeneca's *hCB*₂R ligand **1**,⁵² a dual-active *hCB*₂R agonist / BChE inhibitor **2**⁵³ and a dual-active *hH*₃R antagonist / ChE inhibitor **3**⁵⁰.

To keep the low molar mass, both pharmacophores should be combined by merging them into one single entity (cf. chapter 1). The difficulty is to maintain (receptor) affinity and (inhibitory) activity at both targets upon structural changes. In this case, four possible structural characteristics were altered and thus investigated in SARs (**figure 3.2**): a replacement of the core benzimidazole heterocycle by a 2-aminobenzimidazole, a 3-aminoindazole or a

pyridinoimidazole (blue); a substitution of the diethylamide moiety by a hydrogen atom (green); a replacement of the 4-ethoxy benzyl moiety by several aromatic and aliphatic substituents at the 2-amino moiety (yellow) and an introduction of a basic alkylamine at the *N*¹ of the core benzimidazole (red).

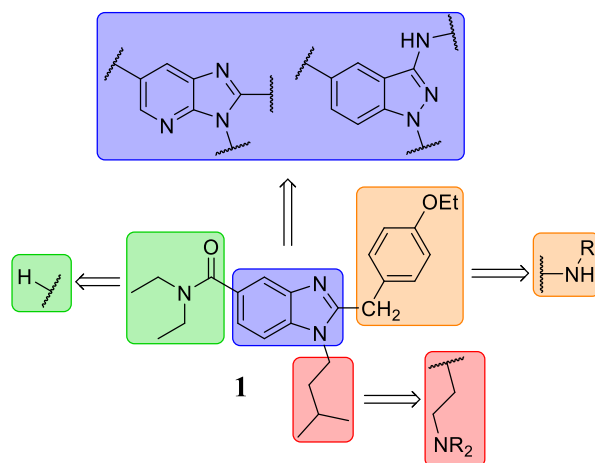
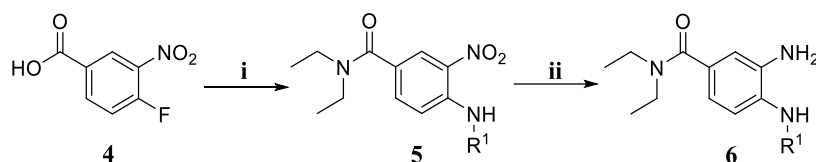


Figure 3.2. Structural alterations of the 2-methylene benzimidazole scaffold derived from AstraZeneca **1**.⁵¹

Depending on the substituents and/or core moieties, different synthetic approaches had to be performed (for detailed description of the synthesis cf. appendix II). In case of the most common 2-methylenebenzimidazoles (synthesized by M. Nimczick in modification to Pagé *et al.*⁵²) and 2-aminobenzimidazoles (synthesized in cooperation with M. Scheiner and J. Ramler in the course of their Bachelor thesis^{54,55}), the same starting material, 4-fluoro-3-nitrobenzoic acid **4**, and the resulting *o*-phenylene diamine precursor **6** could be used.

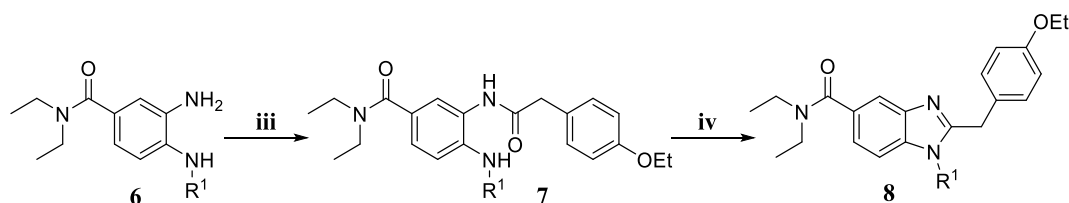
The subsequent description of the synthesis focuses on the core units, 2-methylene benzimidazole and 2-aminobenzimidazole (**schemes 3.1, 3.2 and 3.3**). For a better overview, various substituents are abbreviated as *R*¹ and *R*² (an exact definition of the used substituents *R*¹ and *R*² can be found in appendix II).

First, amide coupling was performed by using HBTU and diethylamine followed by a nucleophilic aromatic substitution with the respective amine to obtain compound **5**. The nitro moiety was then reduced to the *o*-phenylene diamine **6** using tin(II) chloride (**scheme 3.1**).



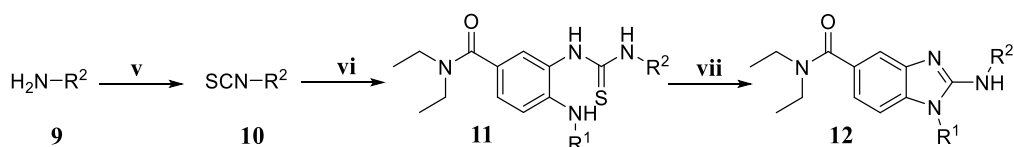
Scheme 3.1. Synthesis of *o*-phenylene diamine **6**. Conditions: i) HNEt₂, HBTU, NEt₃, DMF, rt. → H₂NR¹, NEt₃, EtOH, rt.; ii) SnCl₂ · 2 H₂O, EtOH, reflux.

In case of the 2-methylene benzimidazoles, phenylene diamine **6** was coupled with 2-(4-ethoxyphenyl)acetic acid using HBTU. The resulting amide **7** was cyclized by refluxing in glacial acetic acid to yield compound **8** (**scheme 3.2**). For the synthesis of the pyridinoimidazole core moiety the same synthetic approach was applied using the respective 2,3-pyridine diamine precursor (cf. appendix II).



Scheme 3.2. General synthesis of 2-methylene benzimidazoles. Conditions: iii) 2-(4-ethoxyphenyl)acetic acid, HBTU, NEt₃, DMF, rt.; iv) glacial AcOH, reflux.

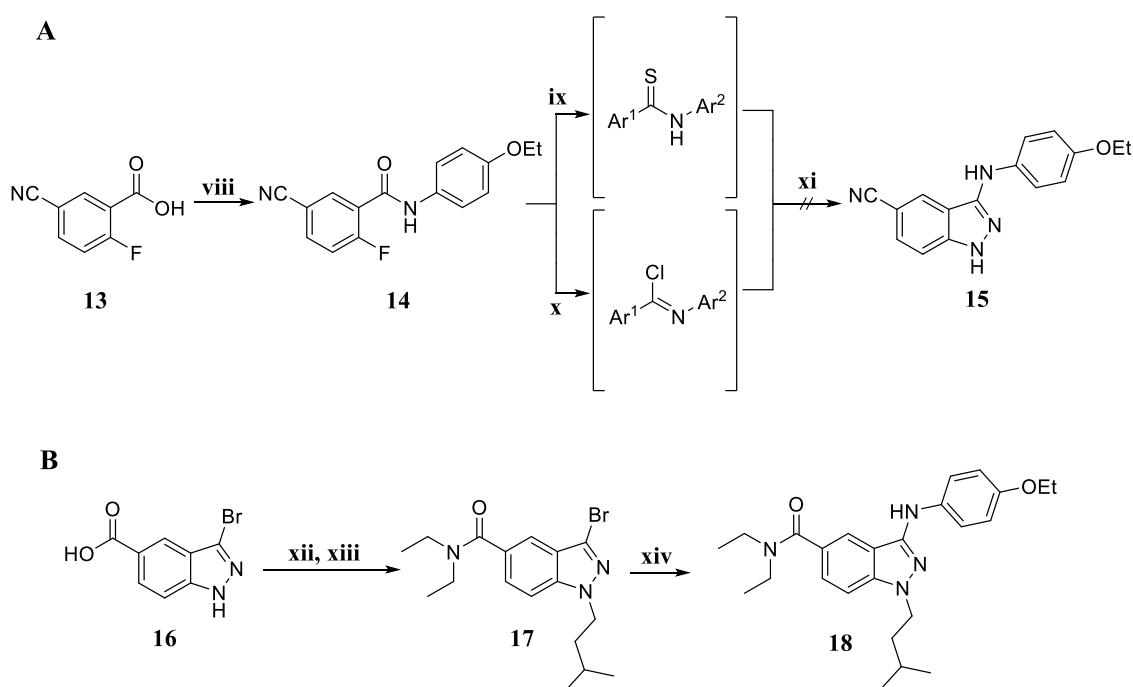
The synthesis of 2-aminobenzimidazoles was established in an earlier Master thesis.⁵⁶ The respective amine **9** was first converted into an isothiocyanate **10** by using carbon disulfide and then reacted with *o*-phenylene diamine **6** to obtain thiourea derivative **11**. To form the 2-aminobenzimidazole **12**, EDCI was used as cyclization agent (**scheme 3.3**).



Scheme 3.3. General synthesis of 2-aminobenzimidazoles. Conditions: v) CS₂, NEt₃, THF, 0 °C → Boc₂O, DMAP, THF, rt.; vi) *o*-phenylene diamine **6**, THF, rt.; vii) EDCI · HCl, NEt₃, THF, reflux.

For the synthesis of the 3-aminoindazole core moiety, a first attempt described by Burke *et al.*⁵⁷ using simple benzoic acid derivatives as building blocks failed. Starting from 5-cyano-2-

fluorobenzoic acid **13**, amide **14** was formed using HBTU. Activation of the carbonyl moiety (by either Lawesson's reagent or phosphoryl chloride) and subsequent cyclization to **15** with hydrazine failed (**scheme 3.4 A**). Instead, a more complex building block – the commercially available 3-bromoindazole derivative **16** – was used. After amide coupling and alkylation, a Buchwald-Hartwig-coupling⁵⁸ with 4-ethoxyaniline was used to obtain the desired 3-aminoindazole **18** (**scheme 3.4 B**).

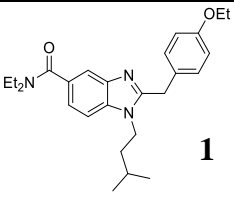
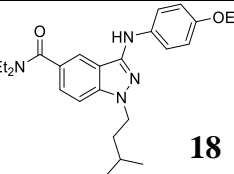
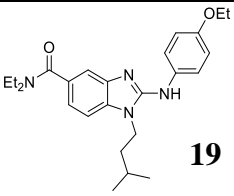
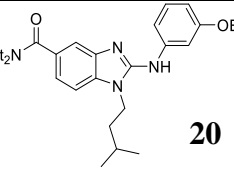
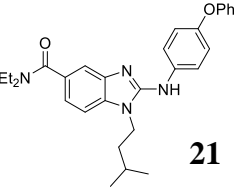
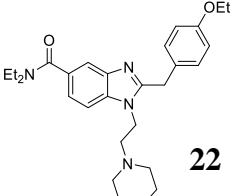
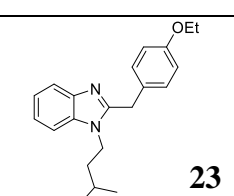


Scheme 3.4. A) Unsuccessful synthesis of 3-aminoindazole using simple building blocks. Conditions: viii) *p*-phenetidine, HBTU, NEt₃, DMF, rt.; ix) Lawesson's reagent, toluene, reflux; x) POCl₃, reflux; xi) hydrazine hydrate. B) Synthesis of 3-aminoindazole using a complex building block. Conditions: xii) HNEt₂, HBTU, NEt₃, DMF, rt.; xiii) isopentylbromide, NaH (60% suspension), DMF, 0 °C → rt.; xiv) *p*-phenetidine, Pd(OAc)₂, xantphos, Cs₂CO₃, dioxane, reflux.

4.2 Pharmacological Evaluation and SARs

All target compounds were tested for receptor affinity to *hCB*₁R and *hCB*₂R in radioligand binding studies (CHO cells stably expressing *hCB*₁R; HEK cells stably expressing *hCB*₂R). For inhibitory activity, target compounds were tested at AChE (*ee*AChE, EC. 3.1.1.7 from electric eel) and at BChE (*eq*BChE, EC. 3.1.1.8 from equine serum). *In vitro* results for selected compounds can be found in **table 3.1**; for detailed *in vitro* results cf. appendix II.

Table 3.1. Results of the biological evaluation of the inhibitory effect on *ee*AChE / *eq*BChE and radioligand binding studies at *hCB*₁R / *hCB*₂R for selected compounds⁵¹ (for complete overview on *in vitro* data cf. appendix II).

Compound	<i>eq</i> BChE IC ₅₀ (pIC ₅₀ ± SD) or % Inhibition	<i>ee</i> AChE IC ₅₀ (pIC ₅₀ ± SD) or % Inhibition	<i>hCB</i> ₂ R K _i (pIC ₅₀ ± SD) or [³ H]CP55,950 displ. at 10 μM	<i>hCB</i> ₁ R K _i (pIC ₅₀ ± SD) or [³ H]CP55,950 displ. at 10 μM
 1	9.7 μM (5.0 ± 0.1)	28 % at 100 μM	36.7 nM (7.4 ± 0.1)	24%
 18	26% at 10 μM	5% at 10 μM	11%	47%
 19	0.7 μM (6.2 ± 0.1)	4 % at 100 μM	1.91 μM (5.7 ± 0.1)	13%
 20	9.1 μM (6.2 ± 0.2)	< 2% at 10 μM	14%	8%
 21	3.7 μM (5.7 ± 0.3)	2% at 10 μM	426.0 nM (6.3 ± 0.2)	45%
 22	2.3 μM (5.6 ± 0.1)	48% at 100 μM	188.0 nM (6.7 ± 0.1)	14%
 23	25% at 10 μM	< 2% at 10 μM	26.0 μM (4.6 ± 0.1)	15%

The first step was to determine inhibitory activity of AstraZeneca's *hCB₂R* ligand **1** to validate the hypothesis that structural similarities to other BChE inhibitors would lead to a similar inhibitory effect at the BChE. In fact, **1** showed moderate inhibitory activity at *eq*BChE as well as selectivity over *ee*AChE ($IC_{50}(eqBChE) = 9.7 \mu M$; $IC_{50}(eeAChE) > 100 \mu M$). Based on these findings, 20 compounds were synthesized, tested and SARs were investigated (results for selected compounds can be found in **table 3.1**; for detailed *in vitro* results cf. appendix II). Depending on the modification, general trends were observed: while an exchange of the 2-methylene benzimidazole core into a 2-aminobenzimidazole maintained receptor affinity and inhibitory activity, the pyridinoimidazole and the 3-indazole scaffolds led to a loss of affinity/activity and were therefore not followed up. In case of the modifications at the 2-position of the 2-aminobenzimidazole scaffold, *m*-/*o*-substitution as well as unsubstituted aromatic scaffolds were not tolerated. The same applies for aliphatic (cyclic and open-chain) substituents. Only a *p*-substitution (even with sterical more demanding substituents) was well tolerated. The introduction of a basic aliphatic amine at the *N*¹ of the benzimidazole core was beneficial for a selective *eq*BChE inhibition and the receptor affinity was almost kept. The removal of the diethylamide functional group at the 5 position, which was expected to be a pharmacophore, led to a complete loss of activity/affinity.

Based on these results, three compounds were selected as 1st generation lead compounds (**figure 3.3**): a *p*-ethoxy phenyl 2-aminobenzimidazole **19** as well as a *p*-phenoxy phenyl 2-aminobenzimidazole **21** and a 2-methylene benzimidazole **22** with a basic aliphatic chain at the *N*¹. Since AstraZeneca's *hCB₂R* ligand **1** acts as an agonist⁵² and was developed and optimized in a drug development program, it was assumed that all synthesized compounds also act as agonists.

A reasonable way to visualize the results for two targets simultaneously is a plot of pIC_{50} values for BChE against pK_i values for *hCB₂R* affinity (**figure 3.3**). Promising compounds with a pIC_{50} / pK_i of least 5 (= 10 μM) are located in the top right quadrant.

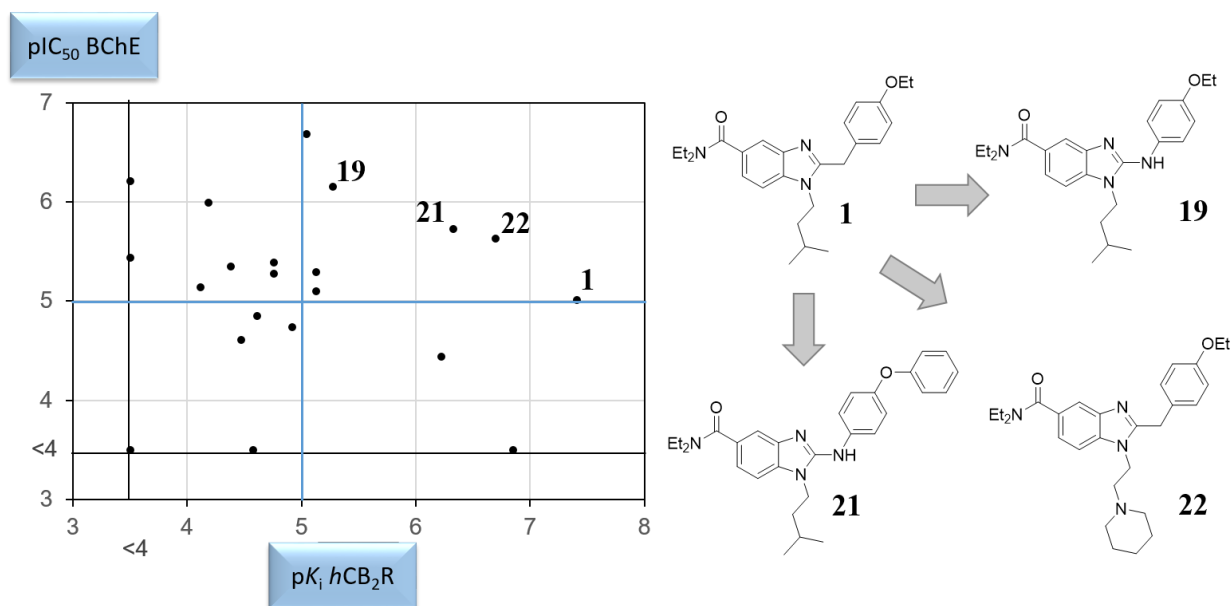


Figure 3.3. Plot of pIC₅₀ values for BChE inhibition against pK_i values for *hCB*₂R affinity of all compounds synthesized.⁵¹ Results for AstraZeneca's ligand **1** and 1st generation lead compounds **19**, **21** and **22** are highlighted. Compounds with no significant affinity for one of the targets are placed on the two black lines. The two blue lines represent the borders for minimum activity/affinity.

4.3 Computational Studies at *hCB*₂R and *hBChE*

To get a closer insight into their binding mode, AstraZeneca's ligand **1** and 2-aminobenzimidazole **19** from the set of 1st generation lead structures were selected. Both compounds show a high structural similarity, but a different activity/affinity profile: although compound **1** is a selective *hCB*₂R ligand with moderate inhibitory activity, 2-aminobenzimidazole **19** shows an increased inhibitory effect, yet with a 100-fold decreased affinity towards *hCB*₂R.

Binding mode at *hCB*₂R was investigated by A. Strasser and H.-J. Wittmann (University of Regensburg) in several MD simulations. A homology model for *hCB*₂R based on the human β₂ adrenergic receptor was used (for further information on the construction of the active-state model of *hCB*₂R cf. appendix II). MD studies revealed a similar binding mode of **1** and **19** in a pocket between transmembranes III, V and VI. The high receptor affinity of **1** can be explained by a positive π-π-interaction between the 2-benzyl moiety and Phe¹⁸³ (**figure 3.4a**). Compound **19** lacks this interaction, due to a slightly different binding mode of the 2-aminobenzimidazole

(**figure 3.4b**). The lone electron pair of the N-H causes the 2-aminobenzimidazole **19** to exhibit a nearly planar conformation (in case of ligand **1**, the CH₂ moiety is sp³-hybridized and therefore more flexible). The fact that **19** still shows one-digit micromolar receptor affinity is due to a water network between the diethylamide function and Trp^{5.43} and Thr^{3.33}, which is also apparent in compound **1**. As already described in the previous chapter, diethylamide is a pharmacophore for *h*CB₂R binding. This is supported by experimental results of compound **23** (cf. **table 3.1**).

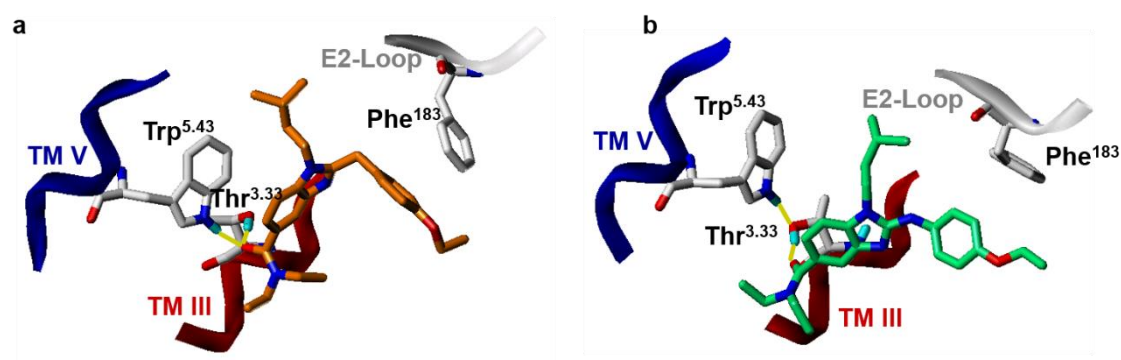


Figure 3.4. Binding conformation of **1** and **19** in the binding site of *h*CB₂R. a) Binding conformation of **1**, b) binding conformation of **19**.⁵¹

Molecular docking and MD at *h*BChE were performed by A. Drakopoulos and C. Sotriffer (for further information on docking studies and MD cf. appendix II). Both compounds **1** and **19** were first docked into the enzyme resulting in a similar binding mode: they are located near the catalytic active site, while the diethylamide function points towards Ala³²⁸. The isopentyl group points towards the oxyanion hole and the *p*-ethoxy phenyl moiety is located near Leu²⁸⁶. MD simulations further proved the docking results. The increased inhibitory activity of **19** (compared to **1**) results from positive interactions (hydrogen bonds) between the N-H of the 2-aminobenzimidazole and Ser²⁸⁷ and Pro²⁸⁵. In addition, polar interactions occur between the N² of the 2-aminobenzimidazole scaffold and Gln¹¹⁹ (**figure 3.5b**). In contrast, 2-methylene benzimidazole **1** lacks these interactions because of an absent N-H moiety. It therefore drifts more into the cavity. The fact that there's still a moderate inhibitory effect of **1** results from a water network between the diethylamide function and Ala³²⁸, Val³³¹ and Tyr³³² making the diethylamide scaffold a pharmacophore for BChE inhibition as well (**figure 3.5a**).

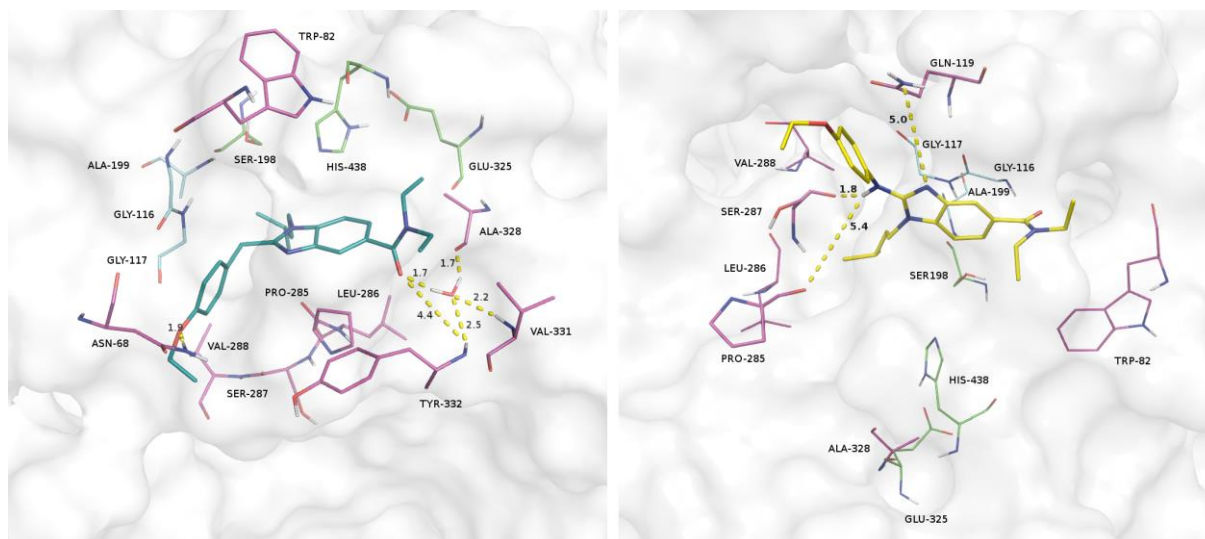



Figure 3.5. a) Binding mode of **1** as observed in the last snapshot of the MD simulation in BChE; interactions of the amide function with a water molecule and Tyr³³², Val³³¹, Ala³²⁸ and the interaction of the ether moiety with Asn⁶⁸ are highlighted. b) Binding mode of **19** as observed in the last snapshot of the MD simulation in BChE; interactions of the anilinic nitrogen atom with Ser²⁸⁷ and Pro²⁸⁵ of the benzimidazole nitrogen with Gln¹¹⁹ are highlighted.⁵¹

4.4 Conclusions

A BChE pharmacophore model was applied to the 2-methylene benzimidazole scaffold developed by AstraZeneca as a selective *h*CB₂R ligand. In fact, the compound shows a moderate inhibitory activity towards *eq*BChE. Based on these observations, 20 novel dual-active BChE inhibitors and *h*CB₂R ligands were synthesized, analyzed and initial SARs were summarized. All compounds show activity/affinity in the micromolar to submicromolar range towards *eq*BChE/*h*CB₂R and selectivity over *ee*AChE/*h*CB₁R. By several computational approaches, binding modes and pharmacophores could be identified. The aim of an upcoming project was to optimize the compounds (“designing in”, “designing out”, “balancing”; cf. chapter 3), to prove agonism and to evaluate them *in vivo*.

5. Structure-Activity Relationships and Computational Investigations into the Development of Potent and Balanced Dual-Acting Butyrylcholinesterase Inhibitors and Human Cannabinoid Receptor 2 Ligands with Pro-Cognitive *in vivo* Profiles⁵⁹

Structure–Activity Relationships and Computational Investigations into the Development of Potent and Balanced Dual-Acting Butyrylcholinesterase Inhibitors and Human Cannabinoid Receptor 2 Ligands with Pro-Cognitive *in Vivo* Profiles

Dominik Dolles,[†] Matthias Hoffmann,[†] Sandra Gunesch,[†] Oliviero Marinelli,[‡] Jan Möller,[§] Giorgio Santoni,[‡] Arnaud Chatonnet,^{||} Martin J. Lohse,[§] Hans-Joachim Wittmann,[⊥] Andrea Strasser,[⊥] Massimo Nabissi,[‡] Tangui Maurice,[#] and Michael Decker^{*,†} 

Author contributions:

D. Dolles (under the supervision of Prof. Dr. M. Decker) performed design and synthesis of the test compounds as well as biological evaluation on *hCB*₁R / *hCB*₂R by radioligand binding studies (Julius Maximilian University Würzburg).

M. Hoffmann and S. Gunesch performed biological evaluation of test compounds on BChE / AChE by Ellmann's assay (Julius Maximilian University Würzburg).

O. Marinelli, G. Santoni and M. Nabissi determined efficacy by cAMP assay and gene expression experiments (University of Camerino)

J. Möller (under the supervision of M. J. Lohse) performed radioligand binding studies at human μ -opioid receptor (Julius Maximilian University Würzburg).

A. Chatonnet and T. Maurice were responsible for behavioral *in vivo* studies in mice (University of Montpellier)

Computational studies at *hCB*₂R were performed by H.-J. Wittman and A. Strasser (University of Regensburg).

5.1 Structure Optimization

In this follow-up project, the compound library was extended and further developed by several common design strategies for multifunctional compounds: “designing in”, “designing out” and “balancing” (cf. chapter 3). Combined with the previously built-up SARs and the resulting 1st generation lead compounds **1-4**, four possible structural modifications were developed (**figure 4.1**): since the diethylamide function at position 5 of the benzimidazole moiety is a pharmacophore for both *h*CB₂R and BChE, different amides (green) and completely novel substituents with similar electronic effects (yellow) were introduced; structural motives of the 1st generation leads were combined (blue) and chain lengths of the basic aliphatic amines at the *N*¹ were modified (red).

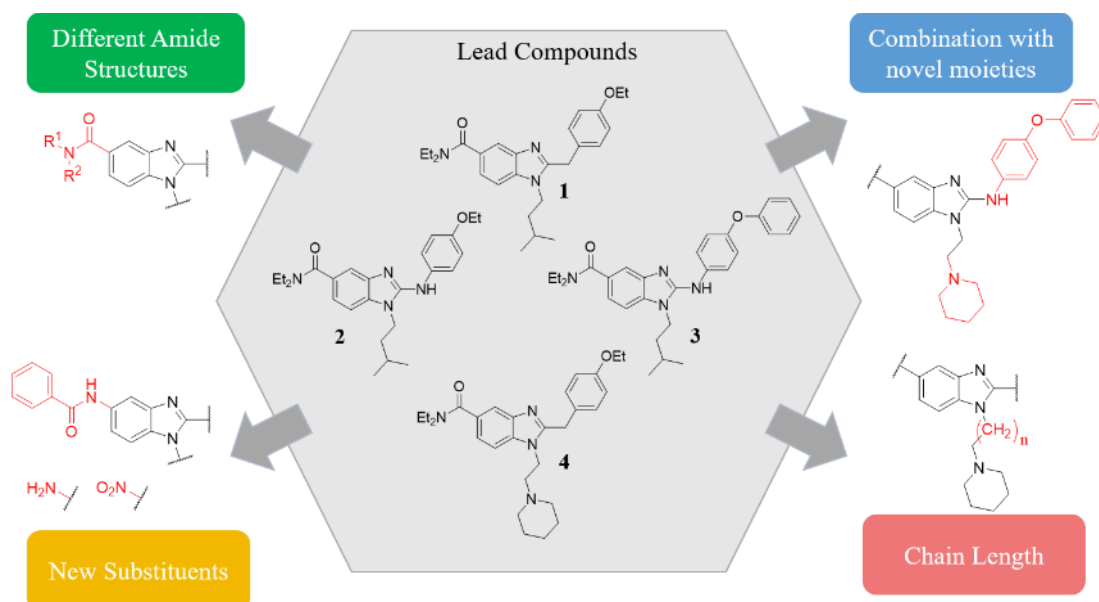
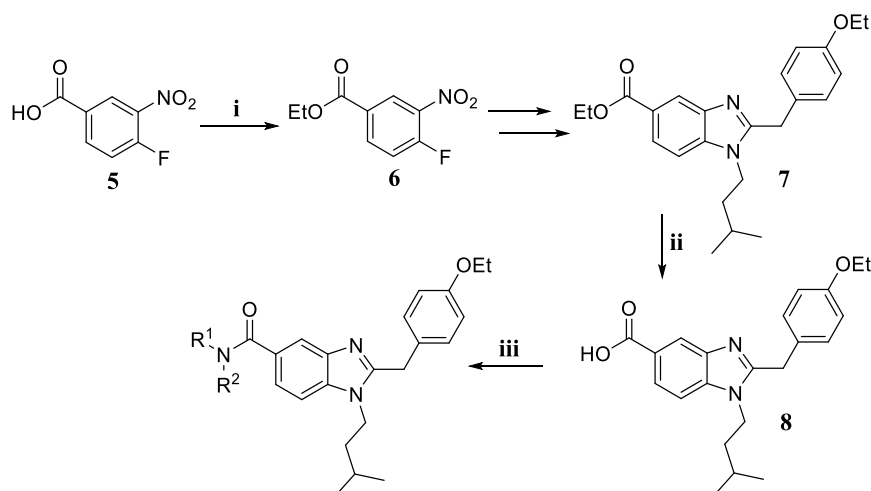


Figure 4.1. Structural modifications on the basis of the 1st generation lead compounds **1-4**.⁵⁹

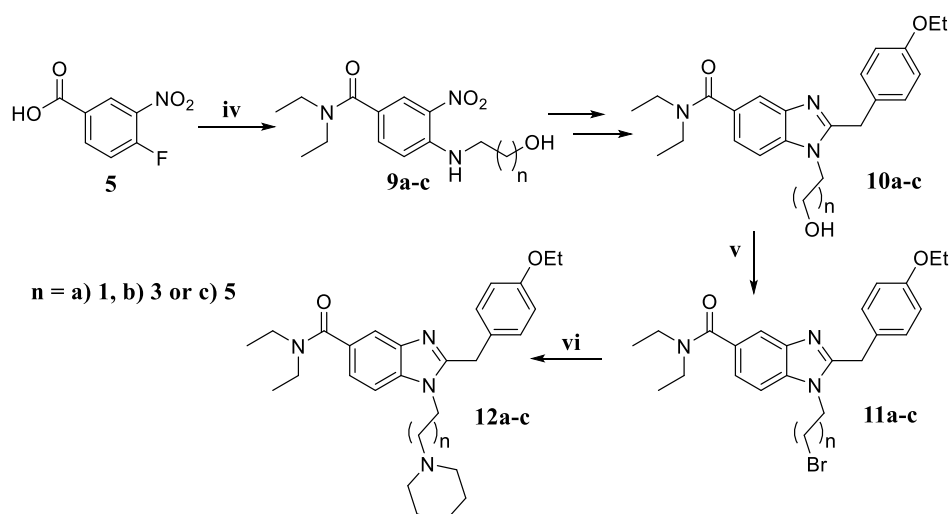
The synthesis of 2-methylene benzimidazoles and 2-aminobenzimidazoles was carried out in the same manner as described in chapter 3.1. Starting from the benzoic acid derivative **5**, a Fischer esterification was performed in the first step to easily introduce different amides at a later stage of the synthesis. After the synthesis of 2-methylene benzimidazole core, the ester **7** was hydrolyzed under basic conditions to afford acid **8**. The respective amides were obtained by coupling reactions using HBTU in the last step (for a better overview, varying substituents

are abbreviated as R¹ and R²; an exact definition of the used substituents R¹ and R² can be found in appendix III).



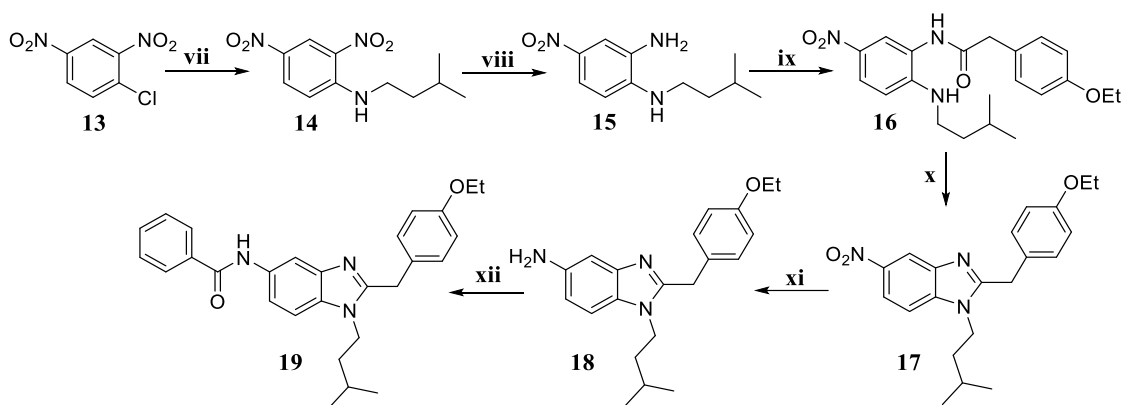
Scheme 4.1. Synthesis of different amides at position 5. Conditions: i) H₂SO₄, EtOH, reflux; ii) LiOH, THF/H₂O, rt.; iii) HNR¹R², HBTU, NEt₃, DMF, rt.

For the introduction of different alkyl chain lengths at the N¹, a modified synthesis was applied (in cooperation with J. Kraus in the course of his bachelor thesis⁶⁰). Starting from the same benzoic acid derivative **5**, amide coupling was performed and amino alcohols with different alkyl chains were introduced by a S_NAr reaction to afford compounds **9a-c**. After the 2-methylene benzimidazole core was synthesized, the alcohol **10a-c** was substituted by a bromide in an Appel-like synthesis using phosphorous tribromide. In the last reaction step, bromide **11a-c** was substituted by piperidine in a S_N2 reaction (**scheme 4.2**).



Scheme 4.2. Synthesis of alkylamines with different chain lengths. Conditions: iv) HNEt₂, HBTU, NEt₃, DMF, rt. → amino alcohol with different chain length, NEt₃, EtOH, rt.; v) PBr₃, CH₂Cl₂, rt.; vi) piperidine, K₂CO₃, DMF, 70 °C.

The exchange of the diethylamide moiety into other substituents (e.g. -NO₂, -NH₂) required the establishment of a novel synthetic pathway (**scheme 4.3**). In this case, 1-chloro-2,4-dinitrobenzene **13** served as starting material. In the first step, chloride was substituted by isopentylamine in a S_NAr reaction. To selectively reduce one nitro moiety and obtain the *o*-phenylene diamine derivative **15**, a basic sodium sulfide solution was used.⁶¹ The resulting *o*-phenylene diamine **15** was then coupled with 2-(4-ethoxyphenyl)acetic acid to obtain amide **16**, which was subsequently cyclized into nitro benzimidazole **17**. To change the electronic properties, the nitro substituent was reduced by tin(II) to afford amine **18**. In the last step, amine **18** was then coupled with benzoic acid to afford amide **19**.



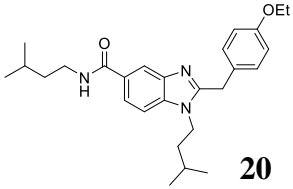
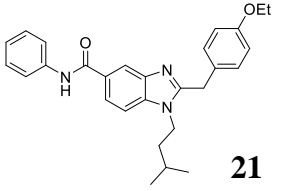
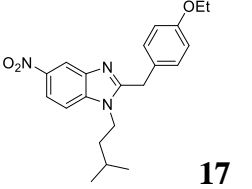
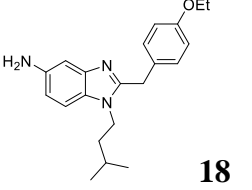
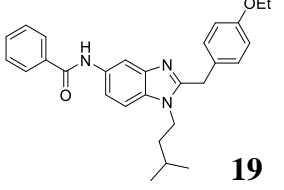
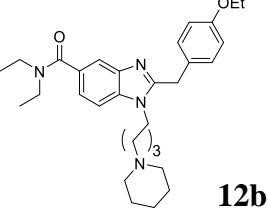
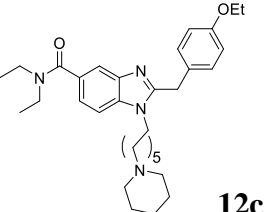
Scheme 4.3. Synthesis of benzimidazoles with electron withdrawing / donating substituents at position 5: vii) isopentylamine, NEt₃, EtOH, rt.; viii) Na₂S · H₂O, NaHCO₃, MeOH/H₂O, reflux; ix) 2-(4-ethoxyphenyl)acetic acid, HBTU, NEt₃, DMF, rt.; x) AcOH, reflux; xi) SnCl₂ · 2 H₂O, EtOH, reflux; xii) benzoic acid, HBTU, NEt₃, DMF, rt.

5.2 Pharmacological Evaluation and SARs

All target compounds were tested for receptor affinity to *hCB*₁R and *hCB*₂R in radioligand binding studies (CHO cells stably expressing *hCB*₁R; HEK cells stably expressing *hCB*₂R). For inhibitory activity, target compounds were tested at AChE (*hAChE* and *eeAChE*, EC. 3.1.1.7 from human erythrocytes and electric eel, respectively) and at BChE (*hBChE*, EC. 3.1.1.8 from human serum). *In vitro* results for selected compounds can be found in **table 4.1**; for detailed *in vitro* results cf. appendix III.

Table 4.1. Results of the biological evaluation of the inhibitory effect on *hAChE* / *hBChE* and radioligand binding studies at *hCB*₁R / *hCB*₂R for selected compounds⁵⁹ (for complete overview on *in vitro* data cf. appendix III).

Dual-Acting BChE Inhibitors and *hCB*₂R Ligands

Compound	<i>h</i> BChE IC ₅₀ (pIC ₅₀ ± SD) or % Inhibition	<i>h</i> AChE IC ₅₀ (pIC ₅₀ ± SD) or % Inhibition	<i>hCB</i> ₂ R K _i (pIC ₅₀ ± SD) or [³ H]CP55,950 displ. at 10 μM	<i>hCB</i> ₁ R K _i (pIC ₅₀ ± SD) or [³ H]CP55,950 displ. at 10 μM
 20	1.6 μM (5.8 ± 0.1)	11% at 10 μM	763.6 nM (6.1 ± 0.1)	37%
 21	1.2 μM (5.9 ± 0.1)	5% at 10 μM	14.4 μM (4.8 ± 0.2)	18%
 17	12 % at 50 μM	14% at 50 μM (tested at <i>ee</i> AChE)	961.8 nM (6.0 ± 0.2)	41%
 18	39 % at 100 μM	15% at 100 μM (tested at <i>ee</i> AChE)	21.0 μM (4.7 ± 0.1)	27%
 19	25 % at 10 μM	2% at 10 μM (tested at <i>ee</i> AChE)	4.3 μM (5.4 ± 0.4)	36%
 12b	2.7 μM (5.6 ± 0.1)	60.1 μM (4.2 ± 0.2)	4.8 μM (5.3 ± 0.2)	2%
 12c	8.2 μM (5.1 ± 0.1)	20.0 μM (4.7 ± 0.1)	1.0 μM (5.9 ± 0.1)	4%

Based on the considerations for structural alterations discussed in chapter 4.1, 13 novel compounds were synthesized, tested and SARs investigated (results for selected compounds can be found in **table 4.1**; for detailed *in vitro* results cf. appendix III). All test compounds show

selectivity over *hCB*₁R and *hAChE*, if not otherwise stated. The exchange of the diethylamide function by an electron-donating (-NH₂, **18**) or an electron-withdrawing substituent (-NO₂, **17**), as well as the “combination” of structural motives from 1st generation lead compounds led to a strongly decreased activity/affinity. The variation of the chain length of the basic alkylene at the *N*¹ (compounds **12b** and **12c**, see **table 4.1**), which was developed to positively interact with the oxyanion hole of the *hBChE* and therefore increase the inhibitory activity, slightly increased inhibitory activity at the *hBChE*, but led to a loss of selectivity towards *hAChE*. The most promising results were obtained by the introduction of different amides: while aromatic and/or sterically demanding substituents (e.g. **21**) decreased activity/affinity, straight or branched alkyl chains (e.g. **20**) afforded well-balanced activities/affinities in the (sub-)micromolar range. Interestingly, the orientation of the amide seems to strongly influence activity/affinity for both targets. The “initial” amide scaffold with the carbonyl part attached to the benzimidazole core is well tolerated (see **21**, **table 4.1**), while the “inverted” amide with the amine part attached to the benzimidazole core lost inhibitory activity (see **19**, **table 4.1**). It is further remarkable that the use of the *hBChE* (instead of the *eqBChE*) led to dramatically different results. All 1st generation lead compounds (**figure 4.1**), which showed at least one-digit micromolar inhibition at *eqBChE*, completely lost inhibitory activity towards *hBChE*, while results for *hAChE* and *eeAChE* stayed nearly in the same range. An earlier sequence alignment has shown that for *AChE*, the active center is highly conserved. Based on these very different results, this might not be the case for *BChE*.

For a better overview on the results, pIC₅₀ values for *BChE* were plotted against p*K*_i values for *hCB*₂R affinity (**figure 4.2**). Promising compounds with a pIC₅₀ / p*K*_i of at least 5 (= 10 μM) are located in the top right quadrant. As 2nd generation lead compound, isopentylamide **20** was chosen because of its balanced activity/affinity profile.

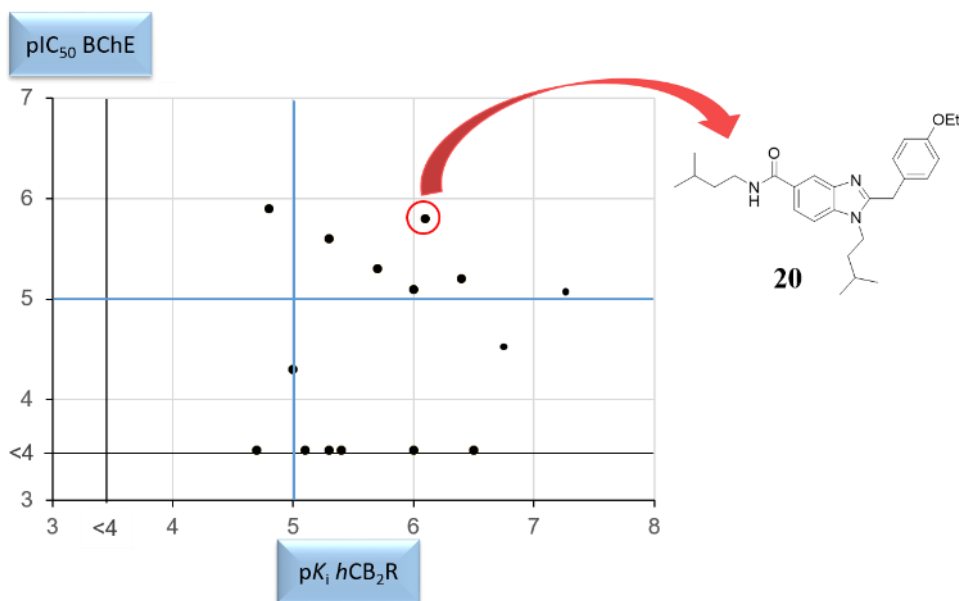


Figure 4.2. Plot of pIC₅₀ values for BChE inhibition against pK_i values for *hCB*₂R affinity of all compounds synthesized.⁵⁹ Results for 2nd generation lead compound **20** is highlighted. Compounds with no significant affinity for one of the targets are placed on the two black lines. The two blue lines represent the borders for minimum activity/affinity.

Since AstraZeneca's *hCB*₂R agonist **1** was derived from a drug development program, it was assumed that all similar compounds do also behave as agonists.⁵² To prove this assumption, M. Nabissi and Co-Workers (University of Camerino) investigated intrinsic activity in a cAMP assay and a downstream gene expression experiment. The *hCB*₂R is G_{i/o} coupled and therefore negatively regulates adenylate cyclase. An agonist reverts forskolin-stimulated cAMP production, while an antagonist/inverse agonist enhances the production. In fact, all test compounds showed agonistic behavior in the cAMP assay. In addition, intracellular cAMP concentration regulates the expression of several genes, which are regulated by the transcription factor cAMP-response element binding (CREB) protein to upstream cAMP response elements (CREs). One of the regulated genes is the macrophage migration factor (MIF), which is located in proximity to a CRE. The same applies to the signal transducer and activator of transcription (STAT-3), which is also under CRE promoter control.⁶²⁻⁶⁶ In fact, gene expression correlates with the results obtained by the cAMP assay and further proves agonist behavior of all compounds tested (**figure 4.3**; for complete overview cf. appendix III).⁵⁹

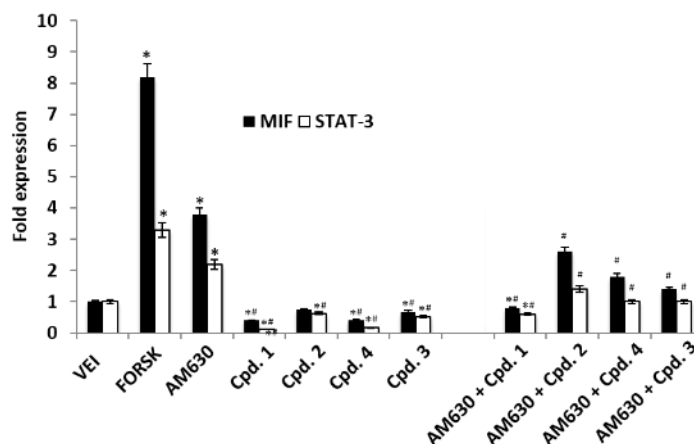


Figure 4.3. Selected test compounds reduce MIF and STAT-3 gene expression.⁵⁹ U266 cells were treated with test compounds (50 μ M), Forskolin (10 μ M) or AM630 (25 μ M) for 2 hours. In combination experiment (AM630 plus test compounds), U266 cells were pre-incubated with AM630 for 30 minutes before adding test compounds. MIF and STAT-3 mRNA levels were determined by qRT-PCR. GAPDH was used for normalization. Data are expressed as relative fold with respect to vehicle treated cells used as the control. Data are expressed as mean \pm SD. * p <0.01 vs untreated; # vs AM630.

When using “privileged structures” (small chemical entities that provide affinities to various targets due to their size, polarity and/or rigidity and do therefore appear in many drugs) such as benzimidazoles, it is important to check for unwanted side-interactions with other targets and to avoid them in future compound design efforts (“designing out”). In this case, Etonitazene⁶⁷, a μ -opioid receptor (MOP) agonist developed in the 1960s, showed a high degree of structural similarities: a benzimidazole as core structure, an electron-withdrawing substituent at position 5 (red), a *p*-ethoxy benzyl moiety at position 2 (green) and a basic alkyl chain attached to the *N*¹ (blue) (**figure 4.4**). Radioligand binding studies performed by J. Möller at the MOP receptor (HEK cells transiently transfected with the *hMOP* receptor) confirmed our assumptions.⁵⁹ Compound **4**, a first generation lead structure with the highest structural similarities, showed affinity in the nanomolar range. For compounds **1** and **2**, which lack structural similarities, affinity is decreased (**figure 4.4**).

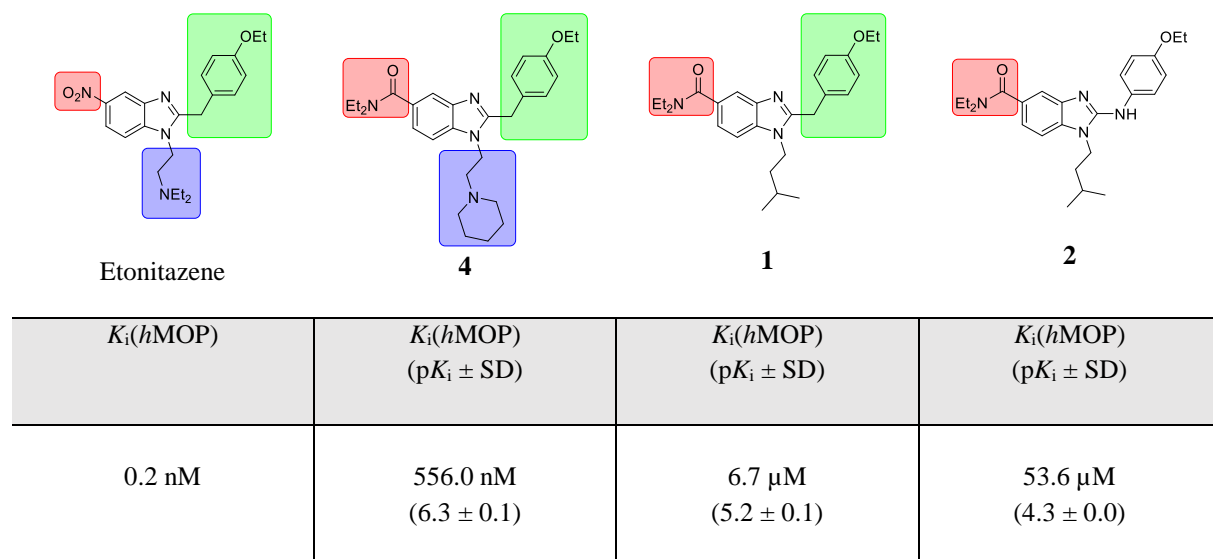


Figure 4.4. Structural similarities between Etonitazene⁶⁷ and lead compounds **1**, **2** and **4**: an electron-withdrawing substituent at position 5 (red), a basic alkyl chain at the *N*¹ (blue) and a *p*-ethoxy benzyl moiety at position 2 of the benzimidazole core (green).

5.3 Computational Studies

After elucidating the role of the diethylamide moiety of AstraZeneca's ligand **1** and 1st generation lead compound **2** as pharmacophore for *hCB*₂R, the newly developed 2nd generation lead compound **20** with a modified amide was investigated.

Binding mode at *hCB*₂R was investigated by A. Strasser and H.-J. Wittmann (University of Regensburg) in several MD simulations.⁵⁹ In contrast to the previous project, a homology model for *hCB*₂R based on a recently published⁶⁸ *hCB*₁R crystal structure in complex with the agonist AM11542 was used, because of a higher degree of homology (for further information on the construction of the active-state model of *hCB*₂R cf. appendix III).

The orthosteric binding pocket of the *hCB*₂R is mainly formed by aromatic amino acids, which results in a preferred binding of the ligands *p*-ethoxy benzyl moiety to this region. MD simulations also revealed an extended water network between the orthosteric binding site and the Asp^{2.50} of the allosteric binding site. By this means, it may be possible that a ligand, which binds to the orthosteric binding site, may transfer signals for receptor downstream-activation not only by the highly conserved amino acids but also via the discovered water network (**figure 4.5**).

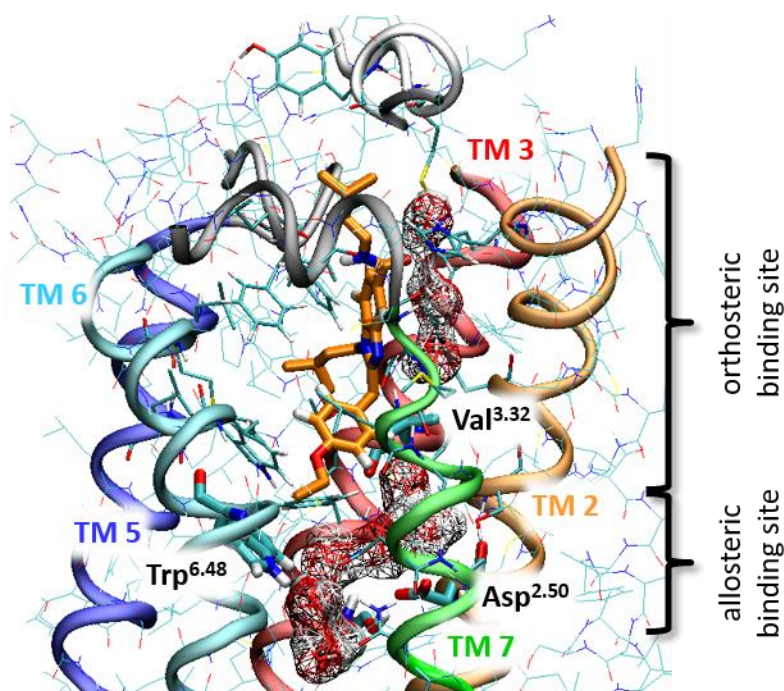


Figure 4.5. Orthosteric binding pocket of the *hCB₂R* in complex with compound **20** as well as the internal water network between the orthosteric (Val^{3.32}) and the allosteric (Asp^{2.50}) binding site, as obtained by the MD simulations.⁵⁹

5.4 *In vivo* Studies

Ultimately, AstraZeneca's *hCB₂R* ligand **1**, 1st generation lead compound **2** (improved BChE inhibition) and 2nd generation lead compound **20** (well-balanced activity/affinity profile) were tested for their neuroprotective and pro-cognitive effects in an AD *in vivo* model by A. Chatonnet and T. Maurice (University of Montpellier).⁵⁹ This study is one of the very few examples described in the literature, where addressing BChE led to improved cognition and memory. In a recent *in vivo* study, BChE knockout-mice showed enhanced learning abilities in memory tests compared to the wildtypes.⁴⁰ In another study, Kosak *et al.*⁴¹ applied selective BChE inhibitors to mice. Here, cognitive deficits in healthy mice were scopolamine-induced. Upon administration of BChE inhibitors, animals subsequently showed improved memory and learning abilities in several *in vivo* tests.

Neuroinflammation and cognitive deficits were induced by injection (*i.c.v.*) of oligomerized A β ₂₅₋₃₅ into the mouse brains (male swiss mice, 6 weeks old). The test compounds were administered (*i.p.*) to the test group in three different doses (0.3 mg/kg, 1.0 mg/kg and 3.0 mg/kg) between day 1 and 7. On day 8, spontaneous alternation performances (addressing

short-term memory) were tested in a Y-maze. On days 9 and 10, step-through passive avoidance (addressing long-term memory) was tested (for detailed experimental procedures cf. appendix III).

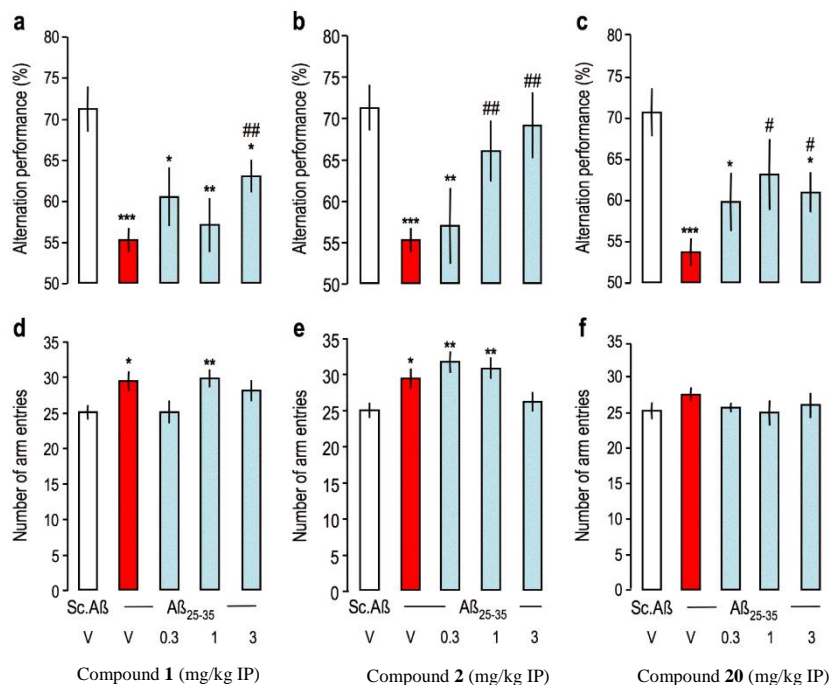


Figure 4.5. Effect of test compounds **1**, **2** and **20** on A β_{25-35} -induced spontaneous alternation deficits in mice.⁵⁹ Animals received A β_{25-35} or Sc.A β peptide (9 nmol *i.c.v.*) on day 1 and the test compounds (0.3 mg/kg *i.p.*) or vehicle solution (V, DMSO 20% in saline or DMSO 20%, Tween-80 2% in saline) *o.d.* between days 1 to 7. Alternation performance was tested on day 8. Data shown mean \pm SEM. ANOVA: $F_{(4,54)} = 6.55$, $p < 0.001$, $n = 9-14$ per group in (a); $F_{(4,54)} = 5.43$, $p < 0.001$, $n = 8-14$ per group in (b); $F_{(4,57)} = 4.05$, $p < 0.01$, $n = 9-14$ per group in (c); $F_{(4,54)} = 2.72$, $p < 0.05$ in (d); $F_{(4,54)} = 4.70$, $p < 0.01$ in (e); $F_{(4,57)} = 0.59$, $p > 0.05$ in (f). * $p < 0.05$, ** $p < 0.01$, *** $p < 0.001$ vs. (Sc.A β +V)-treated group; ## $p < 0.01$, ### $p < 0.001$ vs. (A β_{25-35} +V)-treated group; Dunnett's test.

Regarding short-term memory, compound **1** only attenuated spontaneous alternation deficits at the highest dose tested (**figure 4.5a,d**). Compounds **2** and **20** (both with improved inhibition of BChE) significantly prevented deficits already at a dosage of 1 mg/kg (**figure 4.5b,e** and **figure 4.5c,f**).

In terms of long-term memory, compound **1** failed to show any beneficial effect (**figure 4.6a,d**). Both dual-acting compounds with an improved BChE inhibition showed a significant prevention. For compound **2** prevention could be achieved at the highest dose tested (**figure 4.6b,e**) and for compound **20**, a significant improvement was already achieved at a dosage of 1 mg/kg (**figure 4.6c,f**).

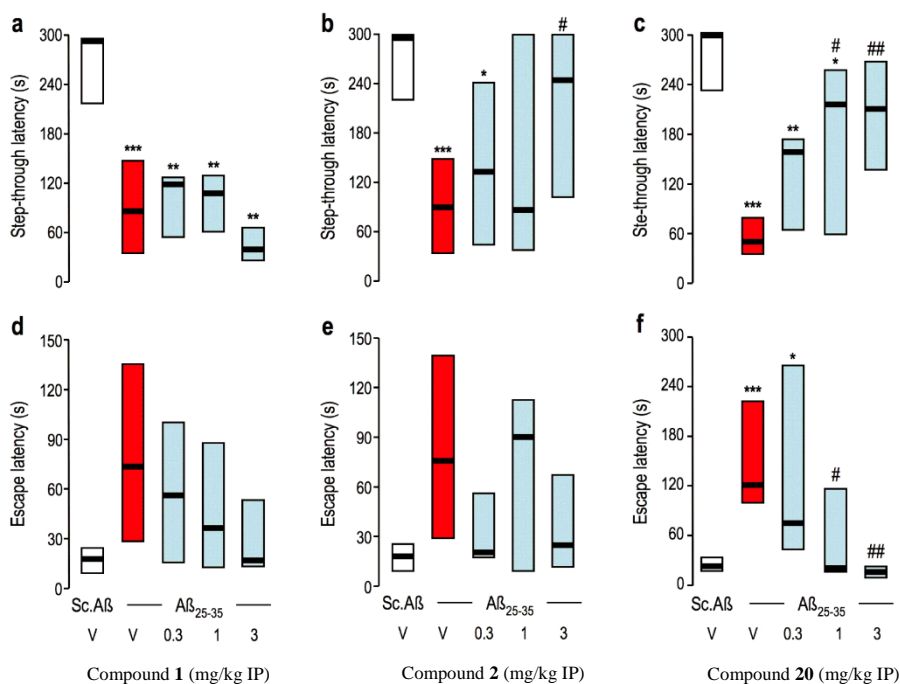


Figure 4.6. Effect of test compounds **1**, **2** and **20** on A β_{25-35} -induced passive avoidance deficits in mice.⁵⁹ Animals received A β_{25-35} or Sc.A β peptide (9 nmol *i.c.v.*) on day 1 and the test compounds (0.3 mg/kg *i.p.*) or vehicle solution (V, DMSO 20% in saline or DMSO 20%, Tween-80 2% in saline) *o.d.* between says 1 to 7. Training was performed on day 9 and retention measured on day 10. Data show median and interquartile range. Kruskal-Wallis ANOVA: $H = 19.0$, $p < 0.001$, $n = 9-14$ per group in (a); $H = 15.0$, $p < 0.01$, $n = 8-14$ per group in (b); $H = 21.1$, $p < 0.001$, $n = 11-14$ in (c); $H = 6.89$, $p > 0.05$ in (d); $H = 6.34$, $p > 0.05$ in (e); $H = 19.7$, $p < 0.001$ in (f). * $p < 0.05$, ** $p < 0.01$, *** $p < 0.001$ vs. (Sc.A β +V)-treated group; # $p < 0.05$, ## $p < 0.01$ vs. (A β_{25-35} +V)-treated group; Dunn's test.

5.5 Conclusions

An extended compound library based on 2-methylene benzimidazoles and 2-aminobenzimidazoles was synthesized and SARs were investigated. Compounds could be further improved by applying literature-known design approaches: “designing in”, “designing out” and “balancing”. All compounds show both a well-balanced activity/affinity profile at *hBChE/hCB*₂R and selectivity over *hCB*₁R and *hAChE*. Intrinsic activity was investigated by applying a cAMP assay and a gene expression experiment proved that all compounds tested act as agonists. By exchanging certain structural elements, unwanted off-target interactions with the MOP receptor could be designed out. A homology model for the *hCB*₂R (based on a recent *hCB*₁R crystal structure) elucidated ligand binding to the orthosteric binding site, which is linked over a water-network to an “allosteric” binding site. *In vivo* studies in mice showed

improved memory and cognition after selected compounds (dual-active and well-balanced) were administered at a dosage of 1 mg/kg to 3 mg/kg.

6. The First Photochromic Affinity Switch for the Human Cannabinoid Receptor 2⁶⁹

FULL PAPER

Photopharmacology

ADVANCED
THERAPEUTICS
www.advtherap.com

The First Photochromic Affinity Switch for the Human Cannabinoid Receptor 2

*Dominik Dolles, Andrea Strasser, Hans-Joachim Wittmann, Oliviero Marinelli, Massimo Nabissi, Roger G. Pertwee, and Michael Decker**

The *hCB₂R* plays an important role in the immune system and is centrally expressed in microglia. The *hCB₂R* activated by agonists hold great therapeutic potential, e.g., in neuroinflammation. It is currently not yet elucidated how pathophysiological processes are mediated by the *hCB₂R*. Here, photochromic affinity switches based on a drugable benzimidazole core through azologization and computational studies are developed. Structure-activity relationships (SARs) lead to compounds with high selectivity over *hCB₁R* that can be reversibly switched to a higher affinity *cis*-form proved on the receptor level by radioligand binding studies and translating into an affinity change in a functional GTP γ S assay. cAMP ELISA and the change in expression level of two genes regulated by CREB proves that the compounds act as partial agonists.

Author contributions:

D. Dolles (under the supervision of Prof. Dr. M. Decker) performed design and synthesis of the test compounds as well as determination of photophysical properties and biological evaluation on *hCB₁R* / *hCB₂R* by radioligand binding studies (Julius Maximilian University Würzburg).

Computational studies at *hCB₂R* were performed by H.-J. Wittman and A. Strasser (University of Regensburg).

O. Marinelli and M. Nabissi determined efficacy by cAMP and gene expression assay (University of Camerino).

R. G. Pertwee performed GTP γ S assay (University of Aberdeen).

6.1 Introduction

As discussed in chapter 1, *hCB₂R* agonists are capable of reducing both the number of activated glia cells surrounding A β plaques and the amount of pro-inflammatory cytokines. What is still unknown is the time-frame, how these effects are mediated and in which sequence pathophysiologic activation takes place.⁷⁰ To further investigate these processes, it is beneficial to use tool compounds. A widely used approach is photopharmacology (**figure 5.1**), which makes use of a hybrid consisting of a biologically active compound and a photochromic (often referred to as “photoswitchable”) moiety. Thus, it is possible to fast and reversibly change the chemical structure (e.g. geometry, polarity, electronic properties) by light. Ideally, these hybrids then exhibit a different binding to the target and certain biological functions can be controlled.⁷¹

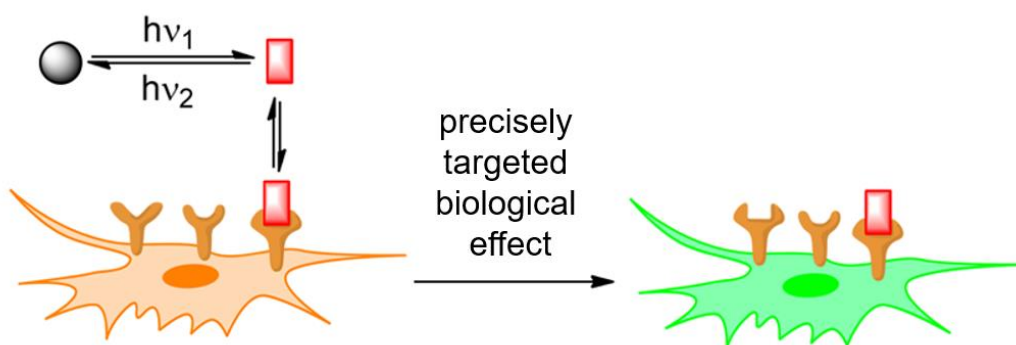


Figure 5.1. Principal of photopharmacology.⁷¹

In the literature, the most common photochromic moieties are azobenzenes, which consist of two benzene rings connected by an azo function (**figure 5.2**). Azobenzenes exist in two stereoisomers: the stable *trans*-isomer and the less stable / unstable *cis*-isomer. Upon irradiation with UV light, isomerization from *trans* to *cis* takes place resulting in a change in geometry and dipole moment / polarity ($\Delta\mu_{trans} = 0$ vs. $\Delta\mu_{cis} = 3$). Depending on the overall chemical structure, azobenzenes are thermally stable and remain in the *cis*-form for several hours if kept in darkness. Upon exposing to daylight, azobenzenes re-isomerize to the stable *trans*-form. This switching process can typically be repeated over multiple cycles.⁷²

What makes azobenzenes more suitable compared to other photochromic moieties with similar properties (e.g. diarylethenes) is their size. Azobenzenes can easily be introduced into

biologically active compounds / drugs without dramatically altering the overall structure and losing affinity. A common principle to introduce azobenzenes into already existing compounds was proposed by Trauner and colleagues: azologization.⁷³ This rational approach is based on the principle of bioisosters. Similar structural motives (e.g. styrenes, ethers, amides etc.) are simply replaced by azobenzene (**figure 5.2**). Another approach is the so-called “azo-extension”.⁷³ By carefully analyzing SARs, suitable position, where an azobenzene might be tolerated at the target, can be investigated (**figure 5.2**).

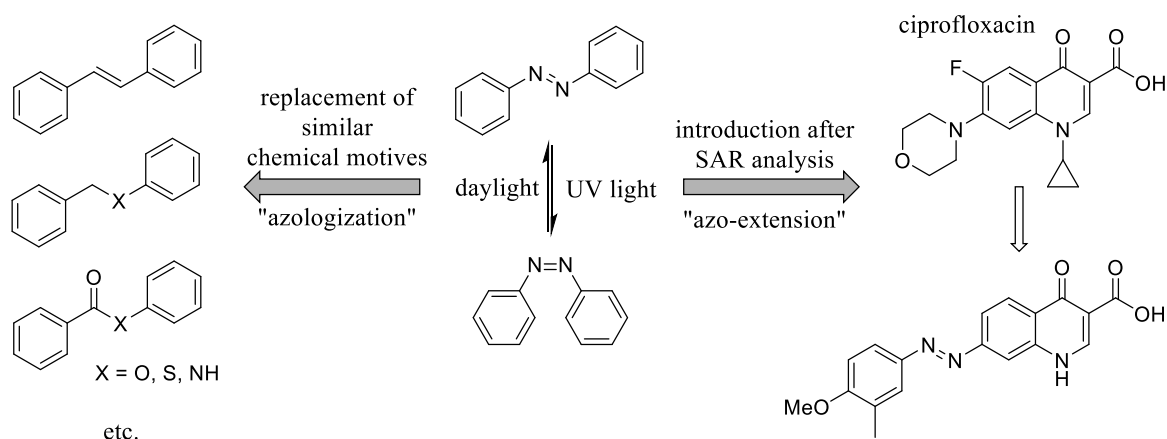


Figure 5.2. Center: isomerization of *trans*-azobenzene to *cis*-azobenzene upon UV light / daylight; left: azologization approach; right: azo-extension approach (as exemplified by Feringa’s quinolone based on ciprofloxacin).^{71,73}

Photopharmacology has been successfully applied at several targets including enzymes, GPCRs and ion channels (for review see reference 72). Ideally, activation upon irradiation is desired: photochromic compounds exhibit no (or at least a weaker) biological effect in their (stable) ground state, but upon isomerization, biological activity is then increased. The following project presents the first GPCR ligand that exhibits increased affinity towards *hCB₂R* upon irradiation.⁶⁹ So far, only ligands that are active in their ground state and can be deactivated upon irradiation were known to literature.^{73,74}

6.2 Design and Development

Based on the insights gained by SARs on benzimidazoles as *hCB₂R* agonists / BChE inhibitors (cf. chapter 4 and 5), a suitable position, which may tolerate an introduction of an azobenzene scaffold was investigated. As described by Trauner and colleagues, it is possible to replace several chemical scaffolds by azobenzenes.⁷³ By this means, the diethylamide moiety at position 5 of the benzimidazole core was replaced (**figure 5.3**).

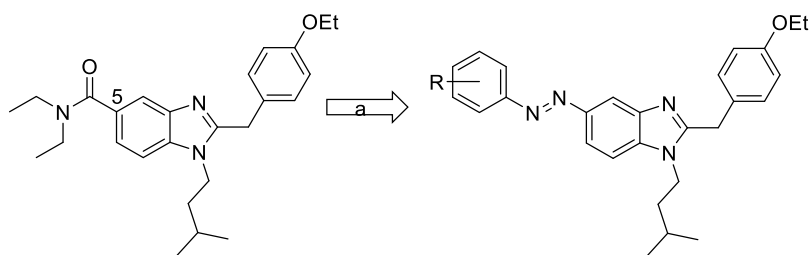
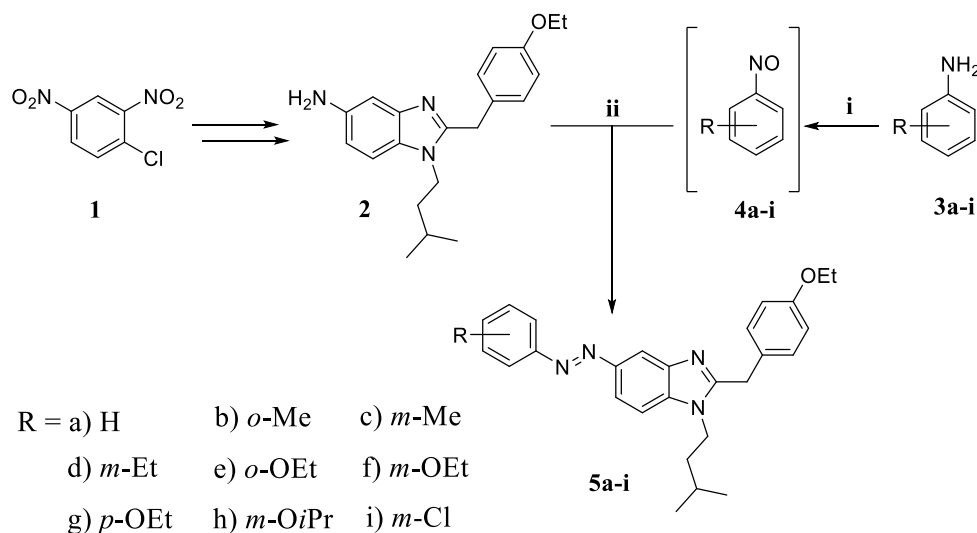


Figure 5.3. Azo-extension of the diethylamide moiety to obtain 5-substituted benzimidazole azobenzenes.

As synthetic approach, a similar synthesis as described in chapter 4.1 was applied. 1-Chloro-2,4-dinitrobenzene **1** was used as starting material. After several reaction steps, 5-aminobenzimidazole **2** was obtained and used as a common intermediate. To couple amine **2** in a Mills reaction⁷⁶ with the respective nitroso compound **4a-i**, it was necessary to partially oxidize the respective anilines (**3a-i**) by oxone.⁷⁷ By this means, 9 (un-)substituted benzimidazole azobenzenes (**5a-i**) were obtained (for detailed experimental procedures cf. appendix IV).



Scheme 5.1. Synthesis of 5-azobenzene benzimidazoles. Conditions: i) oxone, CH₂Cl₂/H₂O, rt.; ii) AcOH, rt.

All compounds synthesized could be isomerized quantitatively from the initial *trans*-form to the *cis*-form by UV light ($\lambda = 366$ nm) showing the typical behavior of azobenzenes with $\pi\text{-}\pi^*$ and $n\text{-}\pi^*$ transitions at absorption maxima of around 325 nm and 430 nm, respectively. Repeated isomerization to *cis* and re-isomerization to *trans* (using daylight) for several cycles was possible. If kept in darkness at room temperature, all compounds remain stable in the *cis*-state for several hours (**figure 5.4**).

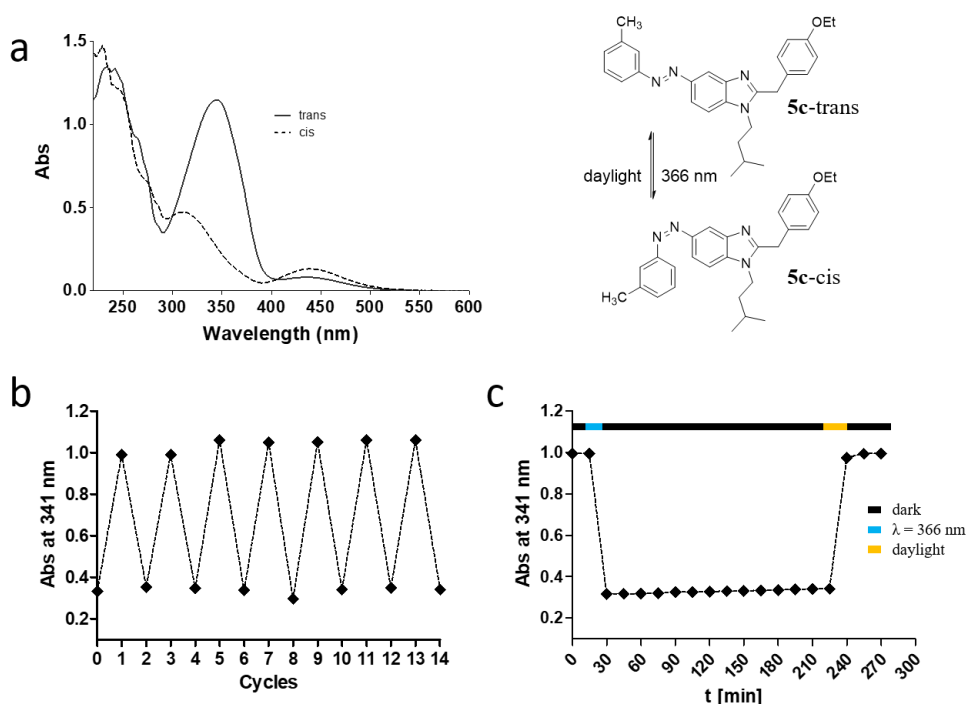


Figure 5.4. Photophysical properties of 5-azobenzene benzimidazoles as represented by compound **5c**.⁶⁹ a) UV-spectrum of **5c** (*trans*: solid line, *cis*: dotted line); b) switching cycles of **5c**; c) thermal stability of **5c-cis** at room temperature over a period of >3h.

6.3 Pharmacological Evaluation

All target compounds were tested for receptor affinity to *hCB₁R* and *hCB₂R* in radioligand binding studies (CHO cells stably expressing *hCB₁R*; HEK cells stably expressing *hCB₂R*; results for *hCB₂R* affinity for all compounds presented as pIC_{50} values can be found in **figure 5.5**; for detailed *in vitro* results cf. appendix IV).

For photoswitchable compounds that serve as tool compounds for receptor investigations, the aim was not just to obtain a high affinity towards *hCB₂R* for both isomers, but to induce a change of affinity upon irradiation.

In fact, all compounds tested showed high affinity towards *hCB₂R* within the two- and three-digit nanomolar range (pIC_{50} values from 6.4 to 7.8; **figure 5.5**) and selectivity over *hCB₁R*. Upon irradiation, all compounds showed an increased affinity, which is a novelty for GPCR ligands. In the literature, only compounds, which are deactivated upon irradiation were reported. While an *o*- or *p*-substitution show almost no difference upon irradiation, the biggest difference between *trans* and *cis* was obtained by a *m*-substitution. An *m*-CH₃ substituent (**5c**) showed the best results with an approx. 8-fold difference upon irradiation.

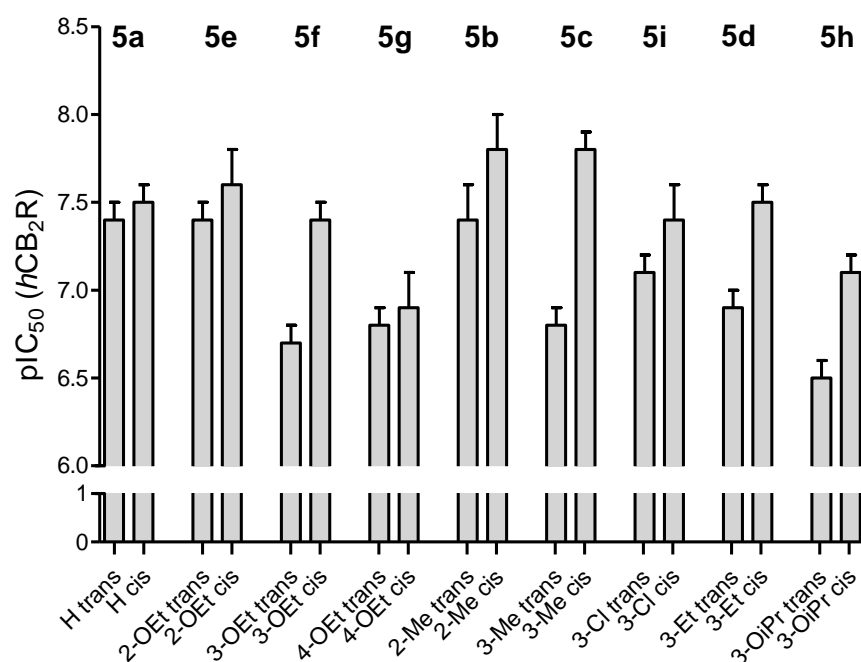


Figure 5.5. Results (presented as pIC_{50} values) obtained from radioligand binding studies at *hCB₂R*.

6.4 Computational Studies

Binding mode at *hCB₂R* was investigated by A. Strasser and H.-J. Wittmann by docking the unsubstituted 5-azobenzene benzimidazole (**5a-trans** and **5a-cis**) into the homology model of

hCB₂R. The homology model for *hCB₂R* was based on a recently published *hCB₁R* crystal structure in complex with the agonist AM11542⁶⁸ (for further information on the construction of the active-state model of *hCB₂R* cf. appendix IV).

The compounds were docked into the orthosteric binding site. For **5a-trans** the azobenzene moiety is located in an aromatic side pocket formed by Phe^{3.36}, Trp^{5.43} and Trp^{6.48}. For **5a-cis** the azobenzene moiety is embedded in an aromatic side pocket formed by Phe¹⁸³, Tyr^{5.39} and Trp^{5.43} (**figure 5.6**).

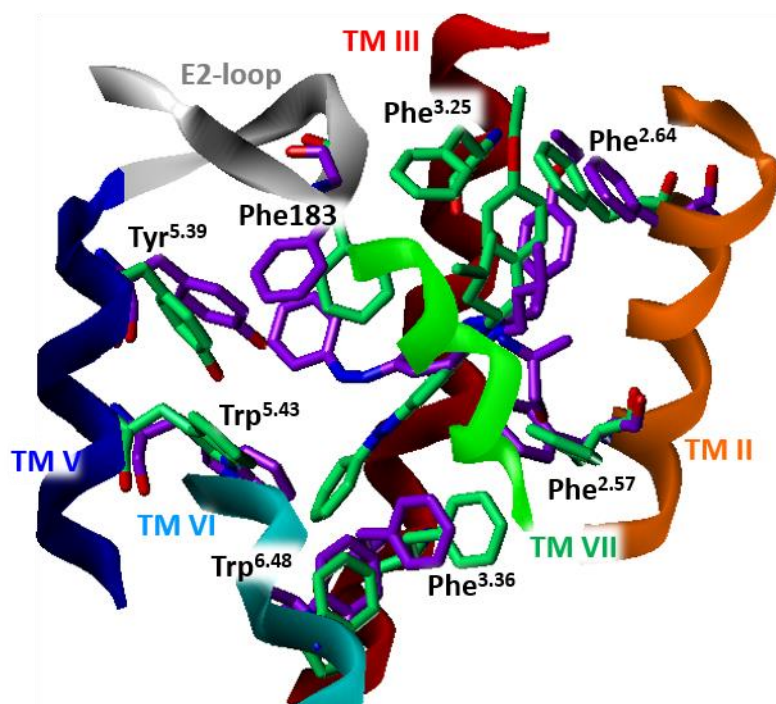


Figure 5.6. Overlay of the binding mode of **5a-trans** (green) and **5a-cis** (purple) in binding pocket of the *hCB₂R* obtained by docking studies.⁶⁹

To explain affinity differences for different substituent patterns, a closer look at the binding of the azobenzene ring had to be taken (**figure 5.7**). For *m*-substitution a steric clash of the *trans* isomer with Thr^{3.37} is observed. In case of the *cis* isomer, the *m*-substituent fits well into a small cavity. This results in a higher affinity of the *m*-substituted *cis* isomer. Regarding *o*-substitution, no difference for *trans*- and *cis*-isomer was found. This results from a small gap in the binding site, where the *o*-substituent is able to bind. For *p*-substitution no vacant gap was observed resulting in a decreased binding affinity for both isomers.

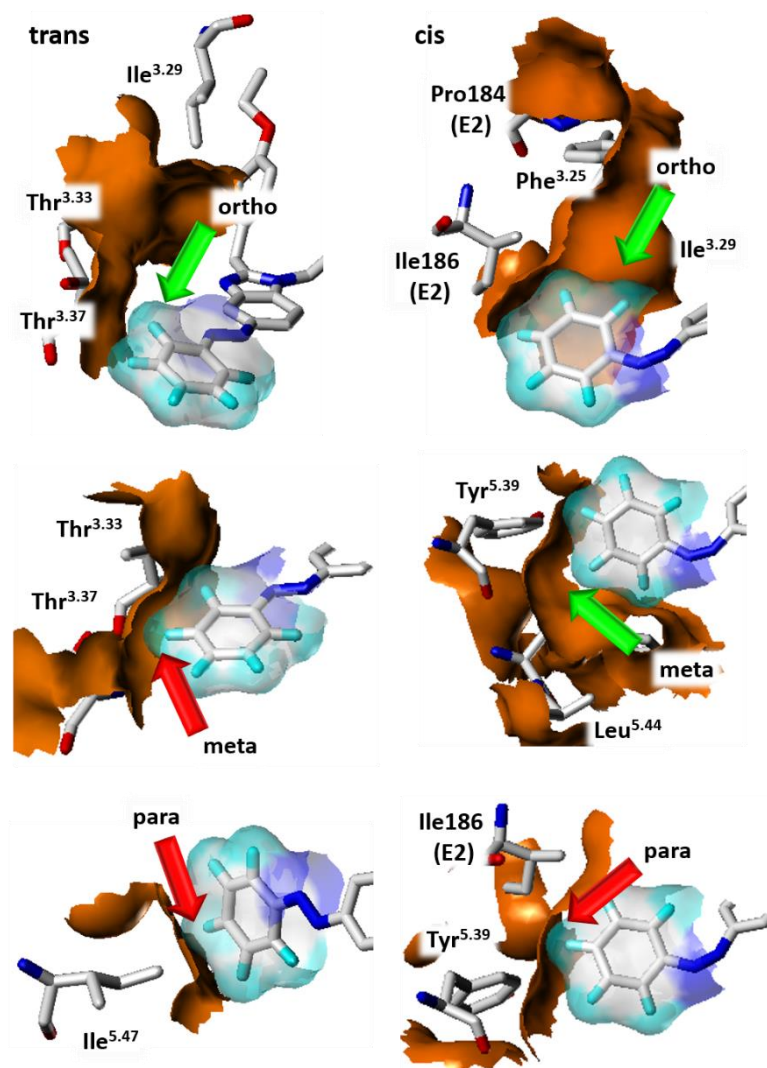


Figure 5.7. *5a-trans* (left) and *5a-cis* (right) docked into the binding pocket of the *hCB₂R*. Shown in the presence (green arrow) or absence (red arrow) of additional gaps for small substituents at the azobenzene moiety in *o*-, *m*- and *p*-position.⁶⁹

7. Summary and Outlook

While life expectancy increases worldwide, treatment of neurodegenerative diseases such as AD becomes a major task for industrial and academic research. Currently, a treatment of AD is only symptomatic and limited to an early stage of the disease by inhibiting AChE. A cure for AD might even seem far away. A rethinking of other possible targets is therefore necessary. Addressing targets that can influence AD even at later stages might be the key. Even if it is not possible to find a cure for AD, it is of great value for AD patients by providing an effective medication. The suffering of patients and their families might be relieved and remaining years may be spent with less symptoms and restrictions.

It was shown that a combination of *hCB₂R* agonist and BChE inhibitor might exactly be a promising approach to combat AD. In the previous chapters, a first investigation of dual-acting compounds that address both *hCB₂R* and BChE was illustrated (**figure 6.1**).

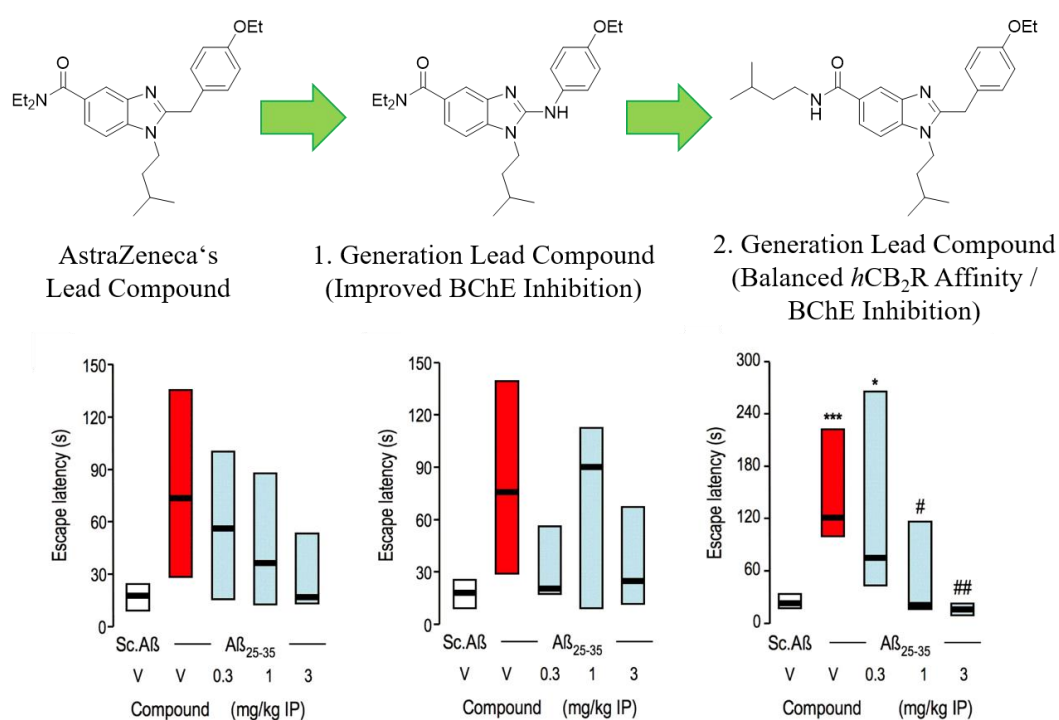


Figure 6.1. Development of dual-acting *hCB₂R* agonists / BChE inhibitors and their improved *in vivo* profile (as exemplified by the results from passive avoidance tests⁵⁹).

A set of over 30 compounds was obtained by applying SARs from BChE inhibitors to a *hCB₂R* selective agonist developed by AstraZeneca. In a first *in vitro* evaluation compounds showed selectivity over *hCB₁R* and AChE. Further investigations could also prove agonism and showed that unwanted off-target affinity to *hMOP* receptor could be designed out. The development of a homology model for *hCB₂R* (based on a novel *hCB₁R* crystal) could further elucidate the mode of action of the ligand binding. Lastly, first *in vivo* studies showed a beneficial effect of selected dual-acting compounds regarding memory and cognition.

Since these first *in vivo* studies mainly aim for an inhibition of the BChE, it should be the aim of upcoming projects to proof the relevance of *hCB₂R* agonism *in vivo* as well. In addition, pharmacokinetic as well as solubility studies may help to complete the overall picture.

Currently, hybrid-based dual-acting *hCB₂R* agonists and selective BChE inhibitors are under investigation in our lab. First *in vitro* evaluations showed improved BChE inhibition and selectivity over AChE compared to tacrine.⁷⁸ Future *in vitro* and *in vivo* studies will clarify their usage as drug molecules with regard to hepatotoxicity and blood-brain barrier penetration.

Since the role of *hCB₂R* is not yet completely elucidated, the use of photochromic tool-compounds becomes an area of interest. These tool-compounds (and their biological effect) can be triggered upon irradiation with light and thus help to investigate time scales and ligand binding.

A set of 5-azobenzene benzimidazoles was developed and synthesized. In radioligand binding studies, affinity towards *hCB₂R* could be increased upon irradiation with UV-light (**figure 6.2**). This makes the investigated compounds the first GPCR ligands that can be activated upon irradiation (not *vice versa*).

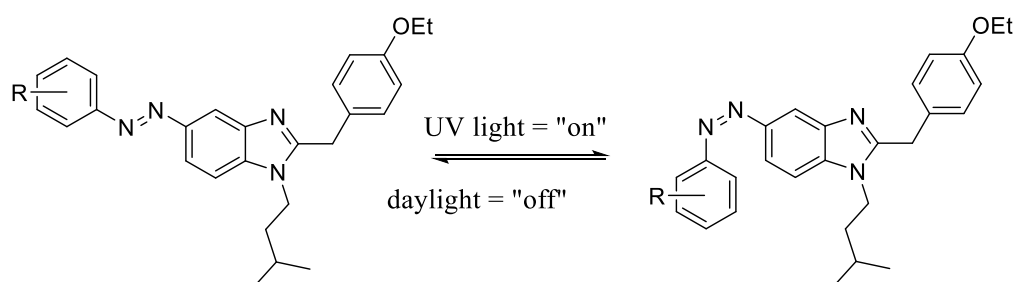


Figure 6.2. Chemical structure of the developed 5-azobenzene benzimidazoles. Affinity towards *hCB₂R* is increased upon irradiation with UV light.

The aim of upcoming research will be the triggering of a certain intrinsic activity by an “efficacy-switch”. For this purpose, several attempts are currently under investigation: an introduction of an azobenzene moiety at the 2-position of the benzimidazole core already led to a slight difference in efficacy upon irradiation with UV light. Another approach going on in our lab is the development of *hCB₁R* switches based on the selective *hCB₁R* inverse agonist rimonabant. First *in vitro* results are not yet available (**figure 6.3**).

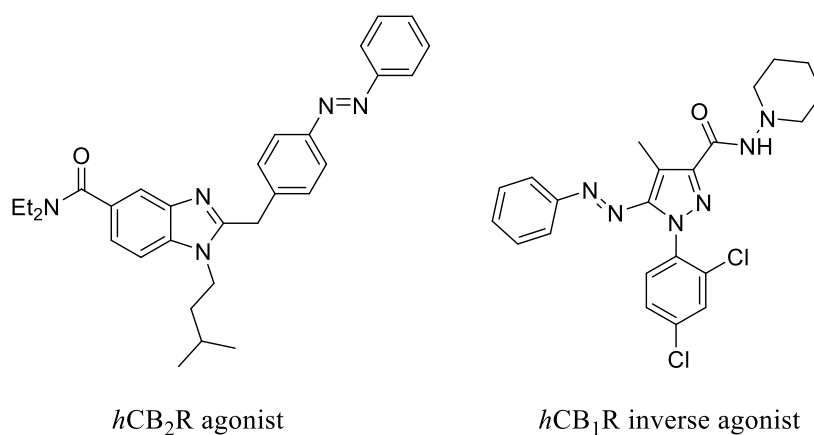


Figure 6.3. Chemical scaffolds for “efficacy switches” at the two CBR subtypes.

8. Zusammenfassung und Ausblick

Durch die weltweit steigende Lebenserwartung rückt die Behandlung von neurodegenerativen Krankheiten, wie der Alzheimer'schen Krankheit, immer mehr in den Fokus der industriellen und akademischen Forschung. Momentan erfolgt die Behandlung der Alzheimer'schen Krankheit durch die Blockade der AChE nur symptomatisch und in einem Frühstadium. Eine Heilung scheint dabei in weiter Ferne zu liegen, weshalb ein Umdenken nach neuen Ansätzen stattfinden sollte. Der Schlüssel könnte darin liegen, dass man biologischen Funktionen adressiert, die den Verlauf der Alzheimer'schen Krankheit auch in einem späteren Stadium beeinflussen. Selbst wenn eine Heilung in absehbarer Zeit unmöglich bleibt, ist es für die betroffenen Patienten eine erhebliche Erleichterung auf eine effektive Medikation zurückgreifen zu können. Das Leid der Patienten und ihrer Familien könnte dadurch gelindert und die verbleibenden Lebensjahre ohne Symptome und Einschränkungen genossen werden.

In den vorangegangenen Kapiteln wurde bereits gezeigt, dass die Kombination aus einem *hCB₂R* Agonisten und einem BChE Hemmer genau diesen vielversprechenden Ansatz verfolgt. Ein erster Entwicklungsansatz von dual-aktiven *hCB₂R* Agonisten / BChE Hemmern wurde in den Kapiteln 3 und 4 ausführlich dargestellt (**Abb. 7.1**).

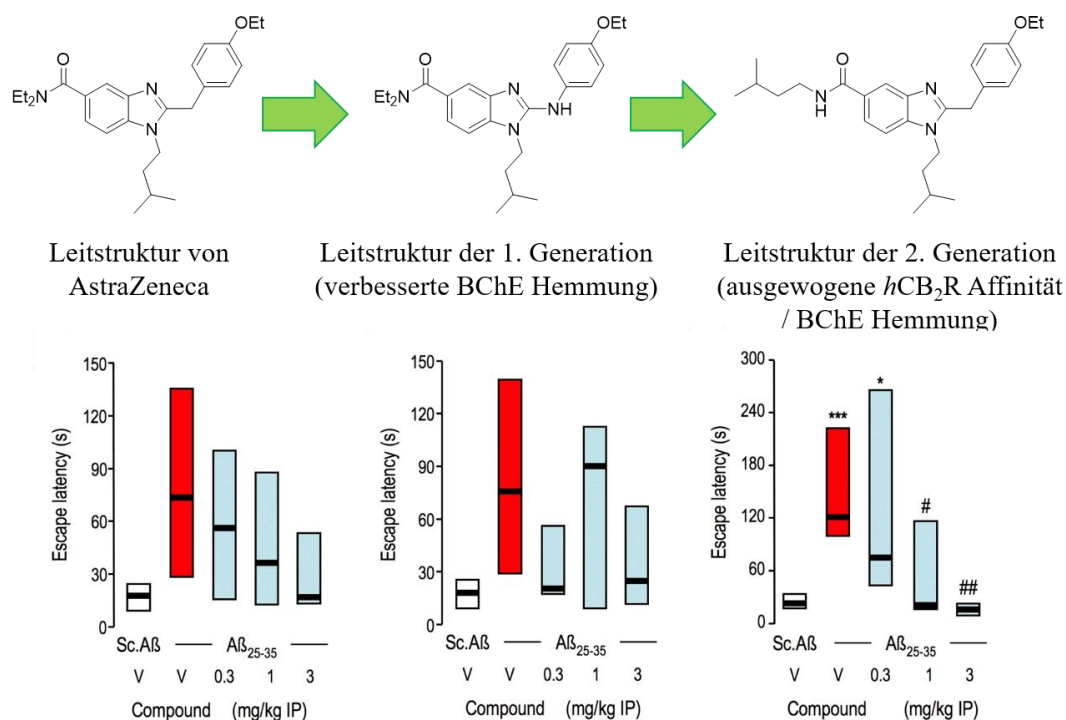


Abb. 7.1. Entwicklung von dual-aktiven *hCB₂R* Agonisten / BChE Hemmern und ihr daraus resultierendes verbessertes *in vivo* Profil (beispielhaft dargestellt durch die Ergebnisse des *passive avoidance tests*⁵⁹).

Ein Set von 30 verschiedenen Verbindungen wurde synthetisiert, indem die Erkenntnisse der Struktur-Wirkungsbeziehungen von anderen BChE Hemmern auf einen von AstraZeneca entwickelten selektiven *hCB₂R* Agonisten angewendet wurden. Erste *in vitro* Untersuchungen zeigten eine hohe Selektivität gegenüber *hCB₁R* und AChE auf. Desweiteren verhielten sich alle getesteten Substanzen wie Agonisten. Nachdem ausgewählte Substanzen auf ihre „*off-target*“ Wechselwirkung mit dem *hMOP* Rezeptor untersucht wurden, konnten diese strukturellen Merkmale in nachfolgenden Entwicklungsbemühungen berücksichtigt werden. Die Entwicklung eines *hCB₂R* Homologiemodells (basierend auf einer erst kürzlich veröffentlichten *hCB₁R* Kristallstruktur) lieferte wertvolle Informationen zum Bindemodus und der Wirkweise der Liganden am Rezeptor. Schlussendlich konnte in einer ersten *in vivo* Studie bewiesen werden, dass ausgewählte dual-aktive Substanzen eine positive Auswirkung auf das Gedächtnis und die kognitiven Eigenschaften haben.

Da diese *in vivo* Untersuchungen hauptsächlich die Hemmung der BChE berücksichtigen, wäre es sinnvoll, in zukünftigen Studien den Einfluss der *hCB₂R* Agonisten zu untersuchen. Pharmakokinetik- und Löslichkeitsstudien könnten zudem helfen, das Gesamtbild zu komplettieren.

Im Moment befinden sich auch dual-aktive *hCB₂R* Agonisten / BChE Hemmer in der Entwicklung, die den Hybrid-Ansatz verfolgen. Erste *in vitro* Untersuchungen dazu ergaben vielversprechende Ergebnisse mit einer guten Selektivität gegenüber AChE und einer erhöhten Hemmung der BChE verglichen mit Tacrin.⁷⁸ Es wird Gegenstand zukünftiger *in vitro* und *in vivo* Untersuchungen sein, herauszufinden, ob sich diese Hybride mit Hinblick auf Hepatotoxizität und Blut-Hirnschrankgängigkeit als Wirkstoffe eignen.

Da die Rolle des *hCB₂R* noch nicht komplett erforscht ist, erfreut sich die Entwicklung von sog. „*tool-compounds*“ großen wissenschaftlichen Interesses. Durch die Bestrahlung mit Licht können diese „*tool-compounds*“ (und ihr nachgeschalteter biologischer Effekt) gesteuert werden. Eine genauere Untersuchung von Zeitskalen und Ligandbindung an den Rezeptor wird dadurch ermöglicht.

Ein Set von 5-Azobenzolbenzimidazolen wurde zu diesem Zwecke entwickelt und synthetisiert. In Radioligandbindungsstudien konnte gezeigt werden, dass sich die Affinität gegenüber dem *hCB₂R* durch die Bestrahlung mit UV-Licht erhöhen lässt (**Abb. 7.2**). Diese Eigenschaft macht

die entwickelten Substanzen zu den ersten GPCR-Liganden, die durch Licht aktiviert werden können (nicht umgekehrt wie bei den bisher beschriebenen photochromen GPCR-Liganden).

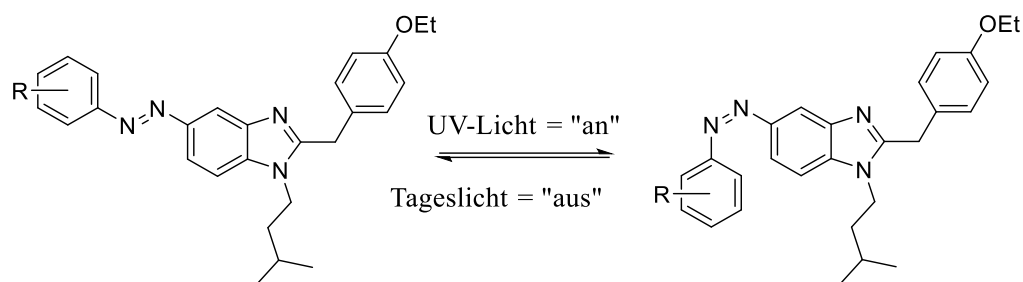


Abb. 7.2. Chemische Struktur der entwickelten 5-Azobenzol Benzimidazole. Die Affinität gegenüber dem hCB_2R kann durch Bestrahlung mit UV-Licht erhöht werden.

Ziel zukünftiger Forschungsbemühungen wird die Steuerung einer bestimmten intrinsischen Aktivität / Effekts durch die Bestrahlung mit Licht sein. Zu diesem Zwecke werden aktuell mehrere Herangehensweisen untersucht: die Einführung eines Azobenzol-Strukturelements an Position 2 des Benzimidazol-Grundgerüsts zeigte in ersten *in vitro* Untersuchungen bereits Unterschiede bei Bestrahlung mit UV-Licht. Eine weitere Herangehensweise ist die Entwicklung von „Photo-Schaltern“ auf Basis von Rimonabant, einem selektiven hCB_1R inversen Agonisten. Hier stehen erste *in vitro* Ergebnisse jedoch noch aus (**Abb. 7.3**).

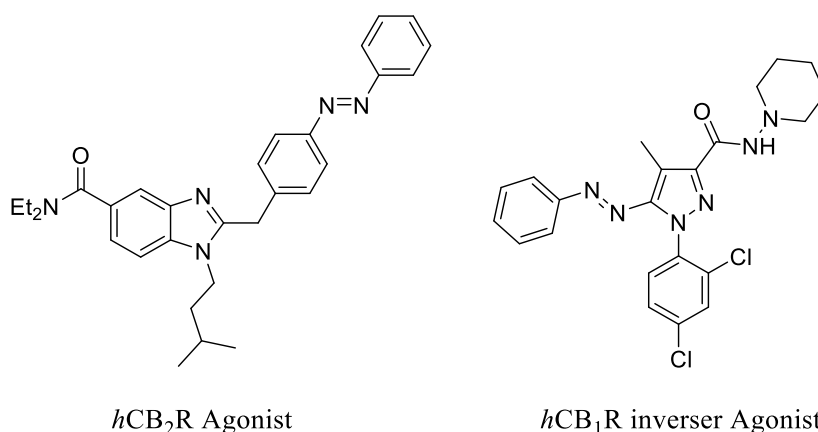


Abb. 7.3. Chemische Strukturen, die als „Efficacy-Schalter“ an zwei verschiedenen Rezeptoren dienen.

9. References

- [1] Maurer, K.; Volk, S.; Gerbaldo, H. Auguste D and Alzheimer's disease. *Lancet* **1997**, *349*, 1546 – 1549.
- [2] Alzheimer, A. Über eine eigenartige Erkrankung der Hirnrinde. *Allgemeine Zeitschrift für Psychiatrie und Psychisch-gerichtliche Medizin* **1907**, *64*, 146 – 148.
- [3] Prince, M.; Comas-Herrera, A.; Knapp, M.; Guerchet, M.; Karagiannidou, M. *World Alzheimer Report 2016; Improving healthcare for people living with dementia; Coverage, quality and costs now and in the future*. Alzheimer's Disease International (ADI): London, 2016.
- [4] Reitz, C.; Mayeux, R. Alzheimer's Disease: Epidemiology, Diagnostic Criteria, Risk Factors and Biomarkers. *Biochem. Pharmacol.* **2014**, *88*, 640 – 651.
- [5] Hammel, P.; Larrey, D.; Bernuau, J.; Kalafat, M.; Fréneaux, E.; Babany, G.; Degott, C.; Feldmann, G.; Pessayre, D.; Benhamou, J.-P. Acute Hepatitis after Tetrahydroaminoacridine Administration for Alzheimer's Disease. *J. Clin. Gastroenterol.* **1990**, *12*, 329 – 331.
- [6] Zemek, F.; Drtinova, L.; Nepovimova, E.; Sepsova, V.; Korabecny, J.; Klimes, J.; Kuca, K. Outcomes of Alzheimer's disease therapy with acetylcholinesterase inhibitors and memantine. *Expert Opin. Drug Saf.* **2014**, *6*, 759 – 774.
- [7] Puzzo, D.; Gulisano, W.; Arancio, O.; Palmeri, A. The Keystone of Alzheimer Pathogenesis might be sought in A β Physiology. *Neuroscience* **2015**, *307*, 26 – 36.
- [8] Hardy, J. A.; Higgins, G. A. Alzheimer's Disease: The Amyloid Cascade Hypothesis. *Science* **1992**, *256*, 184 – 185.
- [9] Hardy, J. A. The Amyloid Hypothesis for Alzheimer's Disease: A Critical Reappraisal. *J. Neurochem.* **2009**, *110*, 1129 – 1134.
- [10] Wyss-Coray, T. Inflammation in Alzheimer's disease: driving force, bystander or beneficial response? *Nat. Med.* **2006**, *12*, 1005 – 1015.
- [11] Perry, V. H.; Nicoll, J. A. R.; Holmes, C. Microglia in neurodegenerative disease. *Nat. Rev. Neurol.* **2010**, *6*, 193 – 201.

- [12] Ballard, C.; Gauthier, S.; Corbett, A.; Brayne, C.; Aarsland, D.; Jones, E. Alzheimer's Disease. *Lancet* **2011**, *377*, 1019 – 1026.
- [13] Ferrer, I. Defining Alzheimer as a common age-related neurodegenerative process not inevitably leading to dementia. *Prog. Neurobiol.* **2012**, *97*, 38 – 51.
- [14] Gaoni, Y.; Mechoulam, R. The isolation and structure of delta-1-tetrahydrocannabinol and other neutral cannabinoids from hashish. *J. Am. Chem. Soc.* **1971**, *93*, 217 – 224.
- [15] Matsuda, L. A.; Lolait, S. J.; Brownstein, M. J.; Young, A. C.; Bonner, T. I. Structure of a cannabinoid receptor and functional expression of the cloned cDNA. *Nature* **1990**, *346*, 561 – 564.
- [16] Howlett, A. C.; Barth, F.; Bonner, T. I.; Cabral, G.; Casellas, P.; Devane, W. A.; Felder, C. C.; Herkenham, M.; Mackie, K.; Martin, B. R.; Mechoulam, R.; Pertwee, R. G. International Union of Pharmacology. XXVII. Classification of cannabinoid receptors. *Pharmacol. Rev.* **2002**, *54*, 161 – 202.
- [17] Pertwee, R. G.; Holwett, A. C.; Abood, M. E.; Alexander, S. P. H.; di Marzo, V.; Elphick, M. R.; Greasley, P. J.; Hansen, H. S.; Kunos, G.; Mackie, K.; Mechoulam, R.; Ross, R. A. International Union of Basic and Clinical Pharmacology. LXXIX. Cannabinoid receptors and their ligands: beyond CB₁ and CB₂. *Pharmacol. Rev.* **2010**, *62*, 588 – 631.
- [18] Núñez, E.; Benito, C.; Pazos, M. R.; Barbachano, A.; Fajardo, O.; González, S.; Tolón R. M.; Romero, J. Cannabinoid CB₂ receptors are expressed by perivascular microglial cells in the human brain: an immunohistochemical study. *Synapse* **2004**, *53*, 208 – 213.
- [19] Lange, J. H. M.; Kruse, C. G. Medicinal chemistry strategies to CB₁ cannabinoid receptor antagonists. *Drug Discov. Today* **2005**, *10*, 693 – 702.
- [20] Benito, C.; Tolón, R. M.; Pazos, M. R.; Núñez, E.; Castillo, A. I.; Romero, J. Cannabinoid CB₂ receptors in human brain inflammation. *Br. J. Pharmacol.* **2008**, *153*, 277 – 285.
- [21] Gómez-Gálvez, Y.; Palomo-Garo, C.; Fernández-Ruiz, J.; García, C. Potential of the cannabinoid CB₂ receptor as a pharmacological target against inflammation in Parkinson's disease. *Prog. Neuro-Psychopharmacol. Biol. Psychiatry* **2015**, *64*, 200 – 208.
- [22] Grünblatt, E.; Zander, N.; Bartl, J.; Jie, L.; Monoranu, C. M.; Arzberger, T.; Ravid, R.; Roggendorf, W.; Gerlach, M.; Riederer, P. Comparison analysis of gene expression patterns between sporadic Alzheimer's and Parkinson's disease. *J. Alzheimer Dis.* **2007**, *12*, 291 – 311.

- [23] Kho, D. T.; Glass, M.; Graham, E. S. Is the Cannabinoid CB2 Receptor a Major Regulator of the Neuroinflammatory Axis of the Neurovascular Unit in Humans? In *Cannabinoid Pharmacology*; Kendall, D.; Alexander, S. P. H., Eds.; Elsevier: Cambridge, 2017; Vol. 8, pp. 367 -396.
- [24] Solas, M.; Francis, P. T.; Franco, R.; Ramirez, M. J. CB2 receptor and amyloid pathology in frontal cortex of Alzheimer's disease patients. *Neurobiol. Aging* **2013**, *34*, 805 – 808.
- [25] Fakhfouri, G.; Ahmadiani, A.; Rahimian, R.; Grolla, A. A.; Moradi, F.; Haeri, A. WIN55212-2 attenuates amyloid-beta-induced neuroinflammation in rats through activation of cannabinoid receptors and PPAR- γ pathway. *Neuropharmacology* **2012**, *63*, 653 – 666.
- [26] Janefjord, E.; Maag, J. L.; Harvey, B. S.; Smid, S. D. Cannabinoid effects on beta amyloid fibril and aggregate formation, neuronal and microglial-activated neurotoxicity in vitro. *Cell. Mol. Neurobiol.* **2014**, *34*, 31 – 42.
- [27] Wu, J.; Bie, B.; Yang, H.; Xu, J. J.; Brown, D. L.; Naguib, M. Activation of the CB₂ receptor system reverses amyloid-induced memory deficiency. *Neurobiol. Aging* **2013**, *34*, 791 – 804.
- [28] Martin-Moreno, A. M.; Brera, B.; Spuch, C.; Carro, E.; Garcia-Garcia, L.; Delgado, M.; Pozo, M. A.; Innamorato, N. G.; Cuadrado, A.; de Ceballos, M. L. Prolonged oral cannabinoid administration prevents neuroinflammation, lower β -amyloid levels and improves cognitive performance in Tg APP 2576 mice. *J. Neuroinflammation* **2012**, *9*, 8 – 12.
- [29] Bisogno, T.; Oddi, S.; Piccoli, A.; Fazio, D.; Maccarone, M. Type-2 cannabinoid receptors in neurodegeneration. *Pharmacol. Res.* **2016**, *111*, 721 – 730.
- [30] Ramer, R.; Hinz, B. Cannabinoids as Anticancer Drugs. In *Cannabinoid Pharmacology*; Kendall, D.; Alexander, S. P. H., Eds.; Elsevier: Cambridge, 2017; Vol. 8, pp. 397 – 436.
- [31] Starowicz, K.; Finn, D. P. Cannabinoids and Pain: Sites and Mechanisms of Action. In *Cannabinoid Pharmacology*; Kendall, D.; Alexander, S. P. H., Eds.; Elsevier: Cambridge, 2017; Vol. 8, pp. 437 – 475.
- [32] Davies, P.; Maloney, A. J. F. Selective loss of central cholinergic neurons in Alzheimer's disease. *Lancet* **1976**, *2*, 1403.
- [33] Bartus, R. T.; Dean, R. L.; Beer, B.; Lippa, A. S. The cholinergic hypothesis of geriatric memory dysfunction. *Science* **1982**, *217*, 408 – 417.

- [34] Giacobini, E. Cholinergic function and Alzheimer's disease. *Int. J. Geriatr. Psychiatry* **2003**, *18*, 1 – 5.
- [35] Darvesh, S.; Hopkins, D. A.; Geula, C. Neurobiology of butyrylcholinesterase. *Nat. Rev. Neurosci.* **2003**, *4*, 131 – 138.
- [36] Nordberg, A.; Ballard, C.; Bullock, R.; Darreh-Shori, T.; Somogyi, M. A. Review of butyrylcholinesterase as a therapeutic target in the treatment of Alzheimer's disease. *Prim. Care Companion CNS Discord.* **2013**, *15*, 2.
- [37] Macdonald, I. R.; Rockwood, K.; Martin, E.; Darvesh, S. Cholinesterase inhibition in Alzheimer's disease: is specificity the answer? *J. Alzheimer Dis.* **2014**, *42*, 379 – 384.
- [38] Mesulam, M. M.; Geula, C. Butyrylcholinesterase reactivity differentiates the amyloid plaques of aging from those of dementia. *Ann. Neurol.* **1994**, *36*, 722 – 727.
- [39] Guillozet, A. L.; Smiley, J. F.; Mash, D. C.; Mesulam, M. M. Butyrylcholinesterase in the life cycle of amyloid plaques. *Ann. Neurol.* **1997**, *42*, 909 – 918.
- [40] Maurice, T.; Strehaiano, M.; Siméon, N.; Bertrand, C.; Chatonnet, A. Learning performances and vulnerability to amyloid toxicity in the butyrylcholinesterase knockout mouse. *Behav. Brain Res.* **2016**, *296*, 351 – 360.
- [41] Kosak, U.; Brus, B.; Knez, D.; Sink, R.; Zakelj, S.; Trontelj, J.; Pisljar, A.; Slenc, J.; Gobec, M.; Zivin, M.; Tratnjek, L.; Perse, M.; Salat, K.; Podkova, A.; Filipek, B.; Nachon, F.; Brazzolotto, X.; Wieckowska, A.; Malawska, B.; Stojan, J.; Mlinaric Rascan, I.; Kos, J.; Coquelle, N.; Colletier, J.-P.; Gobec, S. Development of an *in vivo* active reversible butyrylcholinesterase inhibitor. *Sci. Rep.* **2016**, *6*, 39495 – 39510.
- [42] Wright, C. I.; Geula, C.; Mesulam, M. M. Neurological cholinesterases in the normal brain and in Alzheimer's disease: relationship to plaques, tangles, and patterns of selective vulnerability. *Ann. Neurol.* **1993**, *34*, 373 – 384.
- [43] Dolles, D.; Decker, M. Dual-Acting Compounds acting as Receptor Ligands and Enzyme Inhibitors. In *Design of Hybrid Molecules for Drug Development*; Decker, M., Ed.; Elsevier: Oxford, 2017; pp 137 – 165.
- [44] Morphy, R.; Rankovic, Z. Designed multiple ligands. An emerging drug discovery paradigm. *J. Med. Chem.* **2005**, *48*, 6523 – 6543.

- [45] Lipinski, C. A.; Lombardo, F.; Dominy, B. W.; Feeney, P. J. Experimental and computational approaches to estimate solubility and permeability in drug discovery and development settings. *Adv. Drug Deliv. Rev.* **1997**, *23*, 3 – 25.
- [46] Montanari, S.; Scalvini, L.; Bartolini, M.; Belluti, F.; Gobbi, S.; Andrisano, V.; Ligresti, A.; Di Marzo, V.; Rivara, S.; Mor, M.; Bisi, A.; Rampa, A. Fatty Acid Amide Hydrolase (FAAH), Acetylcholinesterase (AChE), and Butyrylcholinesterase (BChE): Networked Targets for the Development of Carbamates as Potential Anti-Alzheimer Disease Agents. *J. Med. Chem.* **2016**, *59*, 6387 – 6406.
- [47] Nimczick, M.; Decker, M. New Approaches in the Design and Development of Cannabinoid Receptor Ligands: Multifunctional and Bivalent Compounds. *ChemMedChem* **2015**, *10*, 773 – 786.
- [48] Renton, P.; Green, B.; Maddaford, S.; Rakhit, S.; Andrews, J. S. NOpiates: Novel Dual Action Neuronal Nitric Oxide Synthase Inhibitors with μ -Opioid Agonist Activity. *ACS Med. Chem. Lett.* **2012**, *3*, 227 – 231.
- [49] Stöbel, A.; Schlenk, M.; Hinz, S.; Küppers, P.; Heer, J.; Gütschow, M.; Müller, C. E. Dual Targeting of Adenosine A_{2A} Receptors and Monoamine Oxidase B by 4*H*-3,1-Benzothiazin-4-ones. *J. Med. Chem.* **2013**, *56*, 4580 – 4596.
- [50] Darras, F. H.; Pockes, S.; Huang, G.; Wehle, S.; Strasser, A.; Wittmann, H.-J.; Nimczick, M.; Sotriffer, C. A.; Decker, M. Synthesis, Biological Evaluation, and Computational Studies of Tri- and Tetracyclic Nitrogen-Bridgehead Compounds as Potent Dual-Acting AChE Inhibitors and hH₃ Receptor Antagonists. *ACS Chem. Neurosci.* **2014**, *5*, 225 – 242.
- [51] Dolles, D.; Nimczick, M.; Scheiner, M.; Ramler, J.; Stadtmüller, P.; Sawatzky, E.; Drakopoulos, A.; Sotriffer, C.; Wittmann, H.-J.; Strasser, A.; Decker, M. Aminobenzimidazoles and Structural Isomers as Templates for Dual-Acting Butyrylcholinesterase Inhibitors and hCB₂R Ligands to Combat Neurodegenerative Disorders. *ChemMedChem* **2016**, *11*, 1270 – 1283.
- [52] Pagé, D.; Balaux, E.; Boisvert, L.; Liu, Z.; Milburn, C.; Tremblay, M.; Wei, Z.; Woo, S.; Luo, X.; Cheng, Y.-X.; Yang, H.; Srivastava, S.; Zhou, F.; Brown, W.; Tomaszewski, M.; Walpole, C.; Hodzic, L.; St-Onge, S.; Godbout, C.; Salois, D.; Payza, K. Novel benzimidazole derivatives as selective CB₂ agonists. *Bioorg. Med. Chem.* **2008**, *18*, 3695 – 3700.

- [53] González-Naranjo, P.; Pérez-Macias, N.; Campillo, N. E.; Pérez, C.; Arán, V. J.; Girón, R.; Sánchez-Robles, E.; Martín, M. I.; Gómez-Canas, M.; García-Arencibia, M.; Fernández-Ruiz, J.; Páez, J. A. Cannabinoid agonists showing BuChE inhibition as potential therapeutic agents for Alzheimer's disease. *Eur. J. Med. Chem.* **2014**, *73*, 56 – 72.
- [54] Scheiner, M. Synthese von 2-Aminobenzimidazolen zur Aufstellung von Struktur-Wirkungsbeziehungen für dual aktive CB₂R-Liganden / BChE Inhibitoren. Bachelor Thesis, Julius Maximilian University Würzburg, 2015.
- [55] Ramler, J. Synthese von heterozyklischen GPCR-Liganden mit enzyminhibierender Wirkung. Bachelor Thesis, Julius Maximilian University Würzburg, 2015.
- [56] Dolles, D. Design und Synthese von dual-aktiven Butyrylcholinesterase-Hemmern und CB₂-Rezeptor Agonisten. Master Thesis, Julius Maximilian University Würzburg, 2014.
- [57] Burke, M. J.; Trantow, B. M. An efficient route to 3-aminoindazoles and 3-amino-7-azaindazoles. *Tetrahedron Lett.* **2008**, *49*, 4579 – 4581.
- [58] Lohou, E.; Collot, V.; Stiebing, S.; Rault, S. Direct access to 3-aminoindazoles by Buchwald-Hartwig C-N coupling reaction. *Synthesis* **2011**, *16*, 2651–2663.
- [59] Dolles, D.; Hoffmann, M.; Gunesch, S.; Marinelli, O.; Möller, J.; Santoni, G.; Chatonnet, A.; Lohse, M. J.; Wittmann, H.-J.; Strasser, A.; Nabissi, M.; Maurice, T.; Decker, M. Structure-Activity Relationships and Computational Investigations into the Development of Potent and Balanced Dual-Acting Butyrylcholinesterase Inhibitors and Human Cannabinoid Receptor 2 Ligands with Pro-Cognitive *in vivo* Profiles. *J. Med. Chem.* **2018**, *61*, 1646 – 1663.
- [60] Kraus, J. Synthese von N1-funktionalisierten Benzimidazolen als dual-aktive Wirkstoffe. Bachelor Thesis, Julius Maximilian University Würzburg, 2016.
- [61] Freitag, M.; Schemies, J.; Larsen, T.; El Gaghlab, K.; Schulz, F.; Rumpf, T.; Jung, M.; Link, A. Synthesis and biological activity of splitomicin analogs targeted at human NAD⁺-dependent histone deacetylases (sirtuins). *Bioorg. Med. Chem.* **2011**, *19*, 3669 – 3677.
- [62] Williams, C. cAMP detection methods in HTS: selecting the best from the rest. *Nat. Rev. Drug Discov.* **2004**, *3*, 125 – 135.
- [63] Zheng, Y.; Wang, Q.; Li, T.; Qian, J.; Lu, Y.; Li, Y.; Bi, E.; Reu, F.; Qin, Y.; Drazba, J.; Hsi, E.; Yang, J.; Cai, Z.; Yi, Q. Role of Myeloma-Derived MIF in Myeloma Cell Adhesion to

Bone Marrow and Chemotherapy Response. *J. Natl. Cancer Inst.* **2016**, *108*, DOI: 10.1093/jnci/djw131.

[64] Waeber, G.; Thompson, N.; Chautard, T.; Steinmann, M.; Nicod, P.; Pralong, F. P.; Calandra, T.; Gaillard, R. C. Transcriptional activation of the macrophage migration-inhibitory factor gene by the corticotropin-releasing factor is mediated by the cyclic adenosine 3',5'-monophosphate responsive element-binding protein CREB in pituitary cells. *Mol. Endocrinol.* **1998**, *12*, 698 – 705.

[65] Alas, S.; Bonavida, B. Inhibition of constitutive STAT3 activity sensitizes resistant non-Hodgkin's lymphoma and multiple myeloma to chemotherapeutic drug-mediated apoptosis. *Clin. Cancer Res.* **2003**, *9*, 316 – 326.

[66] Kato, K.; Nomoto, M.; Izumi, H.; Ise, T.; Nakano, S.; Niho, Y.; Kohno, K. Structure and functional analysis of the human STAT3 gene promoter: alteration of chromatin structure as a possible mechanism for the upregulation in cisplatin-resistant cells. *Biochim. Biophys. Acta* **2000**, *1493*, 91 – 100.

[67] Hunger, A.; Keberle, J.; Rossi, A.; Hoffmann, K. Benzimidazol-Derivate und verwandte Heterocyclen III. Synthese von 1-Aminoalkyl-2-benzyl-nitro-benzimidazolen. *Helv. Chim. Acta* **1960**, *43*, 1032 – 1046.

[68] Hua, T.; Vemuri, K.; Nikas, S. P.; Laprairie, R. B.; Wu, Y.; Qu, L.; Pu, M.; Korde, A.; Jiang, S.; Ho, J. H.; Han, G. W.; Ding, K.; Li, X.; Liu, H.; Hanson, M. A.; Zhao, S.; Bohn, L. M.; Makriyannis, A.; Stevens, R. C.; Liu, Z. J. Crystal structures of agonist-bound human cannabinoid receptor CB₁. *Nature* **2017**, *547*, 468 – 471.

[69] Dolles, D.; Strasser, A.; Wittmann, H.-J.; Marinelli, O.; Nabissi, M.; Pertwee, R. G.; Decker, M. The First Photochromic Affinity Switch for the Human Cannabinoid Receptor 2. *Adv. Therap.* **2018**, DOI: 10.1002/adtp.201700032.

[70] Aso, E.; Ferrer, I. Cannabinoids for treatment of Alzheimer's disease: moving toward the clinic. *Front. Pharmacol.* **2014**, *5*, 37.

[71] Velema, W. A.; Szymanski, V.; Feringa, B. L. Photopharmacology: Beyond Proof of Principle. *J. Am. Chem. Soc.* **2014**, *136*, 2178 – 2191.

[72] Agnetta, L.; Decker, M. Photoresponsive Hybrid Compounds. In *Design of Hybrid Molecules for Drug Development*; Decker, M., Ed.; Elsevier: Oxford, 2017; pp 279 – 316.

- [73] Broichhagen, J.; Frank, J. A.; Trauner, D. A Roadmap to Success in Photopharmacology. *Acc. Chem. Res.* **2015**, *48*, 1947 – 1960.
- [74] Agnetta, L.; Kauk, M.; Canizal, M. C. A.; Messerer, R.; Holzgrabe, U.; Hoffmann, C.; Decker, M. A Photoswitchable Dualsteric Ligand Controlling Receptor Efficacy. *Angew. Chem. Int. Ed.* **2017**, *56*, 7282 – 7287; *Angew. Chem.* **2017**, *129*, 7388 – 7393.
- [75] Westphal, M. V.; Schafroth, M. A.; Sarott, R. C.; Imhoff, M. A.; Bold, C. P.; Leippe, P.; Dhopeswar A.; Grandner, J. M.; Katritch, V.; Mackie, K.; Trauner, D.; Carreira, E. M.; Frank, J. A. Synthesis of Photoswitchable Δ^9 -Tetrahydrocannabinol Derivatives Enables Optical Control of Cannabinoid Receptor 1 Signaling. *J. Am. Chem. Soc.* **2017**, *139*, 18206 – 18212.
- [76] Mills, C. XCIII. – Some New Azo-compounds. *J. Chem. Soc. Trans.* **1895**, *67*, 925 – 933.
- [77] Schönberger, M.; Trauner, D. A Photochromic Agonist for μ -Opioid Receptors. *Angew. Chem. Int. Ed.* **2014**, *53*, 3264 – 3267.
- [78] Scheiner, M. Synthese und biologische Charakterisierung von dual-aktiven CB₂-Liganden mit Cholinesterase-inhibierender Wirkung. Master Thesis, University of Bayreuth, 2017.

10. Abbreviations

A β	-	amyloid β
Abs.	-	absorbance
ACh	-	acetylcholine
AChE	-	acetylcholinesterase
AcOH	-	acetic acid
AD	-	Alzheimer's disease
ANOVA	-	analysis of variance
APP	-	amyloid precursor protein
BChE	-	butyrylcholinesterase
Boc ₂ O	-	di- <i>tert</i> -butyl dicarbonate
cAMP	-	cyclic adenosine monophosphate
CHO	-	Chinese hamster ovary
CNS	-	central nervous system
Cpd.	-	compound
CRE	-	cAMP response element
CREB	-	cAMP response element binding protein
DMAP	-	4-dimethylaminopyridine
DMF	-	dimethylformamide
DMSO	-	dimethylsulfoxide
<i>ee</i>	-	electric eel
EDCI	-	1-Ethyl-3-(3-dimethylaminopropyl)carbodiimide
<i>eq</i>	-	equine
EtOH	-	ethanol
FAAH	-	fatty acid amide hydrolase
Forsk.	-	forskolin
GAPDH	-	Glyceraldehyde 3-phosphate dehydrogenase
GPCR	-	G-protein coupled receptor

Abbreviations

<i>h</i>	-	human
HBTU	-	2-(1 <i>H</i> -benzotriazol-1-yl)-1,1,3,3-tetramethyluronium (PF ₆ ⁻)
<i>hCB</i> _{1/2} R	-	human cannabinoid receptor subtype 1/2
HEK	-	human embryonic kidney
<i>i.c.v.</i>	-	intracerebroventricular
<i>i.p.</i>	-	intraperitoneal
MD	-	molecular dynamics
MIF	-	macrophage migration inhibitory factor
MOP	-	μ-opioid
<i>o.d.</i>	-	oculus dextrus
qRT-PCR	-	quantitative reverse transcription polymerase chain reaction
rt.	-	room temperature
SAR	-	structure-activity relationship
Sc.Aβ	-	scrambled amyloid β
SD.	-	standard deviation
S _N 2	-	nucleophilic substitution
S _N Ar	-	nucleophilic aromatic substitution
STAT	-	signal transducer and activator of transcription
THF	-	tetrahydrofuran
V / VEI	-	vehicle

11. Appendix

Appendix I:

- Dolles, D.; Decker, M. Dual-Acting Compounds acting as Receptor Ligands and Enzyme Inhibitors. In *Design of Hybrid Molecules for Drug Development*; Decker, M., Ed.; Elsevier: Oxford, 2017; pp 137 – 165.

Appendix II:

- Dolles, D.; Nimczick, M.; Scheiner, M.; Ramler, J.; Stadtmüller, P.; Sawatzky, E.; Drakopoulos, A.; Sotriffer, C.; Wittmann, H.-J.; Strasser, A.; Decker, M. Aminobenzimidazoles and Structural Isomers as Templates for Dual-Acting Butyrylcholinesterase Inhibitors and *h*CB₂R Ligands to Combat Neurodegenerative Disorders. *ChemMedChem* **2016**, *11*, 1270 – 1283.
- Supporting Information

Appendix III:

- Dolles, D.; Hoffmann, M.; Gunesch, S.; Marinelli, O.; Möller, J.; Santoni, G.; Chatonnet, A.; Lohse, M. J.; Wittmann, H.-J.; Strasser, A.; Nabissi, M.; Maurice, T.; Decker, M. Structure-Activity Relationships and Computational Investigations into the Development of Potent and Balanced Dual-Acting Butyrylcholinesterase Inhibitors and Human Cannabinoid Receptor 2 Ligands with Pro-Cognitive *in vivo* Profiles. *J. Med. Chem.* **2018**, *61*, 1646 – 1663.
- Supporting Information

Appendix IV:

- Dolles, D.; Strasser, A.; Wittmann, H.-J.; Marinelli, O.; Nabissi, M.; Pertwee, R. G.; Decker, M. The First Photochromic Affinity Switch for the Human Cannabinoid Receptor 2. *Adv. Therap.* **2018**, DOI: 10.1002/adtp.201700032.
- Supporting Information

Appendix I

Dolles, D.; Decker, M. Dual-acting compounds acting as receptor ligands and enzyme inhibitors. In *Design of Hybrid Molecules for Drug Development*; Decker, M.; Ed.; Elsevier: Oxford, 2017; pp. 137 – 165.

Copyright (2018), with permission from Elsevier.

<https://www.sciencedirect.com/science/article/pii/B9780081010112000052>

Dual-Acting Compounds Acting as Receptor Ligands and Enzyme Inhibitors

Dominik Dolles, Michael Decker

JULIUS MAXIMILIAN UNIVERSITY OF WÜRZBURG, WÜRZBURG, GERMANY

5.1 Introduction

Everyone knows the Swiss Army knife. It's not only a simple knife, but also a helpful tool. It can additionally be equipped with screwdrivers, saws, etc., and thereby adjusted to the user's needs. This makes it an excellent example of multifunctionality. A drug with the same multifunctional profile, that can specifically address different targets, would also be a powerful tool against various diseases, especially multifactorial ones.

In the literature, there are two main types of multifunctional compounds:^{1–3} hybrids and merged ligands (often referred to as “chimeric” or “fused”). Hybrid molecules combine two active compounds with a linker (i.e., chemically only marginally altered). Merged ligands combine pharmacophores into one (small) molecule. Pharmacophores are structural chemical features of a biologically active molecule that are responsible for addressing a certain biological target (Fig. 5-1).

Both types have their own specific advantages and disadvantages. An obvious benefit of hybrid molecules is their simplicity. A molecule that already shows activity at a target is very likely to show this same activity when it's combined with another entity over a linker. The disadvantages of such hybrids connected over a molecular spacer are the high, which therefore makes these molecules often not stick to Lipinski's rule of five. Merged ligands overcome this problem by using only the relevant pharmacophores. Unnecessary parts are omitted. However, their disadvantage is the difficulty of fusing pharmacophores into one ligand, while not losing activity at one of the two targets. There's only a small scope where the activity at both targets is balanced and maintained (as discussed below).

A good example of a hybrid molecule is the CB₁R inverse agonist and acetylcholinesterase (AChE) inhibitor **3** (Fig. 5-2A), which both contain the 1,2-diarylimidazole-based CB₁R inverse agonist **1** and tacrine **2** largely unaltered. Both entities show activity on their own and are still active when they are linked over a butylene spacer.⁴

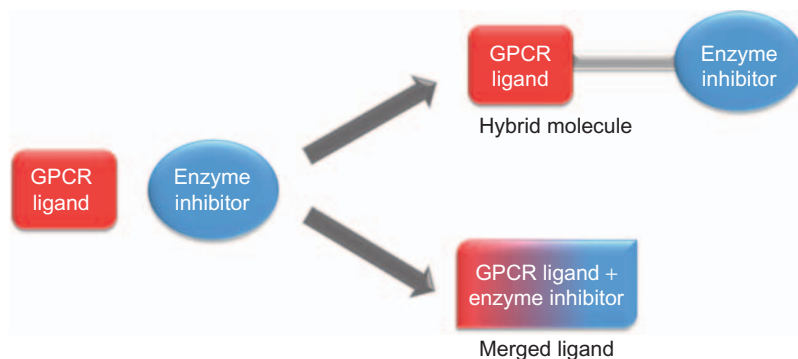


FIGURE 5-1 Schematic concept of a hybrid molecule and a merged ligand.

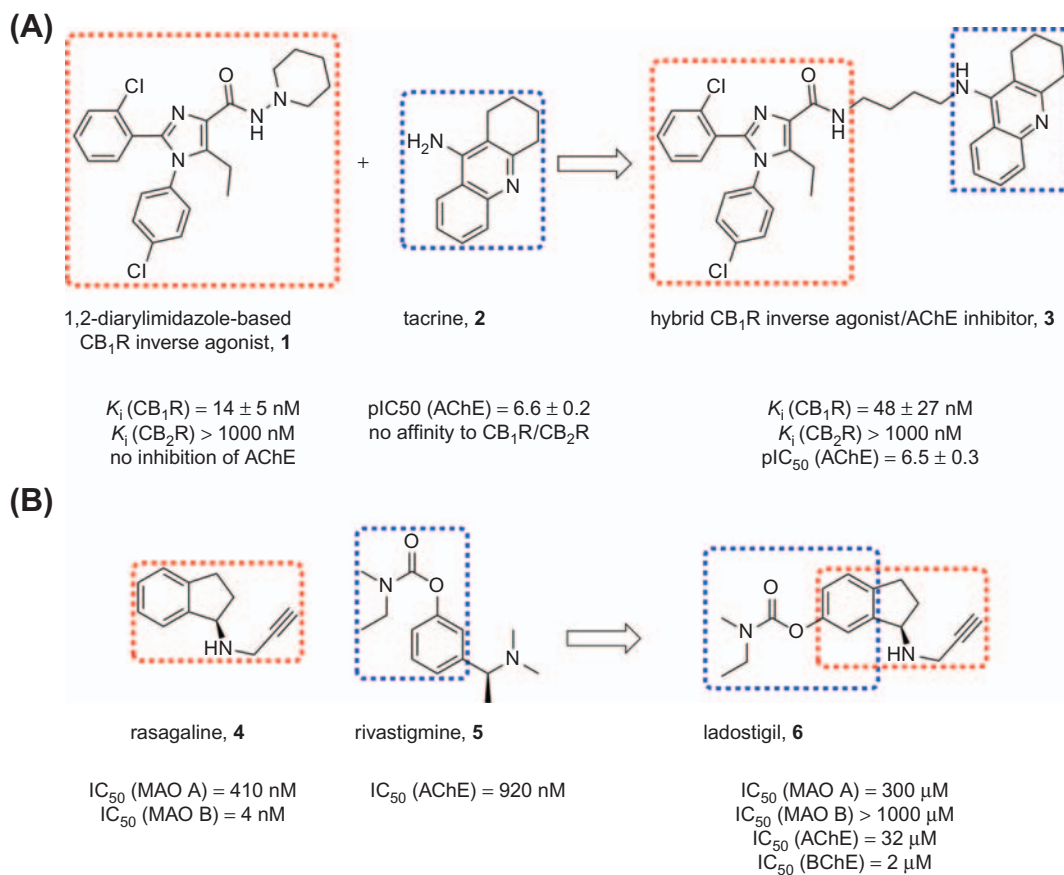


FIGURE 5-2 Examples of multitarget drugs: (A) hybrid CB₁R inverse agonist and AChE inhibitor **3** derived from CB₁R inverse agonist **1** and tacrine **2**⁴; (B) ladostigil **6**, an AChE/BChE and MAO A inhibitor merged from rasagaline **4** and rivastigmine **5**⁵.

An illustrative example of a merged molecule is ladostigil **6**, a reversible AChE and butyrylcholinesterase (BChE) and irreversible monoamine oxidase A (MAO A) inhibitor (Fig. 5-2B). The structure derives from rasagaline **4**, a MAO A/B inhibitor, and rivastigmine **5**, an irreversible AChE inhibitor. Here, only the needed pharmacophores were adopted, resulting in a (small) molecule with both modes of action. Ladostigil **6** was developed by Avraham Pharma and is currently in clinical trials.⁵

Returning to our Swiss Army knife example, we can see that the development of a multitarget drug is not simple; in fact, it bears many questions and problems. In this chapter, the difficulties with regard to the design and development of such compounds and selected examples from state-of-the-art literature are presented.

5.2 Challenges

Promising targets are G-protein coupled receptors (GPCRs). All GPCRs are composed of seven transmembrane α -helices that are embedded into the cell membrane. The whole family of GPCRs contains more than 1000 members that are involved in almost every function of an organ system. This fact makes them important therapeutic targets for central nervous system (CNS) disorders, pain treatment, or cardiac dysfunction.^{6–8} In addition to GPCRs, enzymes are highly attractive drug targets as well. Enzymes are essential for every organism and catalyze biochemical reactions. Due to their obvious relevance, it seems highly desirable to combine chemical features or the structures of a GPCR ligand and an enzyme inhibitor. With this combination a novel drug molecule can be realized by addressing two very distinct protein structures. In a later part of this chapter insight into the variety of combinations of GPCR ligands and enzyme inhibitors will be given.

The main advantage of dual-active compounds is also its main challenge: addressing two different targets. This challenge can be depicted as a pair of scales. If the activity/affinity is increased at one target, it's very likely to lose it at the other target. The challenge is to increase the activity/affinity at both targets by identifying a common chemical space for compound optimization, but to keep it balanced. The latter means that the concentration ranges in which the targets are addressed are in a similar range and/or in the physiologically relevant one.

When it comes to the development of a multitarget compound there are three stages: lead generation (“lead phase”), optimization, and biological evaluation. In most cases, lead generation is determined by a knowledge-based approach that relies on existing data about one or more established experimental therapeutics with a promising biological profile and/or well-known structure-activity relationship study (SAR) on the selected target.

Later, the optimization/synthesis phase is aimed at adjusting the activity/affinity ratio of the involved targets and at improving the pharmacological parameters. To improve the biological properties of the lead compound and to establish a multitarget mode of action, its structure is synthetically altered and a compound library, which is a set of derivatives, is produced. These derivatives are then pharmacologically evaluated by suitable biological

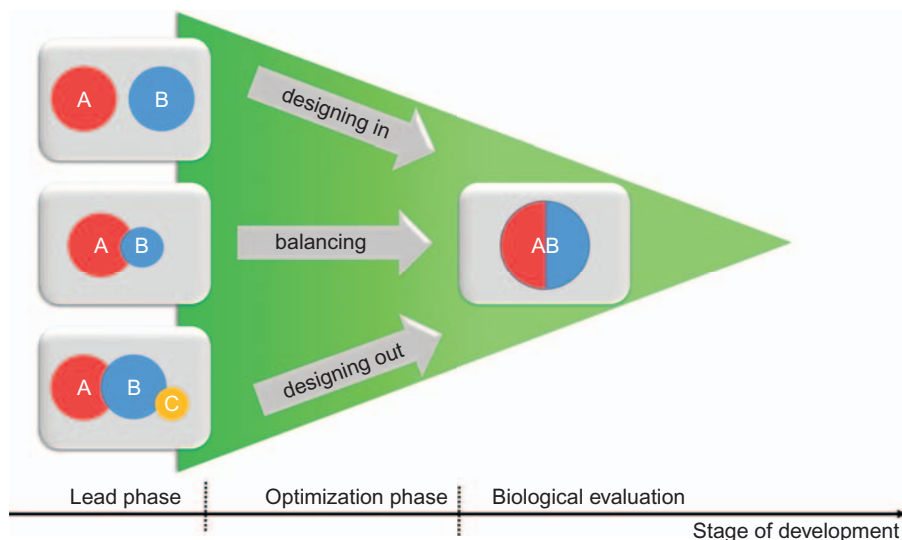


FIGURE 5-3 Schematic overview of the development of a multitarget compound.

evaluation systems. In a laborious process, SAR studies at both targets have to be conducted. In the literature three general possibilities are described concerning how the lead generation can be modified and optimized (Fig. 5-3): if the lead generation provides two known compounds, A and B, which are highly selective and active each at one target, the structural elements of the two ligands are combined (“designing in”); if the selected lead generation AB shows good activity/affinity at one target, but weak at the second target, the aim is to balance both activities/affinities (“balancing”); in the third scenario the lead generation AB has already moderate activity/affinity at the two desired targets, but also has undesirable activity at a third target C, thus the aim is to minimize or even to disable this activity (“designing out”).¹ If there’s a compound with an improved profile either due to increased or better balanced activity/affinity, the second-generation lead structure is obtained. To further improve a compound’s biological properties, the above steps are repeated.

The result of these SAR studies should ideally lead to a compound with well-established pharmacophores and well-balanced activities/affinities with an optimized selectivity profile at the desired targets.

5.3 Approaches and Examples

Since multifactorial diseases like neurodegenerative ones can and should be effectively addressed at diverse targets such as GPCRs and enzymes, and additionally by counteracting oxidative stress (see Chapter 2), quite a plethora of combinations of targets for multitarget compounds can be chosen. To yield effective compounds and choose targets that hold

realistic potential for successful compound development, careful selection of targets, identification of leads, and compound design are of utmost importance. In this section, several examples from recent literature, with regard to design and development of such merged GPCR ligands/enzyme inhibitors, are presented.

5.4 Multifunctional Ligands for the Treatment of Pain

Activating the opioid GPCRs by agonists was and still is the state-of-the-art target when it comes to the treatment of severe pain issues. There are four main subtypes that belong to the opioid receptor family: the μ -, κ -, δ -, and ϵ -receptor. The functions all of these subtypes are still not completely known.⁹ For the treatment of pain, addressing of the μ -opioid receptor (MOP) is necessary. Classical commercially available drugs such as morphine **7**, fentanyl **8**, or tramadol **9**, act as MOP agonists (Fig. 5-4).

On the one hand, MOP agonists are successfully used for pain treatment, but on the other hand they also show unwanted side effects including addiction, respiratory depression, development of tolerance, etc. There's still continued interest in opiates, especially to reduce their side effects as much as possible. A possible approach is the development of drugs using multiple mechanisms of action. These compounds might show improved efficacy and reduced side effects.

Another promising target for pain treatment is nitric oxide synthase (NOS). Several studies showed amelioration of neuropathic pain in animal models by inhibition of NOS. In the body, nitric oxide is produced from *L*-arginine and regulates neurotransmission, blood pressure, and inflammatory responses. It is synthesized by three isoforms: neuronal NOS (nNOS), endothelial NOS (eNOS), and inducible NOS (iNOS). Among these isoforms, nNOS is found to play an important role in the modulation of opioid analgesia and tolerance.^{10,11}

In 2012, Renton et al.¹² were the first to focus on the development of a dual-active MOP agonist and nNOS inhibitor. As lead structures etonitazene **10**, a MOP agonist¹³ ($K_i = 0.2$ nM), and a set of indole-based NOS inhibitors **11**¹⁴ were selected. A brief look at the designated lead structures shows the similarities and the overlap of the two pharmacophoric structures (Fig. 5-5).

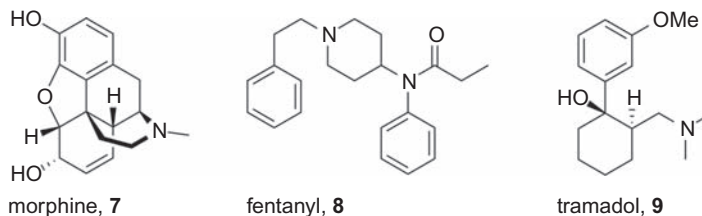


FIGURE 5-4 Therapeutically applied MOP agonist morphine **7**, fentanyl **8**, and tramadol **9**.

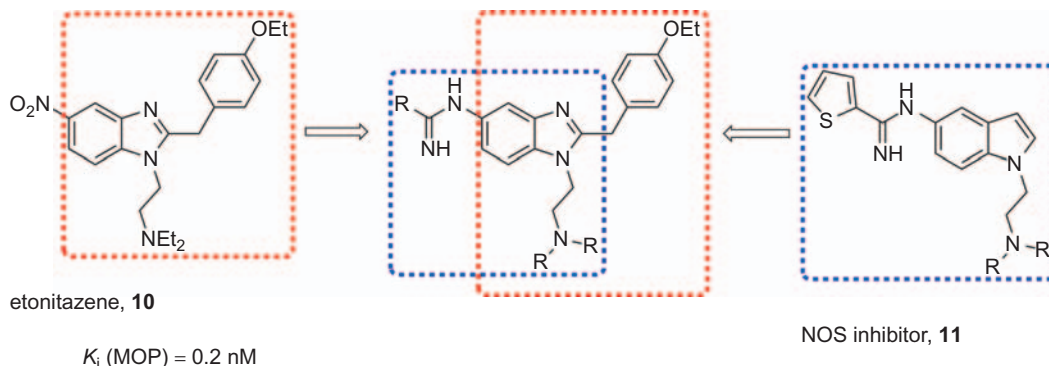


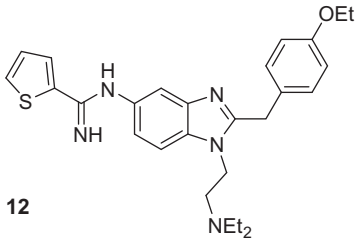
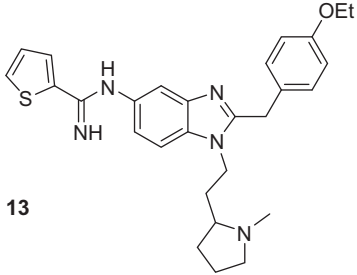
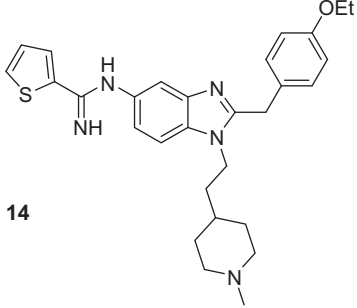
FIGURE 5-5 “Designing in” approach to developing a dual-active MOP agonist and nNOS inhibitor from etonitazene **9**¹³ and NOS inhibitors **10**.¹⁴

A classical “designing in” approach was selected to develop and achieve the bifunctionality: since the central aryl scaffolds (indole and benzimidazole, respectively) and the basic tertiary amine side chain are present in both lead molecules, they were retained. Because of its bidentate interaction with the glutamic acid residue at the arginine binding site of the NOS, the amidine isostere at the 5 position of the benzimidazole of the NOS inhibitors was also retained. According to the literature, antinociceptive activity was not limited to a nitro moiety at this position. Based on these considerations, a set of derivatives was synthesized in a six-step synthesis. Biological evaluation was then performed with a NOS inhibition assay (*L*-NMMA as reference; i.e., a nonselective NOS inhibitor), a competitive radioligand binding assay, to determine the binding affinity at the MOP receptor and a MOP cellular functional cyclic adenosine monophosphate (cAMP) assay, respectively. The result of these first efforts was a set of highly active and selective dual-action nNOS inhibitors and MOP agonists (see [Table 5-1](#)).

Among the most potent compounds, **12** showed the best affinity combined with agonist activity and a good selectivity of nNOS over eNOS and iNOS. It should be the aim of future research to develop a more balanced compound (currently affinity at MOP receptor is approximately 100-fold higher) and to investigate the effectiveness of such compounds *in vivo*.

Another approach to treating neuropathic pain is to inhibit the norepinephrine reuptake (NER). Depending on the location of action in the body, norepinephrine acts both as a hormone and neurotransmitter. In the case of physiological alert, it can be released from the adrenal glands to the blood to increase blood pressure. In the CNS, it is involved in the regulation and stimulation of emotions, sleep, and alertness. NER inhibitors bind to norepinephrine transporters (NET), which results in an inhibition of the reuptake and thus increased postsynaptic concentration of the neurotransmitter. A consequence is the sustained activation of the descending pain inhibitory pathway. The efficiency of NER inhibitors was shown in several animal studies and in clinical observations.¹⁵

Table 5-1 Inhibition of NOS Enzymes and MOP Binding/Functional Data From Selected Compounds¹²

Compound	IC ₅₀ (nNOS) [μM]	IC ₅₀ (eNOS) [μM]	IC ₅₀ (iNOS) [μM]	Binding Studies K _i (hMOP) [nM]	Functional Assay EC ₅₀ (hMOP) [nM]
 12	0.44	4.74	55.2	5.41	340
 13	1.77	4.04	not tested	170	2200
 14	12.8	8.00	not tested	2900	not tested

In 2012, Mladenova et al.¹⁶ merged a NER and a NOS inhibitor by combining the two pharmacophores using a “designing in” strategy. As lead structure for nNOS inhibitors, again the indole-based scaffold **11** was used. The highlighted areas are prominent in both structures and were retained in the final compound (Fig. 5-6). Both inhibitory effects were determined with an inhibition assay using *L*-NMMA as reference for nNOS inhibition and protriptyline as reference for NET inhibition.

Here, the outcome was a dual-active inhibitor with good activity and selectivity (IC₅₀ (nNOS) = 0.56 μM and IC₅₀ (NET) = 1.0 μM).¹⁶ It should be noted that in this compound the activities are balanced, which has not been achieved except in very few cases.

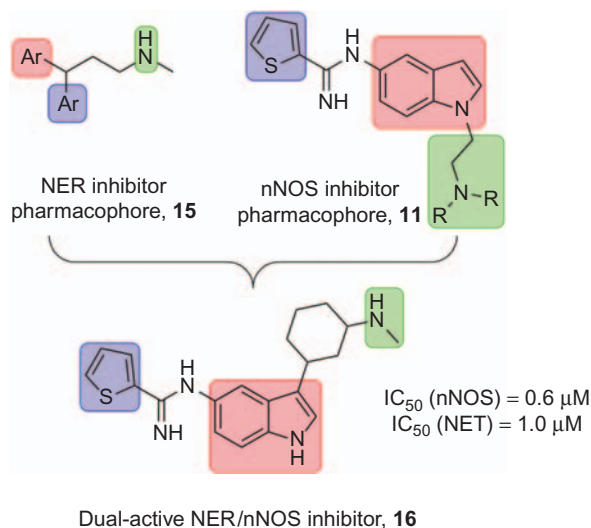


FIGURE 5-6 Dual-acting NER/nNOS inhibitor **16**,¹⁶ which was developed by a “designing in” approach from the NER inhibitor pharmacophore model **15** and the nNOS inhibitor pharmacophore **11**. The highlighted areas show similarities in both scaffolds and in the obtained dual-acting compound.

5.5 Multifunctional Ligands for the Treatment of CNS Diseases

With the number of elderly people in society continuing to increase, the consequences of neurodegenerative diseases affecting the CNS are being seen. Alzheimer’s and Parkinson’s diseases, to name only two forms of neurodegenerative disorders, are causing enormous suffering and thousands of deaths every year. The pathophysiological reasons for these diseases are diverse and multifactorial in nature, which makes the development of a single effective drug extremely complex. Although there are several theories, there hasn’t been any breakthrough yet in combating these diseases. Their complexity and diversity necessitates the development of novel multitarget drugs that address more than one target. Detailed descriptions of the pathophysiology and therapeutic approaches for treating these diseases are discussed in chapters 6, 8 and 10 of this book.

With regard to merged GPCR ligands/enzyme inhibitors, in 2013 Stößel et al.¹⁷ studied the development of a dual-active compound against Parkinson’s disease (PD). PD is characterized by a loss of dopaminergic neurons in the *substantia nigra*, a region of the midbrain. In PD, decreases in dopamine cause major symptoms such as rigidity, shaking, and general motoric dysfunction. The causes of the disease are thought to be genetic or environmental in nature. Current therapy involves levodopa (*L*-DOPA), a natural precursor of dopamine that minimizes symptoms, but ongoing neurodegeneration cannot be stopped. While *L*-DOPA minimizes some symptoms it also causes several negative side effects

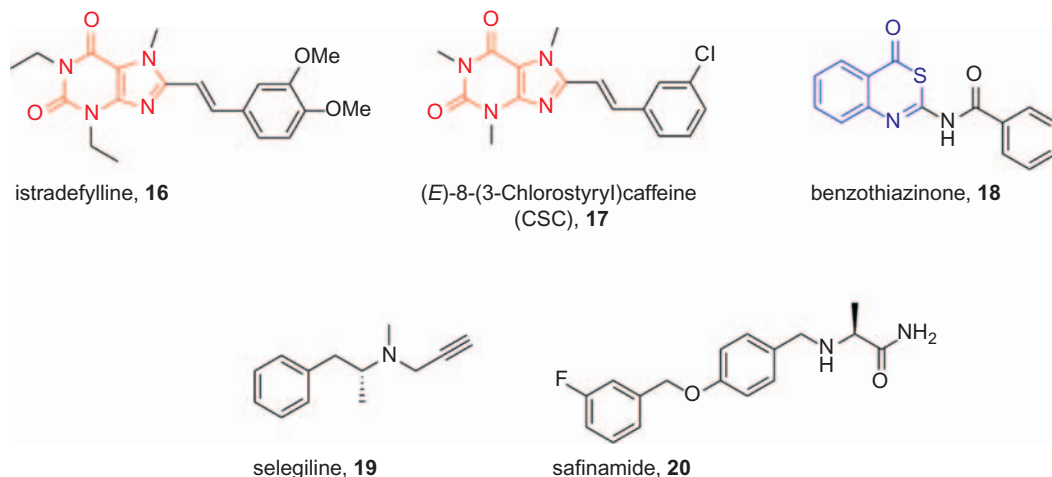


FIGURE 5-7 Above: A_{2A} AR antagonists istradefylline **16** and CSC **17** (the xanthine core is highlighted in red)¹⁷; an antagonist based on a benzothiazinone core **18** (highlighted in blue)²⁰; below: structurally similar MAO B inhibitors selegiline **19** and safinamide **20**.²¹

(e.g., dyskinesia). Treatment that does not necessitate administration of *L*-DOPA is therefore desirable.¹⁸ The A_{2A} adenosine receptor (AR), a GPCR, is a promising target for drugs against PD. The AR, which is activated by adenosine, has four subtypes: A_1 , A_{2A} , A_{2B} , and A_3 . The differences between each subtype are characterized in affinity for adenosine, in recruitment of G proteins, and in their signaling pathways. What makes the A_{2A} AR interesting as a target for the treatment of PD is its appearance in dopamine-innervated areas. It is able to form heterodimeric A_{2A}/D_2 receptor complexes. Both receptors have opposing effects: the inhibition of the A_{2A} leads to increased function of the D_2 receptor and thus enhances the dopamine neurotransmission, and activation of A_{2A} AR inhibits D_2 receptor signaling and leads to reduced affinity of dopamine and other dopamine agonists for their binding site at the heterodimeric complex. An antagonist that blocks the A_{2A} AR is thus promising.¹⁹ Based on these findings, some A_{2A} antagonists have been identified and are currently in clinical trials. These antagonists are mainly based on the structure of xanthines (**16** and **17**) or adenine.¹⁷ Through screening efforts benzothiazinones **18**, based on a structurally different template, have been identified (Fig. 5-7).²⁰

Another pharmacotherapeutic approach to combatting PD is based on inhibition of monoamine oxidase B (MAO B). MAO B is a metabolizing enzyme and one of two isoforms (A and B) that catalyze oxidative deamination of monoamines (e.g., dopamine, adrenaline, etc.). Both isoforms are mainly expressed in the brain and neurons. It has been shown that the expression of MAO B activity increases with age. A clinically applied inhibitor is selegiline **19**, and safinamide **20** is in a Phase III of clinical trials; both are similar in their chemical structure (Fig. 5-7).^{21,22}

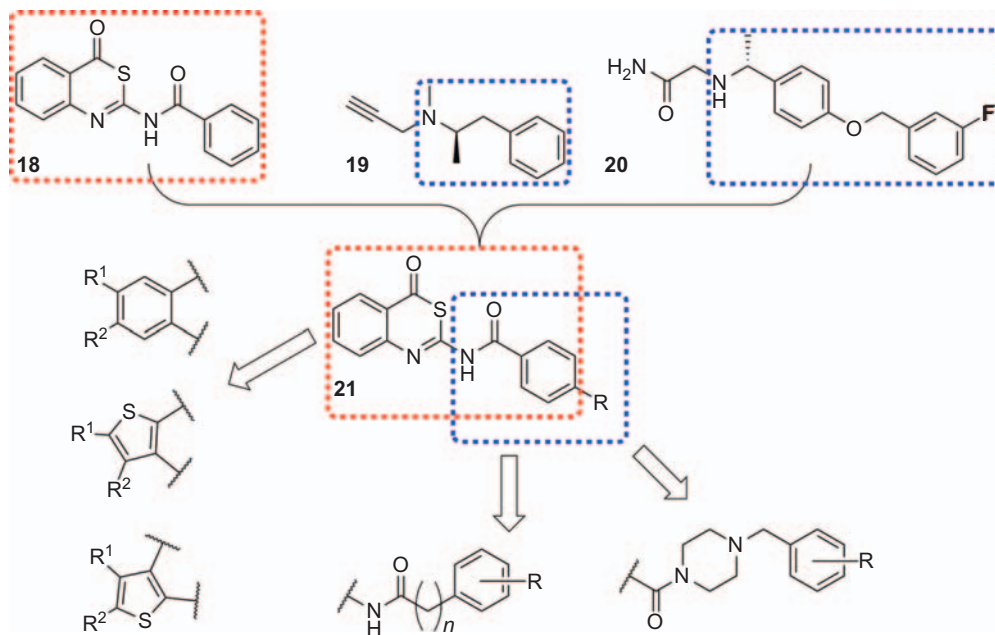


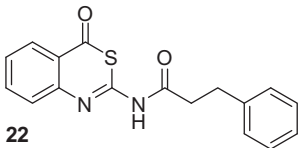
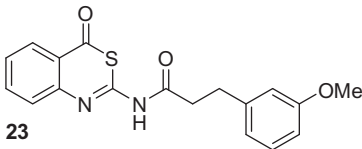
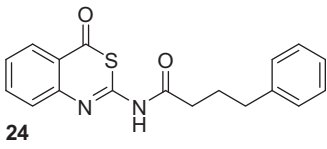
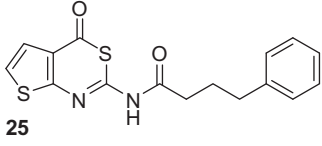
FIGURE 5-8 “Designing in” strategy of a dual-active A_{2A} AR antagonist and MAO B inhibitor **21** starting from the lead compounds **18**, **19**, and **20**.¹⁷

On the basis of these considerations, Stößel et al.¹⁷ developed a set of benzothiazinone derivatives on the basis of the “designing in” paradigm. As lead structures the A_{2A} AR antagonistic benzothiazinone **18** and the two established MAO B inhibitors selegiline **19** and safinamide **20** were used (Fig. 5-8). The benzothiazinone scaffold was synthetically obtained in three steps starting from anthranilic acid. The scaffold was synthetically altered at three positions: the condensed benzene ring was substituted and/or changed into the bioisosteric thiophene; the alkyl chain at the amide moiety was extended and/or several phenyl substituents were introduced; and the benzyl amide moiety was extended with a piperazine amide (Fig. 5-8).

The synthesized compound library contained 30 different target molecules, which were then biologically evaluated to establish SAR studies. To determine affinity at the different ARs, radioligand binding studies were performed. Antagonist behavior was proven by a functional cAMP assay and inhibitory potencies at MAO A and B were evaluated. Furthermore, the mechanistic mode of inhibition was investigated by Lineweaver-Burk plots based on enzyme kinetics. The results of the biological evaluation for some selected compounds are presented in Table 5-2.

Coming back to the challenges in the development of a multitarget compound, one of the major ones is the limited common chemical space or—in a more metaphoric view—the behavior of a pair of scales. If you compare compounds **22** and **24**, the only chemical

Table 5-2 Selected Dual-Acting A_{2A} AR Antagonist and MAO B Inhibitors¹⁷

Compound	$K_i \pm \text{SEM}$ [nM]	A _{2A} Selectivity			IC ₅₀ \pm SEM [nM]	
		<i>hA</i> ₁ : <i>hA</i> _{2A}	<i>hA</i> _{2B} : <i>hA</i> _{2A}	<i>hA</i> ₃ : <i>hA</i> _{2A}	<i>hMAO</i> B	<i>hMAO</i> A
 22	80.9 \pm 21.3	13	5	5	17.6 \pm 3.7	>10 ⁵
 23	64.9 \pm 12.4	21	4	3	95.3 \pm 8.8	>10 ⁵
 24	39.5 \pm 5.8	63	>25	>25	34.9 \pm 2.5	>10 ⁵
 25	82.5 \pm 29.5	4	4	12	69.7 \pm 6.1	>10 ⁵

difference is the length of the carbon chain. With regard to their biological profile, there's a huge difference between the two compounds: one additional CH₂ breaks selectivity and affinity.

Among the most potent compounds, **22** shows the best selectivity at both targets and high potency as well. This work is a perfect example of a classical approach to the design and development of multitarget compounds and goes along with the scheme described in Fig. 5-4: one lead structure was derived from screening efforts and the other was a commercially available drug; SAR studies were performed by synthesizing a compound library with accordance to the “designing in” paradigm; and state-of-the-art biological evaluations were applied to determine the most potent compound **22**, which now serves as a second-generation lead structure for further investigation and as a pharmacological tool for in vivo studies.

Another form of dementia is Alzheimer's disease (AD). Similar to PD, there are several theories describing the cause of AD. The interplay of the formation of β -amyloid plaques, hyperphosphorylation of τ -proteins, interactions of reactive oxygen species, and the irreversible loss of cholinergic neurons is yet unsolved, which makes AD still incurable.²³ In the last

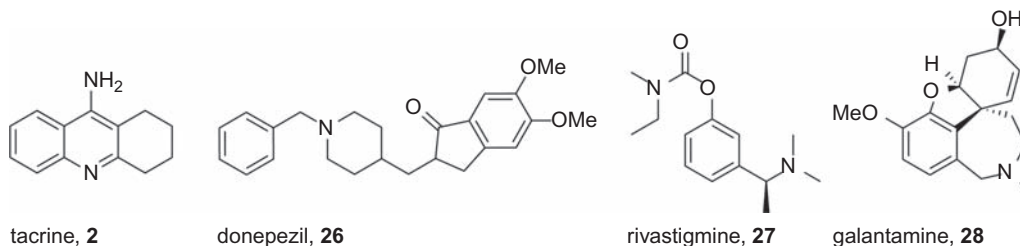


FIGURE 5-9 Therapeutically applied AChE inhibitors.

few years, there have been several promising attempts at addressing different biological and biochemical processes simultaneously.

One of the earliest and most (until now) investigated theories on AD is the cholinergic hypothesis. Here, it is assumed that the cognitive deficits derive from a loss of the neurotransmitter acetylcholine (ACh) in the brain. In the human body, ACh is hydrolyzed into choline and acetate by the two enzymes AChE and BChE.²⁴ This observation led to the development of AChE inhibitory drugs. Among this class of drugs tacrine **2**, donepezil **26**, rivastigmine **27**, and galantamine **28** are therapeutically applied (Fig. 5-9).

Despite their clinical efficiency at improving cognitive deficits in patients suffering from AD, their application is limited to early stages of the disease. Furthermore, tacrine shows severe hepatotoxicity, which was the reason for its withdrawal from the market in several countries.

Besides AChE inhibitors, the histamine H₃ receptor (H₃R) is postulated to be a GPCR drug target for cognitive disorders. The H₃R is part of the histamine receptor family, which also contains the H₁, H₂, and H₄ receptors. The H₃R is responsible for the release of neurotransmitters such as histamine, ACh, serotonin, etc. A blockade of the H₃R by an antagonist might therefore be a promising approach to the upregulation of ACh and to the treatment of AD.^{25,26} There have already been several attempts to synthesize a multitarget compound able to address both targets (Fig. 5-10A).²⁷

Unfortunately, both compounds **29** and **30** (Fig. 5-10A) are imperfect. Compound **29** may show hepatotoxicity due to the tacrine moiety, and compound **30** showed an unbalanced activity profile.^{28,29} The literature-known H₃R antagonists **31** and **32** (Fig. 5-10B) were obtained after SARs. The H₃R ligands show a prototypical pharmacophore collocation for H₃R antagonist activity: a piperidinylpropoxyphenyl pharmacophore plus an amine moiety (highlighted in red).^{30,31}

Combining human histamine receptor 3 antagonists and ChE inhibitors was investigated by Darras et al. in 2014.²⁷ A combination of the above structures was designed and achieved based on a set of previously synthesized and structurally similar tetra- and tricyclic AChE/BChE inhibitors (Fig. 5-10C and Fig. 5-11) on the basis of quinazolines or quinazolinones. Again, the “designing in” strategy was adopted by incorporating the piperidinylpropoxyphenyl pharmacophore for hH₃ antagonism.

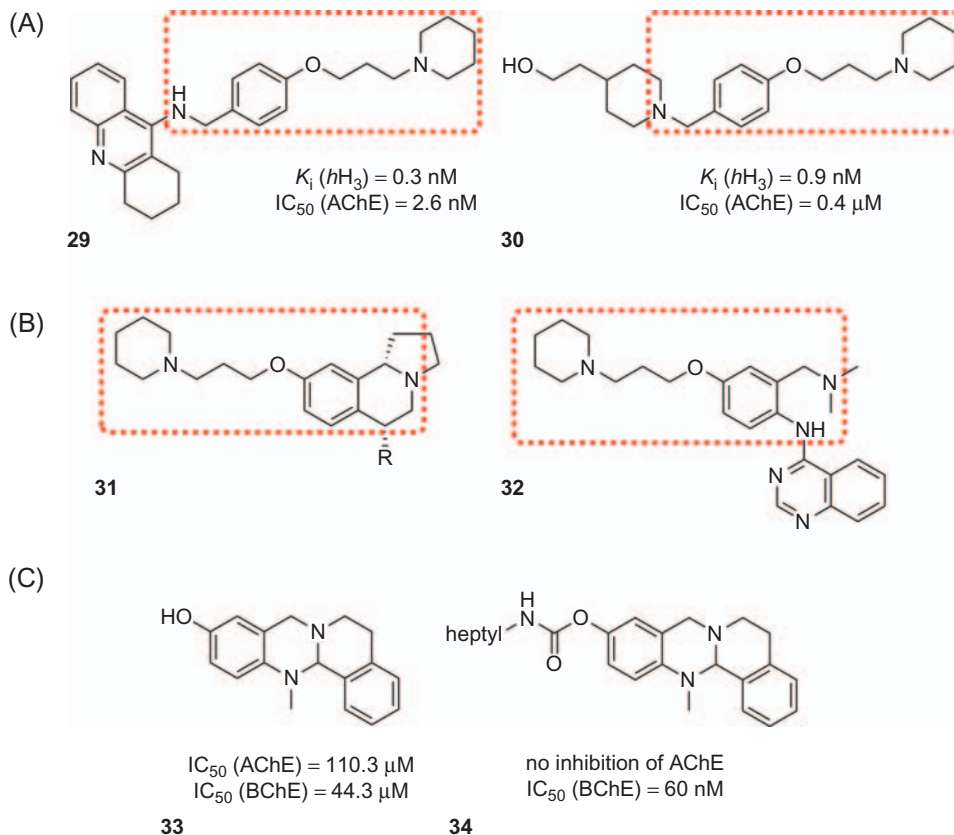


FIGURE 5-10 : (A) Literature-known AChE inhibitors/ hH_3R antagonists **29** and **30**^{28,29}; (B) literature-known H_3R antagonists^{30,31}; H_3R pharmacophore (piperidinylpropoxyphenyl and amine/aminal moiety) is highlighted in red; (C) previously developed AChE/BChE inhibitors **33** and **34** by Darras et al.²⁷

In different synthetic approaches, 10 tetracyclic and 10 tricyclic molecules with different functionalities were obtained: different chain lengths and cycle sizes at the phenoxy side chain and different saturated and unsaturated quinazolinone or quinazolinone core moieties. All compounds were then tested for their inhibition of $hAChE$, $eeAChE$, and $eqBChE$ and for their affinity at the hH_3R (Table 5-3). Regarding receptor affinity, the most potent compounds were tested as well at the other histamine receptors to determine selectivity for the H_3R .²⁷

Among all investigated compounds, **44** shows the best pharmacological profile concerning activity/affinity and balancing. To get better insight into the mode of action of these compounds, intrinsic activity was evaluated by a steady-state GTPase activity assay and mechanistic mode of inhibition was determined by a Lineweaver-Burk plot based on enzyme kinetics. All presented compounds (Table 5-3) showed antagonistic behavior.

Because of their highly active profile further studies were applied to determine the preferred binding mode. Several tri- and tetracyclic quinazolinones were docked into a

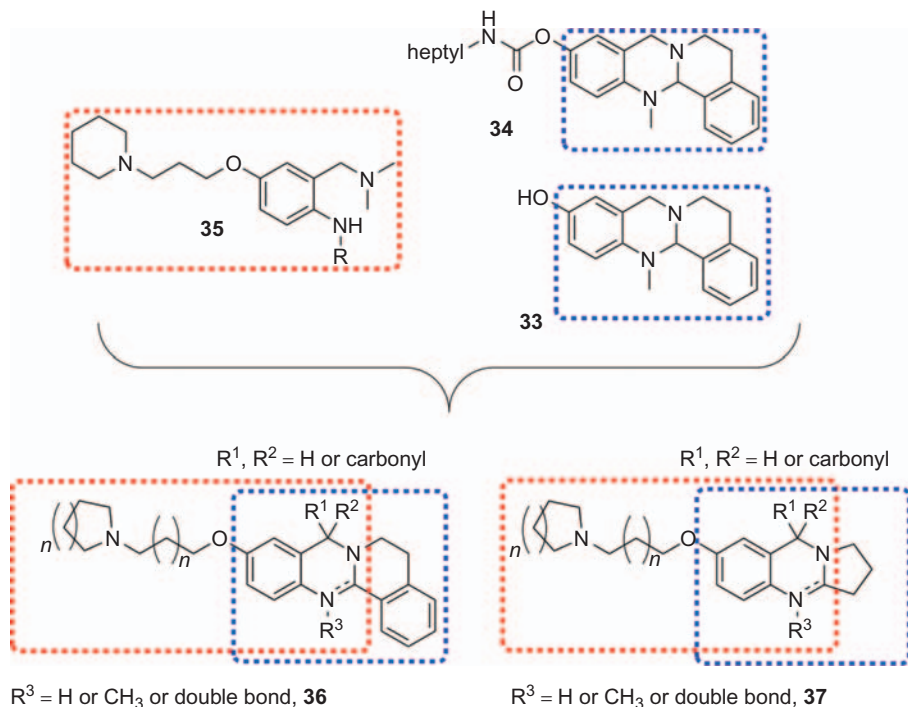


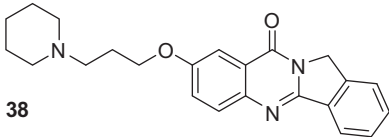
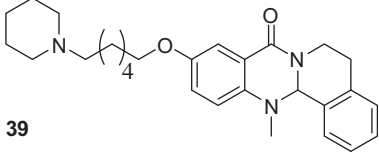
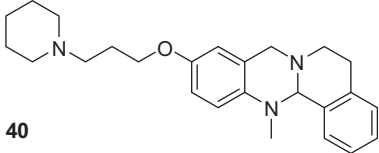
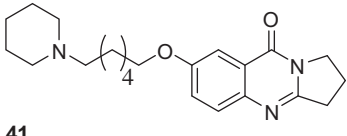
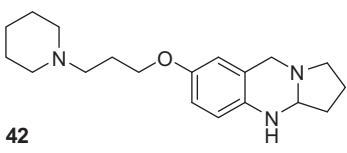
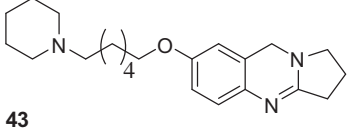
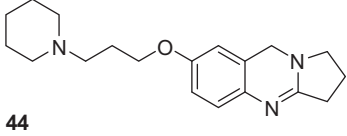
FIGURE 5-11 Design and development of a set of dual-active AChE inhibitors and H₃R antagonists **36** and **37** starting from the lead compounds **33**–**35**. The colored areas mark structural similarities.

high-resolution *h*AChE crystal structure in relation to results obtained by experimental SARs. It was assumed that the “classical orientation” locating the heterocycle in the active site would be found, but an alternative binding mode was found instead. The “inverted” binding mode locates the basic aliphatic side chain into the active center, which points out its necessity (Fig. 5-12).^{27,32}

To complete the development, compound **44** was investigated *in vivo* by conducting cognition experiments. In rats it was shown that **44** dose-dependently increased performance and enhanced precognitive effects. Additionally, in another *in vivo* memory model, compound **44** ameliorated amnesic effects induced by the *N*-Methyl-*D*-Aspartate (NMDA) antagonist dizocilpine. It was the first demonstration showing that dual-active H₃R antagonist and AChE inhibitors can improve retrieval processes and therefore are useful for the treatment of cognitive disorders. Interestingly, a quinazolinone compound with a similar, but only micromolar activity profile, was also able to ameliorate both scopolamine—as well as dizocilpine—induced memory deficits.³³

This work is an excellent example of how methods from different fields can be used for the investigation of a multitarget compound.

Table 5-3 Selected Dual-Active hH_3 Antagonists and Selective AChE Inhibitors^{27,32}

Compound	IC ₅₀ [nM] (pIC ₅₀ ± SEM)			K _i [nM] (pK _i ± SEM)
	<i>h</i> AChE	<i>ee</i> AChE	<i>eq</i> BChE	<i>h</i> H ₃
 38	n.d.	6.9 (8.2 ± 0.0)	4140 (3.4 ± 0.0)	n.d.
 39	n.d.	230 (6.6 ± 0.2)	1820 (5.7 ± 0.1)	361.4 (6.4 ± 0.2)
 40	1980 (5.7 ± 0.1)	530 (6.3 ± 0.1)	1800 (5.7 ± 0.1)	57.7 (7.2 ± 0.1)
 41	n.d.	390 (6.4 ± 0.1)	8600 (5.1 ± 0.1)	924.8 (6.0 ± 0.1)
 42	670 (6.2 ± 0.1)	510 (6.3 ± 0.1)	1590 (5.8 ± 0.1)	37.0 (7.4 ± 0.1)
 43	39 (7.4 ± 0.1)	88 (7.1 ± 0.1)	1300 (5.9 ± 0.0)	113.4 (5.9 ± 0.0)
 44	33 (7.5 ± 0.1)	67 (7.2 ± 0.1)	8200 (5.1 ± 0.1)	76.2 (7.1 ± 0.1)

With regard to the neuroinflammatory component of AD, there's another promising GPCR target: the endocannabinoid system, which consists of two subtypes CB₁R and CB₂R. While the CB₁R is mainly expressed in the terminals of neurons and neuroglia where it affects cognition, emotions, control of motoric functions, and memory, the CB₂R is mainly expressed in immune cells and the peripheral system, but also in microglial cells and

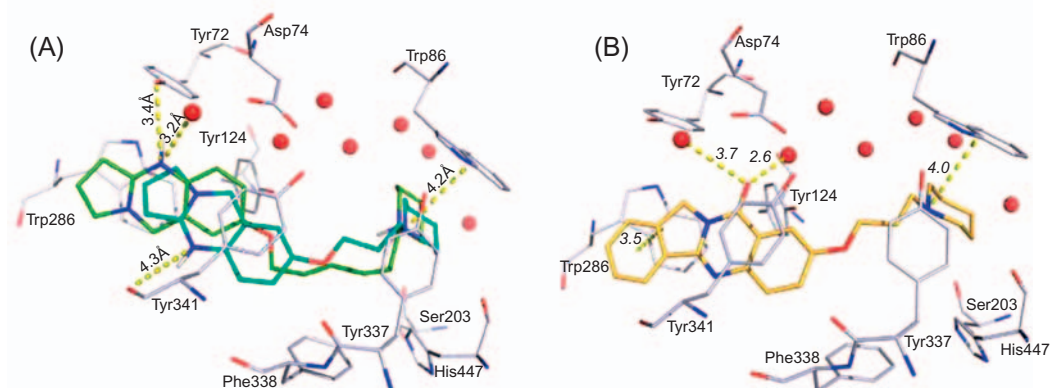


FIGURE 5-12 (A) docking poses of **44** (cyan) and **43** (green)²⁷; (B) docking pose of **38**³²; both showing the “inverted” binding mode with the basic aliphatic side chain pointing into the active center.

neurons. According to the latest research, there’s an overexpression of the CB₂R in the brains of patients suffering from AD, which correlates with an increased occurrence of β -amyloid and senile plaques. The activation of CB₂R by agonists led to several positive effects concerning AD: a suppression of microglial activation and a decreased level of cytokine, nitric oxide, and reactive oxygen species, which decreased neuroinflammation and improved neuroprotection; and a reduction of β -amyloid, proliferation of neuronal progenitor cells, neurogenesis, and τ -protein processing led to an improvement of memory and cognitive performance. This is the reason why an addressing of the CB₂R is in the focus of drug development.²

As already described, AChE inhibitors are classical drugs in the treatment of AD. Alongside AChE, the BChE is the other enzyme that hydrolyzes ACh to choline and acetate. In the course of the disease, the amount of AChE decreases, which makes AChE inhibitors only beneficial at early stages of the disease. In the same way AChE decreases, the concentration of BChE in AD-affected brains seems to increase.³⁴ In a recent study, BChE knockout mice showed improved learning abilities in memory tests, which was triggered when β -amyloid was injected into the mice brains.³⁵

Based on these findings, González-Naranjo et al.³⁶ developed a dual-acting BChE inhibitor and CB₂R agonist. In contrast to the above described works, their first effort was to build up a virtual compound library. This virtual library was obtained by several docking studies on the basis of the scaffolds of the two cannabinoid agonists JWH-015 **45** and WIN 55,212-2 **46**. The fact that in vitro studies also showed AChE inhibition for these two compounds made them even more interesting as lead structures. Combined with the findings that indazole ethers show both cholinergic properties and cannabinoid effects, this marked the starting point.³⁷ A virtual library was developed with regard to group interactions at position 1 and 3 with the CB₂R, structural variability and synthetic accessibility.

The core of the molecule was virtually changed from an indole scaffold into a bioisosteric indazole ring with an ether moiety at position 3. Hereupon, the nitrogen atom at position 1,

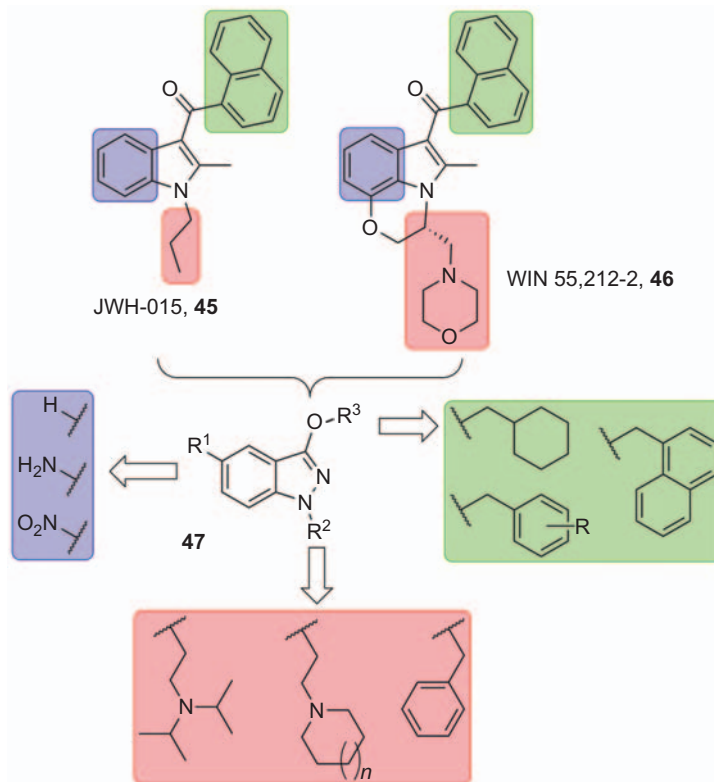


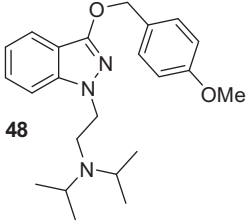
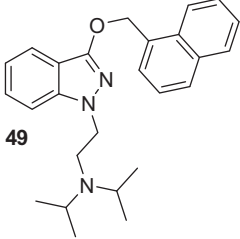
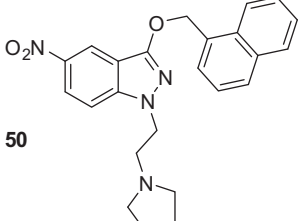
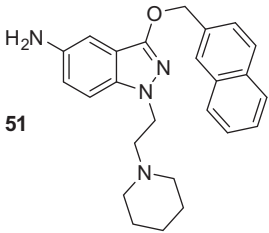
FIGURE 5-13 Development of a multitarget BChE inhibitor and CB₂R agonist **47** based on literature-known CB₂R agonist JWH-015 **45** and WIN 55,212-2 **46**.

was linked to different aminoalkyl substituents (*red*) and several saturated and unsaturated cycles were attached to the ether (*green*). At position 5 of the indazole moiety no substituent or the introduction of an activating or deactivating nitrogen moiety (e.g., nitro or amine) seemed promising (*blue*) (Fig. 5-13).³⁶

Based on this virtual screening, the most promising compounds were synthesized over one to three steps. The resulting set of compounds was then biologically evaluated. The receptor binding was quantified with a radioligand binding assay and intrinsic activity was determined by an isolated tissue assay. The extent of inhibition and the type of inhibition were determined by inhibition assays and a Lineweaver-Burk plot. Furthermore, the oxygen radical absorbance capacity (ORAC) was determined as a measure of antioxidant capacity.

From the 25 compounds synthesized, 22 showed affinity at the CB₂R. Considering the *in silico* approach this is a very remarkable result. Among the 22 active compounds, **48** and **51** were the most potent molecules. Both show selectivity for CB₂R and BChE and a balanced activity/affinity (one digit micromolar at both targets). Furthermore, both compounds act as agonists and show significant antioxidant capacity (Table 5-4).

Table 5-4 Biological Data From Selected Dual-Active CB₂R Agonists and BChE Inhibitors³⁶

Compound	IC ₅₀ [μM] ± SEM		Type of Inhibition ^a	K _i [μM] ± SEM		ORAC ^b
	<i>h</i> AChE	<i>h</i> BChE		CB ₁ R	CB ₂ R	
 48	24 ± 2.0	4.8 ± 0.3	nc	>40	7.7 ± 2.0	1.0
 49	42 ± 3.0	0.1 ± 0.03	c	>40	5.4 ± 2.6	n.d.
 50	45 ± 3.0	4.5 ± 1.7	c	0.6 ± 0.2	0.1 ± 0.02	n.d.
 51	13 ± 4.0	1.8 ± 0.01	m	>40	2.0 ± 1.0	0.8

^aBChE inhibition type, c, competitive; nc, noncompetitive; m, mixed.

^bData are expressed as μmol of Trolox equivalents/μmol of tested compound.

Another approach to developing a dual-acting CB₂R agonist and BChE inhibitor was performed by Dolles et al. in 2016.³⁸ Here, the starting point was a selective benzimidazole-based CB₂R agonist developed by AstraZeneca.

Compared with the quinazoline-based BChE inhibitors/H₃R antagonists **39–44** from Darras et al.²⁷ and other dual-active CB₂R agonists/BChE inhibitors **48–51** from González-Naranjo et al.³⁶ structural similarities with the benzimidazole-based CB₂R agonist **52** from

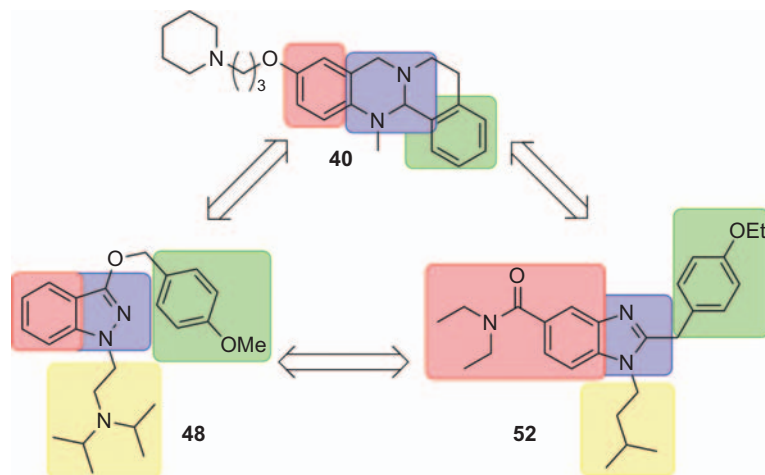


FIGURE 5-14 Simplified pharmacophore model of a prototypical BChE inhibitor based on BChE inhibitors/H₃R antagonists **40** (Darras et al.²⁷), BChE inhibitors/CB₂R agonists **48** (González-Naranjo et al.³⁶), and CB₂R agonist **52** by AstraZeneca.³⁹

AstraZeneca³⁹ and a simplified pharmacophore model of prototypical BChE inhibitors were obtained: a substituted ring (*red*), a condensed basic heterocycle (*blue*), an aromatic (*green*), and/or hydrophobic moiety (*yellow*) (Fig. 5-14).

The structural similarities between **40** and **48** identified by the pharmacophore model are also apparent for the CB₂R agonist **52**, which was therefore tested for inhibition of ChEs. Indeed, moderate activity (two-digit micromolar) as a BChE inhibitor was found for AstraZeneca's compound **52**.

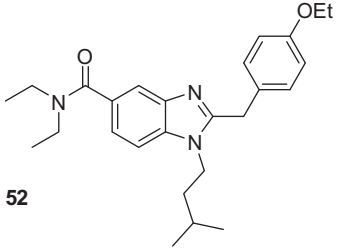
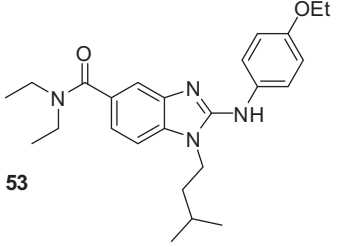
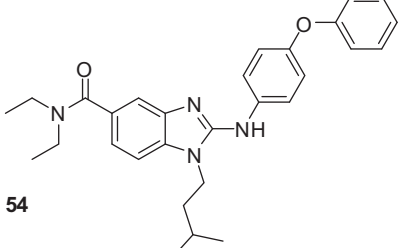
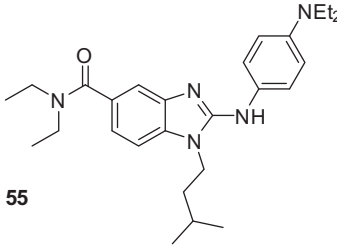
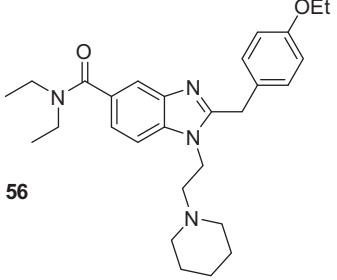
In a first approach to increase potency, AstraZeneca's benzimidazole **52** was structurally altered into a 2-aminobenzimidazole core **53**. The resulting guanidine structure was assumed to be more basic (predicted pK_a = 5.72; experimentally determined pK_a = 6.08) and therefore to positively affect BChE inhibition. Biological evaluation showed a 10-fold increased inhibitory effect at the BChE, but a decrease of affinity at the CB₂R (Table 5-5). Compounds **52** and **53** then served as first- and second-generation lead structures.

Based on this first approach and the prototypical pharmacophore model for BChE inhibitors, several structural alterations were considered. The diethyl amide moiety was replaced with an hydrogen atom to confirm its necessity as CB₂R/BChE pharmacophore. Like González-Naranjo et al. a basic side chain was introduced and the core moiety was altered in an indazole heterocycle. The core structure was changed to an imidazopyridine and the methylene unit of the benzimidazole core was substituted to get a set of 2-aminobenzimidazoles (Fig. 5-15).³⁸

In parallel, molecular docking studies into BChE were conducted as well as molecular dynamics (MD) simulations into the CB₂R in order to relate the altered structural features into the binding and inhibition profiles determined (Fig. 5-16).

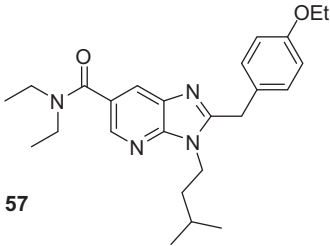
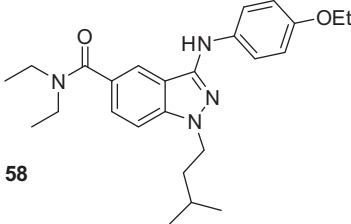
Altogether, 15 novel and structurally diverse 2-aminobenzimidazoles (aromatic and aliphatic), three benzimidazoles, one pyridinoimidazole, and one indazole were synthesized

Table 5-5 Selected Dual-Acting BChE Inhibitors and CB₂R Agonists³⁸

Compound	IC ₅₀ (pIC ₅₀ ± SD) or inhibition		K _i (pK _i ± SD) or radiolig. displ. @ 10 μM	
	eeAChE	eqBChE	hCB ₁ R	hCB ₂ R
 <p>52</p>	28% @ 100 μM	9.7 μM (5.0 ± 0.1)	24%	36.7 nM (7.4 ± 0.1)
 <p>53</p>	4% @ 100 μM	0.7 μM (6.2 ± 0.0)	13%	1.91 μM (5.7 ± 0.1)
 <p>54</p>	2% @ 10 μM	3.7 μM (5.7 ± 0.3)	45%	426.0 nM (6.3 ± 0.2)
 <p>55</p>	10% @ 10 μM	0.2 μM (6.7 ± 0.1)	4%	8.1 μM (5.1 ± 0.1)
 <p>56</p>	48% @ 100 μM	2.3 μM (5.6 ± 0.1)	14%	188.0 nM (6.7 ± 0.1)

(Continued)

Table 5-5 (Continued)

Compound	IC ₅₀ (pIC ₅₀ ± SD) or inhibition		K _i (pK _i ± SD) or radiolig. displ. @ 10 μM	
	eeAChE	eqBChE	hCB ₁ R	hCB ₂ R
 57	7% @ 10 μM	39% @ 10 μM	13%	127.0 nM (6.9 ± 0.1)
 58	5% @ 10 μM	26% @ 10 μM	47%	11%

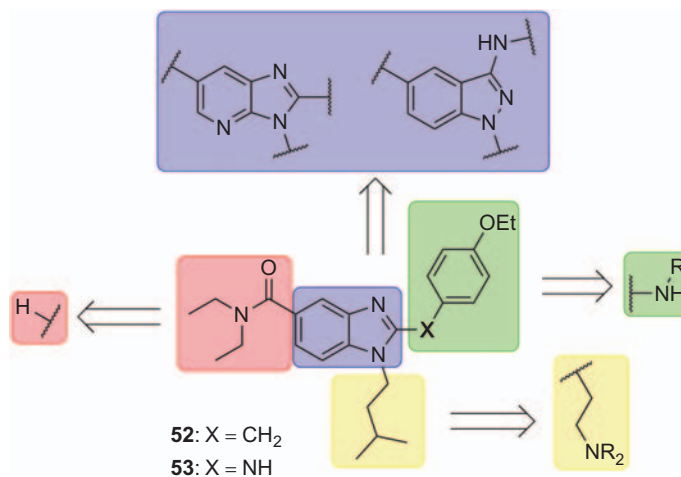


FIGURE 5-15 Structural alterations based on AstraZeneca's benzimidazole **52** and a novel 2-aminobenzimidazole **53** to investigate SAR.

to cover sufficient chemical space for SARs at the two targets (BChE and hCB₂R; actually four targets when including AChE and CB₁R since selectivity is of high importance). These compounds were biologically tested for their activity at both enzymes AChE and BChE (inhibition assay) and for their affinity at the CB₁R and CB₂R (radioligand binding assay). Since lead

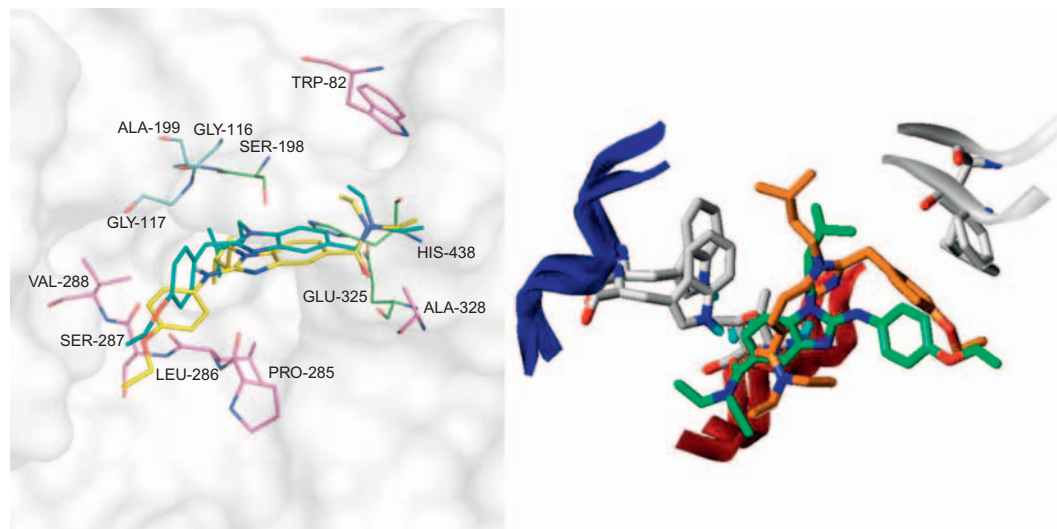


FIGURE 5-16 Left: docking poses of ligand **52** (turquoise) and **53** (yellow) in the CAS of the BChE; right: overlay of the binding conformation of **52** (orange) and **53** (green) in the binding site of *hCB₂R*.

compound **52** is a proven agonist, it was assumed that all synthesized derivatives would show agonist behavior. Determination of the compounds' intrinsic activity later confirmed this.

The selected compounds (Table 5-5) are good examples of the difficulty of the development of a dual-acting compound and the limited common chemical space. Based on the consideration that an additional nitrogen atom positively affects BChE inhibition, one would expect compound **55** to be a more potent inhibitor. Actually this is not the case. The inhibition of BChE is only slightly improved, while affinity at the *hCB₂R* drops by a factor of approximately 10. A similar problem applies for the pyridinoimidazole **57**. The extra nitrogen atom improves affinity at *hCB₂R* by a factor of approximately 1000, but the inhibitory effect at the BChE is completely lost.

In the case of the indazole derivative **58** this behavior is even more pronounced. The compound was developed as a kind of upgrade of the compounds from González-Naranjo et al.³⁶ (micromolar *hCB₂R* agonists/BChE inhibitors; see page 151) and possessed the diethylamide moiety, which is necessary for a *CB₂R* agonist. Surprisingly, the compound totally lost activity at both targets.

Nevertheless, there were two compounds that showed the desired profile of a dual-active compound. Compared to the second-generation lead structure, compounds **54** and **56** showed improved affinity at the *hCB₂R* and only a slightly decreased inhibitory effect at BChE.

From a multitarget compound point of view, the compounds from González-Naranjo et al.³⁶ and Dolles et al.³⁸ show the desired profile: activity at two different targets. However, both sets of compounds show deficits. While González-Naranjo et al.³⁶ developed a balanced activity profile, the compounds still lack potency (activity/affinity in the micromolar range).

For Dolles et al.³⁸ it's vice versa: their compounds show high affinity in the nanomolar range, but lack a balanced profile (affinity at *hCB₂R* in nanomolar range; inhibition of BChE in micromolar range). From a more general therapeutic point of view, these compounds appear to be less potent than available (single target) drugs. That is the reason further investigations and optimizations on this scaffold are ongoing.

5.6 Multitarget Compounds for the Treatment of Cardiovascular Diseases

In addition to neurodegenerative diseases, cardiovascular diseases are also disease states that cause numerous deaths every year. The reasons for this are multifactorial and include increased average life expectancy as well as individual causes such as smoking, obesity, and stress.

The renine-angiotensin-aldosterone system (RAAS), a circuit of different hormones and enzymes, mainly regulates the concentration of the plasma sodium level and arterial blood pressure. It is therefore a natural regulator of the cardiovascular system. The RAAS cascade starts with the release of the protein/enzyme renine from the kidney. Renine then cleaves its substrate angiotensinogen, which results in the formation of the decapeptide angiotensin I (Ang I). In the next step, Ang I is converted by angiotensin-converting enzyme (ACE) to the octapeptide angiotensin II (Ang II). Ang II is able to bind to the two GPCRs AT₁ and AT₂ and thus leads to vasoconstriction, water retention, and the release of vasopressin and aldosterone. Addressing AT₁ and AT₂ by an antagonist is therefore a useful tool to combat cardiovascular diseases.^{40,41}

Other promising targets are the endothelin receptors ET_A and ET_B, which are GPCRs as well. Similar to AT_{1/2}, ET_A is mainly responsible for vasoconstriction. ET_B instead promotes the synthesis of the vasodilators prostacycline and nitric oxide, which counteracts these effects. Both isoforms are activated by the physiological agonists endothelin 1 (ET-1), ET-2, and ET-3. A synthetic antagonist for ET_A might therefore be a powerful drug against cardiovascular diseases.^{40,42}

An approach to developing a dual-active AT₁ and ET_A antagonist was taken up by Murugesan et al.,⁴³ who started from lead compounds **59**, a known ET_A antagonist, and irbesartan **60**, a therapeutically applied drug that acts as an AT₁ antagonist. In a “designing in” attempt, they merged the ET_A pharmacophore, a biphenyl sulfonamide attached to a 5-isoxazole (*red*), and the AT₁ pharmacophore, a biphenyl imidazolone (*blue*). In previous studies, a positive effect of substitution at the biphenyl moiety was observed.⁴⁴ To improve metabolic stability, the 5-isoxazole was replaced with a 3-isoxazole. The resulting compound **61** showed a balanced profile in vitro at the targets (Fig. 5-17).⁴³

In several in vivo evaluations of **61**, pharmacokinetic properties such as oral bioavailability, half-life in plasma, and C_{max}/T_{max} were determined. Compound **61** showed reduced blood pressure in rats and longer duration compared to **59** and **60**.⁴³

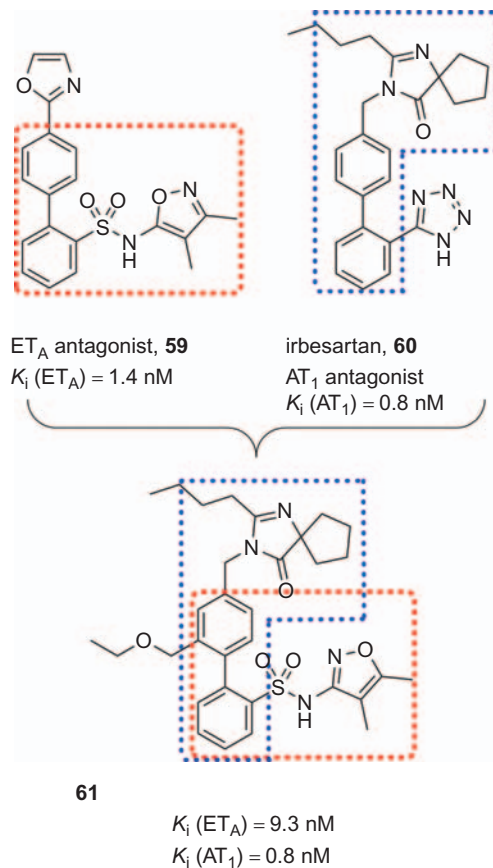


FIGURE 5-17 "Designing in" attempt of the ET_A antagonist **59** and irbesartan **60** in order to develop the dual-active compound **61**.^{43,44}

The multifactorial character of cardiovascular diseases led to addressing of the peroxisome proliferator-activated receptor γ ($PPAR\gamma$), an intracellular nuclear hormone receptor. The $PPAR\gamma$ is responsible for the regulation of glucose metabolism and insulin and is therefore a molecular target when it comes to the prevention of diabetes.^{40,45} According to the American Heart Association there's a strong correlation between diabetes and cardiovascular diseases. Casimiro-Garcia et al.⁴⁶ from Pfizer Global Research and Development therefore aimed to develop a dual-active AT_2 antagonist and $PPAR\gamma$ agonist. Their starting point was telmisartan **62**, a therapeutically applied AT_1 antagonist and the $PPAR\gamma$ agonist **63**.⁴⁷ Through a cross-screening approach, which means that structurally similar compounds were both tested for activity at the AT_1 receptor and at the $PPAR\gamma$, a general pharmacophore to address both receptors could be obtained: an acidic head group (*red*) that interacts with the three clamp residues Tyr 327, His449, and His323; a nonpolar phenyl linker (*blue*); and a hydrophobic tail (*green*) (Fig. 5-18).⁴²

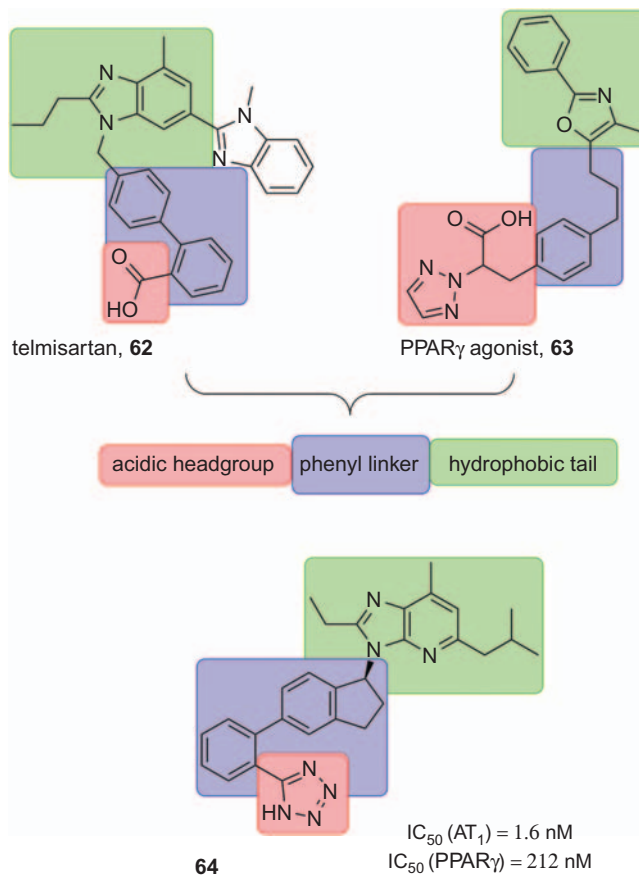


FIGURE 5-18 Development of the general pharmacophore (highlighted in red/blue/green) for a dual-active AT₁ antagonist/PPAR γ agonist based on telmisartan **62** and a previously developed PPAR γ agonist **63**.^{46,47}

Some structural changes were applied (Fig. 5-18): the carboxylic acid was replaced with its bioisostere tetrazole ring, which has the same physicochemical properties, but bigger size. This fact makes the binding site sterically packed, but keeps the desired interactions. The biphenyl linker from telmisartan (generally a key structural element of sartans) was taken up and complemented with an annulated cyclopentyl ring in order to make it more unpolar. In docking studies at the PPAR γ a flipped binding mode could be observed. From these findings, the original benzimidazole was replaced with a pyridine imidazole in order to improve the interactions with the charged binding site (Fig. 5-19). Based on these considerations, a set of 15 molecules was synthesized and compound **64** was identified as the most potent one and with the best activity profile for both receptors.⁴⁶

In two well-validated in vivo models a beneficial effect could be observed with Zucker diabetic fatty rats and spontaneously hypertensive rats, where compound **61** was seen to lower blood pressure for a longer timeframe than the marketed drug telmisartan.⁴⁶

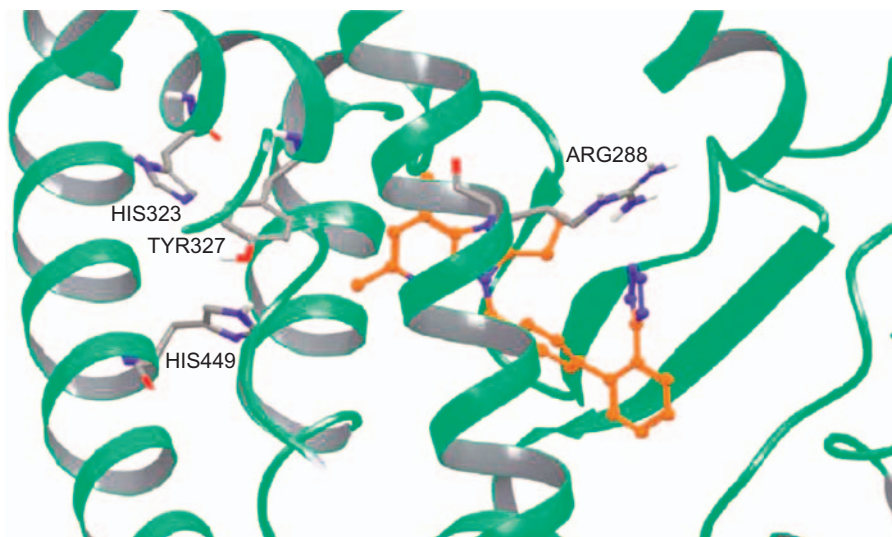


FIGURE 5-19 Docking model of the flipped binding mode of **61** in the active site of PPAR- γ .⁴⁶

5.7 Conclusion

This chapter provided an overview of the development of multitarget compounds with regard to the latest research in the field of different (multifactorial) diseases.

The examples show that the development of dual-active compounds is not only possible but promising. While their physicochemical and biological properties show high potential for future therapeutic appliance, development is difficult, because it requires the work of all disciplines. To validate biological data and to investigate SARs it is necessary to correlate biological data with the 3D structures of the target proteins. In the course of development, there are often surprising SAR results that were not expected and that “crash” previous assumptions. To avoid this problem a large compound library must be synthesized and—of course—biologically evaluated. Structure-based ligand design is necessary to keep the amount of work reasonable. Research in this field should also take into account that balanced affinity does not only mean that the activity at both targets should have the same numerical value. In fact, the expression of a target in the pathophysiological state is the “pace maker” that determines balanced affinity. Therefore it is inevitable not only to investigate *in vitro* but also *in vivo* behavior.

If all these requirements are fulfilled, it might really be possible to develop several powerful “Swiss Army knives” against crucial diseases.

References

1. Morphy, R.; Rankovic, Z. Designed Multiple Ligands. An Emerging Drug discovery Paradigm. *J. Med. Chem.* **2005**, *21*, 6523–6543.
2. Nimczick, M.; Decker, M. New Approaches in the Design and Development of Cannabinoid Receptor Ligands: Multifunctional and Bivalent Compounds. *ChemMedChem* **2015**, *10*, 773–786.

- Bansal, Y.; Silakari, O. Multifunctional Compounds: Smart Molecules for Multifactorial Diseases. *Eur. J. Med. Chem.* **2014**, *76*, 31–42.
- Lange, J. H. M.; Coolen, H. K. A.; Van der Neut, M. A. W.; Borst, A. J. M.; Stork, B.; Verveer, P. C., et al. Design, Synthesis, Biological Properties, and Molecular Modeling Investigations of Novel Tacrine Derivatives with a Combination of Acetylcholinesterase Inhibition and Cannabinoid CB₁ Receptor Antagonism. *J. Med. Chem.* **2010**, *53*, 1338–1346.
- Sterling, J.; Herzig, Y.; Goren, T.; Finkelstein, N.; Lerner, D.; Goldenberg, W., et al. Novel Dual Inhibitors of AChE and MAO Derived from Hydroxy Aminoindan and Phenethylamine as Potential Treatment for Alzheimer's Disease. *J. Med. Chem.* **2002**, *45*, 5260–5279.
- Filmore, D. It's a GPCR World. *Mod. Drug Discov.* **2004**, *11*, 24–28.
- Jazayeri, A.; Dias, J. M.; Marshall, F. H. From G Protein-coupled Receptor Structure Resolution to Rational Drug Design. *J. Biol. Chem.* **2015**, *32*, 19489–19495.
- Heifetz, A.; Schertler, G. F. X.; Seifert, R.; Tate, C. G.; Sexton, P. M.; Gurevich, V. V., et al. GPCR Structure, Function, Drug Discovery and Crystallography: Report From Academia-Industry International Conference (UK Royal Society). *Naunyn Schmiedebergs Arch. Pharmacol.* **2015**, *388*, 883–903.
- Feng, Y.; He, X.; Yang, Y.; Chao, D.; Lazarus, L. H.; Xia, Y. Current Research on Opioid Receptor Function. *Curr. Drug Targets* **2012**, *13*, 230–246.
- Schmidtke, A.; Tegeder, I.; Geisslinger, G. No NO, no pain? The Role of Nitric Oxide and cGMP in Spinal Pain Processing. *Trends Neurosci.* **2009**, *32*, 339–346.
- Tanabe, M.; Nagatani, Y.; Saitoh, K.; Takasu, K.; Ono, H. Pharmacological Assessments of Nitric Oxide Synthase Isoforms and Downstream Diversity of NO Signaling in the Maintenance of Thermal and Mechanical Hypersensitivity after Peripheral Nerve Injury in Mice. *Neuropharmacology* **2009**, *56*, 702–708.
- Renton, P.; Green, B.; Maddaford, S.; Rakhit, S.; Andrews, J. S. NOPiates: Novel Dual Action Neuronal Nitric Oxide Synthase Inhibitors with μ -Opioid Agonist Activity. *ACS Med. Chem. Lett.* **2012**, *3*, 227–231.
- Hunger, A.; Keberle, J.; Rossi, A.; Hoffmann, K. Benzimidazol-Derivate und Verwandte Heterocyclen III. Synthese Von 1-aminoalkyl-2-benzyl-nitro-benzimidazol. *Helv. Chim. Acta* **1960**, *43*, 1032–1046.
- Renton, P.; Speed, J.; Maddaford, S.; Annedi, S. C.; Ramnauth, J.; Rakhit, S. 1,5-Disubstituted Indole Derivatives as Selective Human Neuronal Nitric Oxide Synthase Inhibitors. *Bioorg. Med. Chem. Lett.* **2011**, *21*, 5301–5304.
- Leventhal, L.; Smith, V.; Hornby, G.; Andree, T. H.; Brandt, M. R.; Rogers, K. E. Differential and Synergistic Effects of Selective Norepinephrine and Serotonin Reuptake Inhibitors in Rodent Models of Pain. *J. Pharm. Exp. Ther.* **2007**, *320*, 1178–1185.
- Mladenova, G.; Annedi, S. C.; Ramnauth, J.; Maddaford, S. P.; Rakhit, S.; Andrews, J. S., et al. First-in-Class, Dual-Action, 3,5-Disubstituted Indole Derivatives Having Human Nitric Oxide Synthase (nNOS) and Norepinephrine Reuptake Inhibitory (NERI) Activity for the Treatment of Neuropathic Pain. *J. Med. Chem.* **2012**, *55*, 3488–3501.
- Stößel, A.; Schlenk, M.; Hinz, S.; Küppers, P.; Heer, J.; Gütschow, M., et al. Dual Targeting of Adenosine A_{2A} Receptors and Monoamine Oxidase B by 4H-3,1-Benzothiazin-4-ones. *J. Med. Chem.* **2013**, *56*, 4580–4596.
- Samii, A.; Nutt, J. G.; Ransom, B. R. Parkinson's Disease. *Lancet* **2004**, *363*, 1783–1793.
- Armentero, M. T.; Pinna, A.; Ferré, S.; Lanciego, J. L.; Müller, C. E.; Franco, R. Past, Present and Future of A_{2A} Adenosine Receptor Antagonists in the Therapy of Parkinson's Disease. *Pharmacol. Ther.* **2011**, *132*, 280–299.
- Gütschow, M.; Schlenk, M.; Gäb, J.; Paskaleva, M.; Alnouri, M. W.; Scolari, S. W., et al. Benzothiazinones: A Novel Class of Adenosine Receptor Antagonists Structurally Unrelated to Xanthine and Adenine Derivatives. *J. Med. Chem.* **2012**, *55*, 3331–3341.
- Schapira, A. H. V. Monoamine Oxidase B Inhibitors for the Treatment of Parkinson's Disease: A Review of Symptomatic and Potential Disease-Modifying Effects. *CNS Drugs* **2011**, *25*, 1061–1071.

22. Youdim, M. B.; Bakhle, Y. S. Monoamine Oxidase: Isoforms and Inhibitors in Parkinson's Disease and Depressive Illness. *Br. J. Pharmacol.* **2006**, *147*, 287–296.
23. Blennow, K.; de Leon, M.; Zetterberg, H. Alzheimer's Disease. *Lancet* **2006**, *368*, 387–403.
24. Claassen, J. A.; Jansen, R. W. Cholinergically Mediated Augmentation of Cerebral Perfusion in Alzheimer's Disease and Related Cognitive Disorders: The Cholinergic-Vascular Hypothesis. *J. Gerontol. A Biol. Sci. Med. Sci.* **2006**, *61*, 267–271.
25. Arrang, J.-M.; Garbarg, M.; Schwartz, J.-C. Auto-Inhibition of Brain Histamine Release Mediated by a Novel Class (H₃) of Histamine Receptor. *Nature* **1983**, *302*, 832–837.
26. Singh, M.; Jadhav, H. R. Histamine H₃ Receptor Function and Ligands: Recent Developments. *Mini-Rev. Med. Chem.* **2013**, *13*, 47–57.
27. Darras, F. H.; Pockes, S.; Huang, G.; Wehle, S.; Strasser, A.; Wittman, H.-J., et al. Synthesis, Biological Evaluation, and Computational Studies of Tri- and Tetracyclic Nitrogen-Bridgehead Compounds as Potent Dual-Acting AChE Inhibitors and hH₃ Receptor Antagonists. *ACS Chem. Neurosci.* **2014**, *5*, 225–242.
28. Melo, T.; Videira, R. A.; André, S.; Maciel, E.; Francisco, C. S.; Oliveira-Campos, A. M., et al. Tacrine and Its Analogues Impair Mitochondrial Function and Bioenergetics: A Lipidomic Analysis in Rat. *Brain J. Neurochem.* **2012**, *120*, 998–1013.
29. Bembenek, S. D.; Keith, J. M.; Letavic, M. A.; Apodaca, R.; Barbier, A. J.; Dvorak, L., et al. Lead Identification of Acetylcholinesterase Inhibitors-Histamine H₃ Receptor Antagonists Form Molecular Modeling. *Bioorg. Med. Chem.* **2008**, *16*, 2968–2973.
30. Keith, J. M.; Gomez, L. A.; Wolin, R. L.; Barbier, A. J.; Wilson, S. J.; Boggs, J. D., et al. Pyrrolidino-Tetrahydroisoquinolines as Potent Dual H₃ Antagonist and Serotonin Transporter Inhibitors. *Bioorg. Med. Chem. Lett.* **2007**, *17*, 2603–2607.
31. Roche, O.; Rodríguez Sarmiento, R. M. A New Class of Histamine H₃ Receptor Antagonists Derived from Ligand Based Design. *Bioorg. Med. Chem. Lett.* **2007**, *17*, 3670–3675.
32. Darras, F. H.; Wehle, S.; Huang, G.; Sotriffer, C. A.; Decker, M. Amine Substitution of Quinazolinones Leads to Selective Nanomolar AChE Inhibitors with 'inverted' Binding Mode. *Bioorg. Med. Chem.* **2014**, *22*, 4867–4881.
33. Khan, N.; Saad, A.; Nurulain, S. M.; Darras, F. H.; Decker, M.; Sadek, B. The Dual-Acting H₃ Receptor Antagonist and AChE Inhibitor UW-MD-71 Dose-Dependently Enhances Memory Retrieval and Reverses Dizocilpine-Induced Memory Impairments in Rats. *Behav. Brain Res.* **2016**, *297*, 155–164.
34. Greig, N. H.; Utsuki, T.; Yu, Q.; Zhu, X.; Holloway, H. W.; Perry, T., et al. A New Therapeutic Target in Alzheimer's Disease Treatment: Attention to Butyrylcholinesterase. *Curr. Med. Res. Opin.* **2001**, *17*, 159–165.
35. Maurice, T.; Strehaiano, M.; Siméon, N.; Bertrand, C.; Chatonnet, A. Learning Performances and Vulnerability to Amyloid Toxicity in the Butyrylcholinesterase Knockout Mouse. *Behav. Brain Res.* **2016**, *296*, 351–360.
36. González-Naranjo, P.; Pérez-Macias, N.; Campillo, N. E.; Pérez, C.; Arán, V. J.; Girón, R., et al. Cannabinoid Agonists Showing BuChE Inhibition as Potential Therapeutic Agents for Alzheimer's Disease. *Eur. J. Med. Chem.* **2014**, *73*, 56–72.
37. Páez, J. A.; Campillo, N. E.; González-Naranjo, P.; Pérez, C.; Arán, V. J.; Martín Fontelles, M. I. et al.; Preparation of 3-Indazolyl Ethers with Cannabinoid and/or Cholinergic Properties Useful for Treating Various Diseases, Universidad Rey Juan Carlos, Spain, ES 2378139 (Oct 1, 2009), WO 2011039388 (Sep 30, 2010).
38. Dolles, D.; Nimczick, M.; Scheiner, M.; Ramler, J.; Stadtmüller, P.; Sawatzky, E., et al. Aminobenzimidazoles and Structural Isomers as Templates for Dual-Acting Butyrylcholinesterase Inhibitors and hCB₂R Ligands To Combat Neurodegenerative Disorders. *ChemMedChem* **2016**, *11*, 1270–1283.
39. Pagé, D.; Balaux, E.; Boisvert, L.; Liu, Z.; Milburn, C.; Tremblay, M., et al. Novel Benzimidazole Derivatives as Selective CB₂ Agonists. *Bioorg. Med. Chem. Lett.* **2008**, *18*, 3695–3700.
40. Bisi, A.; Gobbi, S.; Belluti, F.; Rampa, A. Design of Multifunctional Compounds for Cardiovascular Disease: From Natural Scaffolds to "Classical" Multitarget Approach. *Curr. Med. Chem.* **2013**, *20*, 1759–1782.

41. Goodfried, T. L.; Elliott, M. E.; Catt, K. J. Angiotensin Receptors and Their Antagonists. *N. Engl. J. Med.* **1996**, *334*, 1649–1654.
42. Rodríguez-Pascual, F.; Busnadiego, O.; Lagares, D.; Lamas, S. Role of Endothelin in the Cardiovascular System. *Pharm. Res.* **2011**, *63*, 463–472.
43. Murugesan, N.; Gu, Z.; Fadnis, L.; Tellew, J. E.; Baska, R. A. F.; Yang, Y., et al. Dual Angiotensin II and Endothelin A Receptor Antagonists: Synthesis of 2'-Substituted N-3-Isoxazolyl Biphenylsulfonamides with Improved Potency and Pharmacokinetics. *J. Med. Chem.* **2005**, *48*, 171–179.
44. Murugesan, N.; Tellew, J. E.; Gu, Z.; Kunst, B. L.; Fadnis, L.; Cornelius, L. A., et al. Discovery of N-isoxazolyl Biphenylsulfonamides as Potent Dual Angiotensin II and Endothelin A Receptor Antagonists. *J. Med. Chem.* **2002**, *45*, 3829–3835.
45. Benson, S. C.; Pershadsingh, H. A.; Ho, C. I.; Chittiboyina, A.; Desai, P.; Pravenec, M., et al. Identification of Telmisartan as a Unique Angiotensin II Receptor Antagonist with Selective PPAR {gamma}-modulating Activity. *Hypertension* **2004**, *43*, 993–1002.
46. Casimiro-Garcia, A.; Filzen, G. F.; Flynn, D.; Bigge, C. F.; Chen, J.; Davis, J. A., et al. Discovery of a Series of Imidazo[4,5-*b*]pyridines with Dual Activity at Angiotensin II Type 1 Receptor and Peroxisome Proliferator-Activated Receptor- γ . *J. Med. Chem.* **2011**, *54*, 4219–4233.
47. Casimiro-Garcia, A.; Bigge, C. F.; Davis, J. A.; Padalino, T.; Pulaski, J.; Ohren, J. F., et al. Synthesis and Evaluation of Novel α -heteroaryl-phenylpropanoic Acid Derivatives as PPAR α/γ Dual Agonists. *Bioorg. Med. Chem.* **2009**, *17*, 7113–7125.

Appendix II

Dolles, D.; Nimczick, M.; Scheiner, M.; Ramler, J.; Stadtmüller, P.; Sawatzky, E.; Drakopoulos, A.; Sotriffer, C.; Wittmann, H.-J.; Strasser, A.; Decker, M. Aminobenzimidazoles and Structural Isomers as Templates for Dual-Acting Butyrylcholinesterase Inhibitors and *h*CB₂R Ligands to Combat Neurodegenerative Disorders. *ChemMedChem* **2016**, *11*, 1270 – 1283.

Copyright (2016) Wiley-VCH Verlag GmbH & Co. KGaA, Weinheim. Reproduced with permission.

<http://onlinelibrary.wiley.com/doi/10.1002/cmdc.201500418/abstract>

SPECIAL
ISSUE

Aminobenzimidazoles and Structural Isomers as Templates for Dual-Acting Butyrylcholinesterase Inhibitors and *hCB₂R* Ligands To Combat Neurodegenerative Disorders

Dominik Dolles,^[a] Martin Nimczick,^[a] Matthias Scheiner,^[a] Jacqueline Ramler,^[a] Patricia Stadtmüller,^[a] Edgar Sawatzky,^[a] Antonios Drakopoulos,^[a] Christoph Sotriffer,^[a] Hans-Joachim Wittmann,^[b] Andrea Strasser,^[b] and Michael Decker^{*,[a]}

Dedicated to Professor John L. Neumeyer on the occasion of his 85th birthday.

A pharmacophore model for butyrylcholinesterase (BChE) inhibitors was applied to a human cannabinoid subtype 2 receptor (*hCB₂R*) agonist and verified it as a first-generation lead for respective dual-acting compounds. The design, synthesis, and pharmacological evaluation of various derivatives led to the identification of aminobenzimidazoles as second-generation leads with micro- or sub-micromolar activities at both targets and excellent selectivity over *hCB₁* and AChE, respectively. Computational studies of the first- and second-generation lead

structures by applying molecular dynamics (MD) on the active *hCB₂R* model, along with docking and MD on *hBChE*, has enabled an explanation of their binding profiles at the protein levels and opened the way for further optimization. Dual-acting compounds with “balanced” affinities and excellent selectivities could be obtained that represent leads for treatment of both cognitive and pathophysiological impairment occurring in neurodegenerative disorders.

Introduction

For a considerable number of diseases, drugs (and experimental therapeutics) are unavailable not only because the pathological causes are yet unknown, but because interaction and temporal sequence of the individual pathophysiological processes have not been elucidated. Many pathophysiological processes do not run consecutively, but in parallel and interdependently. Such diseases include idiopathic hypertension and neurodegenerative disorders, such as Parkinson's and Alzheimer's disease (AD). In AD, the interactions of β -amyloid (A β) plaque formation, τ -protein hyperphosphorylation, the formation and subsequent reactions of reactive oxygen species (ROS), and cell changes leading to irreversible loss of neurons, especially cholinergic neurons, are yet unsolved.^[1] It thus seems promising to address different processes simultaneously.^[2] Therefore, in recent years several approaches in medicinal

chemistry have emerged in which different biological and pharmacological activities are combined in a single experimental therapeutic: multipotent (also known as multitarget) compounds, hybrid molecules, and dual-active compounds.^[2,3] The majority of these approaches deals with “hybrids”, i.e., the combination of two distinct active molecules being covalently connected. Although the hybrid approach has been applied quite successfully, the combination of chemically fairly unchanged molecules by a molecular spacer leads to an increase in various molecular parameters which then violate Lipinski's “rule of five”,^[4] leading to decreased oral bioavailability and—of even higher importance for prospective central nervous system (CNS) drugs—to (putatively) massive decrease in penetration of the blood–brain barrier (BBB).^[3]

A solution of the above problem might be the development of “dual-acting” or “multitarget” compounds in which two biologically active molecules are “superimposed” or merged, so that the overall molar mass changes only slightly (“small molecules”), while activities at both targets are maintained.^[5,6] Because structure–activity relationships (SARs) might be (but do not have to be) different or even divergent at the targets to be addressed, this approach can be highly challenging and demands a considerable amount of synthetic work.^[7,8]

In the work presented herein we aimed to develop dual-acting butyrylcholinesterase (BChE) inhibitors with affinity at the human cannabinoid subtype 2 receptor (*hCB₂R*). The endocannabinoid system has been shown to modulate processes that already occur during the “silent” period of AD before cognitive decline, when neuroinflammation, oxidative stress, and mitochondrial dysfunction take place. *CB₂R*s are localized in

[a] D. Dolles, M. Nimczick, M. Scheiner, J. Ramler, P. Stadtmüller, E. Sawatzky, A. Drakopoulos, Prof. Dr. C. Sotriffer, Prof. Dr. M. Decker
Pharmaceutical and Medicinal Chemistry, Institute of Pharmacy and Food Chemistry, Julius-Maximilians-Universität Würzburg, Am Hubland, 97074 Würzburg (Germany)
E-mail: michael.decker@uni-wuerzburg.de

[b] Dr. H.-J. Wittmann, Dr. A. Strasser
Pharmaceutical and Medicinal Chemistry II, Institute of Pharmacy, University of Regensburg, 95053 Regensburg (Germany)

Supporting information for this article is available on the WWW under <http://dx.doi.org/10.1002/cmdc.201500418>: preparation and spectral characterization data of all novel compounds, details of biological evaluations, and additional information about computational studies.

SPECIAL
ISSUE

This article is part of a Special Issue on Polypharmacology and Multitarget Drugs. To view the complete issue, visit: <http://onlinelibrary.wiley.com/doi/10.1002/cmdc.v11.12/issuetoc>.

the immune system and modulate immune cell migration and cytokine release. Within the nervous system, CB₂R are located mainly in microglia. Pronounced overexpression of CB₂R and fatty acid amide hydrolase (FAAH) is observed in neuroinflammatory processes in the brain and specifically in glia cells that surround A β plaques.^[9] The expression level correlates well with the A β ₄₂ level and plaque formation, although not directly with cognitive status, indicating that pathogenic processes lead to CB₂R overexpression.^[10] It was shown that both selective CB₂R agonists (JWH-015 and JWH-133) and also unselective CB₁R/CB₂R agonists (D9-THC and HU-210) are able to protect neuronal cells against A β -induced neurotoxicity.^[11,12] Cognitive deficits in mice caused by injection of A β were ameliorated by the application of exogenous CB₂R agonists.^[13] The effect was more pronounced the earlier the agonists were applied in disease progression, demonstrating their neuroprotective and preventive character. The reason for this behavior is yet unknown. The effect of cannabinoids on A β processing is remarkable, as CB₂R-mediated activation of macrophages enables A β clearance,^[13] and it was shown that an endocannabinoid as well as a synthetic CBR agonist were able to cause A β clearance through the BBB.^[14] Neuroinflammation, first manifested in the activation of microglia cells, represents a core process in the irreversible decline of neurons in AD pathology.^[15] CB₂R are expressed in activated microglia. It was shown in several in vitro assays that CB₂R agonists decrease both the number of activated microglia cells surrounding A β plaques and the level of pro-inflammatory cytokines. The same effects were observed in two transgenic amyloid precursor protein (APP) mice models.^[16]

The three most important and currently approved drugs for symptomatic cognition improvement in AD patients are acetylcholinesterase (AChE) inhibitors. AChE inhibitors are only efficient in early disease stages, because the amount of AChE significantly decreases during disease development. It was shown that the amount of the second human cholinesterase, BChE, in AD brains does not decrease, as does AChE; moreover, BChE is able to compensate for the decreased function of AChE.^[17,18] This shows the potential of BChE inhibitors to stabilize cognitive decline in more advanced disease stages as well, either in addition to AChE inhibition or through selective BChE inhibition.^[19]

BChE also seems to play a direct role in cholinergic transmission, because it is found in neurons and proximal dendrites and it is overexpressed and co-localized with neuritic plaques and neurofibrillary tangles, the neuropathological hallmarks of AD.^[20] A very recent study using behavioral experiments with BChE knockout mice showed that these animals have enhanced learning abilities in memory tests, and after intracerebroventricular injection of A β _{25–35}, memory impairment was significantly attenuated.^[21] Whether these effects are mediated at the molecular level by classical BChE action is yet unclear. These findings, and the fact that the highly selective AChE inhibitor (–)-huperzine A does not show positive clinical evidence, makes BChE a promising molecular target in AD therapy.

Of particular relevance with regard to dual-acting BChE inhibitors and CB₂R ligands is the fact that activated glia cells, the target of potential application of CB₂R agonists in AD pharmacotherapy, are the source of BChE production.^[20,22] Therefore, dual-acting compounds may act in closely co-localized or even the same physiological compartments.

Multitarget-directed ligands, hybrid molecules and dual-acting compounds are of special importance for the potential therapy of neurodegenerative disorders.^[3,5,23,24] Over-synergistic effects can result with the use of these compounds, and they show one coherent pharmacokinetic profile, in contrast to the administration of two single substances. Both effects can result in an improved side-effect profile.^[3,25] In a dual-acting compound, pharmacophores for separate targets are formally merged and superimposed into one molecule (with therefore lower molar mass). A rational fragment-based approach for dual-active compounds acting on two enzymes was recently published.^[26] Development of dual-acting compounds is a challenging task because: 1) the successful combination of pharmacophores and their spatial relations must be maintained for both targets, 2) SARs for the improvement of affinity/activity and selectivity can be different or even divergent at the two targets, 3) in the case of successful combination, the biological activities of the molecule should be within similar concentration ranges, and 4) the resulting dual-acting compound should preferably optimize—or at least retain—the good ADME profile of the parent drugs.^[3,25] The concentrations necessary for activity at both targets depend on the occurrence and localization of the targets and must be addressed for each dual-acting compound. Because BChE and CB₂R are expressed in microglia cells and their environment, a similar concentration range seems advantageous.

Despite the difficulties, several dual-acting compounds have been specifically designed and developed. There are also several examples of dual-active compounds for which the dual-acting character was attributed only retrospectively. One of the few “rationally designed” examples combined enzyme-inhibiting properties (for monoamine oxidase B) with GPCR affinity and selectivity (antagonism at the adenosine A_{2A} receptor) by applying a 4*H*-3,1-benzothiazin-4-one scaffold.^[25,27] The authors achieved not only receptor subtype selectivity and selectivity toward MAO-B, but also affinity in the two-digit nanomolar range at both targets (“balanced affinity”), which is rarely reached due to the above described difficulties. In a second example, our research group was able to combine antagonism at the human histamine subtype 3 receptor (*h*H₃R) with ChE inhibition (Figure 1). After synthesis of a compound library, in vitro evaluations and computational studies, we were able to combine *h*H₃ antagonism and ChE inhibition into one “small molecule” by introduction of a common pharmacophore for

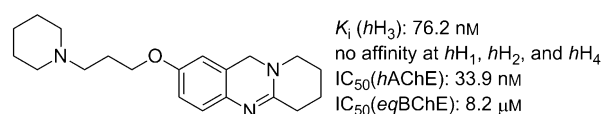


Figure 1. A dual-acting AChE inhibitor and selective *h*H₃ antagonist acting in the same concentration range.^[8]

*h*H₃ antagonists—the piperidinepropoxyphenyl group—into heterocyclic ChE inhibitors previously described by us^[8] (Figure 1).

Several preliminary efforts into the development of multifunctional CBR ligands have been described:^[28,29,30] In an initial work, the combination of a CB₁R antagonist with the AChE inhibitor tacrine in the form of a hybrid molecule was achieved.^[29] In a second work, CB₂R agonists with BChE-inhibitory properties were prepared and investigated. Although the best compounds showed only moderate affinities (mostly in the two-digit micromolar range),^[30] and selectivity at the CBRs and ChEs were not pronounced, this study has very valuable explorative character and is the first to achieve such a dual-acting compound.

Based on our previous work on the development of both reversible and irreversible heterocyclic BChE inhibitors,^[8,31,32] we investigated the structural requirements of a chemical structure for BChE inhibition:^[8,33,34] First, the condensation of a (substituted) aromatic system to a basic (N-containing) heterocycle (Figure 2), and second, connection to a sterically demanding hydrophobic moiety (the active center and surrounding area of BChE contain fewer aromatic residues than those of AChE and can therefore accommodate such moieties).^[33]

Our knowledge about the orientation of pharmacophores for BChE inhibitors led to the observation that the pharmacophore model also applies to: 1) the benzimidazole-based CB₂R agonist described by AstraZeneca^[35] (Figure 2) that we had used as parent ligand in the preparation of bivalent CB₂R li-

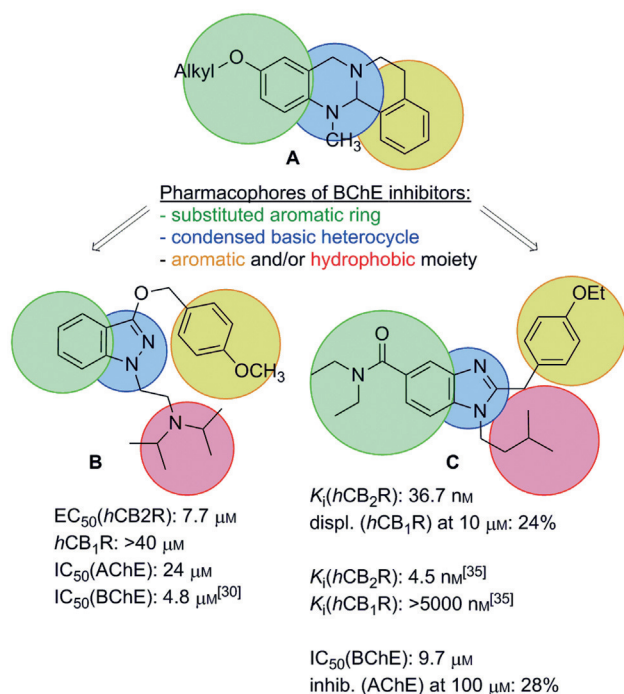


Figure 2. Simplified pharmacophore model (pharmacophores circled) of a prototypical competitive BChE inhibitor **A**^[31,32] and application of this model on a recently described dual-acting compound with an indazole ether scaffold (**B**)^[30] and on a CB₂R-selective ligand described by AstraZeneca (**C**)^[35]

gands,^[36] and 2) the dual-acting ligand described by González-Naranjo et al. (Figure 2).^[30] There was a recent report on (unselective) ChE inhibitors based on a benzimidazole core, adding further support to the hypothesis that such benzimidazoles might inhibit ChEs.^[37]

In this study we therefore examined the inhibition of both AChE and BChE by this CB₂R ligand. After verifying inhibition of BChE (see below), we conducted “dual” SAR studies, i.e., toward the two ChEs as well as toward both CBRs, modifying all core structural features of the molecule. Computational studies, including molecular docking and molecular dynamics (MD) simulations were performed to explain the interactions of the ligands with BChE, and to investigate the molecular requirements for binding and activation of the *h*CB₂R.

Results and Discussion

Chemistry

The difficult task in designing dual-active structures is to maintain affinity for *both* targets. For the benzimidazole derivative **1**, four possible structural changes were investigated (Figure 3): 1) Replacement of the diethylamide moiety with

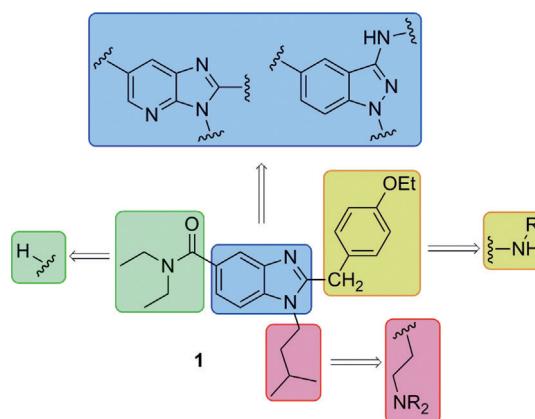


Figure 3. Structural changes to investigate SARs at AChE, BChE and CB₂R, CB₁R, respectively.

a hydrogen atom and therefore confirmation of its necessity as a CB₂R and BChE pharmacophore (highlighted in green); 2) introduction of a basic center into the hydrophobic alkyl chain attached to the imidazole nitrogen atom (highlighted in red); 3) modification of the structure of the moiety attached to the imidazole carbon atom (labeled in orange); and 4) alteration of the structure of the heterocycle (highlighted in blue).

The necessity of a diethylamide moiety for CB₂R affinity was previously demonstrated by Nimczick et al.,^[36] who replaced the amide moiety with an ethyl ester, resulting in complete loss of activity at CB₂R. In this work we therefore focused on a different set of variations, but checked whether this moiety is also necessary for BChE inhibition. The methylene unit of the benzyl moiety was replaced by an amino group. This change led to a more basic 2-aminobenzimidazole/guanidine system

(**16a**: predicted $pK_a=5.72$, experimentally determined $pK_a=6.08$; see Supporting Information). The introduction of this group might enable interaction with hydrogen-bond-donating as well as -accepting parts of the enzyme and receptor, and therefore we expected a higher BChE inhibitory potency and/or CB₂R affinity. With the aim to increase basicity/polarity the isopentyl alkyl chain (highlighted in red), it was changed into a more polar alkyl chain with a terminal amino function.

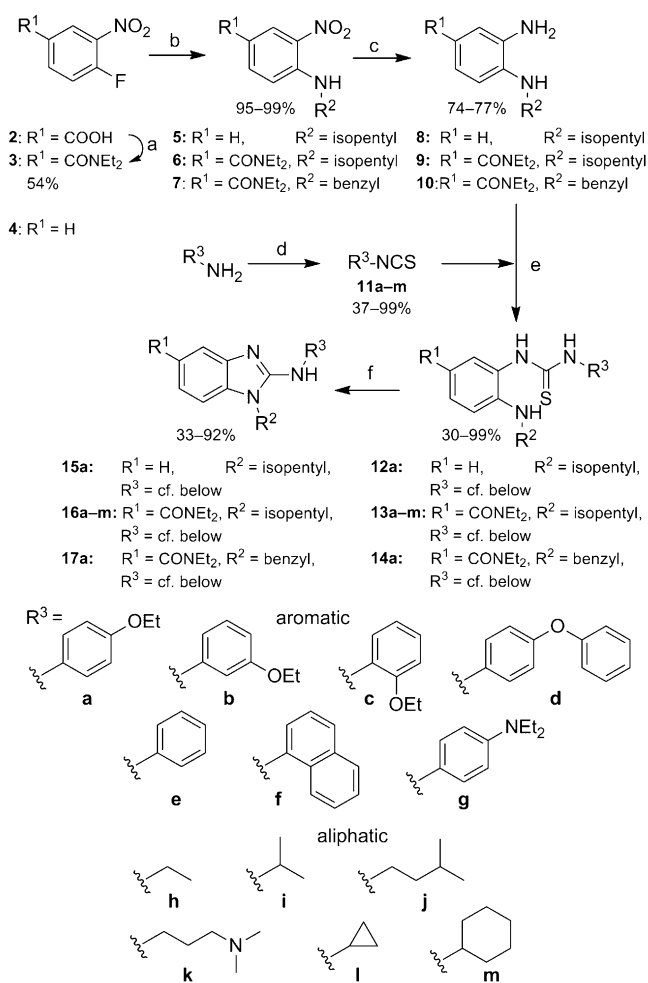
Of special interest was the change of the core heterocycle from a benzimidazole to an imidazopyridine or 3-aminoindazole as structural isomers of 2-aminobenzimidazole, since these heterocycles open the path to novel structural templates.

Based on these design strategies, the first step was to gain easy synthetic access to a set of 2-aminobenzimidazoles with a variety of substituents (aromatic, aliphatic, polar, nonpolar, sterically hindered, and non-hindered moieties). With these SAR variations it is possible to get further insight into both ligand–receptor and inhibitor–enzyme interactions.

For the synthesis of the 2-aminobenzimidazole, 4-fluoro-3-nitrobenzoic acid **2** (in the case of a diethylamide-substituted target structure) or 1-fluoro-2-nitrobenzene **4** (Scheme 1) were used as starting materials. To form the diethylamide compound **3**, 2-(1*H*-benzotriazol-1-yl)-1,1,3,3-tetramethyluronium hexafluorophosphate (HBTU) and diethylamine were used. In the next step, nucleophilic substitution with isopentylamine/benzylamine in ethanol afforded compounds **5–7**, respectively, in good yields. Reduction of the nitro group was carried out in two alternative ways, with Béchamp reaction conditions—using iron powder in acidic ethanol—giving higher yields, but making necessitating additional purification. Because of the tendency of *o*-phenylenediamines to oxidize and thus lead to instability, a different reduction method was chosen by using a tin(II) species.^[38] This method required longer reaction time and afforded lower yields than Béchamp reaction conditions, but provided higher purity without the need for further time-consuming chromatographic purification.

Özden et al.^[39] had synthesized 2-aminobenzimidazoles by the formation of a urea derivative, reacting the 1,2-diamino compounds with 1,1'-carbonyldiimidazole (CDI). In the next step the urea derivative was activated with phosphoryl chloride, and the resulting chloro compound was then substituted with the respective amine. Even after trying several reaction conditions (e.g., different solvent, reflux, or microwave conditions), in our case the desired product could not be obtained.

In an alternative reaction pathway, the 2-aminobenzimidazole core structure was synthesized using isothiocyanates. The required isothiocyanates **11a–m** were obtained by reacting the appropriate amine with carbon disulfide (dithiocarbamate intermediate) and Boc₂O in good yields.^[40] The resulting isothiocyanates **11a–m** were then reacted with diamines **8–10** to form thiourea derivatives **12a**, **13a–m**, and **14a**. For cyclization, various methods were investigated, such as mercury(II) salts, *N,N'*-dicyclohexylcarbodiimide (DCC) and 1-ethyl-3-(3-dimethylaminopropyl)carbodiimide (EDCI).^[41] Among these, only DCC and EDCI led to the desired target structures **15a**, **16a–m**, and **17a** (Scheme 1).

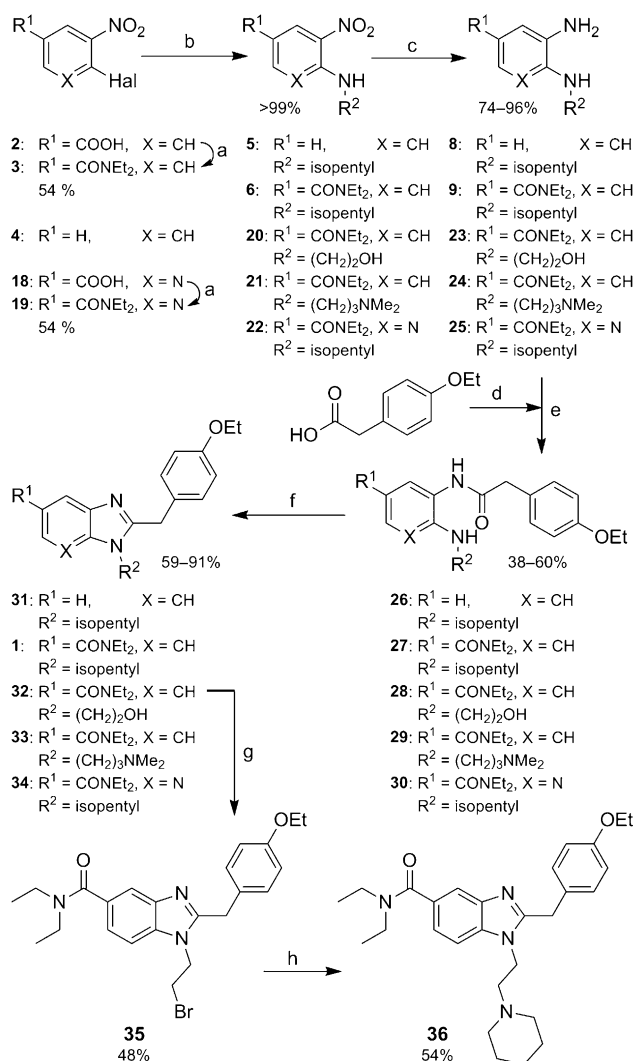


Scheme 1. Synthesis and list of 2-aminobenzimidazoles. *Reagents and conditions:* a) HBTU, HNEt₃, NEt₃, DMF, RT; b) isopentylamine or benzylamine, NEt₃, EtOH, 50 °C; c) SnCl₂·2H₂O, EtOH, reflux; d) CS₂, NEt₃, 0 °C → RT, then Boc₂O, DMAP, RT; e) THF, RT; f) EDCI·HCl, NEt₃, THF, 80 °C.

For modification of the alkyl chain (highlighted in red, Figure 3), the synthesis described by Pagé et al.^[35] was modified (see Scheme 2).

The initial three reaction steps were performed in the same manner as described in Scheme 1 to give the diamine compounds **8**, **9**, **23**, and **24** in high yields. For the formation of the acetamides **26–29**, 2-(4-ethoxyphenyl)acetic acid was activated with CDI and then reacted with the diamino compounds **8**, **9**, **23**, **24**. Cyclization to the benzimidazole core was performed in acetic acid under reflux, obtaining the target structures **1** and **31–33** in high yields. To get facile access to the amino-substituted alkyl chain in the lower part of the molecule, precursor **35** was synthesized in an Appel reaction from compound **32** using carbon tetrabromide and triphenylphosphine.^[42] In the last reaction step, the bromine atom was substituted with piperidine under basic conditions to obtain compound **36**.

Finally, the structure of the core heterocycle was altered. As variants, imidazopyridine and 3-aminoindazole structures were chosen which both represent structural isomers of the 2-ami-

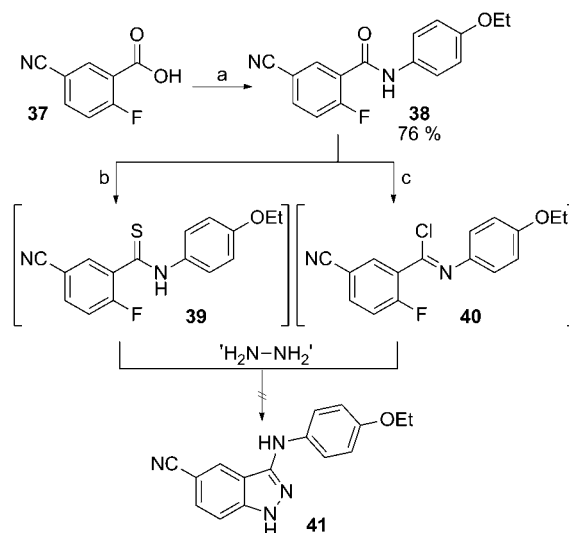


Scheme 2. Synthesis of benzimidazole and imidazopyridine derivatives. *Reagents and conditions:* a) HNEt₂, HBTU, NEt₃, DMF; b) isopentylamine/2-aminoethanol/*N,N'*-dimethylpropane-1,3-diamine, NEt₃, EtOH, 50 °C; c) SnCl₂·2H₂O, EtOH, 80 °C; d) CDI, THF, 50 °C; e) AcOH, 120 °C, g) CBr₄, PPh₃, THF, RT; h) piperidine, K₂CO₃, acetonitrile, 70 °C.

nobenzimidazole. The synthesis of the imidazopyridine was carried out in a manner analogous to that of the benzimidazole derivatives, by starting from 6-chloro-5-nitroindole-3-carboxylic acid **18**, which was first treated with diethylamine and HBTU to obtain compound **19**. Substitution with isopentylamine yielded compound **22**. The nitro moiety was then reduced with tin(II) chloride to the corresponding diamine **25**, which was treated with CDI-activated 2-(4-ethoxyphenyl)acetic acid to form compound **30**. In the final step, cyclization was performed in acetic acid at reflux to obtain target structure **34** (Scheme 2).

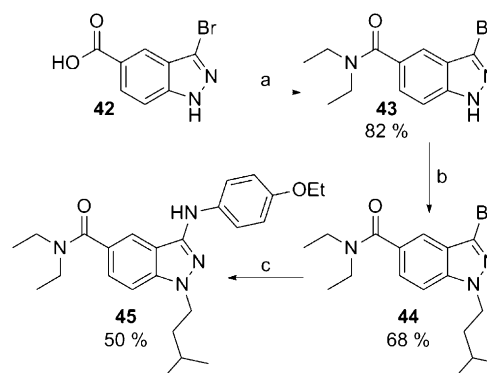
The first approach for the synthesis of the indazole derivative **45** was carried out according to Burke et al.^[43] Starting from 5-cyano-2-fluorobenzoic acid **37**, amide **38** was synthesized in good yield with HBTU and *p*-phenethidine. To activate the carbonyl moiety, thioamide **39** was used as an intermediate which was prepared by applying Lawesson's reagent. By adding hydrazine, cyclization was expected to take place, but

indazole derivative **41** could not be obtained this way. In another synthetic approach, amide **38** was activated by refluxing in phosphoryl chloride to form the imidoyl chloride **40** as intermediate. As in the first synthetic pathway, hydrazine was added to obtain the indazole derivative **41**. Again, this method did not provide the desired product (Scheme 3).



Scheme 3. Synthetic pathway for the formation of a 3-aminoindazole derivative. *Reagents and conditions:* a) *p*-phenethidine, HBTU, NEt₃, DMF, RT; b) Lawesson's reagent, toluene, 120 °C; c) POCl₃, 120 °C.

Ultimately, the synthesis of the indazole derivative then started from 3-bromo-1*H*-indazole-5-carboxylic acid **42** (Scheme 4), which was first treated with diethylamine and HBTU to form amide **43**. Alkylation was performed under basic conditions using isopentyl bromide to obtain compound **44** in 68% yield. In a last reaction step, a Buchwald–Hartwig cross-coupling^[44] was performed using palladium(II) acetate, xantphos, and *p*-phenethidine to obtain target structure **45** in 50% yield.



Scheme 4. Synthesis of indazole **45**. *Reagents and conditions:* a) HNEt₂, HBTU, NEt₃, DMF, RT; b) isopentyl bromide, NaH, DMF, 0 °C → RT; c) *p*-phenethidine, Pd(OAc)₂, xantphos, Cs₂CO₃, dioxane, reflux.

Inhibition of cholinesterases

All target compounds were tested for their ability to inhibit acetylcholinesterase (*ee*AChE, EC.3.1.1.7 from electric eel) and butyrylcholinesterase (*eq*BChE, EC.3.1.1.8 from equine serum) (Table 1). Sequence alignment had shown that both isoforms exhibit very high sequence homology to the human enzymes (88 and 84% sequence identity, respectively).^[33]

In the initial step, the inhibitory effect of the lead structure **1** was determined at both ChEs, yielding $IC_{50}(\text{BChE})=9.7\ \mu\text{M}$ and $IC_{50}(\text{AChE})>100\ \mu\text{M}$ (Table 1). This confirmed our initial assumption that compound **1** is a suitable lead structure for dual-acting compounds with desired selectivity, but with moderate inhibitory activity at BChE and “unbalanced” affinity profiles. Starting from this point, the 2-aminobenzimidazole derivatives **15a**, **16a–16m**, and **17a** were synthesized. Compound **16a**, being most similar to the lead structure **1**, already shows a 13-fold increased inhibitory effect and high selectivity for BChE ($IC_{50}(\text{BChE})=0.7\ \mu\text{M}$; Table 1); *para*-substitution of the benzene ring is necessary to maintain sub-micromolar inhibitory activity (cf. **16b**: $IC_{50}(\text{BChE})=9.1\ \mu\text{M}$ and **16c**: $IC_{50}(\text{BChE})=8.9\ \mu\text{M}$). Replacing the ethoxy group with other electron-donating groups such as phenoxy (**16d**) or diethylamine (**16g**) moieties, inhibition and selectivity were kept in the same range or even slightly increased (**16d** $IC_{50}(\text{BChE})=3.7\ \mu\text{M}$ and **16g** $IC_{50}(\text{BChE})=0.24\ \mu\text{M}$; Table 1). Replacement of the (substituted) phenyl group with an alkyl substituent (cyclic and linear) resulted in a decrease of inhibition. Just by adding a terminal amine to the alkyl chain, inhibition could be preserved, albeit at the cost of selectivity over AChE (**16k**: $IC_{50}(\text{BChE})=1.0\ \mu\text{M}$; Table 1). Structural isomers, i.e., using the aminoindazole core, resulted in almost complete loss of inhibitory activity. Modifications of the alkyl chain at position 1 of the benzimidazole core (**36**: $IC_{50}(\text{BChE})=2.3\ \mu\text{M}$) led to a slightly increased inhibitory effect (compared with first-generation lead structure **1**). Taken together, apart from the inactive structural isomers, all benzimidazoles and aminobenzimidazoles prepared inhibit BChE in the sub-micromolar to two-digit micromolar range with good to excellent selectivity over AChE.

Radioligand binding studies at *hCB₁R* and *hCB₂R*

All compounds were tested for affinity to *hCB₁R* and *hCB₂R* in radioligand binding studies (either HEK cells stably expressing *hCB₂R*, or CHO cells stably expressing *hCB₁R*; see the Experimental Section below for details). Lead structure **1** is an optimized *CB₂R* ligand from an AstraZeneca drug development program, and we therefore regarded it as the gold standard in terms of affinity [$K_i(\text{hCB}_2\text{R})=37\ \text{nM}$ in our tests] and selectivity over *hCB₁R* [24% replacement (*hCB₁R*) of radioligand at $10\ \mu\text{M}$] for the compounds described in this work. For compound **1** an $EC_{50}(\text{hCB}_2\text{R})$ of $2.9\ \text{nM}$ had been determined in a GTP γ S assay.^[35] This value is higher than that observed in our radioligand binding studies, which we had observed before. This might be due to the different test system applied and/or the equilibrium conditions used.^[36]

In the first set of compounds the methylene group of the lead was replaced with an amino moiety (2-aminobenzimidazoles). Compound **16a** shows the highest similarity to lead structure **1**. Although a significant loss of affinity was observed for compound **16a**, it still shows high selectivity and moderate affinity ($K_i(\text{hCB}_2\text{R})=1.9\ \mu\text{M}$; Table 1). Comparing the donor-substituted compound **16a** to the unsubstituted compound **16e** (12% displacement at $10\ \mu\text{M}$, being ~30-fold less active) shows the necessity of an electron-donating substituent. Varying the position of the ethoxy group around the phenyl ring showed the importance of *para* substitution, as a complete loss of affinity in case of the *meta* position (**16b**: 17% displacement at $10\ \mu\text{M}$) and a 4-fold lower affinity of the *ortho*-substituted phenyl ring compound (**16c**: $6.6\ \mu\text{M}$) was observed (Table 1). Exchange to different donor substituents leads to compounds with roughly the same affinity and selectivity as for a diethylamine moiety **16g** ($8.1\ \mu\text{M}$) or even increased affinity for the *para*-phenoxy compound **16d** ($0.4\ \mu\text{M}$), but with lower selectivity. Replacement of the aromatic with an alkyl system (cyclic and acyclic, **16h–16m**) led to decreased affinity (in the two-digit micromolar range; Table 1). In a second set of compounds, structural isomers of the 2-aminobenzimidazoles were synthesized and evaluated. Here, the imidazopyridine **34** shows a 15-fold increased affinity ($K_i(\text{hCB}_2\text{R})=127\ \text{nM}$) relative to **16a**, again with high selectivity over the *hCB₁R*. In contrast, the structural change to the 3-aminoindazole scaffold resulted in a complete loss of affinity for *hCB₂R*. In the third set, modifications to the alkyl chain at position 1 of the benzimidazole core were performed, giving access to compounds **33** and **36**, which are both substituted with terminal amines instead of the isopentyl chain. Compared with lead structure **1**, both structures show decreased affinity for *hCB₂R* ($K_i(\text{hCB}_2\text{R})=577\ \text{nM}$ for **33** and $K_i(\text{hCB}_2\text{R})=188\ \text{nM}$ for **36**), but a 5- to 10-fold increased affinity with respect to the 2-aminobenzimidazole structures (Table 1).

Taken together, nearly all compounds prepared lack any affinity for *hCB₁R* and therefore maintain selectivity with affinity ranging from $127\ \text{nM}$ (**34**) to $26\ \mu\text{M}$ (**31**). There are two inactive compounds: **15a** and **40**. The highest-affinity compound **34** is 4-fold less active than the lead structure **1**. The amino benzimidazoles show micromolar to sub-micromolar affinities (still with high selectivity over *hCB₁R*).

For correlating the results of the SARs obtained at BChE to those at *CB₂R*, the pIC_{50} and pK_i values at each target were plotted in the graph shown as Figure 4. Interpretation is simplified by the fact that the majority of compounds still show high selectivity over both AChE and *hCB₁R*.

Compound **31** (which is very similar to the lead structure **1**, but lacks the diethylamide moiety) shows no inhibitory effect at both ChEs, whereas the respective amino benzimidazole compound **15a** shows a significant inhibitory effect at BChE ($IC_{50}=4.2\ \mu\text{M}$). The importance of the diethylamide moiety for BChE inhibition is therefore pronounced (see Molecular Docking section below). Both compounds have lower (**31**: $K_i(\text{hCB}_2\text{R})=26.0\ \mu\text{M}$) or no affinity (**15a**) for the *CB₂R* than lead structure **1**.

Table 1. Results of biological evaluations of the inhibitory effects of AChE/BChE and radioligand binding studies at hCB_1R/hCB_2R .

Compd	X	Y	R ¹	R ²	R ³	IC ₅₀ (pIC ₅₀ ± SD) or Inhibition [%]		K _i (pIC ₅₀ ± SD) or [³ H]CP55,940 displ. @ 10 μM	
						BChE ^[a]	AChE ^[b]	hCB_2R ^[c]	hCB_1R ^[d]
tacrine						3.3 nM ^[45] (8.5 ± 0.1)	15.6 nM ^[45] (7.8 ± 0.1)	ND	ND
rimonabant						ND	ND	4.0%	143.0 nM (6.8 ± 0.1) 25.0 nM ^[46]
SR-144,528						ND	ND	19.7 nM (7.7 ± 0.1) 5.6 nM ^[47]	687.0 nM (6.1 ± 0.1) 254.0 nM ^[47]
1	CH	CH ₂	CONEt ₂			9.7 μM (5.0 ± 0.1)	28% @ 100 μM	36.7 nM (7.4 ± 0.1) 4.5 nM ^[35]	24% > 5 μM ^[35]
15a	CH	NH	H			4.2 μM (5.4 ± 0.1)	24% @ 10 μM	10%	4%
16a	CH	NH	CONEt ₂			0.7 μM (6.2 ± 0.0)	4% @ 100 μM	1.91 μM (5.7 ± 0.1)	13%
16b	CH	NH	CONEt ₂			9.1 μM (6.2 ± 0.2)	< 2% @ 10 μM	14%	8%
16c	CH	NH	CONEt ₂			8.9 μM (5.1 ± 0.1)	10% @ 10 μM	6.7 μM (5.1 ± 0.2)	4%
16d	CH	NH	CONEt ₂			3.7 μM (5.7 ± 0.3)	2% @ 10 μM	426.0 nM (6.3 ± 0.2)	45%
16e	CH	NH	CONEt ₂			7.2 μM (5.1 ± 0.1)	11% @ 100 μM	12%	21%
16f	CH	NH	CONEt ₂			4.5 μM (5.4 ± 0.1)	19% @ 25 μM	23%	17%
16g	CH	NH	CONEt ₂			0.2 μM (6.7 ± 0.1)	10% @ 10 μM	8.1 μM (5.1 ± 0.1)	4%
16h	CH	NH	CONEt ₂			20.1 μM (4.7 ± 0.1)	< 2% @ 10 μM	10.9 μM (4.9 ± 0.2)	2%
16i	CH	NH	CONEt ₂			15.5 μM (4.9 ± 0.1)	6% @ 100 μM	32%	12%
16j	CH	NH	CONEt ₂			5.1 μM (5.3 ± 0.1)	18% @ 100 μM	7.0 μM (5.1 ± 0.1)	12%
16k	CH	NH	CONEt ₂			1.0 μM (6.0 ± 0.1)	58% @ 100 μM	16%	7%
16l	CH	NH	CONEt ₂			27.4 μM (4.6 ± 0.1)	31% @ 100 μM	16%	2%
16m	CH	NH	CONEt ₂			5.7 μM (5.3 ± 0.1)	19% @ 100 μM	35%	4%
17a	CH	NH	CONEt ₂			4.1 μM (5.4 ± 0.1)	8% @ 100 μM	37%	9%
31	CH	CH ₂	H			25% @ 10 μM	< 2% @ 10 μM	26.0 μM (4.6 ± 0.1)	15%
33	CH	CH ₂	CONEt ₂			36.3 μM (4.4 ± 0.1)	55% @ 100 μM	577.0 nM (6.2 ± 0.1)	7%
34	N	CH ₂	CONEt ₂			39% @ 10 μM	7% @ 10 μM	127.0 nM (6.9 ± 0.1)	13%

Compd	X	Y	R ¹	R ²	R ³	IC ₅₀ (pIC ₅₀ ± SD) or Inhibition [%]		K _i (pIC ₅₀ ± SD) or [³ H]CP 55,940 displ. @ 10 μM							
						BChE ^[a]	AChE ^[b]	hCB ₂ R ^[c]	hCB ₁ R ^[d]						
36	CH	CH ₂	CONEt ₂			2.3 μM (5.6 ± 0.1)	48 % @ 100 μM	188.0 nM (6.7 ± 0.1)	14 %						
						45	CH	NH	CONEt ₂			26 % @ 10 μM	5 % @ 10 μM	11 %	47 %

[a] Values are the mean of at least three determinations; BChE from equine serum. [b] Values are the mean of at least three determinations; AChE from electric eel. [c] Screened on membranes of HEK cells stably expressing hCB₂R, with test compound concentration at 10 μM; values are the mean of at least two independent experiments performed in triplicate. K_i values were determined when the displacement of [³H]CP 55,940 was > 50%; mean values of at least two independent experiments performed in triplicate. [d] Screened on membranes of CHO cells stably expressing hCB₁R, with test compound concentration at 10 μM; values are the mean of at least two independent experiments performed in triplicate. K_i values were determined when the displacement of [³H]CP 55,940 was > 50%; mean values of at least two independent experiments. ND: not determined.

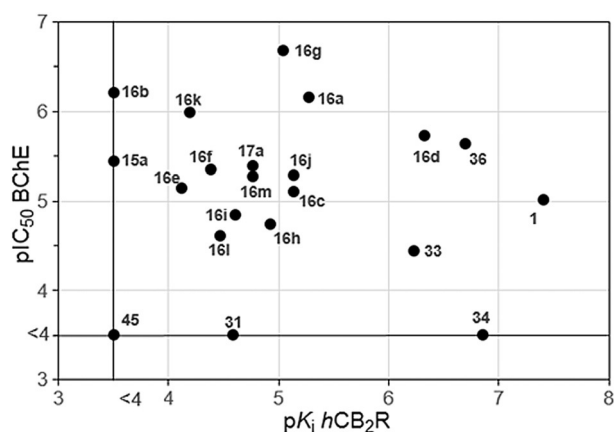


Figure 4. Plot of pIC₅₀ values for BChE inhibition against pK_i values of hCB₂R affinity. Compounds with no significant affinity for one of the targets are placed on the two black lines.

An aromatic system (attached at the 2-position of the 2-aminobenzimidazole or benzimidazole core) is necessary for dual activity. While compounds **16a–16g** have balanced activities regarding both targets, alicyclic compounds **16h–16m** lack these activities.

The piperidine-substituted benzimidazole compound **36** shows potential as a future lead structure for the intended dual-activity due to its micromolar-level inhibition of BChE (IC₅₀ = 2.3 μM) and high affinity for CB₂R (K_i(hCB₂R) = 188.0 nM) (Figure 4). To rationalize the findings with regard to the 3D structures of the targets, computational studies were performed.

Molecular dynamics simulations at the hCB₂R

Construction of the active-state model of hCB₂R

The crystal structure of the active human β₂ adrenergic receptor (PDB ID: 3SN6)^[48] was used as a template to construct the active-state conformation of hCB₂R. For alignment of the amino acid sequences between hβ₂R and hCB₂R, the most conserved residue of each transmembrane (TM) domain according to Ballesteros and Weinstein^[49] was used as reference for all TM helices except TM V, because here, the highly conserved proline is not present in the hCB₂R. Two different sequence alignments for TM V with the hβ₂R as reference have been described.^[50,51] Because there is no information given as to which alignment leads to the better model, in the present study both models of hCB₂R regarding TM V were generated (Figure 5).

Lysozyme, the camelid antibody VHH fragment, and the Gβ and Gγ subunits were deleted. Only the last 20 amino acids of the C terminus of the Gα_s subunit were modelled and mutated into the corresponding amino acids of the Gα_{i/o} subunit. The N terminus of the receptor, which is missing in the crystal structure, was added using the SYBYL 7.0 software package (Tripos Inc.). To obtain an acceptable starting conformation of the N terminus, a short gas-phase MD simulation of the N terminus, by fixing the remaining part of the receptor, was performed with SYBYL 7.0. The “Loop-Search” module of SYBYL 7.0 was used to adopt/complete the E1-, E2-, E3-, I1-, and I3-loops. The last amino acid of the C terminus of the hCB₂R was Leu³¹⁴. Because internal water molecules are suggested to be important for stabilization or activation of family A GPCRs,^[52,53] these internal water molecules were included into the model of active hCB₂R. Compound **1** was docked manually into the binding pocket of both hCB₂R models between TMs III, V, and VI in an analogous manner, using SYBYL 7.0. Several docking poses of **1** were applied by rotation of the ligand or by changing the dihedral angles of rotatable bonds, and an-

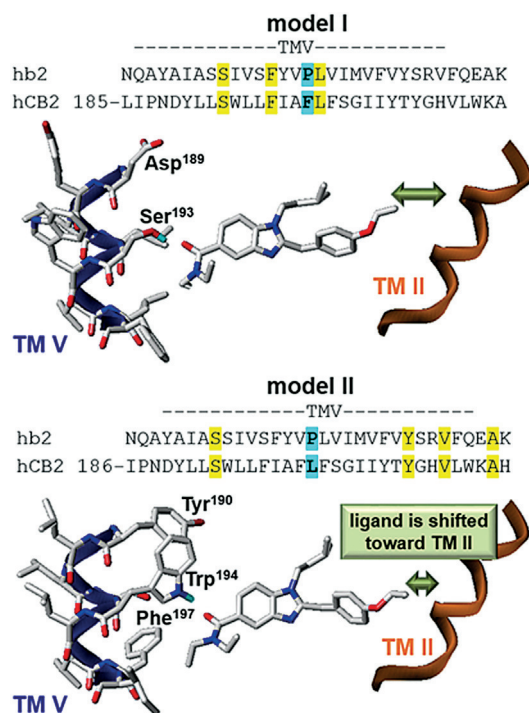


Figure 5. Two different homology models I and II of *hCB₂R* based on two different alignments of TM V with ligand **1** bound to the orthosteric binding site.

alyzed with regard to the best ligand–receptor interaction energy. However, only one ligand–receptor complex was favored with respect to the ligand–receptor interaction energy: Here, the amide moiety was located near Thr^{3.33}, and the phenylene moiety was embedded in an aromatic pocket formed by Phe^{2.57}, Phe^{2.61}, Phe^{2.64}, and Phe¹⁸³ (E2-loop). The lipophilic isopentyl side chain points to the extracellular surface of the *hCB₂R*. The resulting complexes were energetically minimized with SYBYL 7.0 and afterward embedded in a POPC lipid bilayer. Intracellular and extracellular water molecules, as well as five sodium and 12 chloride ions to achieve electroneutrality, were added into the simulation box (7.2×7.2×9.5 nm) using the commands *genbox* and *genion* of the GROMACS 4.0.2 software package (www.gromacs.org). The parameterization for ligands **1** and **16a** was obtained from the PRODRG server (davapc1.bioch.dundee.ac.uk/prodrg/). After minimization of the simulation box with GROMACS 4.0.2, MD simulations (5 ns equilibration phase and 10 ns productive phase) were performed as previously described.^[54,55]

Binding mode of compounds **1** and **16a** at *hCB₂R*

In the case of the active *hCB₂R* model I based on the alignment by Cichero et al.^[51] (Figure 5), ligand **1** remained unstable during the MD simulation, and no hydrogen bond interactions between ligand and receptor were observed. The hydrogen bond between Ser¹⁹³ and **1**, present in the starting structure, disappeared during an early stage of the MD simulation. In contrast, analogous simulations of **1** based on the active *hCB₂R*

model II (Figure 5) based on the alignment of Bramblett et al.^[50] revealed a stable binding mode during the whole productive phase (Figure 6a).

Two stable hydrogen bonds between **1** and the receptor were observed (Figures 6b and 7): The oxygen atom of the amide moiety formed hydrogen bonds with the hydrogen atom of Thr^{3.33} and Trp^{5.43} (Supporting Information Figure 16). At a small number of time steps, an additional hydrogen bond between the oxygen atom of the ethoxy moiety and Ser^{7.39} was observed. Further stabilization of the ligand in the binding pocket was achieved by binding of the phenylene moiety into an aromatic pocket formed by Phe^{2.57}, Phe^{2.61}, Phe^{2.64}, and Phe¹⁸³ (E2-loop). In particular, Phe¹⁸³ (E2-loop) was observed to establish a stacked aromatic interaction with the phenyl moiety of **1** during long periods of the entire simulation (Figure 6b).

MD simulation of **16a**, docked analogously to **1** at the *hCB₂R* (model II), led to a stable binding conformation, which, in contrast to the binding mode of **1**, showed significant differences: For **16a**, only one stable hydrogen bond between the oxygen atom of the amide moiety and Thr^{3.33} was observed, whereas the hydrogen bond between the amide oxygen atom and Trp^{5.43} was completely lost (Figure 7, Figure 8a and 8b, and Supporting Information Figure 17).

In contrast to **1**, the NH group of Trp^{5.43} forms a stable hydrogen bond interaction with the oxygen atom of the Thr^{3.33} side chain (Figure 6b and Figure 8a and 8b). Furthermore, the stacked aromatic interaction between the phenylene moiety

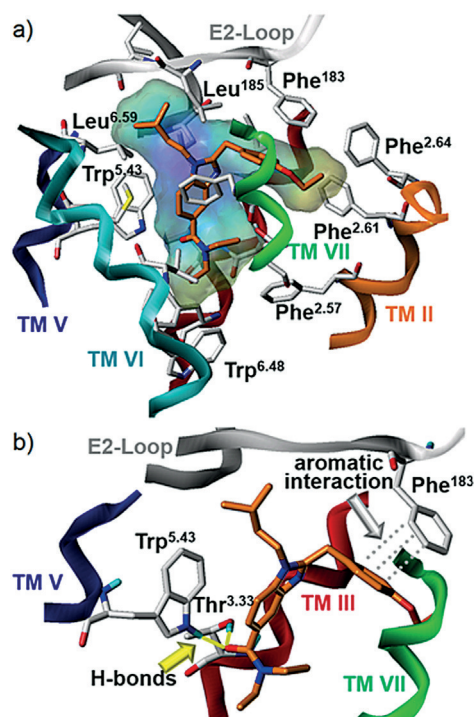


Figure 6. A representative snapshot of **1** in the binding pocket of *hCB₂R* based on MD simulation. a) The most important amino acids forming the binding pocket are shown. b) Hydrogen bonds between Thr^{3.33} or Trp^{5.43} and **1** (yellow lines) and stacked aromatic interaction between Phe¹⁸³ (E2-loop) and the phenylene moiety of **1** (grey dashed lines).

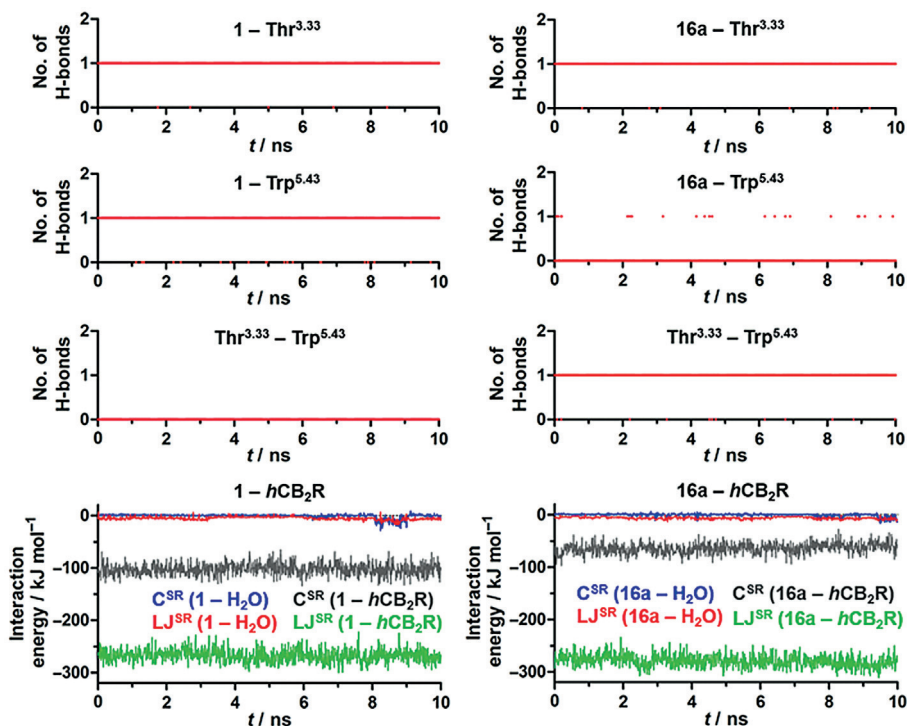


Figure 7. Number of hydrogen bonds between 1 or 16a and Thr^{3.33} or Trp^{5.43}. Interaction energies (short-range Coulomb (C^{SR}) and short-range Lennard-Jones (L^{JSR}), calculated with *g_energy* of GROMACS 4.0.2) between 1 or 16a and the hCB₂R.

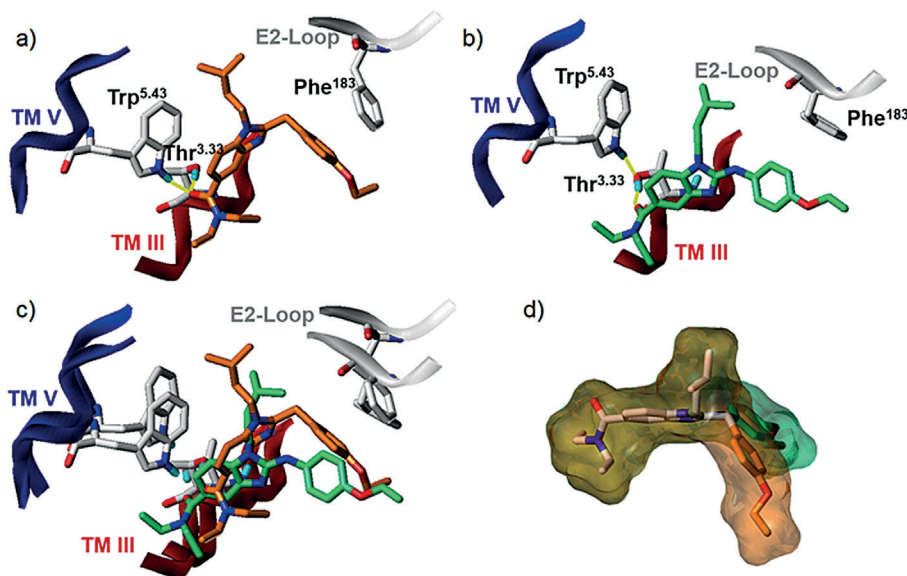


Figure 8. Binding conformation of 1 and 16a in the binding site of hCB₂R. a) Binding conformation of 1, b) binding conformation of 16a, c) overlay of the binding conformation of 1 and 16a in the binding site of hCB₂R, and d) overlay of the energetically preferred conformation of 1 and 16a in the gas phase.

and Phe¹⁸³, as observed for 1, is completely lost (Figure 8a and 8b). During the whole simulation, no interaction of the oxygen atom of the ethoxy moiety or the NH group with the receptor was observed.

Binding of compounds 1 and 16a to hCB₂R

MD studies revealed that 1 and 16a are bound similarly in a pocket between TM III, TM V, and TM VI, as described earlier for other cannabinoid receptor ligands at the CB₁R and CB₂R.^[56–59] Residues Phe^{2.61}, Lys^{3.28}, Thr^{3.33}, Phe^{3.36}, Tyr^{5.39}, Trp^{5.43}, Leu^{6.51}, Asp^{6.58}, Phe^{7.35}, and Ser^{7.39} are the most important amino

acids forming the binding pocket for CP 55,940.^[59] Besides lipophilic ligand–receptor interactions, hydrogen bonds between the ligand CP 55,940 and Lys³²⁸ and Asp⁶⁵⁸ lead to additional stabilization.^[59] However, in contrast to the present study, Trp⁵⁴³ points downward to the intracellular side.^[59]

Experimental data show that the affinity of **1** for *hCB₂R* is about two orders of magnitude higher than that of **16a** (Table 1). As the simulations indicate, the number of hydrogen bonds between **16a** and *hCB₂R* decreased relative to **1** and *hCB₂R* (Figure 7). Furthermore, the aromatic interaction between the phenylene moiety and Phe¹⁸³ in the case of **16a** is reduced (Figure 8a–c). These changes in binding mode are caused by the different electronic behavior of the CH₂ moiety in **1** and the NH moiety in **16a**. Because of the presence of the lone electron pair in the latter, the ligand exhibits a nearly planar conformation of the benzimidazol-2-amine partial structure, indicated by the H–N vector, which is ~30° out of the plane, formed by the hydrogen atom and the two directly attached carbon atoms. In the case of **1**, the analogous carbon atom shows an sp³ hybridization state; therefore, the energetically preferred conformation shows a kink (Figure 8c,d) and thus fits better into the binding pocket of *hCB₂R*. These structural observations are supported by the ligand–receptor interaction energies, which are ~26 kJ mol⁻¹ more favored for **1** (Figure 7). As already pointed out, the hydrogen bonds between the amide moiety of **1** and *hCB₂R* are suggested to be essential for the high affinity of this compound for *hCB₂R*. This is supported by the experimental results presented herein, because for compound **31**, without this amide moiety, the affinity decreased about three orders of magnitude (Table 1).

Molecular docking and MD with hBChE

The catalytic active sites (CAS) of BChE and AChE consist of the residues Ser¹⁹⁸, His⁴³⁸, Glu³²⁵ and Ser²⁰⁰, His⁴⁴⁰, and Glu³²⁷, respectively. These amino acids comprise the catalytic triad and form gorges of 20 Å depth.^[60–63] The binding pocket in BChE is comprised by Leu²⁸⁶ and Val²⁸⁸ in the catalytic triad vicinity, whereas in AChE the equivalent residues are Phe²⁸⁸ and Phe²⁹⁰ (residue numbers from *Torpedo californica* AChE). Other important residues involved in choline hydrolysis in BChE are Trp⁸² and Ala³²⁸. In AChE, this tryptophan is conserved (Trp⁸⁴), whereas the alanine is replaced by Phe³³⁰.^[64] Near the choline binding site of BChE, highly conserved N–H dipoles from Ala¹⁹⁹, Gly¹¹⁶, Gly¹¹⁷ form an oxyanion hole. In the BChE active site, six out of the fourteen bulky aromatic amino acid residues in AChE (Tyr⁷², Tyr¹²⁴, Trp²⁸⁶, Phe²⁹⁵, Phe²⁹⁷, and Tyr³³⁷) are replaced with aliphatic residues (Asn⁶⁸, Gln¹¹⁹, Ala²⁷⁷, Leu²⁸⁶, Val²⁸⁸, and Ala³²⁸). This results in an active site gorge for BChE 200 Å³ larger than that of AChE.^[65] Overall, these differences explain enzyme-specific ligand binding to AChE and BChE.^[66]

Computational docking studies were carried out with GOLD^[67] to investigate the binding mode of aminobenzimidazole **16a** and benzimidazole **1** in BChE. A common cluster of docking poses highly ranked by the DSX scoring function^[68] was obtained for both ligands (rank 1, 3, 6, 9 poses of ligand **1**, and rank 2, 3, 6, 7 poses of ligand **16a**), in agreement with

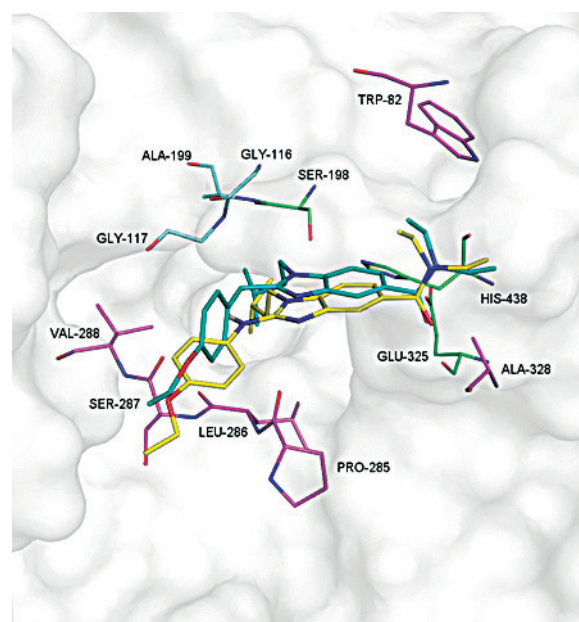


Figure 9. Docking poses of ligand **1** (turquoise) and **16a** (yellow) in the CAS of BChE.

the expectation that these two structurally very similar ligands should exhibit a similar binding mode. As depicted in Figure 9, the aforementioned binding mode suggests that the two ligands are placed near the CAS (residues in green), while their amide groups point toward Ala³²⁸. The isopentyl group of the ligands points toward the residues of the oxyanion hole (residues in light blue), and the ethoxy scaffold is near Leu²⁸⁶ and Val²⁸⁸.

This binding mode suggests that the most important difference between the two ligands is a polar interaction between the backbone carbonyl oxygen atom of Ser²⁸⁷ and the anilinic NH group of ligand **16a**. The lack of this group in ligand **1** can explain its decreased potency compared to ligand **16a**. Furthermore, replacement of the anilinic NH group with a benzylic methylene group in ligand **1** results in a more acute bond angle for the latter.

In a further step, MD simulations using the aforementioned docking poses were carried out to determine whether the proposed binding mode obtained by docking is truly plausible. The MD of ligand **16a** shows that indeed the anilinic NH remains in close proximity to the carbonyl oxygen atom of Ser²⁸⁷ throughout the simulation (Figure 10). A hydrogen bond is formed between the two moieties with an occupancy of 62.3%, interrupted occasionally by a switch of the NH group to the neighboring carbonyl oxygen of Pro²⁸⁵ forming a hydrogen bond with an occupancy of 6.3% (Supporting Information Figures 11 and 12). In addition, polar interactions occur between the N2 of the benzimidazole ring and the NH₂ of the Gln¹¹⁹ side chain (hydrogen bond occupancy: 14.4%; see Supporting Information Figure 10). The aforementioned interactions of the ligand with the protein, primarily those with Ser²⁸⁷, Pro²⁸⁵, and Gln¹¹⁹, result in stabilization of the ligand in its binding mode (Supporting Information Figure 14) after an initial

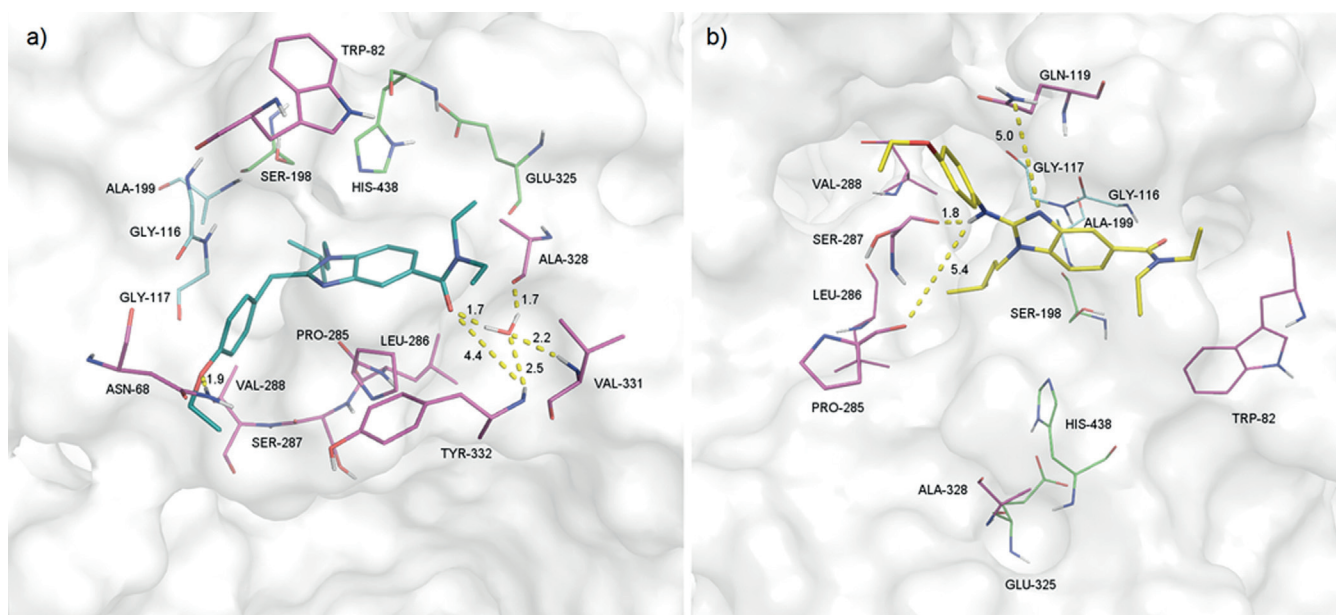


Figure 10. a) Binding mode of **1** as observed in the last snapshot of the MD simulation in BChE; interactions of the amide function with a water molecule and Tyr³³², Val³³¹, Ala³²⁸, and the interaction of the ether moiety with Asn⁶⁸ are highlighted. b) Binding mode of **16a** as observed in the last snapshot of the MD simulation in BChE; interactions of the anilinic nitrogen atom with Ser²⁸⁷ and Pro²⁸⁵ of the benzimidazole nitrogen with Gln¹¹⁹ are highlighted.

slight drift from the starting pose, depicted by an RMSD of 2.19 ± 0.40 Å of the benzimidazole scaffold over the entire simulation (Supporting Information Figure 13).

Because it cannot form the critical polar interaction with Ser²⁸⁷ or Pro²⁸⁵, ligand **1** should be more prone to drift inside the cavity than ligand **16a**. Indeed, the RMSD of the benzimidazole scaffold is 3.54 ± 0.52 Å (Supporting Information Figure 9). The most important polar interaction at the beginning of the MD is between the phenolic OH group of Tyr³³² and the amide oxygen atom of the ligand, which takes place from the beginning of the simulation until 5.5 ns (Supporting Information Figure 6). At this point a conformational change takes place in the protein, causing Tyr³³² to flip. Nonetheless, at 7.7 ns ligand **1** is stabilized by the formation of a polar network with the assistance of a water molecule. The water molecule is pinned to position by hydrogen bonds from the amide oxygen of the ligand, the backbone carbonyl oxygen of Ala³²⁸, and the backbone amide NH group of residues Val³³¹ and Tyr³³² (Supporting Information Figures 1, 3, 4, 7, and 8). This water bridge network is preserved until the end of the simulation and highlights the importance of the amide scaffold of the ligand (Supporting Information Figure 15). In addition, the NH group of Tyr³³² also forms a hydrogen bond directly with the amide oxygen atom of the ligand, which leads to further stabilization of the network motif (Supporting Information Figure 5). Importantly, ligand **31**, which lacks the amide scaffold, shows no enzyme inhibitory potency. Another significant interaction observed is the NH group of Asn⁶⁸ with the ethoxy scaffold of the ligand (Supporting Information Figure 2).

Conclusions

A pharmacophore model for BChE inhibitors was developed and applied to a benzimidazole-based selective *hCB₂R* agonist and identified this compound as a moderately potent BChE inhibitor with selectivity over AChE. In this preliminary study, initial systematic SARs on *hCB₂R* and BChE were conducted by synthesizing and evaluating a library of 21 novel compounds including aminobenzimidazole derivatives, structural isomers of the heterocyclic core, derivatives with modifications of the alkyl chain attached to the heterocycle, and variations of the substitution pattern of the phenyl group. This study is preliminary and currently lacks functional and *in vivo* data. Nevertheless, by MD simulations at the *hCB₂R* subtype and molecular docking of a set of compounds and subsequent MD at *hBChE*, initial insights into molecular understanding of the SARs at the two targets investigated could be obtained (and are illustrated in a 2D plot in the Supporting Information).

Using MD simulations at the *hCB₂R*, a different binding mode of the 2-aminobenzimidazole derivative **16a** relative to that of the benzimidazole lead structure **1** could be observed: while the benzimidazole shows a π - π interaction with Phe¹⁸³, the 2-aminobenzimidazole completely loses this interaction (Figure 8a–c). Compound **16d** offers the possibility to take advantage of the different binding mode: The additional phenyl moiety in compound **16d** might eliminate this effect and leads to improved affinity for the *CB₂R* relative to the other 2-aminobenzimidazoles.

In a docking and MD study on *hBChE*, the inhibitory effect of the benzimidazole lead structure **1** was explained. Here, the inhibitory effect is based on the amide pharmacophore, which forms hydrogen bonds with a water molecule. The water mole-

cule itself also provides hydrogen bonds to the surrounding amino acids (Figure 10). This finding is confirmed by the biological evaluation of **31**, which lacks the amide moiety and no longer shows inhibitory effect at BChE (Table 1). The inhibitory effect of 2-aminobenzimidazole **16a** arises from interactions of the additional nitrogen atom with Ser²⁸⁷ and Pro²⁸⁵ (Figure 10), which provides an advantage over compound **1**. With regard to compounds **1** and **16a** at the CB₂R, docking and MD simulations led to the finding that the affinity difference is not due to increased polarity or basicity of the molecule (provided by the additional nitrogen atom), but to a difference in the geometry of the structure in the binding pocket (Figure 8).

Still, future evaluations of the synthesized compounds in functional assays and thereby differentiation into agonist, partial agonist, antagonist, and inverse agonist properties are crucial to identify suitable leads for the intended development of dual-acting compounds. This is especially true as a lower-affinity compound with pronounced intrinsic activity might be a superior lead when compared with a compound optimized by affinity only. Testing the effects of dual-acting compounds concomitantly in vivo is of special interest, albeit complex. We have conducted such studies for dual-acting AChE inhibitors and h₃R antagonists.^[8,69] For the compounds described herein, neuroinflammatory in vivo models seem appropriate.

Concomitant SARs on several targets (four in this case) are necessarily complex by nature. Nevertheless, we have identified compounds that represent both sub-micromolar BChE inhibitors as well as hCB₂R ligands with selectivity over AChE and hCB₁R. The SARs obtained from these novel lead structures based on an aminobenzimidazole core in combination with computational studies on both target proteins describe a common chemical space for further structural optimization to identify novel leads for putative application as experimental therapeutics for neurodegenerative disorders.

Acknowledgements

M.D. gratefully acknowledges the German Science Foundation (Deutsche Forschungsgemeinschaft) for financial support (DFG DE1546/6-1 and DE1546/4-1) and the Elite Network of Bavaria for awarding a PhD position to A.D. within the International Doctoral Program "Receptor Dynamics". Cell lines stably expressing hCB₁R and hCB₂R were kindly provided by AbbVie (Chicago, IL, USA). We thank S. Kachler and Professor K.-N. Klotz (Institute of Pharmacology and Toxicology, University of Würzburg) for technical support and workspace for radioligand binding studies. We also thank S. Wehle and Y. Narkhede (Pharmaceutical and Medicinal Chemistry, University of Würzburg) for their support with molecular docking and dynamic studies at BChE.

Keywords: Alzheimer's disease • butyrylcholinesterase • cannabinoid receptor ligands • molecular dynamics • multitarget compounds

[1] C. Ballard, S. Gauthier, A. Corbett, C. Brayne, D. Aarsland, E. Jones, *Lancet* **2011**, *377*, 1019–1026.

- [2] W. J. Geldenhuys, M. B. H. Youdim, R. T. Carroll, C. J. Van der Schyf, *Prog. Neurobiol.* **2011**, *94*, 347–359.
- [3] X. Chen, M. Decker, *Curr. Med. Chem.* **2013**, *20*, 1673–1685.
- [4] C. A. Lipinski, F. Lombardo, B. W. Dominy, P. J. Feeney, *Adv. Drug Delivery Rev.* **1997**, *23*, 3–25.
- [5] G. R. Zimmermann, J. Lehar, C. T. Keith, *Drug Discovery Today* **2007**, *12*, 34–42.
- [6] A. Koeberle, O. Werz, *Drug Discovery Today* **2014**, *19*, 1871–1882.
- [7] R. Morphy, C. Kay, Z. Rankovic, *Drug Discovery Today* **2004**, *9*, 641–651.
- [8] F. H. Darras, S. Pockes, G. Huang, S. Wehle, A. Strasser, H.-J. Wittmann, M. Nimczick, C. A. Sotriffer, M. Decker, *ACS Chem. Neurosci.* **2014**, *5*, 225–242.
- [9] C. Benito, E. Núñez, R. M. Tolón, E. J. Carrier, A. Rábano, C. J. Hillard, J. Romero, *J. Neurosci.* **2003**, *23*, 11136–11141.
- [10] M. Solas, P. T. Francis, R. Franco, M. J. Ramirez, *Neurobiol. Aging* **2013**, *34*, 805–808.
- [11] G. Fakhfoury, A. Ahmadiani, R. Rahimian, A. A. Grolla, F. Moradi, A. Haeri, *Neuropharmacology* **2012**, *63*, 653–666.
- [12] E. Janefjord, J. L. V. Maag, B. S. Harvey, S. D. Smid, *Cell. Mol. Neurobiol.* **2014**, *34*, 31–42.
- [13] J. Wu, B. Bie, H. Yang, J. J. Xu, D. L. Brown, M. Naguib, *Neurobiol. Aging* **2013**, *34*, 791–804.
- [14] C. Bachmeier, D. Beaulieu-Abdelahad, M. Mullan, D. Paris, *Mol. Cell. Neurosci.* **2013**, *56*, 255–262.
- [15] K. Hensley, *J. Alzheimer's Dis.* **2010**, *21*, 1–14.
- [16] A. M. Martín-Moreno, B. Brera, C. Spuch, E. Carro, L. García-García, M. Delgado, M. A. Pozo, N. G. Innamorato, A. Cuadrado, M. L. de Ceballos, *J. Neuroinflammation* **2012**, *9*, 8.
- [17] N. H. Greig, T. Utsuki, D. K. Ingram, Y. Wang, G. Pepeu, C. Scali, Q.-S. Yu, J. Mamczarz, H. W. Holloway, T. Giordano, C. DeMao, F. Katsutoshi, S. Kumar, B. Arnold, K. L. Debomoy, *Proc. Natl. Acad. Sci. USA* **2005**, *102*, 17213–17218.
- [18] A. Nordberg, C. Ballard, R. Bullock, T. Darreh-Shori, M. Somogyi, *Prim. Care Companion CNS Disord.* **2013**, *15*, 1–18.
- [19] I. R. Macdonald, K. Rockwood, E. Martin, S. Darvesh, *J. Alzheimer's Dis.* **2014**, *42*, 379–384.
- [20] S. Darvesh, D. A. Hopkins, C. Geula, *Nat. Rev. Neurosci.* **2003**, *4*, 131–138.
- [21] T. Maurice, M. Strehaiano, N. Siméon, C. Bertrand, A. Chatonnet, *Behav. Brain Res.*, DOI: 10.1016/j.bbr.2015.08.026.
- [22] C. I. Wright, C. Geula, M.-M. Mesulam, *Ann. Neurol.* **1993**, *34*, 373–384.
- [23] S. Patyar, A. Prakash, B. Medhi, *J. Pharm. Pharmacol.* **2011**, *63*, 459–471.
- [24] M. Nimczick, M. Decker, *ChemMedChem* **2015**, *10*, 773–786.
- [25] A. Stöbel, M. Schlenk, S. Hinz, P. Küppers, J. Heer, M. Gütschow, C. E. Müller, *J. Med. Chem.* **2013**, *56*, 4580–4596.
- [26] J. Achenbach, F.-M. Klingler, R. Blöcher, D. Moser, A.-K. Häfner, C. B. Rödl, S. Kretschmer, B. Krüger, F. Löhr, H. Stark, B. Hofmann, D. Steinhilber, E. Proschak, *ACS Med. Chem. Lett.* **2013**, *4*, 1169–1172.
- [27] A. Brunschweiler, P. Koch, M. Schlenk, F. Pineda, P. Küppers, S. Hinz, M. Köse, S. Ullrich, J. Hockemeyer, M. Wiese, J. Heer, C. E. Müller, *ChemMedChem* **2014**, *9*, 1704–1724.
- [28] P. Gonzalez-Naranjo, N. E. Campillo, C. Perez, J. A. Paez, *Curr. Alzheimer Res.* **2013**, *10*, 229–239.
- [29] J. H. Lange, H. K. Coolen, M. A. van der Neut, A. J. Borst, P. C. Vermeer, C. G. Kruse, *J. Med. Chem.* **2010**, *53*, 1338–1346.
- [30] P. González-Naranjo, N. Pérez-Macias, N. E. Campillo, C. Pérez, V. J. Arán, R. Girón, E. Sánchez-Robles, M. I. Martín, M. Gómez-Canas, M. García-Arencibia, J. Fernández-Ruiz, J. A. Páez, *Eur. J. Med. Chem.* **2014**, *73*, 56–72.
- [31] F. H. Darras, B. Kling, J. Heilmann, M. Decker, *ACS Med. Chem. Lett.* **2012**, *3*, 914–919.
- [32] G. Huang, B. Kling, F. H. Darras, J. Heilmann, M. Decker, *Eur. J. Med. Chem.* **2014**, *81*, 15–21.
- [33] F. H. Darras, S. Wehle, G. Huang, C. A. Sotriffer, M. Decker, *Bioorg. Med. Chem.* **2014**, *22*, 4867–4881.
- [34] F. Zheng, M. Zhan, X. Huang, M. D. Abdul Hameed, C. G. Zhan, *Bioorg. Med. Chem.* **2014**, *22*, 538–549.
- [35] D. Pagé, E. Balaux, L. Boisvert, Z. Liu, C. Milburn, M. Tremblay, Z. Wei, S. Woo, X. Luo, Y.-X. Cheng, H. Yang, S. Srivastava, F. Zhou, W. Brown, M. Tomaszewski, C. Walpole, L. Hodzic, S. St-Onge, C. Godbout, D. Salois, K. Payza, *Bioorg. Med. Chem.* **2008**, *18*, 3695–3700.

- [36] M. Nimczick, D. Pemp, F. H. Darras, X. Chen, J. Heilmann, M. Decker, *Bioorg. Med. Chem.* **2014**, *22*, 3938–3946.
- [37] J. Zhu, C. F. Wu, X. Li, G. S. Wu, S. Xie, Q. N. Hu, Z. Deng, M. X. Zhu, H. R. Luo, X. Hong, *Bioorg. Med. Chem.* **2013**, *21*, 4218–4224.
- [38] F. D. Bellamy, K. Ou, *Tetrahedron Lett.* **1984**, *25*, 839–842.
- [39] S. Özden, D. Atabey, S. Yildiz, H. Göker, *Eur. J. Med. Chem.* **2008**, *43*, 1390–1402.
- [40] H. Munch, J. S. Hansen, M. Pittelkow, J. B. Christensen, U. Boas, *Tetrahedron Lett.* **2008**, *49*, 3117–3119.
- [41] V. J. Cee, N. S. Downing, *Tetrahedron Lett.* **2006**, *47*, 3747–3750.
- [42] J. E. Toth, P. R. Hamann, P. L. Fuchs, *J. Org. Chem.* **1988**, *53*, 4694–4708.
- [43] M. J. Burke, B. M. Trantow, *Tetrahedron Lett.* **2008**, *49*, 4579–4581.
- [44] E. Lohou, V. Collot, S. Stiebing, S. Rault, *Synthesis* **2011**, 2651–2663.
- [45] X. Chen, S. Wehle, N. Kuzmanovic, B. Merget, U. Holzgrabe, B. König, C. A. Sotriffer, M. Decker, *ACS Chem. Neurosci.* **2014**, *5*, 377–389.
- [46] J. H. M. Lange, H. H. van Stuivenberg, H. K. A. C. Coolen, T. J. P. Adolfs, A. C. McCreary, H. G. Keizer, H. C. Wals, W. Veerman, A. J. M. Borst, W. de Loeff, C. Verveer, C. G. Kruse, *J. Med. Chem.* **2005**, *48*, 1823–1838.
- [47] B. B. Yao, G. C. Hsieh, J. M. Frost, Y. Fan, T. R. Garrison, A. V. Daza, G. K. Grayson, C. Z. Zhu, M. Pai, P. Chandran, A. K. Salyers, E. J. Wensink, P. Honore, J. P. Sullivan, M. J. Dart, M. D. Meyer, *Br. J. Pharmacol.* **2008**, *153*, 390–401.
- [48] S. G. F. Rasmussen, B. T. DeVree, Y. Zou, A. C. Kruse, K. Y. Chung, T. S. Kobilka, F. S. Thain, P. S. Chae, E. Pardon, D. Calinski, J. M. Mathiesen, S. T. Y. Shah, J. A. Lyons, M. Caffrey, S. H. Gellmann, J. Steyaert, G. Skiniotis, W. I. Weis, R. K. Sunahara, B. K. Kobilka, *Nature* **2011**, *477*, 549–555.
- [49] J. A. Ballesteros, H. Weinstein, *Methods Neurosci.* **1995**, *25*, 366–428.
- [50] R. D. Bramblett, A. M. Panu, J. A. Ballesteros, P. H. Reggio, *Life Sci.* **1995**, *56*, 1971–1982.
- [51] E. Cichero, A. Ligresti, M. Allara, V. di Marzo, Z. Lazzati, P. D'Ursi, A. Marabotti, L. Milanese, A. Spallarossa, A. Ranise, P. Fossa, *Eur. J. Med. Chem.* **2011**, *46*, 4489–4505.
- [52] T. E. Angel, M. R. Chance, K. Palczewski, *Proc. Natl. Acad. Sci. USA* **2009**, *106*, 8555–8560.
- [53] W. Liu, E. Chun, A. A. Thompson, P. Chubukov, F. Xu, V. Katritch, G. W. Han, C. B. Roth, L. H. Heitmann, A. P. IJzerman, V. Cherezov, R. C. Stevens, *Science* **2012**, *337*, 232–235.
- [54] A. Strasser, B. Striegl, H. J. Wittmann, R. Seifert, *J. Pharmacol. Exp. Ther.* **2008**, *324*, 60–71.
- [55] P. Igel, R. Geyer, A. Strasser, S. Dove, R. Seifert, A. Buschauer, *J. Med. Chem.* **2009**, *52*, 6297–6313.
- [56] Z. H. Song, C. A. Slowey, D. P. Hurst, P. H. Reggio, *Mol. Pharmacol.* **1999**, *56*, 834–840.
- [57] C. Montero, N. E. Campillo, P. Goya, J. A. Paez, *Eur. J. Med. Chem.* **2005**, *40*, 75–83.
- [58] V. Lucchesi, D. P. Hurst, D. M. Shore, S. Bertini, B. R. Ehrmann, M. Allara, L. Lawrence, A. Ligresti, F. Minutolo, G. Saccomanni, H. Sharir, M. Macchia, V. Di Marzo, M. E. Abood, P. H. Reggio, C. Manera, *J. Med. Chem.* **2014**, *57*, 8777–8791.
- [59] C. Espinosa-Bustos, C. F. Lagos, J. Romero-Parra, A. M. Zárate, J. Mella-Raipán, H. Pessoa-Mahana, G. Recabarren-Gajardo, P. Iturriaga-Vásquez, R. A. Tapia, C. D. Pessoa-Mahana, *Arch. Pharm.* **2015**, *348*, 81–88.
- [60] Y. Nicolet, O. Lockridge, P. Masson, J. C. Fontecilla-Camps, F. Nachon, *J. Biol. Chem.* **2003**, *278*, 41141–41147.
- [61] J. Wiesner, Z. Kriz, K. Kuca, D. Jun, J. Koca, *J. Enzyme Inhib. Med. Chem.* **2007**, *22*, 417–424.
- [62] N. Çokuğraş, *Turk. J. Biochem.* **2003**, *28*, 54–61.
- [63] J. L. Sussman, M. Harel, F. Frolow, C. Oefner, A. Goldman, L. Toker, I. Silman, *Science* **1991**, *253*, 872–879.
- [64] Y. Xu, J.-P. Colletier, M. Weik, H. Jiang, J. Moulton, I. Silman, J. L. Sussman, *Biophys. J.* **2008**, *95*, 2500–2511.
- [65] A. Saxena, A. M. Redman, X. Jiang, O. Lockridge, B. P. Doctor, *Chem.-Biol. Interact.* **1999**, *119–120*, 61–69.
- [66] M. Bajda, A. Więckowska, M. Hebda, N. Guziar, C. A. Sotriffer, B. Malawska, *Int. J. Mol. Sci.* **2013**, *14*, 5608–5632.
- [67] M. L. Verdonk, J. C. Cole, M. J. Hartshorn, C. W. Murray, R. D. Taylor, *Proteins Struct. Funct. Bioinf.* **2003**, *52*, 609–623.
- [68] G. Neudert, G. Klebe, *J. Chem. Inf. Model.* **2011**, *51*, 2731–2745.
- [69] N. Khan, A. Saad, S. N. Nurulain, F. H. Darras, M. Decker, B. Sadek, *Behav. Brain Res.* **2016**, *297*, 155–164.

 Received: September 12, 2015

Published online on November 9, 2015

Supporting Information

Aminobenzimidazoles and Structural Isomers as Templates for Dual-Acting Butyrylcholinesterase Inhibitors and *hCB₂R* Ligands To Combat Neurodegenerative Disorders

Dominik Dolles,^[a] Martin Nimczick,^[a] Matthias Scheiner,^[a] Jacqueline Ramler,^[a] Patricia Stadtmüller,^[a] Edgar Sawatzky,^[a] Antonios Drakopoulos,^[a] Christoph Sotriffer,^[a] Hans-Joachim Wittmann,^[b] Andrea Strasser,^[b] and Michael Decker^{*[a]}

cmdc_201500418_sm_miscellaneous_information.pdf

Supporting Information

Table of Contents

Chemistry	2
General Information	2
Synthesis	3
Biological evaluation.....	45
Inhibition of BChE and AChE	45
Radioligand binding studies on <i>hCB₂R</i> and <i>hCB₁R</i>	45
Computational studies at <i>hBChE</i>	47
Materials and Methods.....	47
MD of benzimidazole 1	49
MD of 2-amino benzimidazole 16a	52
2D docking images	53
References.....	55

Chemistry

General Information

All reagents were used without further purification and bought from common commercial suppliers. For anhydrous reaction conditions, THF and dioxane were dried prior to use by refluxing over sodium slices for at least two days under argon atmosphere.

Thin layer chromatography was performed on silica gel 60 (alumina foils with fluorescent indicator 254 nm). For detection iodine vapor and UV light (254 nm and 366 nm) were used. For column chromatography, silica gel 60 (particle size of 0.040 mm – 0.063 mm) was used.

Nuclear magnetic resonance spectra were recorded with a Bruker AV-400 NMR instrument (Bruker, Karlsruhe, Germany) in CDCl_3 , $\text{DMSO-}d_6$ or CD_3OD , respectively, and chemical shifts are expressed in ppm relative to CDCl_3 (7.26 ppm for ^1H and 77.16 ppm for ^{13}C), $\text{DMSO-}d_6$ (2.49 ppm for ^1H and 39.52 ppm for ^{13}C) and CD_3OD (3.31 ppm for ^1H and 49.00 ppm for ^{13}C)^[1].

The LCMS-system from Shimadzu Products, contained a DGU-20A3R degassing unit, a LC20AB liquid chromatograph and a SPD-20A UV/Vis detector. Mass spectra were obtained by a LCMS 2020. As stationary phase a Synergi 4U fusion-RP (150 * 4.6 mm) column and as mobile phase a gradient of MeOH / water was used. Parameters for method I: A: water with 0.1 % CF_3COOH , B: MeOH with 0.1 % CF_3COOH , $V(\text{B})/(V(\text{A})+V(\text{B})) = 10\%$ to 80% over 10 min, $V(\text{B})/(V(\text{A})+V(\text{B})) = 80\%$ for 5 min, $V(\text{B})/(V(\text{A})+V(\text{B})) = 80\%$ to 10% over 3 min. Parameters for method II: A: water, B: MeOH, $V(\text{B})/(V(\text{A})+V(\text{B})) = 5\%$ to 90% over 10 min, $V(\text{B})/(V(\text{A})+V(\text{B})) = 90\%$ for 5 min, $V(\text{B})/(V(\text{A})+V(\text{B})) = 90\%$ to 5% over 3 min. Both methods were performed with a flow rate of 1.0 mL/min. UV detection was measured at 254 nm.

Synthesis

General procedure I for amide formation (for compounds 3, 19, 43)

The respective acid (1 eq.) was dissolved in DMF and NEt₃ (1.5 eq.), HBTU (1.1 eq.) and the appropriate amine (1 eq.) were added in one portion. The mixture was stirred overnight at room temperature. Then, EtOAc and sat. NaHCO₃ solution were added. The organic layer was washed several times with water and brine and dried over anhydrous Na₂SO₄. The solvent was removed *in vacuo* and product was used without further purification.

General procedure II for aryl halogen substitution (for compounds 5 – 7, 20 – 22)

The respective halogenated aryl compound (1 eq.) was dissolved in EtOH and NEt₃ (1.5 eq.) and the appropriate amine (1.1 eq.) were added. The mixture was stirred overnight at 50 °C. Afterwards, the solvent was removed *in vacuo* and the residue taken up in EtOAc. The organic layer was washed with brine, dried over anhydrous Na₂SO₄ and the solvent removed *in vacuo*. Product was used without further purification.

General procedure III for the reduction of the nitro moiety^[2] (for compounds 8 – 10, 23 – 25)

The respective nitro compound (1 eq.) was dissolved in EtOH and SnCl₂ · 2 H₂O (6.2 eq.) added. The mixture was refluxed overnight under argon atmosphere. After cooling to 0 °C, the mixture was basified (pH = 10) with 1 M NaOH_{aq} until precipitation. The precipitate was filtered off by suction and the solution concentrated *in vacuo*. The residue was suspended in water and extracted with CH₂Cl₂. The organic layer was dried over anhydrous Na₂SO₄ and the solvent was removed *in vacuo*. Product was used without further purification.

General procedure IV for the formation of the isothiocyanates^[3] (for compounds 11a – m)

The respective amine (1 eq.) and NEt₃ (1.2 eq.) were dissolved in anhydrous THF and cooled down to 0 °C. CS₂ (10 eq.) was added dropwise over a period of 20 minutes and the mixture stirred overnight at room temperature. The mixture was again cooled down to 0 °C and a solution of Boc₂O (1 eq.) and DMAP (cat.) in anhydrous THF added dropwise. The reaction was stirred for further 2 h. The solvent was removed *in vacuo* and Et₂O added until precipitation. The precipitate was filtered off and the filtrate was concentrated *in vacuo*. The crude product was purified by column chromatography if necessary.

General procedure V for the thiourea formation (for compounds 12a, 13a – m, 14a)

The respective diamino compound (1 eq.) was dissolved in anhydrous THF and the appropriate isothiocyanate (1.0 eq. to 1.1 eq.) added. The mixture was stirred for 3 to 7 days at room temperature. Afterwards, EtOAc was added and the organic layer washed with brine. The crude product was purified by column chromatography.

General procedure VI for the cyclisation of the 2-amino benzimidazole derivatives^[4] (for compounds 15a, 16a – m, 17a)

The respective thiourea compound (1 eq.) was dissolved in anhydrous THF and NEt₃ (1.5 eq.) and EDCI · HCl (2.5 eq.) were added. The mixture was refluxed for 3 to 5 days. Afterwards, EtOAc was added and the organic layer was washed with brine. The crude product was purified by column chromatography.

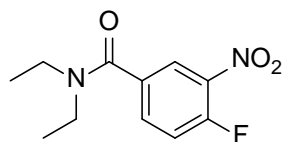
General procedure VII for the formation of the acetamide derivative^[5] (for compounds 26 – 30)

2-(4-Ethoxyphenyl)acetic acid (1 eq.) was dissolved in anhydrous THF and CDI (1 eq.) was added. The mixture was stirred for 1 h at room temperature. Then, a solution of the diamino compound (1 eq.) in anhydrous THF was added and stirred for 3 days at 50 °C. After concentrating the solution *in vacuo*, water was added and the mixture extracted with CH₂Cl₂. The organic layer was dried over anhydrous Na₂SO₄ and solvent evaporated. The crude product was purified by column chromatography.

General procedure VIII for the cyclisation of the benzimidazole derivatives^[5] (for compounds 1, 31 – 34)

The respective acetamide compound (1 eq.) was dissolved in glacial acetic acid, and the mixture refluxed for 1.5 h. The solution was then concentrated *in vacuo*, basified (pH = 10) with NH_{3, aq.} (25%) and extracted with CH₂Cl₂. The organic layer was dried over anhydrous Na₂SO₄, the solvent removed *in vacuo* and the pure product obtained after column chromatography.

Synthesis of *N,N*-diethyl-4-fluoro-3-nitrobenzamide



3

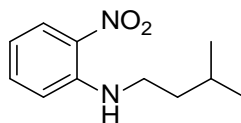
The reaction was carried out according to general procedure **I** using commercially available 4-fluoro-3-nitrobenzoic acid **2** (5.40 mmol, 1.00 g) and HNEt₂ (5.40 mmol, 0.71 mL). Product **3** was obtained as a yellow oil (2.89 mmol, 0.69 g, 54 %).

¹H NMR (CDCl₃, 400 MHz): δ = 1.11 – 1.30 (m, 6 H), 3.18 – 3.65 (m, 4 H), 7.35 (dd, J = 10.4, 8.5 Hz, 2 H), 7.66 – 7.70 ((m, J = 8.5, 4.2, 2.2 Hz, 1 H), 8.11 (dd, J = 7.0, 2.2 Hz, 1 H) ppm.

¹³C NMR (CDCl₃, 101 MHz): δ = 13.99, 43.44, 118.81, 124.42, 133.81, 136.86, 154.11, 156.77, 167.47 ppm.

ESI: m/z calcd for C₁₁H₁₃FN₂O₃ [M+H]⁺: 241.10; found: 241.10.

Synthesis of *N*-isopentyl-2-nitroaniline



5

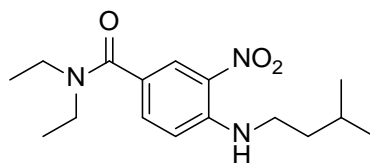
The reaction was carried out according to general procedure **II** using commercially available 1-fluoro-2-nitrobenzene **4** (1.42 mmol, 0.15 mL) and isopentylamine (1.56 mmol, 0.22 mL). Product **5** was obtained as a yellow oil (1.42 mmol, 0.31 g, > 99 %).

¹H NMR (CDCl₃, 400 MHz): δ = 0.98 (d, J = 6.8 Hz, 6 H), 1.64 (q, J = 7.2 Hz, 2 H), 1.78 (m, 1 H), 3.31 (m, 2 H), 6.63 (ddd, J = 8.4, 6.8, 1.2 Hz, 1 H), 6.85 (dd, J = 8.4, 1.2 Hz, 1 H), 7.43 (ddd, J = 8.8, 7.2, 1.6 Hz, 1 H), 8.17 (m, 1 H), 9.76 (s, 1 H, NH) ppm.

¹³C NMR (CDCl₃, 101 MHz): δ = 22.63, 26.14, 37.93, 41.44, 113.95, 115.23, 127.08, 136.33 ppm.

ESI: m/z calcd for C₁₁H₁₆N₂O₂ [M+Na]⁺: 231.11; found: 231.10.

Synthesis of *N,N*-diethyl-4-(isopentylamino)-3-nitrobenzamide



6

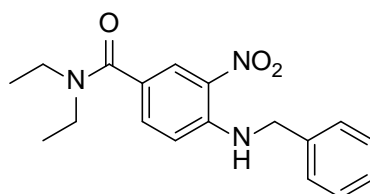
The reaction was carried out according to general procedure **II** using *N,N*-diethyl-4-fluoro-3-nitrobenzamide **3** (4.90 mmol, 1.20 g) and isopentylamine (5.90 mmol, 0.82 mL). Product **6** was obtained as a yellow oil (4.82 mmol, 1.53 g, 95 %).

¹H NMR (CDCl₃, 400 MHz): δ = 0.91 (d, J = 6.8 Hz, 6 H), 1.14 (t, J = 7.0 Hz, 6 H), 1.56 (q, J = 7.1 Hz, 2 H), 1.67 – 1.71 (m, 1 H), 3.27 (t, J = 7.2 Hz, 2 H), 3.37 (q, J = 6.8 Hz, 4 H), 6.81 (d, J = 8.8 Hz, 1 H), 7.48 (dd, J = 8.8, 2.0 Hz, 1 H), 8.07 (br, *NH*), 8.19 (d, J = 2.0 Hz, 1 H) ppm.

¹³C NMR (CDCl₃, 101 MHz): δ = 13.34 – 13.75, 22.44, 25.95, 37.71, 41.37, 40.59 – 43.31, 113.96, 123.18, 125.68, 130.61, 135.22, 146.02, 169.50 ppm.

ESI: m/z calcd for C₁₆H₂₅N₃O₃ [M+H]⁺: 308.20; found: 308.00.

Synthesis of 4-(benzylamino)-*N,N*-diethyl-3-nitrobenzamide



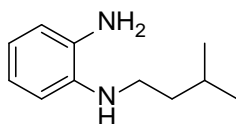
7

The reaction was carried out according to general procedure **II** using *N,N*-diethyl-4-fluoro-3-nitrobenzamide **3** (3.36 mmol, 0.81 g) and benzylamine (3.70 mmol, 0.40 mL). Product **7** was obtained as an orange oil (3.23 mmol, 1.06 g, 96 %).

¹H NMR (CDCl₃, 400 MHz): δ = 1.11 (t, J = 7.2 Hz, 6 H), 3.33 (br, 4 H), 4.48 (d, J = 5.6 Hz, 2 H), 6.76 (d, J = 8.8 Hz, 1 H), 7.24 (m, 5 H), 7.39 (d, J = 8.8 Hz, 1 H), 8.20 (s, 1 H), 8.45 (br, *NH*) ppm.

¹³C NMR (CDCl₃, 101 MHz): δ = 12.72 – 14.39, 39.19 – 44.25, 47.10, 114.41, 124.24, 125.54, 127.02, 127.81, 128.97, 131.16, 135.04, 136.91, 145.65, 169.24 ppm.

Synthesis of *N*¹-isopentylbenzene-1,2-diamine



8

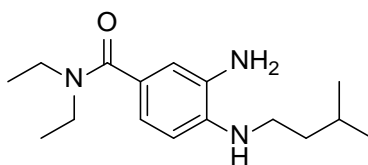
The reaction was carried out according to general procedure III using *N*-isopentyl-2-nitroaniline **5** (1.48 mmol, 0.31 g). Product **8** was obtained as a brown oil (1.12 mmol, 0.20 g, 76 %).

¹H NMR (CDCl₃, 400 MHz): δ = 0.94 (d, J = 6.8 Hz, 6 H), 1.61 (q, J = 7.2 Hz, 2 H), 1.73 (m, 1 H), 3.16 (m, 2 H), 5.30 (s, 2 H, NH₂), 6.73 (m, 1 H), 6.77 (s, 1 H), 6.81 (m, 1 H), 6.83 (m, 1 H), 7.37 (s, 1 H, NH) ppm.

¹³C NMR (CDCl₃, 101 MHz): δ = 22.46, 26.23, 35.93, 46.60, 108.35, 118.14, 120.15, 121.55 ppm.

ESI: m/z calcd for C₁₁H₁₈N₂ [M+H]⁺: 179.15; found: 179.15.

Synthesis of 3-amino-*N,N*-diethyl-4-(isopentylamino)benzamide



9

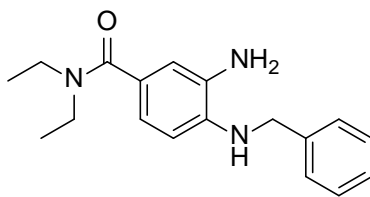
The reaction was carried out according to general procedure III using *N,N*-diethyl-4-(isopentylamino)-3-nitrobenzamide **6** (1.09 mmol, 0.34 g). Product **9** was obtained as colourless oil (0.84 mmol, 0.23 g, 77 %).

¹H NMR (CDCl₃, 400 MHz): δ = 0.88 (d, J = 6.4 Hz, 6 H), 1.09 (t, J = 7.0 Hz, 6 H), 1.49 (q, J = 7.2 Hz, 2 H), 1.67 (m, 1 H), 3.05 (t, J = 7.4 Hz, 2 H), 3.28 – 3.48 (m, 4 H + NH₂), 6.50 (d, J = 8.0 Hz, 1 H), 6.71 (d, J = 1.6 Hz, 1 H), 6.79 (dd, J = 8.0, 1.6 Hz, 1 H) ppm.

¹³C NMR (CDCl₃, 101 MHz): δ = 12.25 – 12.86, 21.63, 25.09, 37.56, 41.19, 39.23 – 41.87, 108.97, 114.46, 118.59, 125.35, 132.27, 138.44, 170.96 ppm.

ESI: m/z calcd for C₁₆H₂₇N₃O [M+H]⁺: 278.22; found: 278.15.

Synthesis of 3-amino-4-(benzylamino)-*N,N*-diethylbenzamide



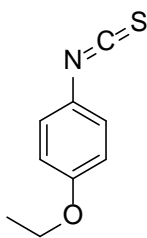
10

The reaction was carried out according to general procedure **III** using 4-(benzylamino)-*N,N*-diethyl-3-nitrobenzamide **7** (3.23 mmol, 1.06 g). Product **10** was obtained as colourless oil (2.42 mmol, 0.72 g, 74 %).

¹H NMR (CDCl₃, 400 MHz): δ = 1.05 (t, J = 7.0 Hz, 6 H), 3.32 (m, 4 H + NH₂), 4.04 (br, NH), 4.19 (d, J = 4.0 Hz, 2 H), 6.44 (d, J = 8.0 Hz, 1 H), 6.68 (m, 2 H), 7.17 (m, 1 H), 7.24 (m, 4 H) ppm.

¹³C NMR (CDCl₃, 101 MHz): δ = 13.06 – 14.18, 38.73 – 44.13, 48.22, 110.41, 115.35, 119.23, 126.69, 127.23, 127.59, 128.59, 133.67, 138.81, 139.22, 171.97 ppm.

Synthesis of 1-ethoxy-4-isothiocyanatobenzene



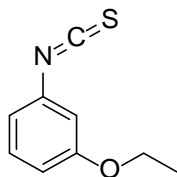
11a

The reaction was carried out according to general procedure **IV** using *p*-phenetidine (4.37 mmol, 0.56 mL). The crude product was purified by column chromatography using pure petroleum ether as eluent system. Product **11a** was obtained as a pale yellow solid (4.13 mmol, 0.74 g, 95 %).

¹H NMR (CDCl₃, 400 MHz): δ = 1.41 (t, J = 6.8 Hz, 3 H), 4.02 (q, J = 8.4 Hz, 2 H), 6.84 (m, 2 H), 7.15 (m, 2 H) ppm.

¹³C NMR (CDCl₃, 101 MHz): δ = 14.84, 64.01, 115.46, 116.36, 127.10, 158.15 ppm.

Synthesis of 1-ethoxy-3-isothiocyanatobenzene



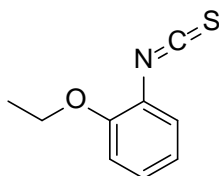
11b

The reaction was carried out according to general procedure **IV** using 3-ethoxyaniline (3.35 mmol, 0.46 g). Product **11b** was obtained without further purification as an orange oil (3.35 mmol, 0.60 g, > 99 %).

¹H NMR (CDCl₃, 400 MHz): δ = 1.41 (t, J = 7.0 Hz, 3 H), 4.00 (q, J = 6.9 Hz, 2 H), 6.71 (m, 1 H), 6.80 (m, 2 H), 7.21 (t, J = 7.2 Hz, 1 H) ppm.

¹³C NMR (CDCl₃, 101 MHz): δ = 14.74, 63.84, 111.67, 114.22, 118.03, 130.24, 132.10, 135.39, 159.73 ppm.

Synthesis of 1-ethoxy-2-isothiocyanatobenzene



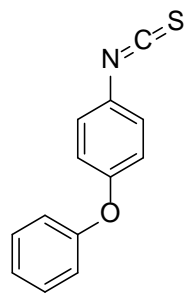
11c

The reaction was carried out according to general procedure **IV** using 2-ethoxyaniline (3.44 mmol, 0.47 g). Product **11c** was obtained without further purification as a brown oil (3.44 mmol, 0.63 g, > 99 %).

¹H NMR (CDCl₃, 400 MHz): δ = 1.49 (t, J = 7.0 Hz, 3 H), 4.10 (q, J = 6.9 Hz, 2 H), 6.87 (m, 2 H), 7.07 (m, 1 H), 7.19 (m, 1 H) ppm.

¹³C NMR (CDCl₃, 101 MHz): δ = 14.72, 64.75, 112.37, 120.59, 121.06, 125.14, 128.23, 141.18, 155.68 ppm.

Synthesis of 1-isothiocyanato-4-phenoxybenzene



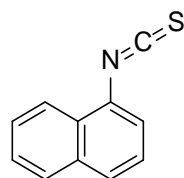
11d

The reaction was carried out according to general procedure **IV** using 4-phenoxyaniline (2.16 mmol, 0.40 g). The crude product was purified by column chromatography using petroleum ether and EtOAc (4:1) as eluent system. Product **11d** was obtained as a colourless oil (0.80 mmol, 0.18 g, 37 %).

¹H NMR (400 MHz, CDCl₃) δ = 6.93 – 6.98 (m, 2 H), 7.00 – 7.05 (m, 2 H), 7.14 – 7.21 (m, 3 H), 7.34 – 7.41 (m, 2 H) ppm.

¹³C NMR (101 MHz, CDCl₃) δ = 119.27, 119.42, 124.13, 125.87, 127.16, 130.01, 135.02, 156.30, 156.58 ppm.

Synthesis of 1-isothiocyanatonaphthalene



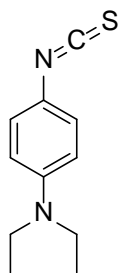
11f

The reaction was carried out according to general procedure **IV** using 1-naphthylamine (3.07 mmol, 0.44 g). Product **11f** was obtained without further purification as a light brown solid (3.07 mmol, 0.59 g, > 99 %).

¹H NMR (CDCl₃, 400 MHz): δ = 7.40 (d, J = 4.8 Hz), 7.58 (m, 2 H), 7.77 (m, 1 H), 7.87 (d, J = 8.0 Hz), 8.11 (d, J = 7.6 Hz) ppm.

¹³C NMR (101 MHz, CDCl₃) δ = 122.78, 123.53, 125.47, 127.20, 127.45, 127.58, 127.78, 128.50, 129.34, 134.07, 136.20 ppm.

Synthesis of *N,N*-diethyl-4-isothiocyanatoaniline



11g

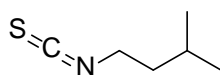
The reaction was carried out according to general procedure **IV** using *N,N*-diethylbenzene-1,4-diamine (6.08 mmol, 1.01 mL). The crude product was purified by column chromatography using petroleum ether and EtOAc (2:1) as eluent system. Product **11g** was obtained as a pale yellow solid (4.80 mmol, 0.99 g, 79 %).

¹H NMR (CDCl₃, 400 MHz): δ = 1.01 (t, *J* = 7.2 Hz, 6 H), 3.19 (q, *J* = 7.0 Hz, 4 H), 6.37 – 6.43 (m, 2 H), 6.87 – 6.94 (m, 2 H) ppm.

¹³C NMR (101 MHz, CDCl₃) δ = 12.58, 44.54, 111.75, 117.37, 126.93, 132.09, 146.58 ppm.

ESI: *m/z* calcd for C₁₁H₁₄N₂S [M+H]⁺: 207.09 found: 207.15.

Synthesis of 1-isothiocyanato-3-methylbutane



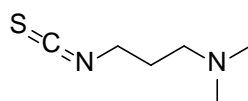
11j

The reaction was carried out according to general procedure **IV** using isopentylamine (3.01 mmol, 0.35 mL). The crude product was purified by column chromatography using pure petroleum ether as eluent system. Product **11j** was obtained as a colourless liquid (2.40 mmol, 0.31 g, 80 %).

¹H NMR (CDCl₃, 400 MHz): δ = 0.91 (d, *J* = 6.4 Hz, 6 H), 1.57 (m, 2 H), 1.73 (m, 1 H), 3.51 (t, *J* = 6.8 Hz, 2 H) ppm.

¹³C NMR (101 MHz, CDCl₃) δ = 22.03, 25.44, 38.60, 43.49, 129.59 ppm.

Synthesis of 3-isothiocyanato-*N,N*-dimethylpropan-1-amine



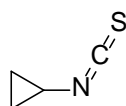
11k

The reaction was carried out according to general procedure **IV** using *N*¹,*N*¹-Dimethylpropane-1,3-diamine (4.40 mmol, 0.45 g). The crude product was purified by column chromatography using pure petroleum ether as eluent system. Product **11k** was obtained as a pale brown liquid (4.40 mmol, 0.70 g, > 99 %).

¹H NMR (CDCl₃, 400 MHz): δ = 1.76 (m, 2 H), 2.14 (s, 6 H), 2.30 (t, *J* = 6.8 Hz, 2 H), m 3.52 (t, *J* = 6.6 Hz, 2 H) ppm.

¹³C NMR (101 MHz, CDCl₃) δ = 28.00, 43.02, 45.42, 56.01, 129.99 ppm.

Synthesis of isothiocyanatocyclopropane



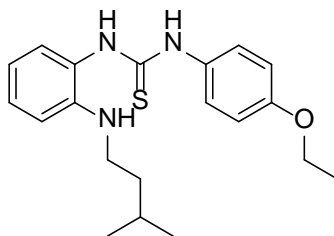
11l

The reaction was carried out according to general procedure **IV** using cyclopropylamine (4.04 mmol, 0.28 mL). Product **11l** was obtained without further purification as an orange liquid (3.80 mmol, 0.39 g, 97 %).

¹H NMR (CDCl₃, 400 MHz): δ = 0.87 (m, 4 H), 2.89 (m, 1 H) ppm.

¹³C NMR (101 MHz, CDCl₃) δ = 8.26, 25.49, 126.85 ppm.

Synthesis of 1-(4-ethoxyphenyl)-3-(2-(isopentylamino)phenyl)thiourea



12a

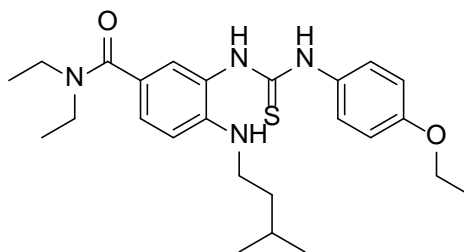
The reaction was carried out according to general procedure **V** using *N*¹-isopentylbenzene-1,2-diamine **8** (0.6 mmol, 0.1 g) and 1-ethoxy-4-isothiocyanatobenzene **11a** (0.62 mmol, 0.11 g). The crude product was purified by column chromatography using petroleum ether and EtOAc (4:1) as eluent system. Product **12a** was obtained as yellow solid (0.28 mmol, 0.10 g, 45 %).

¹H NMR (CDCl₃, 400 MHz): δ = 0.85 (d, *J* = 6.8 Hz, 6 H), 1.37 (m, 2 H), 1.44 (m, 4 H), 3.06 (t, 7.6, 2 H), 4.06 (q, *J* = 7.2 Hz, 2 H), 6.94 (d, *J* = 9.2 Hz, 2 H), 7.10 (d, *J* = 8.8 Hz, 2 H), 7.22 (m, 1 H), 7.33 (m, 1 H), 7.41 (m, 2 H), 12.27 (s, 1 H, NH), 13.71 (s, 1 H, NH) ppm.

^{13}C NMR (CDCl_3 , 101 MHz): δ = 14.88, 22.41, 29.78, 36.77, 45.14, 67.87, 109.99, 115.70, 118.64, 120.08, 124.36, 126.53 ppm.

ESI: m/z calcd for $\text{C}_{19}\text{H}_{25}\text{N}_3\text{OS}$ $[\text{M}+\text{Na}]^+$: 380.18 found: 380.20.

Synthesis of 3-(3-(4-ethoxyphenyl)thioureido)-*N,N*-diethyl-4-(isopentylamino)benzamide



13a

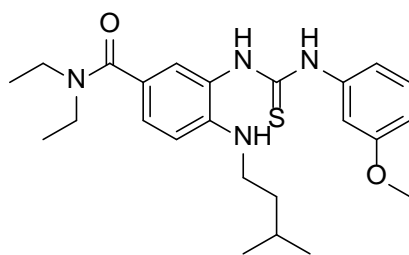
The reaction was carried out according to general procedure **V** using 3-amino-*N,N*-diethyl-4-(isopentylamino)benzamide **9** (1.25 mmol, 0.35 g) and 1-ethoxy-4-isothiocyanatobenzene **11a** (1.43 mmol, 0.26 g). The crude product was purified by column chromatography using CH_2Cl_2 , MeOH and NH_3 , aq. 25% (50:1:0.1) as eluent system. Product **13a** was obtained as a greenish oil (0.72 mmol, 0.32 g, 56 %).

^1H NMR (CDCl_3 , 400 MHz): δ = 0.87 (d, J = 6.8 Hz, 6 H), 1.09 (t, J = 7.0 Hz, 6 H), 1.32 (t, J = 6.8 Hz, 3 H), 1.45 (q, J = 7.3 Hz, 2 H), 1.60 – 1.73 (m, 1 H), 3.02 (q, J = 6.4 Hz, 2 H), 3.35 (d, J = 5.6 Hz, 4 H), 3.94 (q, J = 6.9 Hz, 2 H), 4.24 (br, NH), 6.52 (d, J = 8.4 Hz, 1 H), 6.79 (d, J = 8.8 Hz, 2 H), 7.06 (s, 1 H), 7.12 (d, J = 8.0 Hz, 1 H), 7.27 (d, J = 8.4 Hz, 2 H), 8.02 (br, NH), 8.40 (br, NH) ppm.

^{13}C NMR (CDCl_3 , 101 MHz): δ = 12.75 – 12.48, 14.82, 22.61, 26.08, 38.26, 41.64, 42.28 – 44.74, 63.66, 110.51, 114.67, 122.60, 124.00, 126.79, 127.37, 127.78, 131.06, 146.11, 157.24, 171.52, 181.92 ppm.

ESI: m/z calcd for $\text{C}_{25}\text{H}_{34}\text{N}_4\text{O}_2$ $[\text{M}+\text{Na}]^+$: 479.25; found: 479.15.

Synthesis of 3-(3-(3-ethoxyphenyl)thioureido)-*N,N*-diethyl-4-(isopentylamino)benzamide



13b

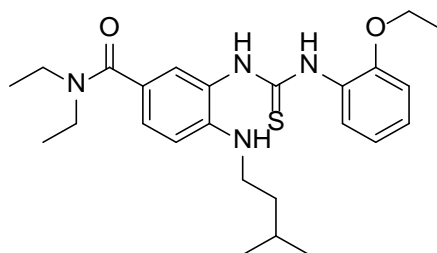
The reaction was carried out according to general procedure **V** using 3-amino-*N,N*-diethyl-4-(isopentylamino)benzamide **9** (1.21 mmol, 0.34 g) and 1-ethoxy-3-isothiocyanatobenzene **11b** (1.01 mmol, 0.18 g). The crude product was purified by column chromatography using petroleum ether and EtOAc (3:2) as eluent system. Product **13b** was obtained as a brown oil (0.30 mmol, 0.14 g, 30 %).

¹H NMR (CDCl₃, 400 MHz): δ = 0.94 (d, J = 6.6 Hz, 6 H), 1.18 (t, J = 6.8 Hz, 6 H), 1.39 (t, J = 7.0 Hz, 3 H), 1.51 (q, J = 14.9, 7.0 Hz, 2 H), 1.63 – 1.75 (m, 1 H), 3.07 (m, 2 H), 3.44 (br, 4 H), 4.02 (q, J = 4.0 Hz, 2 H), 4.25 (br, *NH*), 6.56 (d, J = 8.4 Hz, 1 H), 6.69 – 6.72 (m, 1 H), 7.02 – 7.10 (m, 2 H), 7.13 – 7.19 (m, 1 H), 7.21 (t, J = 8.1 Hz, 1 H), 7.30 (s, 1 H), 8.17 (s, 1 H) ppm.

¹³C NMR (CDCl₃, 101 MHz): δ = 14.79, 22.62, 26.09, 38.27, 41.63, 63.54, 107.82, 110.18, 110.43, 112.09, 115.98, 123.69, 127.14, 127.78, 129.41, 139.80, 146.15, 159.27, 171.79, 181.27 ppm.

ESI: m/z calcd for C₂₅H₃₆N₄O₂S [M+Na]⁺: 479.25; found: 479.30.

Synthesis of 3-(3-(2-ethoxyphenyl)thioureido)-*N,N*-diethyl-4-(isopentylamino)benzamide



13c

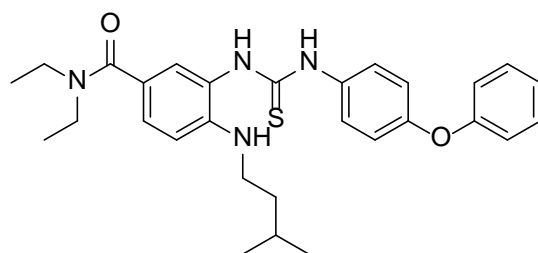
The reaction was carried out according to general procedure **V** using 3-amino-*N,N*-diethyl-4-(isopentylamino)benzamide **9** (1.01 mmol, 0.28 g) and 1-ethoxy-2-isothiocyanatobenzene **11c** (0.84 mmol, 0.15 g). The crude product was purified by column chromatography using petroleum ether and EtOAc (3:2) as eluent system. Product **13c** was obtained as a brown oil (0.41 mmol, 0.19 mg, 49 %).

¹H NMR (CDCl₃, 400 MHz): δ = 0.87 (d, J = 6.4, 6 H), 1.14 (t, J = 7.1 Hz, 6 H), 1.17 – 1.25 (m, 4 H), 1.47 (dd, J = 14.7, 7.1 Hz, 2 H), 1.55 – 1.69 (m, 1 H), 3.11 (t, J = 7.2 Hz, 2 H), 3.39 (d, J = 6.8 Hz, 4 H), 3.92 (q, J = 6.7, 2 H), 4.36 (br, *NH*), 6.66 (d, J = 8.5 Hz, 1 H), 6.79 (d, J = 8.4 Hz, 1 H), 6.89 – 6.93 (m, 1 H), 7.01 – 7.07 (m, 1 H), 7.14 (s, 1 H), 7.31 (d, J = 7.9 Hz, 1 H), 8.05 (br, *NH*), 8.22 (s, 1 H), 8.36 – 8.56 (br, *NH*) ppm.

¹³C NMR (CDCl₃, 101 MHz): δ = 14.68, 22.50, 25.94, 38.09, 41.55, 64.28, 110.68, 111.59, 114.71, 116.61, 120.31, 124.56, 125.56, 127.64, 127.97, 128.92, 143.47, 146.18, 149.76, 170.82 ppm.

ESI: m/z calcd for $C_{25}H_{36}N_4O_2S$ $[M+H]^+$: 457.26; found: 457.25.

Synthesis of *N,N*-diethyl-4-(isopentylamino)-3-(3-(4-phenoxyphenyl)thioureido)benzamide



13d

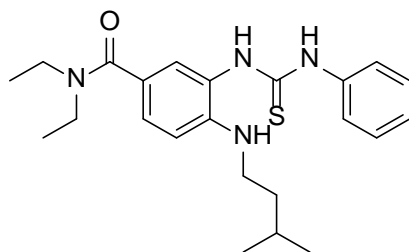
The reaction was carried out according to general procedure **V** using 3-amino-*N,N*-diethyl-4-(isopentylamino)benzamide **9** (0.84 mmol, 0.23 g) and 1-isothiocyanato-4-phenoxybenzene **11d** (0.80 mmol, 0.18 g). The crude product was purified by column chromatography using petroleum ether and EtOAc (1:1) as eluent system. Product **13d** was obtained as a pale brown oil (0.65 mmol, 0.33 g, 87 %).

1H NMR ($CDCl_3$, 400 MHz): δ = 0.94 (d, J = 8.0 Hz, 6 H), 1.17 (t, J = 4.0 Hz, 6 H), 1.51 (q, J = 8.0 Hz, 2 H), 1.64 – 1.75 (m, 1 H), 3.08 (t, J = 8.0 Hz, 2 H), 3.43 (s, 4 H), 4.28 (s, 1 H), 6.57 (d, J = 8.5 Hz, 1 H), 6.57 (d, J = 8.5 Hz, 1 H), 6.93 – 7.03 (m, 4 H), 7.05 – 7.12 (m, 2 H), 7.15 (d, J = 8.0 Hz, 1 H), 7.29 – 7.35 (m, 2 H), 7.50 (d, J = 8.5 Hz, 2 H), 8.19 (s, 1 H), 8.84 (s, 1 H) ppm.

^{13}C NMR ($CDCl_3$, 101 MHz): δ = 12.65 – 14.46, 22.62, 26.10, 38.27, 41.64, 110.42, 118.88, 118.94, 123.35, 123.62, 126.08, 127.10, 127.77, 129.75, 133.99, 146.19, 154.88, 157.12, 171.12, 171.85, 181.77 ppm.

ESI: m/z calcd for $C_{29}H_{36}N_4O_2S$ $[M+Na]^+$: 527.25; found: 527.20.

Synthesis of *N,N*-diethyl-4-(isopentylamino)-3-(3-phenylthioureido)benzamide



13e

The reaction was carried out according to general procedure **V** using 3-amino-*N,N*-diethyl-4-(isopentylamino)benzamide **9** (0.74 mmol, 0.20 g) and commercially available isothiocyanatobenzene **11e** (0.84 mmol, 0.11 g). The crude product was purified by column

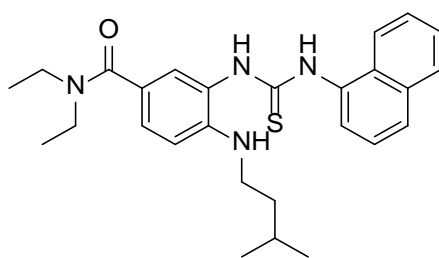
chromatography using CH₂Cl₂, MeOH and NH₃, aq. 25 % (50:1:0.2) as eluent system. Product **13e** was obtained as an orange oil (0.50 mmol, 0.21 g, 70 %).

¹H NMR (CDCl₃, 400 MHz): δ = 0.95 (d, *J* = 6.8 Hz, 6 H), 1.18 (m, 6 H), 1.51 (m, 2 H), 1.70 (m, 1 H), 3.08 (m, 2 H), 3.43 (m, 4 H), 4.26 (br, 1 H, *NH*), 6.57 (d, *J* = 8.4 Hz, 1 H), 7.09 (s, 1 H), 7.17 (m, 2 H), 7.34 (m, 2 H), 7.56 (d, *J* = 8.0 Hz, 2 H), 8.20 (br, 1 H), 8.85 (br, 1 H) ppm.

¹³C NMR (CDCl₃, 101 MHz): δ = 22.68, 26.15, 38.34, 41.70, 110.51, 123.72, 124.33, 125.67, 127.20, 127.84, 128.82, 138.83, 146.24, 171.89, 181.62 ppm.

ESI: *m/z* calcd for C₃₀H₃₂N₄OS [M+H]⁺: 413.23; found: 413.20.

Synthesis of *N,N*-diethyl-4-(isopentylamino)-3-(3-(naphthalen-1-yl)thioureido)benzamide



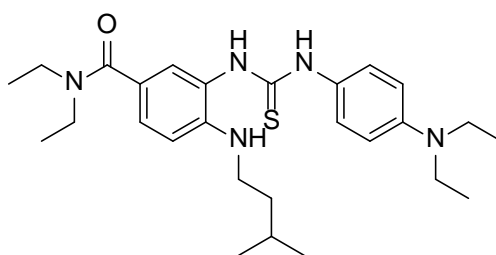
13f

The reaction was carried out according to general procedure **V** using 3-amino-*N,N*-diethyl-4-(isopentylamino)benzamide **9** (0.78 mmol, 0.22 g) and 1-isothiocyanatonaphthalene **11f** (0.90 mmol, 0.17 g). The crude product was purified by column chromatography using CH₂Cl₂, MeOH and NH₃, aq. 25 % (25:1:0.1) as eluent system. Product **13f** was obtained as a beige solid (0.70 mmol, 0.33 g, 91 %).

¹H NMR (CDCl₃, 400 MHz): δ = 0.96 (d, *J* = 6.4 Hz, 6 H), 1.18 (t, *J* = 7.0 Hz, 6 H), 1.51 (m, 2 H), 1.70 (m, 1 H), 3.13 (m, 2 H), 3.43 (d, *J* = 7.2 Hz, 4 H), 4.21 (br, 1 H, *NH*), 6.66 (m, 1 H), 7.28 (m, 3 H), 7.54 (m, 3 H), 7.64 (d, *J* = 7.2 Hz, 1 H), 7.92 (m, 4 H) ppm.

ESI: *m/z* calcd for C₂₇H₃₄N₄OS [M+H]⁺: 463.25; found: 463.30.

Synthesis of 3-(3-(4-(diethylamino)phenyl)thioureido)-*N,N*-diethyl-4-(isopentylamino)benzamide



13g

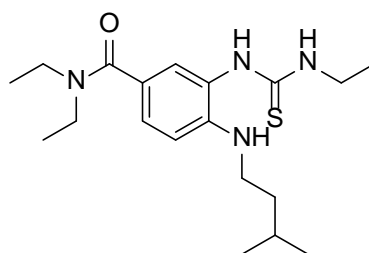
The reaction was carried out according to general procedure **V** using 3-amino-*N,N*-diethyl-4-(isopentylamino)benzamide **9** (2.04 mmol, 0.56 g) and *N,N*-diethyl-4-isothiocyanatoaniline **11g** (2.24 mmol, 0.46 g). The crude product was purified by column chromatography using petroleum ether and EtOAc (1:1) as eluent system. Product **13g** was obtained as a pale brown oil (0.65 mmol, 0.32 g, 32 %).

¹H NMR (CDCl₃, 400 MHz): δ = 0.90 (d, J = 6.6 Hz, 6 H), 1.07 – 1.19 (m, 12 H), 1.48 (q, 7.0 Hz, 2 H), 1.56 – 1.72 (m, 1 H), 3.01 – 3.12 (br, 2 H), 3.29 (q, J = 7.0 Hz, 4 H), 3.37 – 3.47 (br, 4 H), 4.25 – 4.39 (br, NH), 6.56 – 6.61 (m, 2 H), 7.09 – 7.19 (m, 4 H), 7.20 – 7.23 (m, 1 H), 8.15 (br, NH) ppm.

¹³C NMR (CDCl₃, 101 MHz): δ = 12.51, 22.59, 26.04, 38.22, 41.66, 44.41, 108.50, 110.65, 120.86, 127.45, 127.82, 130.88, 131.76, 133.21, 146.00, 169.31, 170.90, 181.69 ppm.

ESI: m/z calcd for C₂₇H₄₁N₅OS [M+H]⁺: 484.30; found: 484.25.

Synthesis of *N,N*-diethyl-3-(3-ethylthioureido)-4-(isopentylamino)benzamide



13h

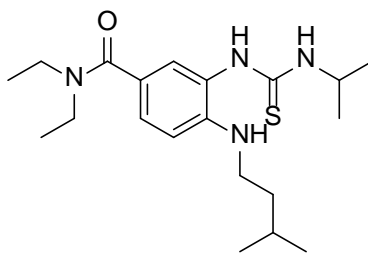
The reaction was carried out according to general procedure **V** using 3-amino-*N,N*-diethyl-4-(isopentylamino)benzamide **9** (1.08 mmol, 0.30 g) and commercially available isothiocyanatoethane **11h** (1.30 mmol, 0.13 g). The crude product was purified by column chromatography using petroleum ether and EtOAc (1:1) as eluent system. Product **13h** was obtained as a brown oil (0.86 mmol, 0.31 g, 80 %).

¹H NMR (CDCl₃, 400 MHz): δ = 0.87 (d, J = 6.6 Hz, 6 H), 1.08 – 1.13 (m, 9 H), 1.42 (q, 7.0 Hz, 2 H), 1.56 – 1.66 (m, 1 H), 3.02 (t, J = 7.3 Hz, 2 H), 3.38 (br, 4 H), 3.54 (q, J = 7.2 Hz, 2 H), 4.23 (br, NH), 6.51 (d, J = 8.5 Hz, 1 H), 6.99 (d, J = 4.0 Hz, 1 H), 7.13 – 7.15 (m, 1 H), 7.86 (br, NH) ppm.

¹³C NMR (CDCl₃, 101 MHz): δ = 14.27, 22.53, 25.96, 38.11, 39.97, 41.46, 110.33, 121.04, 123.96, 127.72, 146.08, 171.33, 181.85 ppm.

ESI: m/z calcd for C₁₉H₃₂N₄OS [M+H]⁺: 365.23; found: 365.20.

Synthesis of *N,N*-diethyl-4-(isopentylamino)-3-(3-isopropylthioureido)benzamide



13i

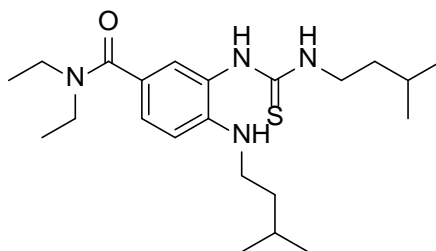
The reaction was carried out according to general procedure **V** using 3-amino-*N,N*-diethyl-4-(isopentylamino)benzamide **9** (0.69 mmol, 0.19 g) and 2-isothiocyanatopropane **11i** (1.21 mmol, 0.12 g). The crude product was purified by column chromatography using CH₂Cl₂, MeOH and NH₃, aq. 25 % (25:1:0.1) as eluent system. Product **13i** was obtained as an orange-brown oil (0.70 mmol, 0.29 g, > 99 %).

¹H NMR (CDCl₃, 400 MHz): δ = 0.89 (d, J = 6.4 Hz, 6 H), 1.13 (m, 12 H), 1.44 (m, 2 H), 1.63 (m, 1 H), 3.03 (m, 2 H), 3.38 (m, 4 H), 4.19 (br, 1 H), 4.47 (m, 1 H), 6.24 (br, 1 H), 6.53 (d, J = 8.4 Hz, 1 H), 7.00 (s, 1 H), 7.16 (d, J = 8.4 Hz, 1 H), 7.74 (br, 1 H) ppm.

¹³C NMR (CDCl₃, 101 MHz): δ = 22.35, 22.54, 25.98, 38.18, 41.48, 46.93, 110.35, 121.30, 124.10, 127.69, 127.81, 146.10, 171.27, 180.86 ppm.

ESI: m/z calcd for C₂₀H₃₄N₄OS [M+H]⁺: 379.25; found: 379.30.

Synthesis of *N,N*-diethyl-4-(isopentylamino)-3-(3-isopentylthioureido)benzamide



13j

The reaction was carried out according to general procedure **V** using 3-amino-*N,N*-diethyl-4-(isopentylamino)benzamide **9** (0.71 mmol, 0.19 g) and 1-isothiocyanato-3-methylbutane **11j** (0.82 mmol, 0.11 g). The crude product was purified by column chromatography using CH₂Cl₂, MeOH and NH₃, aq. 25 % (25:1:0.1) as eluent system. Product **13j** was obtained as a yellow-brown oil (0.60 mmol, 0.24 g, 82 %).

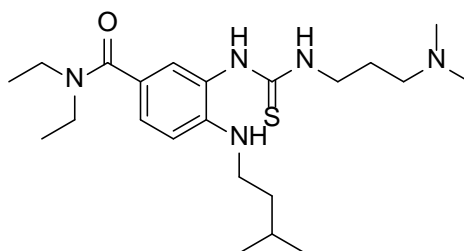
¹H NMR (CDCl₃, 400 MHz): δ = 0.88 (d, J = 6.8 Hz), 0.92 (d, J = 6.8 Hz, 6 H), 1.16 (t, J = 7.0 Hz, 6 H), 1.41 (m, 2 H), 1.47 (m, 2 H), 1.57 (m, 1 H), 1.66 (m, 1 H), 3.07 (m, 2 H), 3.40 (m, 4

H), 3.57 (m, 2 H), 4.23 (br, 1 H), 6.24 (br, 1 H), 6.58 (d, $J = 8.4$ Hz, 1 H), 7.05 (s, 1 H), 7.22 (d, $J = 8.0$ Hz, 1 H), 7.58 (br, 1 H) ppm.

^{13}C NMR (CDCl_3 , 101 MHz): $\delta = 22.57, 22.64, 25.96, 26.07, 37.97, 38.26, 41.57, 43.85, 110.57, 120.74, 124.47, 127.84, 128.32, 146.19, 171.19, 181.97$ ppm.

ESI: m/z calcd for $\text{C}_{22}\text{H}_{38}\text{N}_4\text{OS}$ $[\text{M}+\text{Na}]^+$: 429.27; found: 429.20.

Synthesis of 3-(3-(3-(dimethylamino)propyl)thioureido)-*N,N*-diethyl-4-(isopentylamino)benzamide



13k

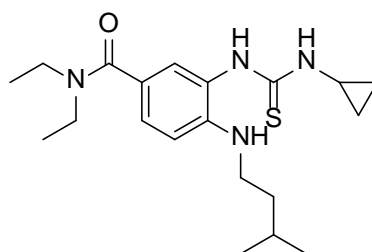
The reaction was carried out according to general procedure **V** using 3-amino-*N,N*-diethyl-4-(isopentylamino)benzamide **9** (0.75 mmol, 0.21 g) and 3-isothiocyanato-*N,N*-dimethylpropan-1-amine **11k** (0.88 mmol, 0.13 g). The crude product was purified by column chromatography using CH_2Cl_2 , MeOH and NH_3 , aq. 25% (20:1:0.1) as eluent system. Product **13k** was obtained as a light brown solid (0.80 mmol, 0.32 g, > 99 %).

^1H NMR (CDCl_3 , 400 MHz): $\delta = 0.93$ (d, $J = 6.8$ Hz, 6 H), 1.15 (t, $J = 7.0$ Hz, 6 H), 1.50 (m, 2 H), 1.61 (m, 2 H), 1.68 (m, 1 H), 1.84 (s, 6 H), 2.28 (m, 2 H), 3.13 (m, 2 H), 3.40 (m, 4 H), 3.66 (m, 2 H), 4.32 (br, 1 H), 6.65 (d, $J = 8.4$ Hz, 1 H), 7.08 (br, 1 H), 7.14 (d, $J = 2.0$ Hz, 1 H), 7.31 (dd, $J_1 = 8.4$ Hz, $J_2 = 1.6$ Hz, 1 H), 8.62 (br, 1 H) ppm.

^{13}C NMR (CDCl_3 , 101 MHz): $\delta = 22.65, 24.37, 26.06, 38.31, 41.55, 44.72, 47.39, 59.40, 110.40, 120.31, 124.98, 128.24, 129.14, 146.42, 170.61, 181.46$ ppm.

ESI: m/z calcd for $\text{C}_{22}\text{H}_{39}\text{N}_5\text{OS}$ $[\text{M}+\text{H}]^+$: 422.29; found: 422.20.

Synthesis of 3-(3-cyclopropylthioureido)-*N,N*-diethyl-4-(isopentylamino)benzamide



13l

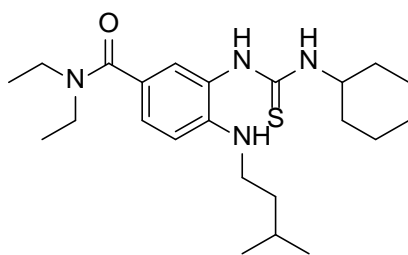
The reaction was carried out according to general procedure **V** using 3-amino-*N,N*-diethyl-4-(isopentylamino)benzamide **9** (0.69 mmol, 0.19 g) and isothiocyanatocyclopropane **11I** (0.81 mmol, 0.08 g). The crude product was purified by column chromatography using CH₂Cl₂, MeOH and NH₃, aq. 25 % (25:1:0.1) as eluent system. Product **13I** was obtained as a brown solid (0.60 mmol, 0.25 g, 95 %).

¹H NMR (CDCl₃, 400 MHz): δ = 0.60 (m, 2 H), 0.83 (m, 2 H), 0.93 (d, *J* = 6.4 Hz, 6 H), 1.15 (m, 7 H), 1.48 (m, 2 H), 1.67 (m, 1 H), 3.07 (m, 2 H), 3.40 (m, 4 H), 4.19 (br, 1 H), 6.57 (d, *J* = 8.4 Hz, 1 H), 6.62 (br, 1 H), 7.03 (s, 1 H), 7.19 (d, *J* = 8.4 Hz, 1 H), 7.69 (br, 1 H) ppm.

¹³C NMR (CDCl₃, 101 MHz): δ = 7.57, 22.66, 26.12, 38.30, 41.66, 110.62, 124.39, 127.80, 146.01, 171.36, 183.77 ppm.

ESI: *m/z* calcd for C₂₀H₃₂N₄OS [M+H]⁺: 377.23; found: 377.20.

Synthesis of 3-(3-cyclohexylthioureido)-*N,N*-diethyl-4-(isopentylamino)benzamide



13m

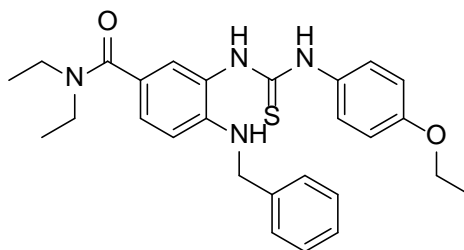
The reaction was carried out according to general procedure **V** using 3-amino-*N,N*-diethyl-4-(isopentylamino)benzamide **9** (0.67 mmol, 0.19 g) and commercially available isothiocyanatocyclohexane **11m** (1.16 mmol, 0.16 g). The crude product was purified by column chromatography using CH₂Cl₂, MeOH and NH₃, aq. 25 % (25:1:0.1) as eluent system. Product **13m** was obtained as a yellow oil (0.60 mmol, 0.25 g, 88 %).

¹H NMR (CDCl₃, 400 MHz): δ = 0.90 (d, *J* = 6.8 Hz, 6 H), 1.11 (m, 9 H), 1.33 (m, 2 H), 1.45 (m, 2 H), 1.55 (m, 1 H), 1.65 (m, 3 H), 1.96 (m, 2 H), 3.05 (m, 2 H), 3.39 (m, 4 H), 4.20 (m, 2 H), 6.22 (br, 1 H), 6.55 (d, *J* = 8.4 Hz, 1 H), 7.01 (s, 1 H), 7.18 (d, *J* = 8.4 Hz, 1 H), 7.71 (br, 1 H) ppm.

¹³C NMR (CDCl₃, 101 MHz): δ = 22.59, 24.75, 25.49, 26.03, 32.60, 38.22, 41.53, 53.68, 110.43, 121.05, 124.22, 127.68, 128.01, 146.09, 171.25, 180.69 ppm.

ESI: *m/z* calcd for C₂₃H₃₈N₄OS [M+H]⁺: 419.28; found: 419.30.

Synthesis of 4-(benzylamino)-3-(3-(4-ethoxyphenyl)thioureido)-*N,N*-diethylbenzamide



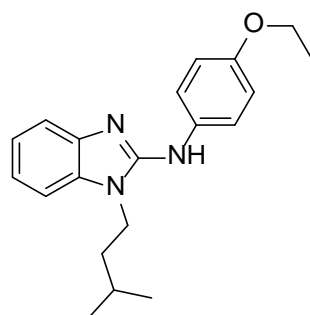
14a

The reaction was carried out according to general procedure **V** using 3-amino-*N,N*-diethyl-4-(benzylamino)benzamide **10** (2.40 mmol, 0.72 g) and 1-ethoxy-4-isothiocyanatobenzene **11a** (2.64 mmol, 0.47 g). The crude product was purified by column chromatography using CH₂Cl₂, MeOH and NH₃, aq. 25 % (50:1:0.1) as eluent system. Product **14a** was obtained as a pale red oil (1.60 mmol, 0.76 g, 66 %).

¹H NMR (CDCl₃, 400 MHz): δ = 1.15 (t, J = 6.8 Hz, 6 H), 1.38 (t, J = 7.0 Hz, 3 H), 3.41 (br, 4 H), 3.98 (q, J = 6.9 Hz, 2 H), 4.26 (d, J = 5.6 Hz, 2 H), 4.99 (br, NH), 6.49 (d, J = 8.4 Hz, 1 H), 6.84 (d, J = 8.8 Hz, 2 H), 7.11 (dd, J = 8.4, 2.0 Hz, 1 H), 7.16 (d, J = 2.0 Hz, 1 H), 7.30 (m, 7 H), 8.53 (br, NH), 8.87 (br, NH) ppm.

¹³C NMR (CDCl₃, 101 MHz): δ = 12.68 – 14.46, 14.87, 39.05 – 44.62, 47.38, 63.64, 110.88, 114.57, 124.09, 126.66, 126.95, 127.25, 127.98, 128.64, 131.40, 138.77, 145.89, 157.04, 171.67, 182.03 ppm.

Synthesis of *N*-(4-ethoxyphenyl)-1-isopentyl-benzoimidazole-2-amine



15a

The reaction was carried out according to general procedure **VI** using 1-(4-ethoxyphenyl)-3-(2-(isopentylamino)phenyl)thiourea **12a** (0.28 mmol, 0.10 g). The crude product was purified by column chromatography using petroleum ether and EtOAc (3:1) as eluent system. Product **15a** was obtained as a white solid (0.18 mmol, 0.06 g, 64 %).

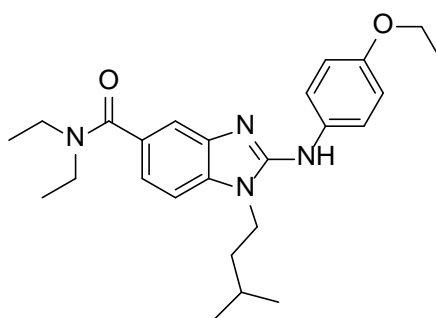
¹H NMR (MeOD, 400 MHz): δ = 1.00 (d, J = 6.4 Hz, 6 H), 1.39 (t, J = 7.0 Hz, 3 H), 1.68 (m, 3 H), 4.04 (q, J = 7.0 Hz, 2 H), 4.18 (m, 2 H), 6.92 (d, J = 8.8 Hz, 2 H), 7.10 (m, 2 H), 7.25 (m, 1 H), 7.32 (m, 1 H), 7.38 (d, J = 9.2 Hz, 2 H) ppm.

¹³C NMR (MeOD, 101 MHz): δ = 15.21, 22.89, 27.09, 38.48, 41.94, 64.85, 109.39, 115.89, 116.17, 116.41, 121.79, 122.76, 123.99, 141.36, 141.25, 159.30 ppm.

ESI: m/z calcd for C₂₀H₂₅N₃O [M+H]⁺: 324.21; found: 324.20.

HPLC purity: 95 % (Retention time: 10.04).

Synthesis of 2-((4-ethoxyphenyl)amino)-*N,N*-diethyl-1-isopentyl-benzimidazole-5-carboxamide



16a

The reaction was carried out according to general procedure **VI** using 3-(3-(4-ethoxyphenyl)thioureido)-*N,N*-diethyl-4-(isopentylamino)benzamide **13a** (0.25 mmol, 0.12 g). The crude product was purified by column chromatography using CH₂Cl₂, MeOH and NH_{3,aq}, 25 % (20:1:0.1) as eluent system. Product **16a** was obtained as a pale red solid (0.12 mmol, 0.05 g, 43 %).

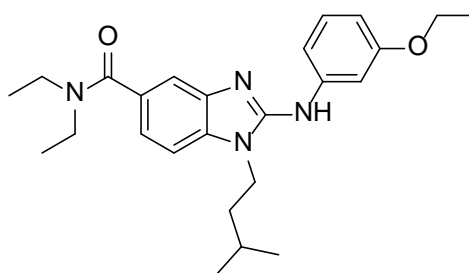
¹H NMR (CDCl₃, 400 MHz): δ = 0.82 (d, J = 6.0 Hz, 6 H), 1.13 (br, 6 H), 1.33 (t, J = 7.0 Hz, 3 H), 1.43 (m, 3 H), 3.40 (br, 4 H), 3.64 (t, J = 7.4 Hz, 2 H), 3.94 (q, J = 7.2 Hz, 2 H), 6.73 (d, J = 8.0 Hz, 1 H), 6.81 (d, J = 8.8 Hz, 2 H), 6.90 (d, J = 8.0 Hz, 1 H), 7.27 (br, NH), 7.38 (s, 1 H), 7.46 (d, J = 8.8 Hz, 2 H) ppm.

¹³C NMR (CDCl₃, 101 MHz): δ = 12.86 – 14.73, 15.06, 22.57, 25.97, 37.67, 41.13, 64.02, 107.79, 114.72, 115.46, 119.43, 121.02, 129.99, 133.41, 134.43, 141.27, 151.46, 154.98, 172.73 ppm.

ESI: m/z calcd for C₂₅H₃₄N₄O₂ [M+H]⁺: 423.27; found: 423.15.

HPLC purity: 97 % (Retention time: 10.30 min).

Synthesis of 2-((3-ethoxyphenyl)amino)-*N,N*-diethyl-1-isopentyl-benzimidazole-5-carboxamide



16b

The reaction was carried out according to general procedure **VI** using 3-(3-(3-ethoxyphenyl)thioureido)-*N,N*-diethyl-4-(isopentylamino)benzamide **13b** (0.30 mmol, 0.14 g). The crude product was purified by column chromatography using petroleum ether and EtOAc (1:10) as eluent system. Product **16b** was obtained as a brown solid (0.11 mmol, 0.05 g, 52 %).

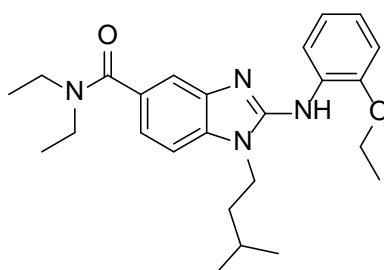
¹H NMR (CDCl₃, 400 MHz): δ = 0.83 (d, J = 6.4 Hz, 6 H), 1.09 – 1.34 (m, 6 H), 1.33 – 1.47 (m, 6 H), 3.39 – 3.65 (br, 4 H), 3.63 (t, J = 7.6, 2 H), 4.03 (q, J = 7.0 Hz, 2 H), 6.49 – 6.52 (m, 1H), 6.71 (d, J = 8.1 Hz, 1 H), 6.87 – 6.94 (m, 1 H), 7.11 – 7.14 (m, 1H), 7.15 – 7.22 (m, 2H), 7.34 (d, J = 4.0 Hz, 1H), 7.76 – 8.03 (br, NH) ppm.

¹³C NMR (CDCl₃, 101 MHz): δ = 14.89, 22.36, 25.70, 37.32, 40.69, 63.28, 104.71, 107.49, 107.99, 110.61, 113.53, 119.09, 128.77, 129.75, 133.68, 140.70, 142.21, 150.56, 159.74, 173.23 ppm.

ESI: m/z calcd for C₂₅H₃₄N₄O₂ [M+H]⁺: 423.27; found: 423.35.

HPLC purity: 95 % (Retention time: 8.49 min).

Synthesis of 2-((2-ethoxyphenyl)amino)-*N,N*-diethyl-1-isopentyl-benzimidazole-5-carboxamide



16c

The reaction was carried out according to general procedure **VI** using 3-(3-(2-ethoxyphenyl)thioureido)-*N,N*-diethyl-4-(isopentylamino)benzamide **13c** (0.41 mmol, 0.19 g).

The crude product was purified by column chromatography using petroleum ether and EtOAc (1:10) as eluent system. Product **16c** was obtained as a brown solid (0.20 mmol, 0.09 g, 52 %).

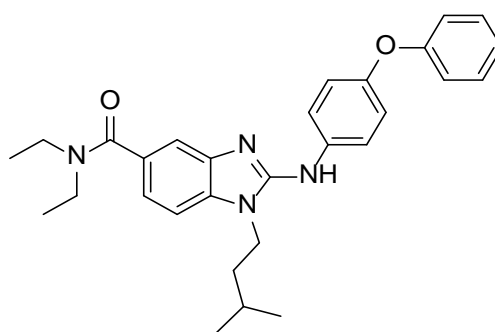
¹H NMR (CDCl₃, 400 MHz): δ = 1.01 (d, J = 6.2 Hz, 6 H), 1.11 – 1.23 (m, 6 H), 1.46 (t, J = 7.0 Hz, 3 H), 1.69 (m, 3 H), 3.46 (br, 4 H), 3.95 – 4.02 (m, 2 H), 4.12 (q, J = 7.0 Hz, 2 H), 6.86 (dd, J = 8.1, 1.2 Hz, 1 H), 6.93 (m, 1 H), 7.01 – 7.05 (m, 1 H), 7.10 (d, J = 8.0 Hz, 2 H), 7.17 (dd, J = 8.1, 1.4 Hz, 1 H), 7.58 (d, J = 1.0 Hz, 1 H), 8.56 (dd, J = 8.0, 1.5 Hz, *NH*) ppm.

¹³C NMR (CDCl₃, 101 MHz): δ = 15.02, 22.46, 25.94, 37.74, 41.00, 64.15, 107.37, 110.56, 115.49, 117.40, 119.48, 121.35, 121.55, 129.08, 130.46, 134.07, 141.69, 146.47, 149.96, 172.19 ppm.

ESI: m/z calcd for C₂₅H₃₄N₄O₂ [M+H]⁺: 423.27; found: 423.25.

HPLC purity: > 99 % (Retention time: 7.66 min).

Synthesis of *N,N*-diethyl-1-isopentyl-2-((4-phenoxyphenyl)amino)-benzimidazole-5-carboxamide



16d

The reaction was carried out according to general procedure **VI** using *N,N*-diethyl-4-(isopentylamino)-3-(3-(4-phenoxyphenyl)thioureido)benzamide **13d** (0.65 mmol, 0.33 g). The crude product was purified by column chromatography using petroleum ether and EtOAc (1:2) as eluent system. Product **16d** was obtained as a brown solid (0.38 mmol, 0.18 g, 58 %).

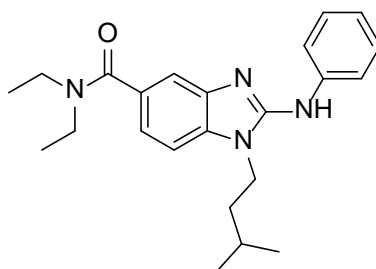
¹H NMR (CDCl₃, 400 MHz): δ = 0.89 (d, J = 6.4 Hz, 6 H), 0.96 – 1.41 (m, 8 H), 1.40 – 1.61 (m, 3 H), 3.33 – 3.69 (m, 4 H), 3.69 (t, J = 8.0 Hz, 2 H), 6.77 (d, J = 8.1 Hz, 1 H), 6.95 (dd, J = 8.1, 1.4 Hz, 1 H), 6.99 – 7.09 (m, 5 H), 7.28 – 7.35 (m, 2 H), 7.38 (s, 1 H), 7.57 (d, J = 8.8 Hz, 2 H), 7.70 (s, 1 H) ppm.

¹³C NMR (CDCl₃, 101 MHz): δ = 22.39, 25.80, 37.37, 40.74, 107.87, 113.69, 117.88, 119.17, 119.61, 120.50, 122.45, 128.96, 129.57, 133.85, 136.75, 140.85, 150.81, 151.09, 158.38, 173.15 ppm.

ESI: m/z calcd for $C_{29}H_{34}N_4O_2$ $[M+H]^+$: 471.27; found: 471.30.

HPLC purity: > 99 % (Retention time: 9.17 min).

Synthesis of *N,N*-diethyl-1-isopentyl-2-(phenylamino)-benzimidazole-5-carboxamide



16e

The reaction was carried out according to general procedure **VI** using *N,N*-diethyl-4-(isopentylamino)-3-(3-phenylthioureido)benzamide **13e** (0.51 mmol, 0.21 g). The crude product was purified by column chromatography using CH_2Cl_2 , MeOH and NH_3 , aq. 25 % (25:1:0.1) as eluent system. Product **16e** was obtained as a yellow-brown solid (0.30 mmol, 0.1 g, 60 %).

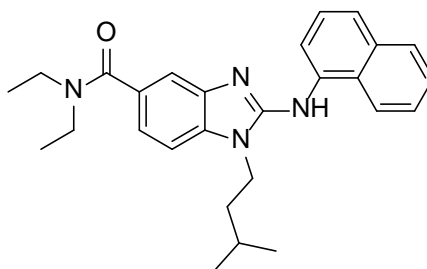
1H NMR ($CDCl_3$, 400 MHz): δ = 0.86 (d, J = 6.4 Hz, 6 H), 1.22 (m, 6 H), 1.40 (m, 2 H), 1.47 (m, 1 H), 3.51 (m, 4 H), 3.67 (t, J = 7.6 Hz, 2 H), 6.73 (d, J = 8.0 Hz, 1 H), 6.92 (dd, J = 8.0, 1.2 Hz, 1 H), 6.98 (m, 1 H), 7.33 (m, 2 H), 7.37 (d, J = 0.8 Hz, 1 H), 7.58 (d, J = 8.6 Hz, 2 H), 7.81 (br, 1 H) ppm.

^{13}C NMR ($CDCl_3$, 101 MHz): δ = 22.49, 25.87, 37.48, 40.83, 108.02, 113.76, 118.22, 119.19, 121.64, 129.01, 129.23, 133.85, 140.89, 140.97, 150.71, 173.33 ppm.

ESI: m/z calcd for $C_{23}H_{32}N_4O$ $[M+H]^+$: 379.24; found: 379.20.

HPLC purity: > 99 % (Retention time: 9.63 min).

Synthesis of *N,N*-diethyl-1-isopentyl-2-(naphthalen-1-ylamino)-benzimidazole-5-carboxamide



16f

The reaction was carried out according to general procedure **VI** using *N,N*-diethyl-4-(isopentylamino)-3-(3-(naphthalen-1-yl)thioureido)benzamide **13f** (0.71 mmol, 0.33 g). The crude product was purified by column chromatography using petroleum ether and EtOAc (1:5) as eluent system. Product **16f** was obtained as a pale red solid (0.50 mmol, 0.23 g, 76 %).

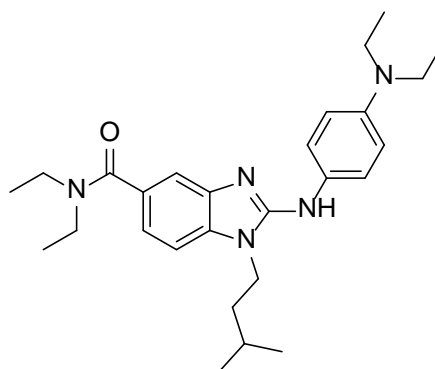
¹H NMR (CDCl₃, 400 MHz): δ = 0.84 (d, *J* = 6.4 Hz, 6 H), 1.18 (m, 7 H), 1.51 (m, 1 H), 1.59 (m, 2 H), 3.44 (m, 4 H), 3.91 (t, *J* = 7.8 Hz, 2 H), 7.05 (d, *J* = 8.0 Hz, 1 H), 7.15 (dd, *J* = 8.2, 1.0 Hz, 1 H), 7.42 (m, 2 H), 7.51 (m, 2 H), 7.61 (m, 2 H), 7.87 (m, 1 H), 8.15 (m, 1 H) ppm.

¹³C NMR (CDCl₃, 101 MHz): δ = 22.45, 25.93, 37.49, 41.73, 108.15, 114.56, 117.25, 119.85, 121.79, 124.03, 126.09, 126.15, 126.27, 127.39, 128.67, 130.40, 134.65, 151.69, 172.27 ppm.

ESI: *m/z* calcd for C₂₇H₃₄N₄O [M+H]⁺: 429.26; found: 429.30.

HPLC purity: 98 % (Retention time: 8.07 min).

Synthesis of 2-((4-(diethylamino)phenyl)amino)-*N,N*-diethyl-1-isopentyl-benzimidazole-5-carboxamide



16g

The reaction was carried out according to general procedure **VI** using 3-(3-(4-(diethylamino)phenyl)thioureido)-*N,N*-diethyl-4-(isopentylamino)benzamide **13g** (0.63 mmol, 0.32 g). The crude product was purified by column chromatography using petroleum ether and EtOAc (1:10) as eluent system. Product **16g** was obtained as a green solid (0.19 mmol, 0.08 g, 33 %).

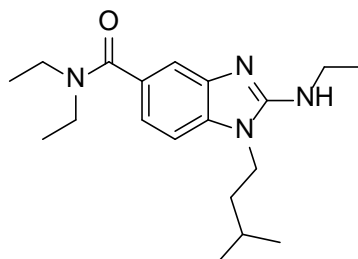
¹H NMR (CDCl₃, 400 MHz): δ = 0.84 (d, *J* = 5.9 Hz, 6 H), 1.01 – 1.35 (m, 12 H), 1.39 - 1.52 (s, 3 H), 3.06 – 3.65 (m, 8 H), 3.67 (s, 2 H), 6.65 (br, 2 H), 6.79 (d, *J* = 7.8 Hz, 1 H), 6.97 (d, *J* = 6.8 Hz, 1 H), 7.22 – 7.66 (m, 3 H) ppm.

¹³C NMR (CDCl₃, 101 MHz): δ = 11.57, 13.10, 21.41, 24.75, 28.67, 36.27, 39.78, 43.96, 106.36, 112.69, 112.90, 117.80, 120.70, 128.21, 133.34, 140.06, 151.27, 171.84 ppm.

ESI: m/z calcd for $C_{27}H_{39}N_5O$ $[M+H]^+$: 450.32; found: 450.35.

HPLC purity: > 99 % (Retention time: 10.81 min).

Synthesis of *N,N*-diethyl-2-(ethylamino)-1-isopentyl-benzoimidazole-5-carboxamide



16h

The reaction was carried out according to general procedure **VI** using *N,N*-diethyl-3-(3-ethylthioureido)-4-(isopentylamino)benzamide **13h** (0.86 mmol, 0.31 g). The crude product was purified by column chromatography using CH_2Cl_2 and MeOH (10:1) as eluent system. Product **16h** was obtained as a brown oil (0.37 mmol, 0.12 g, 43 %).

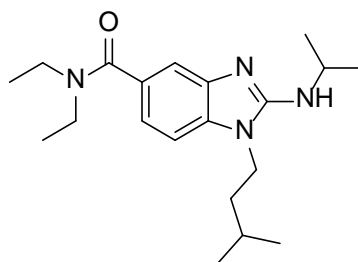
1H NMR ($CDCl_3$, 400 MHz): δ = 0.88 (d, J = 6.4 Hz, 6 H), 1.21 – 1.03 (br, 6 H), 1.25 (t, J = 7.2 Hz, 3 H), 1.41 – 1.57 (m, 3 H), 3.32 (br, 4 H), 3.41 – 3.48 (m, 2 H), 3.61 – 3.68 (t, J = 5.7 Hz, 2 H), 5.04 (br, NH), 6.84 (d, J = 8.0 Hz, 1 H), 6.94 (d, J = 8.0 Hz, 1 H), 7.30 (s, 1 H) ppm.

^{13}C NMR ($CDCl_3$, 101 MHz): δ = 15.07, 22.39, 25.72, 31.17, 38.10, 40.34, 106.84, 113.36, 118.08, 129.35, 134.78, 141.44, 154.84, 172.74 ppm.

ESI: m/z calcd for $C_{19}H_{30}N_4O$ $[M+H]^+$: 331.24; found: 331.30.

HPLC purity: > 99 % (Retention time: 10.25 min).

Synthesis of *N,N*-diethyl-1-isopentyl-2-(isopropylamino)-benzoimidazole-5-carboxamide



16i

The reaction was carried out according to general procedure **VI** using *N,N*-diethyl-4-(isopentylamino)-3-(3-isopropylthioureido)benzamide **13i** (0.76 mmol, 0.29 g). The crude

product was purified by column chromatography using CH₂Cl₂, MeOH and NH₃, aq. 25 % (25:1:0.1) as eluent system. Product **16i** was obtained as a yellow-brown solid (0.70 mmol, 0.24 g, 92 %).

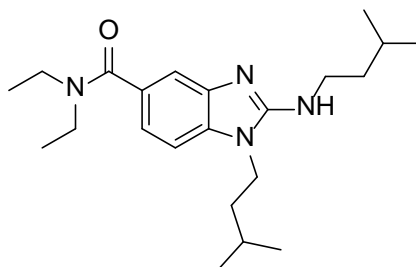
¹H NMR (CDCl₃, 400 MHz): δ = 0.96 (d, *J* = 6.0 Hz, 6 H), 1.16 (m, 6 H), 1.31 (d, *J* = 6.4 Hz, 6 H), 1.59 (m, 3 H), 3.44 (m, 4 H), 3.79 (t, *J* = 7.4 Hz, 2 H), 4.11 (br, 1 H), 4.24 (m, 1 H), 6.97 (d, *J* = 8.0 Hz, 1 H), 7.06 (dd, *J* = 8.0, 1.2 Hz, 1 H), 7.42 (m, 1 H) ppm.

¹³C NMR (CDCl₃, 101 MHz): δ = 22.58, 23.53, 25.84, 37.57, 40.59, 45.22, 107.06, 114.26, 118.63, 130.12, 134.95, 141.90, 154.02, 172.51 ppm.

ESI: *m/z* calcd for C₂₀H₃₂N₄O [M+H]⁺: 345.26; found: 345.20.

HPLC purity: > 99 % (Retention time: 10.80 min).

Synthesis of *N,N*-diethyl-1-isopentyl-2-(isopentylamino)-benzoimidazole-5-carboxamide



16j

The reaction was carried out according to general procedure **VI** using *N,N*-diethyl-4-(isopentylamino)-3-(3-isopentylthioureido)benzamide **13j** (0.59 mmol, 0.24 g). The crude product was purified by column chromatography using CH₂Cl₂, MeOH and NH₃, aq. 25 % (20:1:0.1) as eluent system. Product **16j** was obtained as a white solid (0.50 mmol, 0.20 g, 92 %).

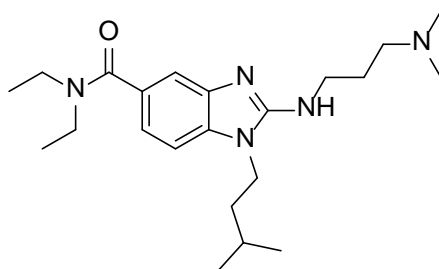
¹H NMR (CDCl₃, 400 MHz): δ = 0.94 (m, 12 H), 1.16 (m, 6 H), 1.51 (m, 2 H), 1.57 (m, 3 H), 1.72 (m, 1 H), 3.44 (m, 6 H), 3.72 (t, *J* = 7.4 Hz, 2 H), 4.44 (br, 1 H), 6.90 (d, *J* = 8.0 Hz, 1 H), 6.99 (dd, *J* = 8.0, 1.2 Hz, 1 H), 7.37 (s, 1 H) ppm.

¹³C NMR (CDCl₃, 101 MHz): δ = 22.56, 22.73, 25.84, 26.15, 37.48, 38.87, 40.53, 41.96, 106.96, 113.98, 118.36, 129.73, 135.05, 141.87, 154.96, 172.69 ppm.

ESI: *m/z* calcd for C₂₂H₃₆N₄O [M+H]⁺: 373.29; found: 373.20.

HPLC purity: 95 % (Retention time: 8.02 min).

Synthesis of 2-((3-(dimethylamino)propyl)amino)-*N,N*-diethyl-1-isopentyl-benzoimidazole-5-carboxamide



16k

The reaction was carried out according to general procedure **VI** using 3-(3-(3-(dimethylamino)propyl)thioureido)-*N,N*-diethyl-4-(isopentylamino)benzamide **13k** (0.75 mmol, 0.32 g). The crude product was purified by column chromatography using CH₂Cl₂, MeOH and NH₃, aq. 25 % (10:1:0.1) as eluent system. Product **16k** was obtained as a pale yellow oil (0.30 mmol, 0.12 g, 40 %).

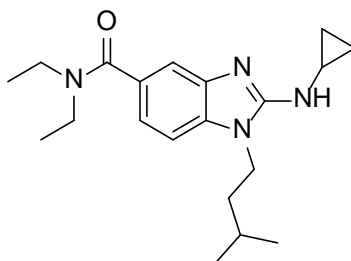
¹H NMR (CDCl₃, 400 MHz): δ 0.99 (d, *J* = 6.4 Hz, 6 H), 1.17 (m, 6 H), 1.63 (m, 3 H), 1.85 (m, 2 H), 2.31 (s, 6 H), 2.41 (br, 1 H), 2.55 (t, *J* = 5.6 Hz, 2 H), 3.43 (m, 4 H), 3.63 (t, *J* = 5.8 Hz, 2 H), 3.79 (m, 2 H), 6.99 (d, *J* = 8.0 Hz, 1 H), 7.07 (dd, *J* = 8.0, 1.6 Hz, 1 H), 7.40 (d, *J* = 1.2 Hz, 1 H) ppm.

¹³C NMR (CDCl₃, 101 MHz): δ = 22.62, 24.95, 26.20, 37.57, 40.92, 44.67, 45.62, 60.10, 106.79, 114.08, 118.47, 129.94, 135.27, 142.20, 155.50, 172.62 ppm.

ESI: *m/z* calcd for C₂₂H₃₇N₅O [M+H]⁺: 388.30; found: 388.20.

HPLC purity: 95 % (Retention time: 6.00 min).

Synthesis of 2-(cyclopropylamino)-*N,N*-diethyl-1-isopentyl-benzoimidazole-5-carboxamide



16l

The reaction was carried out according to general procedure **VI** using 3-(3-(3-cyclopropylthioureido)-*N,N*-diethyl-4-(isopentylamino)benzamide **13l** (0.66 mmol, 0.25 g). The crude product was purified by preparative HPLC (injection: each run 2.0 mL with 9 mg

crude compound in MeOH:H₂O 7:4; method: A: H₂O, B: MeOH, V(B)/(V(A)+V(B)) = 65% to 90% 15 min, V(B)/(V(A)+V(B)) = 90% 2 min, V(B)/(V(A)+V(B)) = 90% to 65% 3 min, V(B)/(V(A)+V(B)) = 65% 2 min; flow rate: 3.0 mL min⁻¹; UV detection: 254 nm). Product **16l** was obtained as a yellow solid (0.40 mmol, 0.13 g, 57 %).

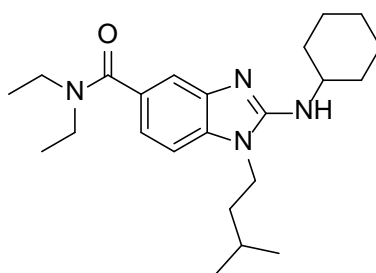
¹H NMR (CDCl₃, 400 MHz): δ = 0.62 (m, 2 H), 0.85 (m, 2 H), 0.91 (d, *J* = 6.4 Hz, 6 H), 1.17 (m, 6 H), 1.48 (m, 2 H), 1.55 (m, 1 H), 2.88 (m, 1 H), 3.44 (m, 4 H), 3.71 (t, *J* = 7.8 Hz, 2 H), 5.14 (br, 1 H), 6.93 (d, *J* = 8.0 Hz, 1 H), 7.04 (d, *J* = 8.0 Hz, 1 H), 7.45 (s, 1 H) ppm.

¹³C NMR (CDCl₃, 101 MHz): δ = 7.45, 22.55, 25.28, 25.88, 37.47, 40.73, 107.26, 114.45, 118.78, 129.79, 134.93, 141.56, 155.20, 172.70 ppm.

ESI: *m/z* calcd for C₂₀H₃₀N₄O [M+H]⁺: 343.24; found: 343.20.

HPLC purity: 98 % (Retention time: 11.39 min).

Synthesis of 2-(cyclohexylamino)-*N,N*-diethyl-1-isopentyl-benzimidazole-5-carboxamide



16m

The reaction was carried out according to general procedure **VI** using 3-(3-cyclohexylthioureido)-*N,N*-diethyl-4-(isopentylamino)benzamide **13m** (0.59 mmol, 0.25 g). The crude product was purified by column chromatography using CH₂Cl₂, MeOH and NH₃, aq. 25 % (25:1:0.1) as eluent system. Product **16m** was obtained as a beige solid (0.50 mmol, 0.21 g, 94 %).

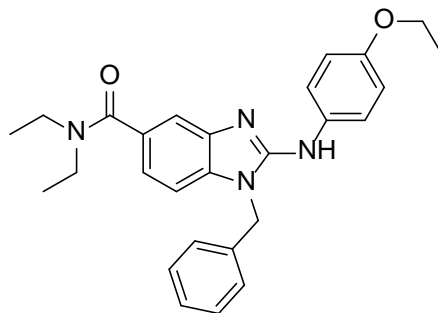
¹H NMR (CDCl₃, 400 MHz): δ = 0.97 (d, *J* = 6.4 Hz, 6 H), 1.20 (m, 9 H), 1.60 (m, 8 H), 2.15 (m, 2 H), 3.43 (m, 4 H), 3.81 (t, *J* = 7.6 Hz, 2 H), 3.94 (m, 2 H), 4.13 (br, 1 H), 6.98 (d, *J* = 8.0 Hz, 1 H), 7.06 (dd, *J* = 8.2, 1.4 Hz, 1 H), 7.43 (d, *J* = 0.8 Hz, 1 H) ppm.

¹³C NMR (CDCl₃, 101 MHz): δ = 22.61, 24.96, 25.81, 25.83, 33.94, 37.59, 40.61, 51.75, 107.04, 114.23, 118.64, 130.18, 134.93, 141.75, 153.89, 172.50 ppm.

ESI: *m/z* calcd for C₂₃H₃₆N₄O [M+H]⁺: 385.29; found: 385.20.

HPLC purity: > 99 % (Retention time: 11.05 min).

Synthesis of 1-benzyl-2-((4-ethoxyphenyl)amino)-*N,N*-diethyl-benzoimidazole-5-carboxamide



17a

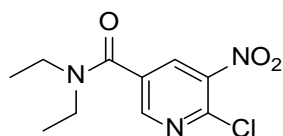
The reaction was carried out according to general procedure **VI** using 3-(3-(4-ethoxyphenyl)thioureido)-*N,N*-diethyl-4-(benzylamino)benzamide **14a** (1.05 mmol, 0.50 g). The crude product was purified by column chromatography using CH₂Cl₂, MeOH and NH_{3,aq,25 %} (50:1:0.1) as eluent system. Product **17a** was obtained as a pale red solid (0.40 mmol, 0.17 g, 39 %).

¹H NMR (CDCl₃, 400 MHz): δ = 1.13 (br, 6 H), 1.32 (t, J = 7.0 Hz, 3 H), 3.39 (br, 4 H), 3.92 (q, J = 7.1 Hz, 2 H), 4.96 (s, 2 H), 6.78 (d, J = 8.8 Hz, 2 H), 6.83 (d, J = 8.4 Hz, 1 H), 6.93 (d, J = 7.6 Hz, 1 H), 7.04 (d, J = 7.2 Hz, 2 H), 7.19 – 7.23 (m, 3 H), 7.32 (d, J = 8.8 Hz, 2 H), 7.40 (s, 1 H) ppm.

¹³C NMR (CDCl₃, 101 MHz): δ = 14.15 – 14.24, 14.90, 45.85, 63.83, 107.75, 114.40, 115.18, 119.23, 120.65, 126.73, 128.00, 129.03, 129.96, 133.12, 134.54, 135.49, 141.35, 151.76, 154.66, 172.69 ppm.

HPLC purity: 96 % (Retention time: 10.50 min).

Synthesis of 6-chloro-*N,N*-diethyl-5-nitronicotinamide



19

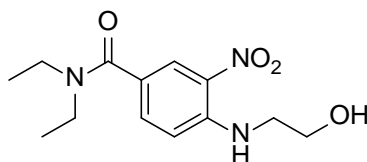
The reaction was carried out according to general procedure **I** using commercially available 6-chloro-5-nitronicotinic acid **18** (3.08 mmol, 0.78 g) and HNEt₂ (3.70 mmol, 0.39 mL). Product **19** was obtained as a yellow oil (2.90 mmol, 0.70 g, 54 %).

¹H NMR (CDCl₃, 400 MHz): δ = 1.23 (t, J = 6.4 Hz, 6 H), 3.45 (m, 4 H), 8.53 (s, 1 H), 8.56 (s, 1 H) ppm.

^{13}C NMR (CDCl_3 , 101 MHz): δ = 13.99, 43.44, 124.42, 133.81, 136.86, 154.11, 156.77, 167.47 ppm.

ESI: m/z calcd for $\text{C}_{10}\text{H}_{12}\text{ClN}_3\text{O}_3$ $[\text{M}+\text{H}]^+$: 258.06; found: 258.20.

Synthesis of *N,N*-diethyl-4-((2-hydroxyethyl)amino)-3-nitrobenzamide



20

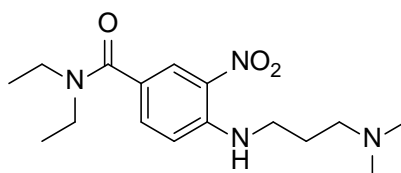
The reaction was carried out according to general procedure II using *N,N*-diethyl-4-fluoro-3-nitrobenzamide **3** (6.58 mmol, 1.58 g) and 2-aminoethanol (7.52 mmol, 0.45 mL). Product **20** was obtained as a red-orange oil (6.50 mmol, 1.99 g, > 99 %).

^1H NMR (CDCl_3 , 400 MHz): δ = 1.20 (t, J = 7.2 Hz, 6 H), 3.22 (br, 1 H), 3.43 (m, 6 H), 3.88 (m, 2 H), 6.85 (d, J = 9.2 Hz, 1 H), 7.48 (dd, J_1 = 9.0 Hz, J_2 = 1.8 Hz, 1 H), 8.23 (d, J = 2.0 Hz, 1 H), 8.32 (m, 1 H) ppm.

^{13}C NMR (CDCl_3 , 101 MHz): δ = 45.20, 60.54, 114.17, 123.55, 125.67, 130.96, 135.05, 146.11, 169.71 ppm.

ESI: m/z calcd for $\text{C}_{13}\text{H}_{19}\text{N}_3\text{O}_4$ $[\text{M}+\text{H}]^+$: 304.13; found: 304.00.

Synthesis of 4-((3-(dimethylamino)propyl)amino)-*N,N*-diethyl-3-nitrobenzamide



21

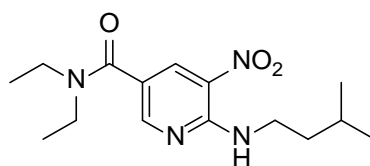
The reaction was carried out according to general procedure II using *N,N*-diethyl-4-fluoro-3-nitrobenzamide **3** (2.50 mmol, 0.60 g) and *N,N'*-dimethylpropane-1,3-diamine (2.81 mmol, 0.35 mL). Product **21** was obtained as an orange oil (2.50 mmol, 0.84 g, > 99 %).

^1H NMR (CDCl_3 , 400 MHz): δ = 1.18 (t, J = 7.0 Hz, 6 H), 1.84 (m, 2 H), 2.23 (s, 6 H), 2.41 (t, J = 6.4 Hz, 2 H), 3.39 (m, 6 H), 6.87 (d, J = 8.8 Hz, 1 H), 7.50 (dd, J_1 = 8.8 Hz, J_2 = 2.0 Hz, 1 H), 8.24 (d, J = 2.0 Hz, 1 H), 8.66 (m, 1 H) ppm.

^{13}C NMR (CDCl_3 , 101 MHz): δ = 26.42, 42.15, 45.50, 57.52, 113.99, 123.38, 125.69, 130.78, 135.11, 146.04, 169.54 ppm

ESI: m/z calcd for $C_{16}H_{26}N_4O_3$ $[M+H]^+$: 323.20; found: 323.60.

Synthesis of *N,N*-diethyl-6-(isopentylamino)-5-nitronicotinamide



22

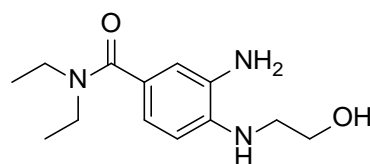
The reaction was carried out according to general procedure **II** using 6-chloro-*N,N*-diethyl-5-nitronicotinamide **19** (0.92 mmol, 0.2 g) and isopentylamine (0.92 mmol, 0.10 mL). Product **22** was obtained as an orange oil (0.89 mmol, 0.24 g, > 99 %).

1H NMR ($CDCl_3$, 400 MHz): δ = 0.97 (d, J = 6.4 Hz, 6 H), 1.23 (t, J = 6.8 Hz, 6 H), 1.61 (m, 2 H), 1.73 (m, 1 H), 3.45 (d, 5.6 Hz, 4 H), 3.72 (s, 2 H), 8.39 (s, 1 H, *NH*), 8.53 (s, 1 H), 8.56 (s, 1 H) ppm.

^{13}C NMR ($CDCl_3$, 101 MHz): δ = 22.60, 26.07, 31.63, 36.68, 38.22, 39.20, 40.30, 120.63, 134.93, 152.29, 153.70, 162.74, 166.97 ppm.

ESI: m/z calcd for $C_{15}H_{24}N_4O_3$ $[M+H]^+$: 309.19; found: 309.10.

Synthesis of 3-amino-*N,N*-diethyl-4-((2-hydroxyethyl)amino)benzamide



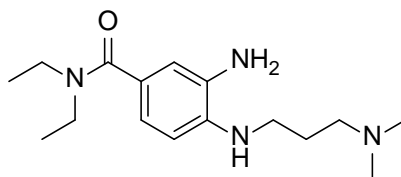
23

The reaction was carried out according to general procedure **III** using *N,N*-diethyl-4-((2-hydroxyethyl)amino)-3-nitrobenzamide **20** (7.04 mmol, 1.98 g). Product **23** was obtained as colourless oil (5.40 mmol, 1.35 g, 76 %).

1H NMR, ^{13}C NMR: no NMR data available.

ESI: m/z calcd for $C_{13}H_{21}N_3O_2$ $[M+H]^+$: 252.16; found: 252.10.

Synthesis of 3-amino-4-((3-(dimethylamino)propyl)amino)-*N,N*-diethylbenzamide



24

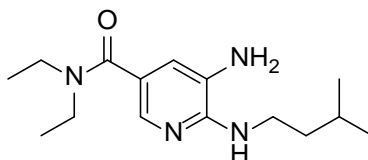
The reaction was carried out according to general procedure III using 4-((3-(dimethylamino)propyl)amino)-*N,N*-diethyl-3-nitrobenzamide **21** (2.61 mmol, 0.84 g). Product **24** was obtained as colourless oil (2.50 mmol, 0.76 g, 96 %).

¹H NMR (CDCl₃, 400 MHz): δ = 1.16 (m, 6 H), 1.84 (m, 2 H), 2.26 (s, 6 H), 2.43 (m, 2 H), 3.20 (m, 2 H), 3.38 (m, 7 H), 6.56 (d, J = 8.0 Hz, 1 H), 6.78 (s, 1 H), 6.84 (d, J = 8.0 Hz, 1 H) ppm.

¹³C NMR (CDCl₃, 101 MHz): δ = 26.87, 43.54, 45.69, 58.63, 110.07, 115.23, 119.60, 126.50, 133.51, 139.39, 172.13 ppm.

ESI: m/z calcd for C₁₆H₂₈N₄O [M+H]⁺: 293.23; found: 293.90.

Synthesis of 5-amino-*N,N*-diethyl-6-(isopentylamino)nicotinamide



25

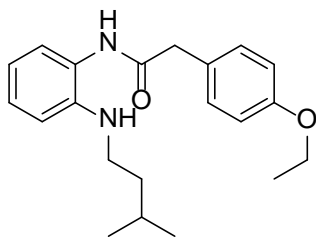
The reaction was carried out according to general procedure III using *N,N*-diethyl-6-(isopentylamino)-5-nitronicotinamide **22** (0.32 mmol, 0.10 g). Product **25** was obtained as pale yellow oil (0.24 mmol, 70.00 mg, 74 %).

¹H NMR (CDCl₃, 400 MHz): δ = 0.89 (d, J = 6.8 Hz, 6 H), 1.15 (t, J = 7.2 Hz, 6 H), 1.52 (dt, J = 15.8, 8.1 Hz, 2 H), 1.69 (m, 1 H), 2.78 (s, 3 H), 3.43 (m, 6 H), 6.89 (d, J = 1.9 Hz, 1 H), 7.69 (d, J = 1.8 Hz, 1 H) ppm.

¹³C NMR (CDCl₃, 101 MHz): δ = 13.63, 22.69, 26.10, 37.90 - 44.49, 38.66, 40.19, 120.22, 121.51, 128.36, 136.54, 190.93 ppm.

ESI: m/z calcd for C₁₅H₂₆N₄O [M+H]⁺: 279.22; found: 279.15.

Synthesis of 2-(4-ethoxyphenyl)-N-(2-(isopentylamino)phenyl)acetamide



26

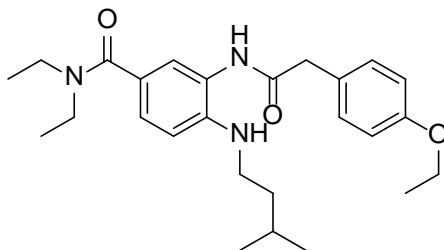
The reaction was carried out according to general procedure **VII** using *N*¹-isopentylbenzene-1,2-diamine **8** (2.39 mmol, 0.43 g). The crude product was purified by column chromatography using petroleum ether and EtOAc (3:1) as eluent system. Product **26** was obtained as a pale red solid (1.44 mmol, 0.49 g, 60 %).

¹H NMR (CDCl₃, 400 MHz): δ = 0.81 (d, *J* = 6.0 Hz, 6 H), 1.42 (t, *J* = 6.8 Hz, 3 H), 1.55 (m, 3 H), 3.03 (m, 2 H), 3.76 (s, 2 H), 4.00 (q, *J* = 7.2 Hz, 2 H), 6.86 (d, *J* = 8.8 Hz, 2 H), 6.97 (m, 2 H), 7.16 - 7.24 (m, 3 H), 7.37 (d, *J* = 8.4 Hz, 2 H), 7.59 (d, *J* = 8.0 Hz, 1 H) ppm.

¹³C NMR (CDCl₃, 101 MHz): δ = 14.98, 22.30, 26.02, 38.37, 43.48, 63.57, 114.97, 116.03, 121.11, 121.38, 126.74, 126.98, 130.58, 130.83, 164.09, 188.58 ppm.

ESI: *m/z* calcd for C₂₁H₂₈N₂O₂ [M+H]⁺: 341.22; found: 341.25.

Synthesis of 3-(2-(4-ethoxyphenyl)acetamido)-N,N-diethyl-4-(isopentylamino)benzamide



27

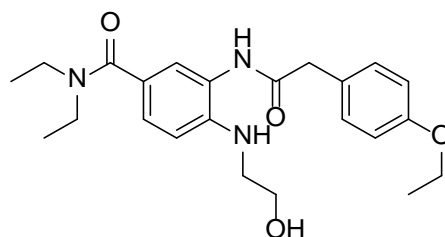
The reaction was carried out according to general procedure **VII** using 3-amino-*N,N*-diethyl-4-(isopentylamino)benzamide **9** (3.71 mmol, 1.03 g). The crude product was purified by column chromatography using petroleum ether, EtOAc, MeOH and NH_{3, aq.} 25 % (6:4:0.4:0.1) as eluent system. Product **27** was obtained as a brown oil (1.70 mmol, 0.79 g, 48 %).

¹H NMR (CDCl₃, 400 MHz): δ = 0.90 (d, *J* = 6.6 Hz, 6 H), 1.15 (m, 6 H), 1.38 (m, 5 H), 1.60 (m, 1 H), 2.93 (m, 2 H), 3.39 (m, 4 H), 3.64 (s, 2 H), 3.78 (br, 1 H), 4.01 (q, *J* = 6.9 Hz, 2 H), 6.45 (d, *J* = 8.4 Hz, 1 H), 6.86 (d, *J* = 8.7 Hz, 2 H), 7.00 (m, 2 H), 7.29 (d, *J* = 8.7 Hz, 2 H), 8.22 (br, 1 H) ppm.

¹³C NMR (CDCl₃, 101 MHz): δ = 14.94, 22.68, 26.03, 38.37, 41.85, 43.18, 63.53, 110.70, 114.96, 122.56, 124.27, 125.17, 125.61, 127.53, 130.38, 144.06, 158.28, 171.17, 172.02 ppm.

ESI: *m/z* calcd for C₂₆H₃₇N₃O₃ [M+H]⁺: 440.28; found: 440.10.

Synthesis of 3-(2-(4-ethoxyphenyl)acetamido)-*N,N*-diethyl-4-((2-hydroxyethyl)amino)benzamide



28

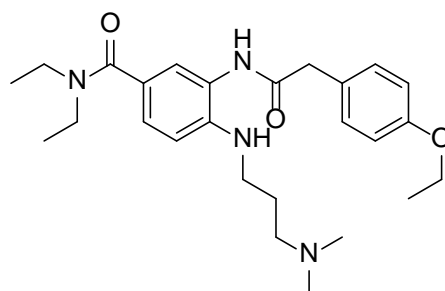
The reaction was carried out according to general procedure **VII** using 3-amino-*N,N*-diethyl-4-((2-hydroxyethyl)amino)benzamide **23** (5.37 mmol, 1.35 g). The crude product was purified by column chromatography using CH₂Cl₂, MeOH and NH₃, aq. 25 % (10:1:0.1) as eluent system. Product **28** was obtained as a brown oil (2.00 mmol, 0.84 g, 38 %).

¹H NMR (CDCl₃, 400 MHz): δ = 1.14 (m, 6 H), 1.39 (t, *J* = 7.0 Hz, 3 H), 3.09 (m, 2 H), 3.38 (m, 4 H), 3.57 (m, 5 H), 4.00 (q, *J* = 6.9 Hz, 2 H), 4.18 (br, 1 H), 6.46 (d, *J* = 8.4 Hz, 1 H), 6.84 (d, *J* = 7.2 Hz, 2 H), 6.96 (dd, *J*₁ = 8.4 Hz, *J*₂ = 1.6 Hz), 7.04 (d, *J* = 2.0 Hz, 1 H), 7.24 (d, *J* = 7.6 Hz, 2 H), 8.36 (br, 1 H) ppm.

¹³C NMR (CDCl₃, 101 MHz): δ = 14.93, 42.96, 45.92, 60.63, 63.58, 111.41, 114.96, 123.37, 124.75, 124.92, 125.39, 127.29, 130.36, 143.52, 158.25, 171.35, 172.06 ppm.

ESI: *m/z* calcd for C₂₃H₃₁N₃O₄ [M+Na]⁺: 436.22; found: 436.15.

Synthesis of 4-((3-(dimethylamino)propyl)amino)-3-(2-(4-ethoxyphenyl)acetamido)-*N,N*-diethylbenzamide



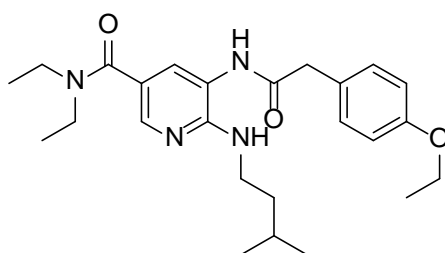
29

The reaction was carried out according to general procedure **VII** using 3-amino-4-((3-(dimethylamino)propyl)amino)-*N,N*-diethylbenzamide **24** (2.60 mmol, 0.76 g). The crude product was purified by column chromatography using CH₂Cl₂, MeOH and NH₃, aq. 25 % (12:1:0.1) as eluent system. Product **29** was obtained as a brown oil (1.4 mmol, 0.65 g, 55 %).

¹H NMR, ¹³C NMR: no NMR data available.

ESI: *m/z* calcd for C₂₆H₃₈N₄O₃ [M+H]⁺: 455.29; found: 455.40.

Synthesis of 5-(2-(4-ethoxyphenyl)acetamido)-*N,N*-diethyl-6-(isopentylamino)nicotinamide



30

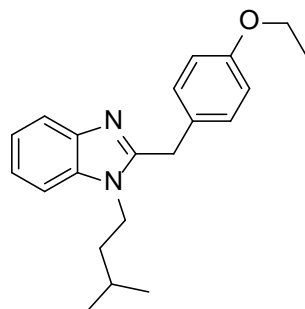
The reaction was carried out according to general procedure **VII** using 5-amino-*N,N*-diethyl-6-(isopentylamino)nicotinamide **25** (0.42 mmol, 0.12 g). The crude product was purified by column chromatography using petroleum ether and EtOAc (1:5) as eluent system. Product **30** was obtained as a brown oil (0.20 mmol, 0.09 g, 46 %).

¹H NMR (CDCl₃, 400 MHz): δ = 0.88 (d, *J* = 6.8 Hz, 6 H), 1.12 (m, 6 H), 1.33 (q, *J* = 7.2 Hz, 2 H), 1.37 (t, *J* = 7.2 Hz, 3 H), 1.56 (m, 1 H), 3.23 (m, 2 H), 3.40 (br, 4 H), 3.63 (s, 2 H), 3.99 (q, *J* = 6.8 Hz, 2 H), 4.52 (t, *J* = 4.0 Hz, 1 H, *NH*), 6.83 (d, *J* = 8.8 Hz, 2 H), 7.13 (d, *J* = 2.0 Hz, 1 H), 7.27 (d, *J* = 8.4 Hz, 2 H), 7.86 (d, *J* = 2.4 Hz, 1 H), 8.92 (s, 1 H, *NH*) ppm.

¹³C NMR (CDCl₃, 101 MHz): δ = 14.90, 22.66, 25.97, 29.76, 38.47, 39.83, 42.42 – 44.58, 43.03, 63.48, 114.87, 117.80, 119.64, 127.43, 130.21, 131.84, 143.14, 153.95, 158.22, 170.39, 171.63 ppm.

ESI: *m/z* calcd for C₂₅H₃₆N₄O₃ [M+H]⁺: 441.30; found: 441.29.

Synthesis of 2-(4-ethoxybenzyl)-1-isopentyl-benzoimidazole



31

The reaction was carried out according to general procedure **VIII** using 2-(4-ethoxyphenyl)-*N*-(2-(isopentylamino)phenyl)acetamide **26** (0.62 mmol, 0.21 g). The crude product was purified by column chromatography using petroleum ether and EtOAc (3:1) as eluent system. Product **31** was obtained as a green-brown oil (0.56 mmol, 0.18 g, 91 %).

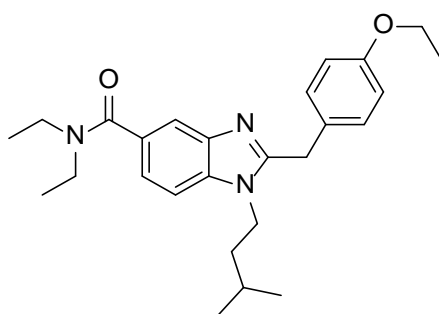
¹H NMR (CDCl₃, 400 MHz): δ = 0.94 (d, *J* = 6.8 Hz, 6 H), 1.38 (t, *J* = 6.8 Hz, 3 H), 1.42 (m, 2 H), 1.61 (m, 1 H), 3.99 (q, *J* = 6.8 Hz, 2 H), 4.12 (m, 2 H), 4.60 (s, 2 H), 6.85 (d, *J* = 8.4 Hz, 2 H), 7.28 (d, 9.6 Hz, 2 H), 7.44 (m, 3 H), 7.98 (m, 1 H) ppm.

¹³C NMR (CDCl₃, 101 MHz): δ = 14.86, 22.38, 26.36, 31.46, 37.64, 43.65, 63.73, 110.89, 115.50, 116.84, 124.69, 125.61, 125.82, 130.10, 132.27, 151.59, 158.89 ppm.

ESI: *m/z* calcd for C₂₁H₂₆N₂O [M+H]⁺: 323.21; found: 323.25.

HPLC purity: 96 % (Retention time: 11.64 min).

Synthesis of 2-(4-ethoxybenzyl)-*N,N*-diethyl-1-isopentyl-benzoimidazole-5-carboxamide



1

The reaction was carried out according to general procedure **VIII** using 3-(2-(4-ethoxyphenyl)acetamido)-*N,N*-diethyl-4-(isopentylamino)benzamide **27** (1.77 mmol, 0.78 g). The crude product was purified by column chromatography using EtOAc and MeOH (100:1) as eluent system. Product **1** was obtained as a light grey solid (1.30 mmol, 0.59 g, 79 %).

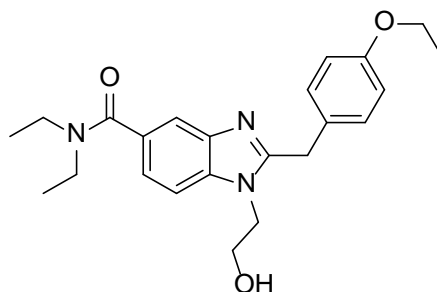
¹H NMR (CDCl₃, 400 MHz): δ = 0.90 (d, *J* = 6.6 Hz, 6 H), 1.21 (m, 6 H), 1.39 (m, 5 H), 1.56 (m, 1 H), 3.46 (m, 4 H), 3.98 (m, 4 H), 4.25 (s, 2 H), 6.83 (d, *J* = 8.4 Hz, 2 H), 7.14 (d, *J* = 8.4 Hz, 2 H), 7.29 (m, 2 H), 7.75 (s, 1 H) ppm.

¹³C NMR (CDCl₃, 101 MHz): δ = 14.93, 22.49, 26.26, 33.99, 38.24, 42.73, 63.60, 109.55, 114.97, 117.71, 121.42, 128.08, 129.60, 131.10, 135.97, 142.24, 154.51, 158.14, 171.95 ppm.

ESI: *m/z* calcd for C₂₆H₃₅N₃O₂ [M+H]⁺: 422.27; found: 422.10.

HPLC purity: > 99 % (Retention time: 8.93 min).

Synthesis of 2-(4-ethoxybenzyl)-*N,N*-diethyl-1-(2-hydroxyethyl)-benzimidazole-5-carboxamide



32

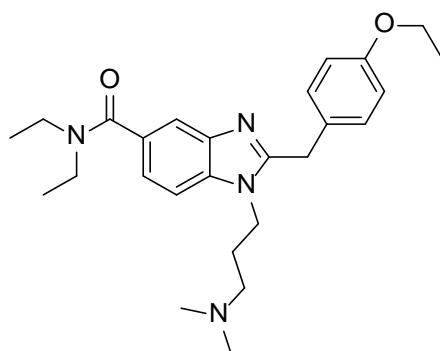
The reaction was carried out according to general procedure **VIII** using 3-(2-(4-ethoxyphenyl)acetamido)-*N,N*-diethyl-4-((2-hydroxyethyl)amino)benzamide **28** (2.03 mmol, 0.84 g). The crude product was purified by column chromatography using CH₂Cl₂, MeOH and NH₃, aq. 25 % (15:1:0.1) as eluent system. Product **32** was obtained as a brown oil (1.70 mmol, 0.66 g, 85 %).

¹H NMR (CDCl₃, 400 MHz): δ = 1.17 (m, 6 H), 1.35 (t, *J* = 7.0 Hz, 3 H), 3.40 (m, 4 H), 3.67 (t, *J* = 5.2 Hz, 2 H), 3.94 (q, *J* = 6.9 Hz, 4 H), 4.06 (m, 4 H), 4.64 (br s, 1 H), 6.75 (d, *J* = 8.8 Hz, 2 H), 7.04 (d, *J* = 8.4 Hz, 2 H), 7.08 (d, *J* = 8.4 Hz, 1 H), 7.17 (d, *J* = 8.4 Hz, 1 H), 7.65 (s, 1 H) ppm.

¹³C NMR (CDCl₃, 101 MHz): δ = 14.89, 33.35, 46.48, 60.48, 63.51, 110.05, 114.86, 117.18, 121.14, 127.99, 129.61, 130.86, 136.13, 141.82, 155.54, 158.00, 172.12 ppm.

ESI: *m/z* calcd for C₂₃H₂₉N₃O₃ [M+H]⁺: 396.22; found: 396.20.

Synthesis of 1-(3-(dimethylamino)propyl)-2-(4-ethoxybenzyl)-*N,N*-diethyl-benzimidazole-5-carboxamide



33

The reaction was carried out according to general procedure **VIII** using 4-((3-(dimethylamino)propyl)amino)-3-(2-(4-ethoxyphenyl)acetamido)-*N,N*-diethylbenzamide **29** (1.43 mmol, 0.65 g). The crude product was purified by column chromatography using CH_2Cl_2 , MeOH and NH_3 , aq. 25 % (20:1:0.1) as eluent system. Product **33** was obtained as a brown oil (0.90 mmol, 0.42 g, 67 %).

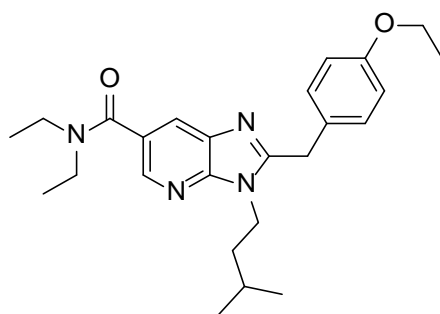
^1H NMR (CDCl_3 , 400 MHz): δ = 1.19 (m, 6 H), 1.36 (t, J = 7.0 Hz, 3 H), 1.71 (m, 2 H), 2.12 (t, J = 6.6 Hz, 2 H), 2.14 (s, 6 H), 3.44 (m, 4 H), 3.97 (q, J = 6.9 Hz, 4 H), 4.06 (t, J = 7.2 Hz, 2 H), 4.29 (s, 2 H), 6.80 (d, J = 8.8 Hz, 2 H), 7.13 (d, J = 8.8 Hz, 2 H), 7.30 (m, 2 H), 7.74 (s, 1 H) ppm.

^{13}C NMR (CDCl_3 , 101 MHz): δ = 14.91, 27.37, 33.62, 41.81, 45.36, 56.03, 63.55, 109.76, 114.93, 117.64, 121.36, 128.28, 129.57, 131.13, 136.07, 142.28, 154.90, 158.08, 171.94 ppm.

ESI: m/z calcd for $\text{C}_{26}\text{H}_{36}\text{N}_4\text{O}_2$ $[\text{M}+\text{H}]^+$: 437.29; found: 437.29.

HPLC purity: 98 % (Retention time: 6.73 min).

Synthesis of 2-(4-ethoxybenzyl)-*N,N*-diethyl-3-isopentyl-3*H*-imidazo[4,5-*b*]pyridine-6-carboxamide



34

The reaction was carried out according to general procedure **VIII** using 5-(2-(4-ethoxyphenyl)acetamido)-*N,N*-diethyl-6-(isopentylamino)nicotinamide **30** (0.20 mmol, 0.09 g). Product **34** was obtained without further purification as a brown oil (0.11 mmol, 0.05 g, 59 %).

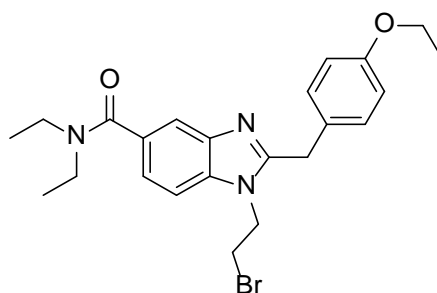
¹H NMR (CDCl₃, 400 MHz): δ = 0.87 (d, *J* = 6.4 Hz, 6 H), 1.24 (m, 6 H), 1.35 (t, *J* = 7.2 Hz, 3 H), 1.47 (m, 2 H), 1.55 (m, 1 H), 3.25 – 3.64 (m, 4 H), 3.97 (q, *J* = 7.2 Hz, 2 H), 5.11 (t, *J* = 8.0 Hz, 2 H), 4.25 (s, 2 H), 6.82 (d, *J* = 8.8 Hz, 2 H), 7.13 (d, *J* = 8.8 Hz, 2 H), 7.99 (d, *J* = 2.0 Hz, 1 H), 8.37 (d, *J* = 2.0 Hz, 1 H) ppm.

¹³C NMR (CDCl₃, 101 MHz): δ = 14.86, 22.45, 26.17, 29.77, 34.34, 38.32, 39.63, 41.57, 43.63, 63.57, 115.03, 124.92, 127.31, 127.72, 129.63, 133.97, 141.93, 148.79, 156.20, 158.20, 169.68 ppm.

ESI: *m/z* calcd for C₂₅H₃₄N₄O₂ [M+Na]⁺: 445.26; found: 445.35.

HPLC purity: > 99 % (Retention time: 10.77 min).

Synthesis of 1-(2-bromoethyl)-2-(4-ethoxybenzyl)-*N,N*-diethyl-benzoimidazole-5-carboxamide



35

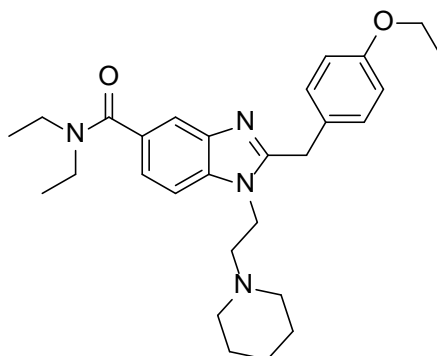
The reaction was carried out according to *Toth et al.*^[6], the hydroxy compound **32** (0.86 mmol, 0.34 g) and PPh₃ (1.11 mmol, 0.29 g) were dissolved in anhydrous THF (5 mL) and a solution of CBr₄ (1.33 mmol, 0.44 g) in anhydrous THF (2 mL) was slowly added at 0 °C. The mixture was stirred overnight at room temperature. Then, water was added, the solution was basified with NH_{3, aq. 25 %} (pH ~ 9-10) and extracted with CH₂Cl₂. The combined organic phases were dried over anhydrous Na₂SO₄. After filtration and removal of solvent *in vacuo* the product was purified by column chromatography using CH₂Cl₂:CH₃OH: NH_{3, aq. 25 %} (20:1:0.1) as eluent system. Product **35** was obtained as a brown oil (0.40 mmol, 0.19 g, 48 %).

¹H NMR (CDCl₃, 400 MHz): δ = 1.36 (t, *J* = 7.0 Hz, 3 H), 3.20 (t, *J* = 7.4 Hz, 2 H), 3.43 (m, 4 H), 3.97 (q, *J* = 6.9 Hz, 4 H), 4.29 (s, 2 H), 4.36 (t, *J* = 7.2 Hz, 2 H), 6.82 (d, *J* = 8.4 Hz, 2 H), 7.14 (d, *J* = 8.4 Hz, 2 H), 7.28 (m, 4 H), 7.75 (s, 1 H) ppm.

^{13}C NMR (CDCl_3 , 101 MHz): δ = 14.84, 27.76, 33.96, 45.40, 63.57, 109.21, 115.14, 117.91, 121.79, 127.57, 129.53, 131.70, 135.48, 142.13, 154.61, 158.24, 171.59 ppm.

ESI: m/z calcd for $\text{C}_{23}\text{H}_{28}\text{BrN}_3\text{O}_2$ $[\text{M}+\text{H}]^+$: 458.14, 460.13; found: 458.10, 460.10.

Synthesis of 2-(4-ethoxybenzyl)-*N,N*-diethyl-1-(2-(piperidin-1-yl)ethyl)-benzimidazole-5-carboxamide



36

Piperidine (0.61 mmol, 0.06 mL) and the bromo compound **35** (0.23 mmol, 0.10 g) were dissolved in acetonitrile (5 mL). Then, K_2CO_3 (1.16 mmol, 0.16 g) was added and the mixture was stirred overnight at 70 °C. After filtration the solvent was removed *in vacuo* and the crude product was purified by column chromatography using CH_2Cl_2 , MeOH and NH_3 , aq. 25 % (20:1:0.1) as eluent system. The pure product **36** was obtained as a yellow-orange oil (0.10 mmol, 0.07 g, 55 %).

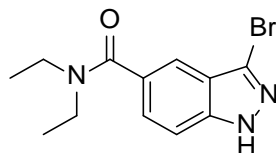
^1H NMR (CDCl_3 , 400 MHz): δ = 1.20 (m, 6 H), 1.40 (m, 5 H), 1.55 (m, 4 H), 2.33 (m, 4 H), 2.38 (t, J = 7.2 Hz, 2 H), 3.46 (m, 4 H), 3.99 (q, J = 6.9 Hz, 2 H), 4.09 (t, J = 7.2 Hz, 2 H), 4.30 (s, 2 H), 6.82 (d, J = 8.8 Hz, 2 H), 7.14 (d, J = 8.4 Hz, 2 H), 7.30 (m, 4 H), 7.74 (s, 1 H) ppm.

^{13}C NMR (CDCl_3 , 101 MHz): δ = 14.93, 24.22, 26.05, 33.83, 42.25, 55.14, 57.70, 63.61, 109.61, 115.01, 117.72, 121.46, 128.21, 129.60, 131.21, 136.04, 142.26, 155.05, 158.14, 171.94 ppm.

ESI: m/z calcd for $\text{C}_{28}\text{H}_{38}\text{N}_4\text{O}_2$ $[\text{M}+\text{H}]^+$: 463.30; found: 463.30.

HPLC purity: > 99 % (Retention time: 11.81 min).

Synthesis of 3-bromo-*N,N*-diethyl-1*H*-indazole-5-carboxamide



43

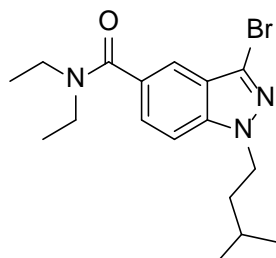
The reaction was carried out according to general procedure I using commercially available 3-bromo-1*H*-indazole-5-carboxylic acid **42** (1.24 mmol, 0.30 g) and HNEt₂ (1.49 mmol, 0.16 mL). Product **43** was obtained as a yellow oil (1.01 mmol, 0.30 g, 82 %).

¹H NMR (CDCl₃, 400 MHz): δ = 1.13 (br, 6 H), 3.11 – 3.60 (br, 4 H), 7.28 (dd, *J* = 8.0, 4.0 Hz, 1 H), 7.35 (d, *J* = 8.0 Hz, 1 H), 7.54 (m, 1 H), 12.58 (s, 1 H) ppm.

¹³C NMR (CDCl₃, 101 MHz): δ = 38.62, 46.89, 111.16, 118.09, 122.23, 122.25, 125.90, 130.00, 141.32, 171.61 ppm.

ESI: *m/z* calcd for C₁₂H₁₄BrN₃O [M+H]⁺: 296.10, 298.03; found: 296.92, 298.20.

Synthesis of 3-bromo-*N,N*-diethyl-1-isopentyl-1*H*-indazole-5-carboxamide



44

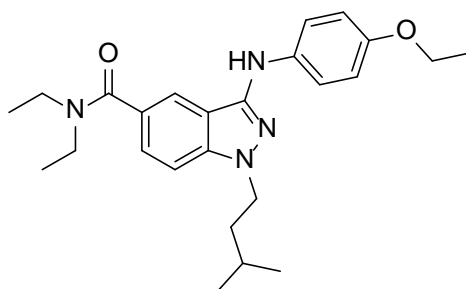
3-bromo-*N,N*-diethyl-1*H*-indazole-5-carboxamide **43** (0.79 mmol, 0.24 g) was dissolved in DMF (3 mL) and cooled down to 0 °C. Then, NaH (60 % suspension in paraffin oil) (1.58 mmol, 0.04 g) was added portionwise and stirring was continued for 10 min. After the addition of isopentylbromide (0.87 mmol, 0.10 mL), the mixture was allowed to warm up to room temperature and stirring was continued for one day. Then, water was added and the organics were extracted with EtOAc. The organic phase was then washed three times with brine, dried over anhydrous Na₂SO₄ and the solvent was removed *in vacuo*. The crude product was purified by column chromatography using petroleum ether and EtOAc (2:1) as eluent system. The pure product **44** was obtained as a light brown solid (0.19 g, 0.52 mmol, 68 %).

¹H NMR (CDCl₃, 400 MHz): δ = 0.90 (d, *J* = 6.6 Hz, 6 H), 1.17 (br, 6 H), 1.52 (m, 1 H), 1.75 (q, *J* = 8.0 Hz, 2 H), 3.38 (br, 4 H), 4.30 (t, *J* = 8.0 Hz, 2 H), 7.38 (m, 2 H), 7.59 (s, 1 H) ppm.

¹³C NMR (CDCl₃, 101 MHz): δ = 22.32, 25.60, 38.42, 47.87, 109.48, 118.77, 120.49, 123.08, 126.19, 130.40, 140.46, 170.89 ppm.

ESI: *m/z* calcd for C₁₇H₂₄BrN₃O [M+H]⁺: 366.11, 368.11; found: 366.20, 368.40.

Synthesis of 3-((4-ethoxyphenyl)amino)-*N,N*-diethyl-1-isopentyl-1*H*-indazole-5-carboxamide



45

The reaction was carried out according Lohou *et al.*^[7], to the anhydrous dioxane (5 mL) Pd(OAc)₂ (0.05 mmol, 0.01 g), xantphos (0.06 mmol, 0.04 g) and *p*-phenethidine (0.62 mmol, 0.08 mL) were added and heated to 100 °C for 5 min. Then, 3-bromo-*N,N*-diethyl-1-isopentyl-1*H*-indazole-5-carboxamide **44** (0.52 mmol, 0.19 g) and Cs₂CO₃ (1.50 mmol, 0.47 g) were added and stirring at 100 °C continued. Then, EtOAc was added and the organic phase was washed twice with brine. The organic phase was then dried over anhydrous Na₂SO₄ and the solvent removed *in vacuo*. The crude product was purified by column chromatography using petroleum ether and EtOAc (2:1) as eluent system. Pure product **45** was obtained as a red solid (0.26 mmol, 0.11 g, 50 %).

¹H NMR (CDCl₃, 400 MHz): δ = 0.95 (d, *J* = 6.6 Hz, 6 H), 1.15 (br, 6 H), 1.38 (t, *J* = 7.0 Hz, 3 H), 1.58 (m, 1 H), 1.75 (q, *J* = 8.0 Hz, 2 H), 3.42 (br, 4 H), 3.99 (q, *J* = 7.0 Hz, 2 H), 4.18 (t, *J* = 8.0 Hz, 2 H), 6.83 (m, 2 H), 6.89 (br, 1 H), 7.14 (d, *J* = 8.7 Hz, 1 H), 7.29 (dd, *J* = 8.6, 1.3 Hz, 1 H), 7.38 (m, 2 H), 7.63 (s, 1 H) ppm.

¹³C NMR (CDCl₃, 101 MHz): δ = 14.98, 22.45, 25.71, 38.32, 46.76, 63.90, 108.35, 114.76, 115.22, 118.08, 119.10, 125.39, 126.95, 136.36, 140.09, 145.15, 153.05, 172.01.

ESI: *m/z* calcd for C₂₅H₃₄N₄O₂ [M+H]⁺: 423.27; found: 423.15.

HPLC purity: > 99 % (Retention time: 11.50 min).

Biological evaluation

Inhibition of BChE and AChE

AChE (E.C. 3.1.1.7, from electric eel) and BChE (E.C. 3.1.1.8, from equine serum) were purchased from Sigma-Aldrich. DTNB (Ellman's reagent), ATC and BTC iodides were obtained from Fluka Analytical, tacrine hydrochloride was purchased from Sigma-Aldrich.

The stock solutions of the test compounds were prepared in ethanol (33.3 mM) and diluted to the desired concentrations. For the testing 50 μ L DTNB and 50 μ L enzyme were added to 1.5 mL of the buffer. After 50 μ L of the test compound was added, the mixture was incubated for 4.5 min. Afterwards, 10 μ L ATC or BTC were added and the mixture was allowed to incubate for further 2.5 min. Enzyme activity was then observed via UV ($\lambda = 412$ nm).

Radioligand binding studies on *hCB₂R* and *hCB₁R*

SR-144,528 (inverse agonist for *hCB₂R*) was bought from Santa Cruz Biotechnology Inc.; unlabeled CP-55,940 (agonist for *hCB₂R* and *hCB₁R*) was bought from Sigma-Aldrich Life Science; radioactive labeled [³H] CP-55,940 was bought from Hartmann Analytic GmbH; Rimonabant (inverse agonist for *hCB₁R*) was obtained by an in-house synthesis.

Cells were a kindly gift from AbbVie Laboratories (Chicago, U. S. A.). Human embryonic kidney cells (HEK) stably expressing the *hCB₂R*-receptor were grown in Dulbecco's modified Eagle's medium containing high glucose supplemented with 8 % fetal calf serum and 25 μ g/ml zeocin in a 37 °C incubator in the presence of 5 % CO₂. Chinese hamster ovary cells (CHO) stably expressing the *hCB₁R*-receptor were grown in Ham's F-12 Nutrient Mix supplemented with 8 % fetal calf serum and 400 μ g/ml geneticin in a 37 °C incubator in the presence of 5 % CO₂. Cells were splitted twice a week.

Cells (either HEK cells stably expressing *hCB₂R* or CHO cells stably expressing *hCB₁R*) were harvested and homogenized in Tris-EDTA buffer (50 mM Tris-HCl pH = 7.4; 1 mM MgCl₂ · 6 H₂O; 1 mM EDTA) using an ultra turax for 2x 15 s bursts. The suspensions were centrifuged for 10 min at 1,408 g at 4 °C. The pellets were discarded and the supernatant was centrifuged at 140,657 g for 50 min at 4 °C. The final membrane pellet was homogenized in binding buffer (50 mM Tris-HCl pH = 7.4; 5 mM MgCl₂ · 6 H₂O; 2.5 mM EDTA), shock frosted with liquid nitrogen and stored at -80 °C until use.

Saturation assays were done similar to S. Murkherjee *et al.*^[8] to determine the K_D-value of the membrane samples. Saturation assays were done with 8 concentrations of [³H] CP-55,940 ranging from 0.088 nM to 4,4 nM. Reactions were started by adding 8 μ g membrane per well of a 96 well Multiscreen filter plate (Millipore) containing the radioligand in assay buffer (50 mM Tris-HCl, pH = 7.4; 5 mM MgCl₂ · 6 H₂O; 2.5 mM EDTA; 2 mg/ml BSA). After 3 h incubation at RT the reaction was stopped by vacuum filtration and each well was washed

4 times with cold binding buffer (50 mM Tris-HCl, pH = 7.4; 5 mM MgCl₂ · 6 H₂O; 2.5 mM EDTA). The filter plate was dried at 40 °C. Activity was counted in a Micro Beta Trilux-Counter (Wallac) using IRGA Safe plus-scintillation cocktail (Perkin Elmer). Competition assays were done with 5-11 concentrations of replacing ligands (0.1 nM – 0.4 mM) and 0.44 nM [³H] CP-55,940. Non-specific binding was determined using 10 μM compound **1** for hCB₂R and 10 μM rimonabant for hCB₁R.

To determine the IC₅₀ values, statistical evaluations and sigmoidal dose-response curve fittings were performed with GraphPad Prism 5 software for Windows (Version 5.01, August 7, 2007) using nonlinear regression and one site fit logIC50 as curve fitting functions.

K_i values was determined when displacement of [³H]-CP 55,940 was higher than 60 % at 100 μM test compound concentration. According to the Cheng-Prusoff equation:

$$K_i = \frac{IC_{50}}{1 + \frac{[L^*]}{K_D}}$$

with [L*] as radioligand concentration (0.44 nM), the K_i value was calculated of at least two individual experiments.

K_D values and standard errors were for CB₂R K_D(hCB₂R) = 4.16 ± 3.04 and for CB₁R K_D(hCB₁R) = 2.24 ± 1.15.

Computational studies at BChE

Materials and Methods

Docking Studies: Docking to BChE was carried out with GOLD v5.2 (GOLDSUITE v5.2, CCDC Software, www.ccdc.cam.ac.uk)^[9] in the 4BDS crystal structure of human BChE (crystallization at pH 6.5, resolution 2.10 Å). The protein was set up for docking by removing all water molecules and non-protein atoms and protonation of the amino acids was performed with MOE 2014.09^[10] using Protonate 3D^[11] at standard conditions. The binding site was defined by the following residues: Asn68, Asp70, Ser79, Trp82, Asn83, Gly115, Gly116, Gly117, Gln119, Thr120, Gly121, Thr122, Leu125, Tyr128, Glu197, Ser198, Ala199, Trp231, Ala277, Leu286, Val288, Glu325, Ala328, Phe329, Tyr332, Trp430, His438, Gly439, Tyr440, Ile442. The ligand structures were either built in MOE (compounds **1** and **16a**) or extracted from the crystal structure (co-crystallized tacrine used for redocking). The pK_a value of compound **1** was experimentally measured using the apparatus SiriusT3 from Sirius Analytical via UV-metric titration (fast UV method); the protonation was set in accordance with the measured value (pK_a = 6.08). The protonation of tacrine was set according to calculations performed with the program MoKa^[12]; the acridinic N was protonated while the anilinic N was not. The ligand structures were energy minimized in MOE with the MMFF94x force field^[13] to an RMS-gradient of 0.001 kcal/(mol·Å).

The best-suited scoring function was selected based on redocking calculations of the ligand tacrine in 4BDS. Unpublished data of our research group (manuscript in preparation) showed that best results for BChE docking are obtained with GoldScore^[14,15], while also the scoring functions ASP^[16] and ChemPLP^[17] rendered good results. Thus, redocking was performed using all aforementioned scoring functions. 50 ligand poses were generated after 500 000 operation cycles. GoldScore resulted in 20/50 poses of tacrine in accordance with the crystal-structure reference, while in 25/50 poses the ligand was found in the reference position, but in a flipped orientation. This was attributed to the high level of symmetry in the structure of tacrine, as the cyclohexane ring only differs from the acridinic benzene ring by a small tilt in the crystal structure. With ASP, 47/50 poses were flipped and 3/50 were in accordance, while with ChemPLP all poses were flipped. After rescoring the poses generated from GoldScore using the scoring function DSX^[18], 9 of the top 10 poses - including the top pose- were in accordance with the reference (RMSD < 1 Å). Thus, this protocol was considered appropriate to proceed with the docking of our ligands.

Molecular Dynamics Simulations: Molecular Dynamics (MD) simulations were performed with ligand-docked BChE complexes of ligands **1** and **16a**. The MD simulations were carried out using AMBER 14^[19-21]. The atom charges of the ligands were calculated via the RESP fitting technique^[22] in AMBER 14 based on the electrostatic potentials obtained from HF/6-31G* calculations with Gaussian 09^[23]. The antechamber and tleap modules were used to assign

the Generalized Amber Force Field (GAFF)^[24] parameters to the ligands and the ff99SB force field parameters^[25] to the enzyme. The complex was neutralized by adding 3 chlorine counterions and was solvated by using boxes of TIP3P water molecules^[26], using a buffer of 10 Å in each direction. Periodic boundary conditions (PBC) were applied to avoid edge effects. The Particle Mesh Ewald (PME)^[27,28] method was used to calculate long-range electrostatic interactions. A 2000-step implicit solvent minimization was initially performed; the first 1000 steps were carried out using the steepest descent algorithm, and the remaining 1000 steps were performed with a conjugate gradient algorithm. After minimization, the system was relaxed and heated in two 50 ps steps using the sander module. At the first step, the system was slowly heated to 300 K in 40 ps and then cooled to 100 K in 10 ps with no restraints to the solvent, but keeping the protein-ligand complex fixed; at the second step the system was heated from 100 K to 300 K in 50 ps without any restraints. The system was then equilibrated in an NPT ensemble without restraints for 50 ps, followed by a production phase of 20 ns for **16a** and 50 ns for **1**.

MD of benzimidazole 1

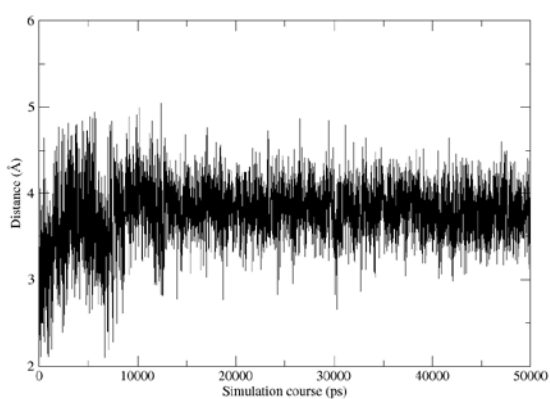


Fig. 1: Distance between Ala³²⁸ (CO) and Val³³¹ (NH).

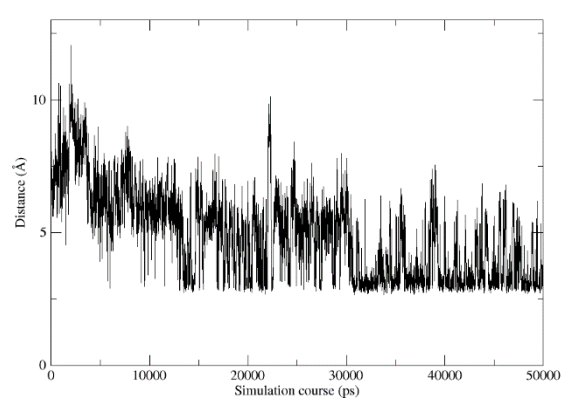


Fig. 2: Distance between Asn⁶⁸ (NH) and the O-atom of the ligand's ethyl ether.

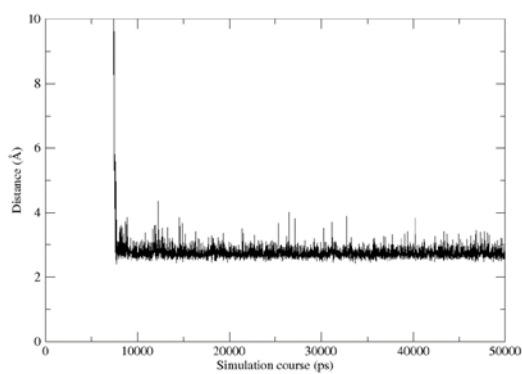


Fig. 3: Distance between Ala³²⁸ and the water molecule.

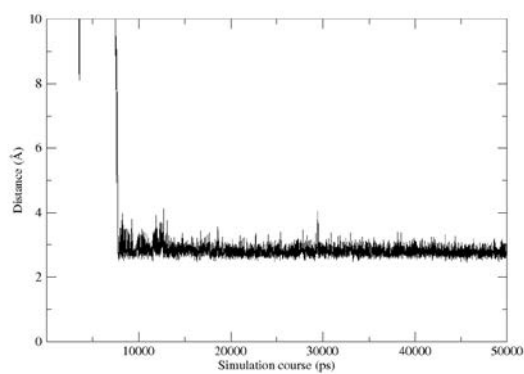


Fig. 4: Distance between the O-atom of the ligand's amide function and the water molecule.

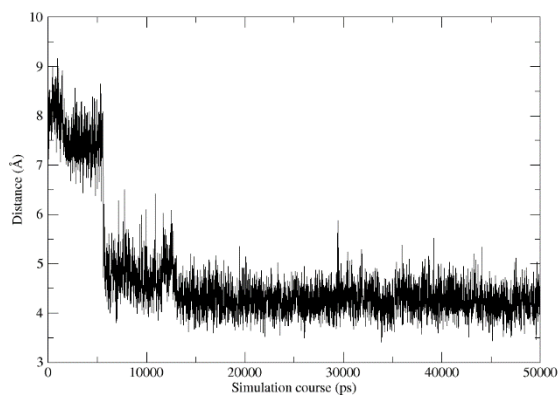


Fig. 5: Distance between Tyr³³² (NH) and the O-atom of the ligand's amide function.

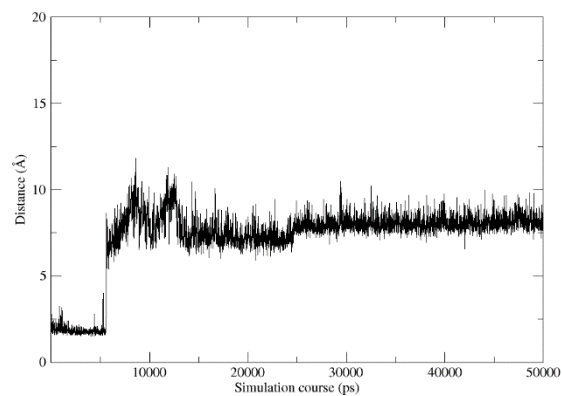


Fig. 6: Distance between Tyr³³² (OH) and the O-atom of the ligand's amide function.

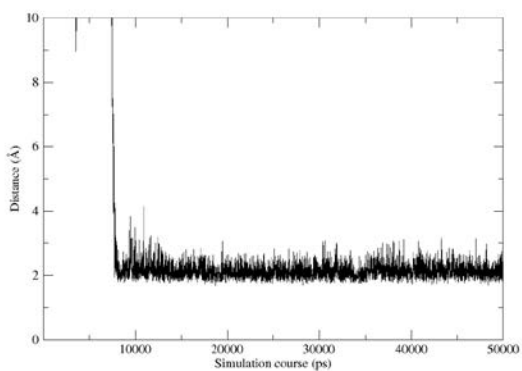


Fig. 7: Distance between Tyr³³² (NH) and the water molecule.

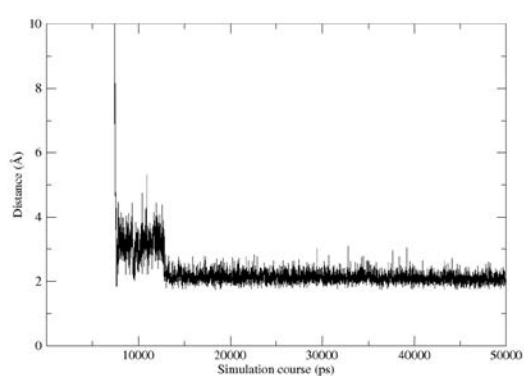


Fig. 8: Distance between Val³³¹ (NH) and the water molecule.

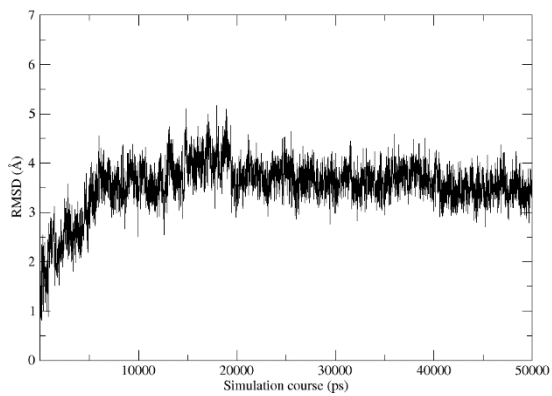


Fig. 9: RMSD of the ligand 1.

MD of 2-amino benzimidazole 16a

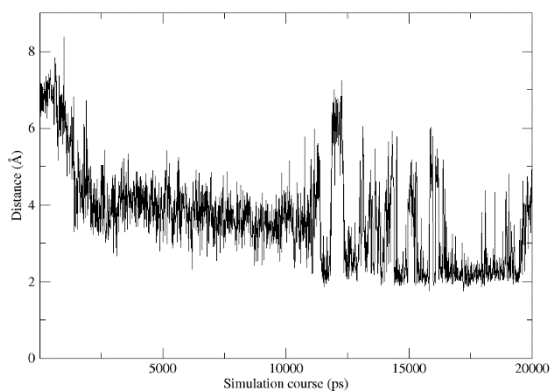


Fig. 10: Distance between Gln¹¹⁹ (NH) and the N-atom of the ligand's benzimidazole core.

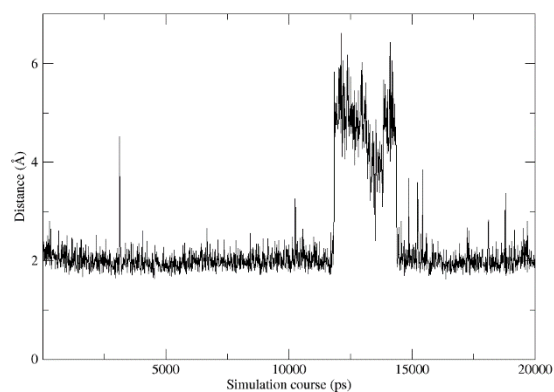


Fig. 11: Distance between Ser²⁸⁷ (CO) and the anilinic N-atom of the ligand.

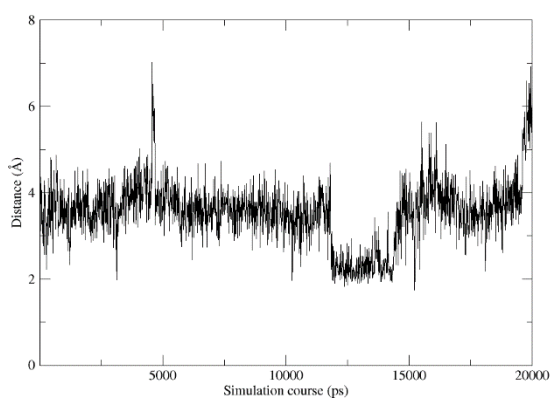


Fig. 12: Distance between Pro²⁸⁵ (CO) and the anilinic N-atom of the ligand.

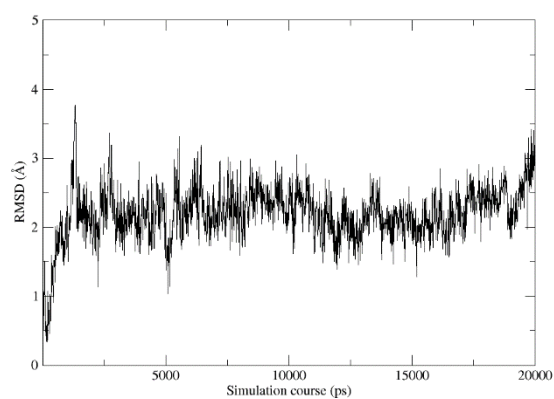


Fig. 13: RMSD of ligand 16a.

2D SAR schemes

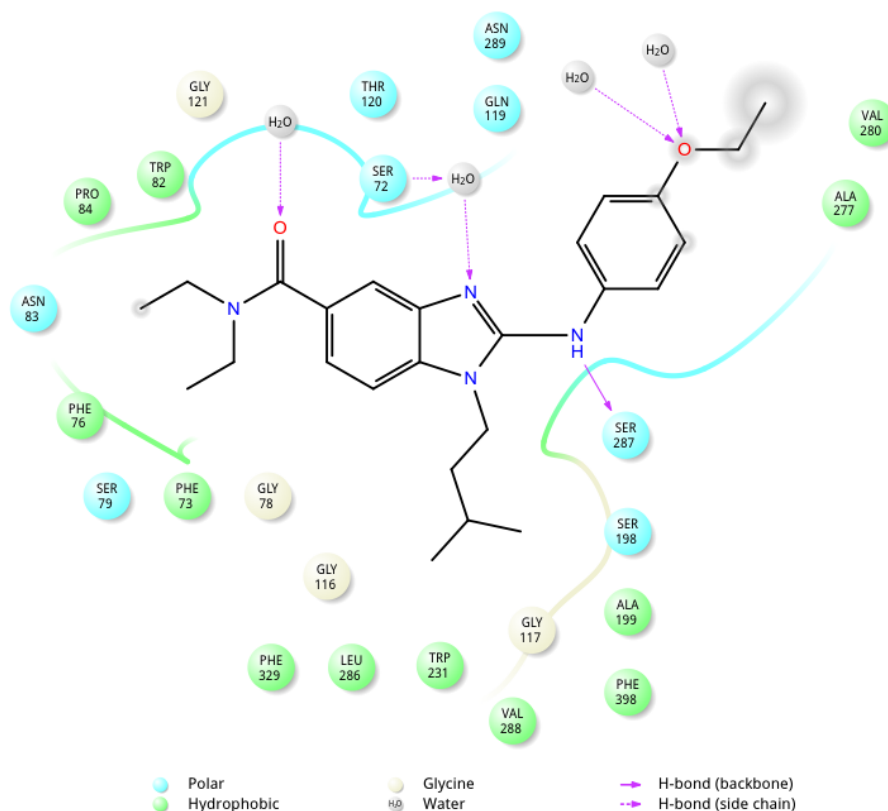


Fig. 14: 2D SAR scheme of ligand **16a** in *hBChE* (generated from the last frame of the MD)

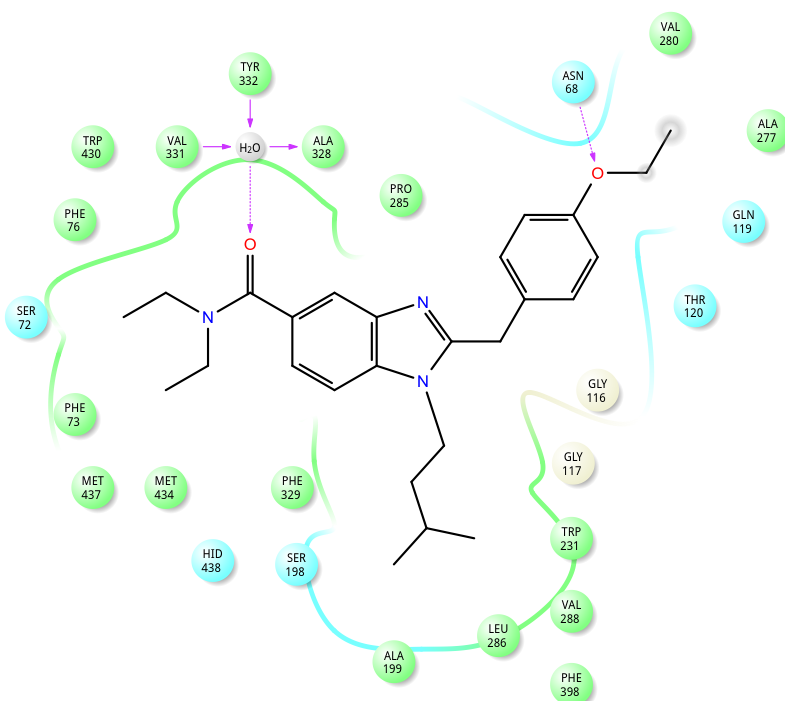


Fig. 15: 2D SAR scheme of ligand **1** in *hBChE* (generated from the last frame of the MD)

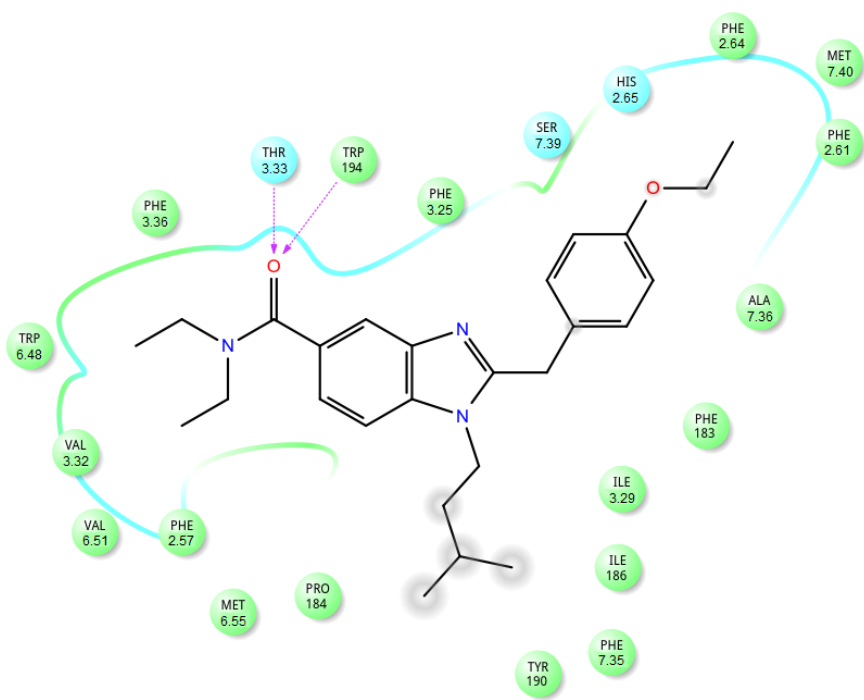


Fig. 16: 2D SAR scheme of ligand **1** in hCB_2R (generated from the last frame of the MD)

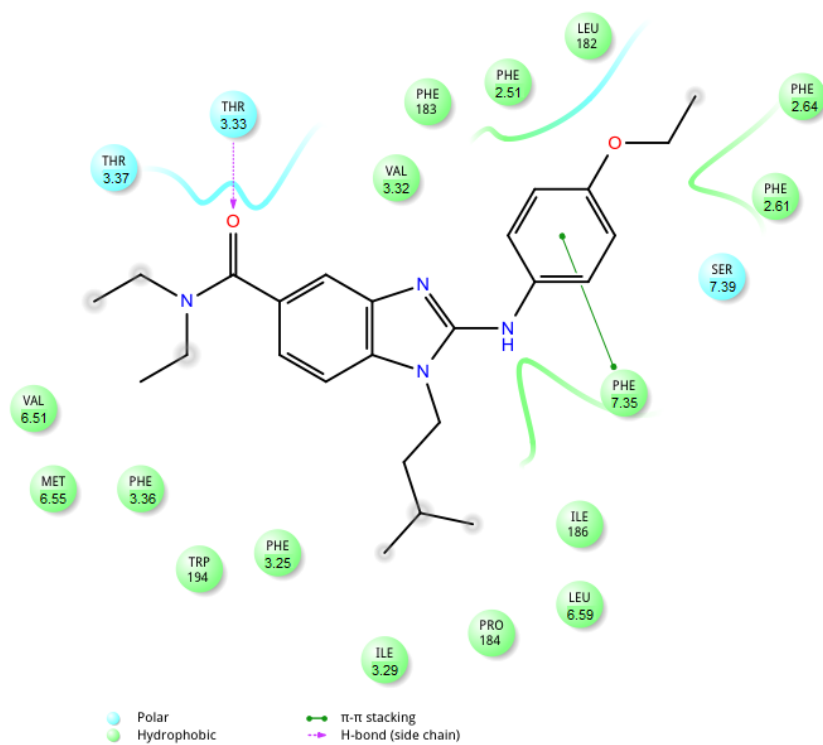


Fig. 17: 2D SAR scheme of ligand **16a** in hCB_2R (generated from the last frame of the MD)

References

- [1] Gottlieb H. E., Kotlyar V., Nudelman A. *J. Org. Chem.* **1997**, *62*, 7512 – 7515.
- [2] Bellamy F. D., Ou K. *Tetrahedron Lett.* **1984**, *25*, 839 – 842.
- [3] Munch H., Hansen J. S., Pittelkow M., Christensen J. B., Boas U. *Tetrahedron Lett.* **2008**, *49*, 3117 – 3119.
- [4] Cee V. J., Downing N. S. *Tetrahedron Lett.* **2006**, *47*, 3747 – 3750.
- [5] Pagé D., Balaux E., Boisvert L., Liu Z., Milburn C., Tremblay M., Wei Z., Woo S., Luo X., Cheng Y.-X., Yang H., Srivastava S., Zhou F., Brown W., Tomaszewski M., Walpole C., Hodzic L., St-Onge S., Godbout C., Salois D., Payza K. *Bioorg. Med. Chem.* **2008**, *18*, 3695 – 3700.
- [6] Toth J. E., Hamann P. R., Fuchs P. L. *J. Org. Chem.* **1988**, *53*, 4694 – 4708.
- [7] Lohou E., Collot V., Stiebing S., Rault S. *Synthesis* **2011**, *16*, 2651 – 2663.
- [8] Murkherjee S., Adams M., Whiteaker K., Daza A., Kage K., Cassar S., Meyer M., Yao B. B. *Eur. J. Pharmacol.* **2004**, *505*, 1 – 9.
- [9] Verdonk M. L., Cole J. C., Hartshorn M. J., Murray C. W.; Taylor R. D. *Proteins* **2003**, *52*, 609 – 623.
- [10] Molecular Operating Environment (MOE), 2013.08; Chemical Computing Group Inc., 1010 Sherbooke St. West, Suite #910, Montreal, QC, Canada, H3A 2R7, **2015**.
- [11] Labute P. Protonate 3D: Assignment of Macromolecular Protonation State and Geometry, **2007**.
- [12] Milletti F., Storchi L., Sforza G., Cruciani G. *J. Chem. Inf. Model.* **2007**, *47*, 2172 – 2181.
- [13] Halgren T. A. *J. Comput. Chem.* **1996**, *17*, 490 – 519.
- [14] Jones G., Willett P., Glen R. C., Leach A. R., Taylor R. *J. Mol. Biol.* **1997**, *267*, 727 – 748.
- [15] Jones G., Willett P., Glen R. C. *J. Mol. Biol.* **1995**, *245*, 43 – 5.
- [16] Mooij W. T. M., Verdonk M. L. *Proteins* **2005**, *61*, 272 – 287.
- [17] Korb O., Stützle T., Exner T. E. PLANTS: Application of Ant Colony Optimization to Structure-Based Drug Design. In *Ant Colony Optimization and Swarm Intelligence*; Dorigo M., Gambardella L. M., Birattari M., Martinoli A., Poli R., Stützle T., Eds.;

Lecture Notes in Computer Science; Springer Berlin Heidelberg: Berlin, Heidelberg, **2006**; Vol. 4150, pp. 247–258

- [18] Neudert G., Klebe G. *J. Chem. Inf. Model.* **2011**, *51*, 2731 – 2745.
- [19] Case D. A., Berryman J. T., Betz R. M., Cerutti D. S., Cheatham T., Darden T. A., Duke R. E., Giese T. J., Gohlke H., Goetz A., Homeyer N., Izadi S., Janowski P., Kaus J., Kovalenko A., Lee T., LeGrand S., Li P., Luchko T., Luo R., Madej B., Merz K. M., Monard G., Needham P., Nguyen H., Nguyen H., Omelyan I., Onufriev A., Roe D. R., Roitberg A., Salomon-Ferrer R., Simmerling C. L., Smith W., Swails J., Walker R. C., Wang J., Wolf R., Wu X., York D. M., Kollman P. A. AMBER 2015, **2015**.
- [20] Salomon-Ferrer R., Case D. A., Walker R. C. *Wiley Interdiscip. Rev. Comput. Mol. Sci.* **2013**, *3*, 198 – 210.
- [21] Case D. A., Cheatham T. E., Darden T., Gohlke H., Luo R., Merz K. M., Onufriev A., Simmerling C., Wang B., Woods R. J. *J. Comput. Chem.* **2005**, *26*, 1668 – 1688.
- [22] Bayly C. I., Cieplak P., Cornell W., Kollman P. A. *J. Phys. Chem.* **1993**, *97*, 10269 – 10280.
- [23] Frisch M. J., Trucks G. W., Schlegel H. B., Scuseria G. E., Robb M. A., Cheeseman J. R., Scalmani G., Barone V., Mennucci B., Petersson G. A., Nakatsuji H., Caricato M., Li X., Hratchian H. P., Izmaylov A. F., Bloino J., Zheng G., Sonnenberg J., Fox D. J. Gaussian 09, **2009**.
- [24] Wang J., Wolf R. M., Caldwell J. W., Kollman P. A., Case D. A. *J. Comput. Chem.* **2004**, *25*, 1157 – 1174.
- [25] Rezácová P., Borek D., Moy S. F., Joachimiak A., Otwinowski Z. *Proteins* **2008**, *70*, 311 – 319.
- [26] Jorgensen W. L., Chandrasekhar J., Madura J. D., Impey R. W., Klein M. L. *J. Chem. Phys.* **1983**, *79*, 926.
- [27] Darden T., York D., Pedersen L. *J. Chem. Phys.* **1993**, *98*, 10089.
- [28] Essmann U., Perera L., Berkowitz M. L., Darden T., Lee H., Pedersen L. G. *J. Chem. Phys.* **1995**, *103*, 8577.

Appendix III

Dolles, D.; Hoffmann, M.; Gunesch, S.; Marinelli, O.; Möller, J.; Santoni, G.; Chatonnet, A.; Lohse, M. J.; Wittmann, H.-J.; Strasser, A.; Nabissi, M.; Maurice, T.; Decker, M. Structure-Activity Relationships and Computational Investigations into the Development of Potent and Balanced Dual-Acting Butyrylcholinesterase Inhibitors and Human Cannabinoid Receptor 2 Ligands with Pro-Cognitive *in vivo* Profiles. *J. Med. Chem.* **2018**, *61*, 1646 – 1663.

Copyright (2018) American Chemical Society.

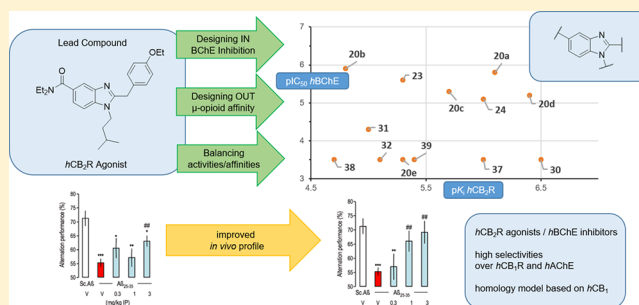
<https://pubs.acs.org/doi/abs/10.1021%2Facs.jmedchem.7b01760>

Structure–Activity Relationships and Computational Investigations into the Development of Potent and Balanced Dual-Acting Butyrylcholinesterase Inhibitors and Human Cannabinoid Receptor 2 Ligands with Pro-Cognitive in Vivo Profiles

Dominik Dolles,[†] Matthias Hoffmann,[†] Sandra Gunesch,[†] Oliviero Marinelli,[‡] Jan Möller,[§] Giorgio Santoni,[‡] Arnaud Chatonnet,^{||} Martin J. Lohse,[§] Hans-Joachim Wittmann,[⊥] Andrea Strasser,[⊥] Massimo Nabissi,[‡] Tangui Maurice,[#] and Michael Decker^{*,†,||}[†]Pharmaceutical and Medicinal Chemistry, Institute of Pharmacy and Food Chemistry, Julius Maximilian University of Würzburg, Am Hubland, D-97074 Würzburg, Germany[‡]School of Pharmacy, Department of Experimental Medicine, University of Camerino, I-62032 Camerino, Italy[§]Institute of Pharmacology and Toxicology, Julius Maximilian University of Würzburg, Versbacher Strabe 9, D-97078 Würzburg, Germany^{||}INRA UMR866, University of Montpellier, F-34060 Montpellier, France[⊥]Pharmaceutical and Medicinal Chemistry II, Institute of Pharmacy, University of Regensburg, D-95053 Regensburg, Germany[#]INSERM UMR-S1198, University of Montpellier, EPHE, F-34095 Montpellier, France

Supporting Information

ABSTRACT: The enzyme butyrylcholinesterase (BChE) and the human cannabinoid receptor 2 (hCB_2R) represent promising targets for pharmacotherapy in the later stages of Alzheimer's disease. We merged pharmacophores for both targets into small benzimidazole-based molecules, investigated SARs, and identified several dual-acting ligands with a balanced affinity/inhibitory activity and an excellent selectivity over both hCB_1R and $hAChE$. A homology model for the hCB_2R was developed based on the hCB_1R crystal structure and used for molecular dynamics studies to investigate binding modes. In vitro studies proved hCB_2R agonism. Unwanted μ -opioid receptor affinity could be designed out. One well-balanced dual-acting and selective $hBChE$ inhibitor/ hCB_2R agonist showed superior in vivo activity over the lead CB_2 agonist with regards to cognition improvement. The data shows the possibility to combine a small molecule with selective and balanced GPCR-activity/enzyme inhibition and in vivo activity for the therapy of AD and may help to rationalize the development of other dual-acting ligands.



INTRODUCTION

Alzheimer's disease (AD) is the most common form of dementia. According to the annual World Alzheimer Report, there are more than 47 million people suffering from AD. By 2050, researchers expect this number to climb up to even more than 130 million.¹ Currently, a cure is pending and pharmacotherapy is very limited. Three acetylcholinesterase (AChE) inhibitors (rivastigmine, donepezil, and galantamine) and one *N*-methyl-D-aspartate receptor (NMDA) antagonist (memantine) are currently available as drugs. Unfortunately, these drugs are only effective in early stages of AD, and they only act symptomatically but do not slow down progression or even cure AD.²

The reasons for an outbreak of this complex disease still remain unknown. AD is pathobiologically characterized by the presence of senile plaques, which consist of β -amyloid ($A\beta$). $A\beta$ is an insoluble peptide and is formed by β/γ -secretase-induced cleavage of the amyloid precursor protein (APP). Another hallmark is the

formation of neurofibrillary tangles, which consist of hyperphosphorylated τ -protein aggregates. Once formed, both $A\beta$ and τ -proteins trigger the progressive loss of muscarinic neurons in the brain and lead to memory deficits and cognitive dysfunction.^{3–5} Moreover, $A\beta$ induces activation of neuroinflammatory pathways characterized by activated microglia and astrocytes as observed in the brains of AD patients.⁶ Neuroinflammation then leads to the production of pro-inflammatory chemokines, cytokines, and neurotoxins, which speed up AD progression by themselves.⁷ The exact sequence of these cascade processes is still under discussion.

In the past years, the human cannabinoid receptors ($hCBRs$) were identified as targets for drug development concerning neurodegenerative disorders. Currently, there are two known subtypes:

Received: November 29, 2017

Published: February 5, 2018

the human cannabinoid receptors 1 (hCB_1R) and 2 (hCB_2R). hCB_1Rs are mainly expressed in the brain;⁸ hCB_2Rs were first described in the peripheral immune system⁹ and then described to occur to a lower extent in the central nervous system (CNS), especially microglia.^{10,11} In the course of AD, expression levels of hCB_1R do not change, but overexpression of hCB_2R is observed in certain brain regions (especially in the hippocampus) of AD patients.¹² Furthermore, CB_2R expression is associated with microglia and astrocytes that are surrounded by neuritic plaques.¹³ The theory that up-regulation of CB_2R signaling leads to reduction of associated inflammatory processes¹⁴ was substantiated in several in vitro studies: hCB_2R agonists reduce the production of neurotoxic factors, such as reactive oxygen species (ROS) and pro-inflammatory mediators (TNF- α and cytokines).^{15–17} Furthermore, in vivo studies support the therapeutic potential of hCB_2R agonists: Wu et al. injected $A\beta_{1-40}$ intracerebrally into rat brains and then treated the animals with MDA7, a known hCB_2R agonist. After 14 days, behavioral tests were performed (place learning in the Morris water maze) and the rat brains slices were then examined. MDA7 was found to promote $A\beta$ clearance, to decrease secretion of proinflammatory mediators and ultimately led to restored synaptic plasticity, cognition, and memory.¹⁸ In another study, transgenic Tg2576 mice that overexpress APP were continuously treated with JWH-133, another known hCB_2R agonist, at different stages of AD. As a result, $A\beta$ production was lowered, reactive microglia cells were reduced, and a positive cognitive performance was observed.¹⁹ The importance of CB_2R in $A\beta$ formation was shown in J20APP mice (overexpression of APP in neocortex and hippocampus). Deletion of CB_2R led to an increased formation and deposition of $A\beta$, which supports CB_2R 's role as a reducing agent of $A\beta$.²⁰ In summary, activation of hCB_2R leads to various beneficial effects concerning AD and additionally seems to play a central role in other neurodegenerative diseases such as Parkinson's and Huntington's disease.²¹

The oldest theory regarding AD pathophysiology is the “cholinergic hypothesis”, which describes the massive loss of cholinergic neurons in AD.²² The amount of acetylcholinesterase (AChE), the metabolizing enzyme of the neurotransmitter acetylcholine (ACh), decreases in the course of AD. However, the concentration of its isoenzyme butyrylcholinesterase (BChE) stays unchanged or even increases and is able to compensate for the loss of AChE, since BChE can also hydrolyze ACh into choline and acetate.^{23,24} Besides that, it was shown that BChE (over-) expression is associated with senile plaques and the transformation of nonfibrillar to fibrillary $A\beta$ plaques.^{25,26} Inhibition of BChE is therefore a promising approach when it comes to combat AD's cognitive deficits, especially in later stages when AChE diminishes.²⁷ In a very recent in vivo study, BChE knockout mice showed enhanced learning abilities in memory tests as compared to wildtype littermates, and after intercerebroventricular injections of $A\beta_{25-35}$ oligomers, BChE knockout mice appeared less sensitive to the learning and memory deficits, oxidative stress, and decrease in hippocampal ACh, as induced by the amyloid peptide in wildtype animals.²⁸ In another study, a sulfonamide-based nanomolar BChE inhibitor was investigated. In one of the very few in vivo studies that applied BChE-selective inhibitors, mice treated with this inhibitor showed improved memory and learning abilities in passive avoidance and Morris water maze tests without producing acute cholinergic adverse effects.²⁹

Furthermore, it is remarkable that there's a colocalization of BChE and hCB_2Rs in microglia cells of the pathophysiologically altered brain. Glia cells play an important role in production of BChE and can be specifically targeted by CB_2R agonists.^{30,31}

The multifactorial character of AD makes it difficult if not impossible to apply the classical “one target—one disease” for successful drug development.³² It is therefore advantageous to develop multitarget drugs, which address different targets simultaneously. These drugs consist of two drug entities either as a hybrid linked by a spacer³³ or merged into one single entity;^{32,34–36} for the latter case, only a few successful examples have been described. (For a review, see ref 35.) Hybrids addressing CBRs as one of the targets have been developed successfully.^{37–39} In a remarkable recent work, Rampa et al. have achieved inhibiting both $hBChE$ and fatty acid amide hydrolase (FAAH) and therefore target both the endocannabinoid and cholinergic system.⁴⁰ The main disadvantage of hybrid molecules is their (often) high molecular weight, which goes along with a violation of Lipinski's rule of five.⁴¹ In contrast, merged ligands are still “small molecules” and their molar mass remains often at the same level as the “single compound”.^{35,36} In return, their development is more laborious. Both drug moieties have to be “fused” into one entity. The problem is that, if affinity is increased at one target, it is very likely decreased at the other one.^{36,37} There are three common approaches to obtain such merged/dual-acting compounds: “designing in”, “designing out”, and “balancing”. The most common approach is “designing in”, where structural elements of two highly selective ligands are combined in one molecule, and the resulting compound then incorporates activity at the two desired targets. In a second approach, a merged compound not only possesses activity for two desired targets but also shows undesirable activity at a third target. In this case, “designing out” aims for excluding activity at the third, undesired target but keeping activity at the other two desired ones. In the third approach, a compound shows a very high affinity for one target but only moderate activity for the other target. Here, the aim is to balance the affinity at both desired targets.^{32,35} Despite these difficulties, there are already several successful examples for merged ligands in the recent literature, such as adenosine A_{2A} receptor/monoamine oxidase B ligands and human histamine H_3 receptor antagonists/AChE inhibitors developed in our group; the latter proved successful even in vivo.^{42,43}

In our previous work,³⁶ we applied a novel pharmacophore model for BChE inhibitors to several benzimidazole-based selective hCB_2R agonists initially developed by AstraZeneca A (Figure 1)⁴⁴ in a “designing in” approach. A related merged structure based on indazole had been described before.⁴⁵ After the synthesis of various heterocyclic templates and applying various substitution patterns, we had obtained a first substance library and some compounds showed activity in the (sub)micromolar range at both targets and an excellent selectivity over both hCB_1R and AChE (Figure 1).³⁶ Furthermore, we conducted molecular dynamics (MD) simulations in both hCB_2R and BChE, which gave the first insights into the binding mode of our lead compounds **A** and **B** and helped the understanding of structure–activity relationships (SARs) at both targets.

In the present study, we developed our compound portfolio further by balancing activities at hCB_2R and BChE and by investigating and designing out unwanted interactions with the μ opioid receptor (MOP). We synthesized and characterized in a portfolio of in vitro assays 13 novel dual-acting hCB_2R ligands and BChE inhibitors. We furthermore investigated for the first time intrinsic activities at the hCB_2R for second and third generation compounds. Finally, we evaluated the ability of our second generation lead compound **B** to fight cognition deficits induced by intracerebroventricular (ICV) $A\beta_{25-35}$ injections in mice, as an in vivo pharmacological model for AD.

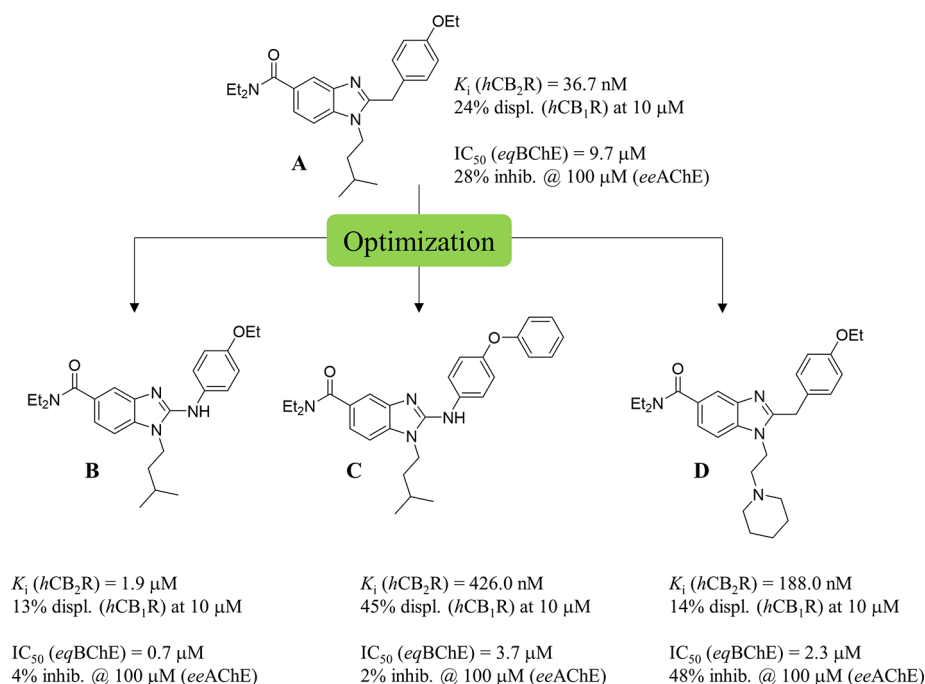


Figure 1. Development of the second generation lead structures B, C, and D starting from AstraZeneca's selective hCB_2R agonist A, the first generation lead.^{36,44}

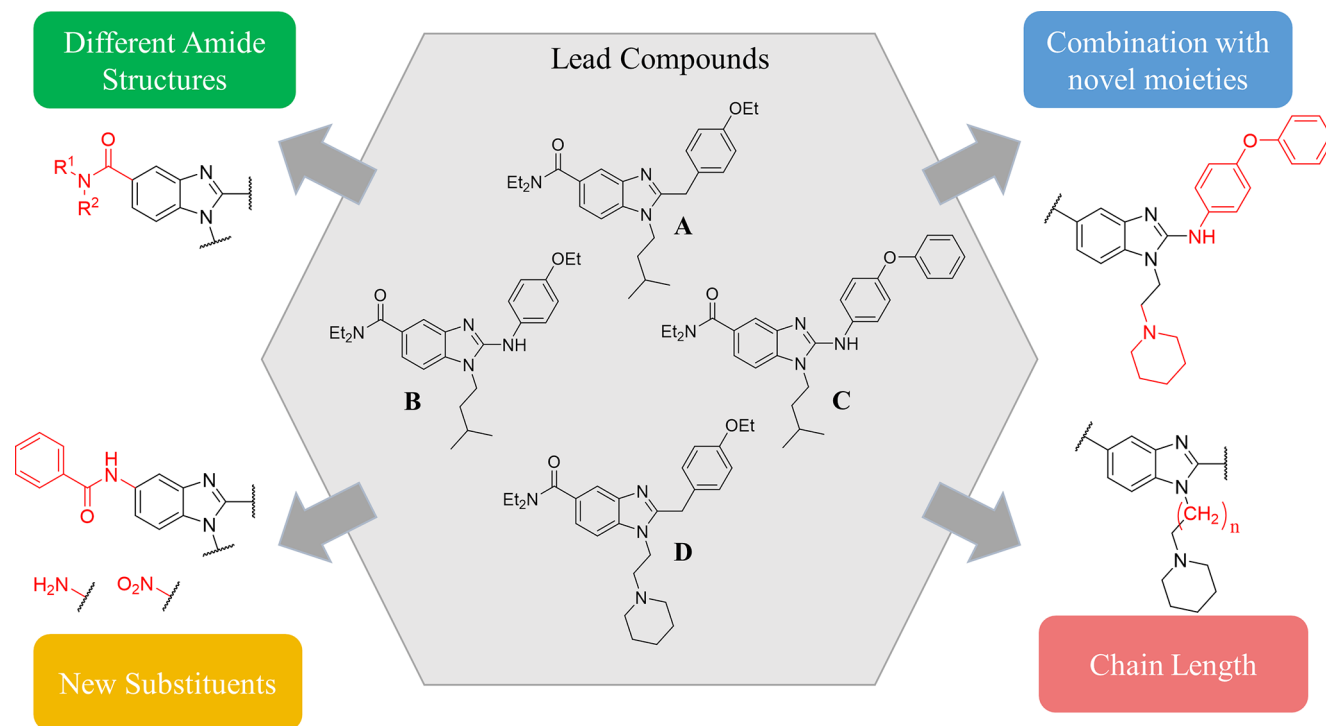


Figure 2. Structural compound design approaches carried out starting from lead compounds A–D.

RESULTS

Chemistry. The difficulty in designing a multitarget compound is to “fuse” drug entities and at the same time to keep or even improve the activity at both targets. The starting point for advanced synthetic approaches are Astra Zeneca's benzimidazole A as well as our second generation lead compounds B, C, and D described very recently (Figures 1 and 2).^{36,44} These compounds already showed either a high affinity at one of the two targets or even a balanced micromolar activity profile. From these results, we followed several design approaches (Figure 2): the introduction of

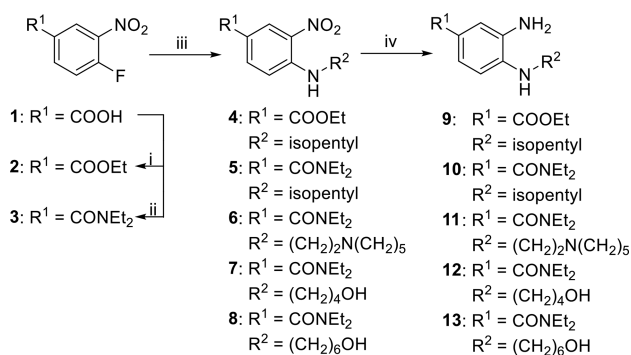
different amides (green) and substituents (yellow) at position 5 of the benzimidazole core, alternation of the chain length (red), and a combination of the most promising substitution patterns (blue). Before, we also had synthesized other heterocyclic templates such as amino-indazoles, but the compounds lost affinity at all targets.³⁶ Therefore, we returned to the initial structural template.

The necessity of a (diethyl)amide for a high hCB_2R affinity had been previously demonstrated,^{36,44} but data for inhibition of either AChE or BChE of several amides was not available. The

electron-withdrawing character of amides led us using substituents with different electronic effects (e.g., nitro and amino) at position 5 of the benzimidazole core. Ethylenepiperidinyl substitution at the N^1 of the benzimidazole core already caused (sub)micromolar activity at both hCB_2R and BChE. The aim was to extend the alkylene chain and to increase lipophilicity and interaction between the side chain and the oxyanion hole of the BChE.³⁶ Lastly, we combined the most promising substituents in order to increase dual-activity.

Specifically, the synthesis of benzimidazoles and 2-amino benzimidazoles was carried out as previously reported starting from 4-fluoro-3-nitrobenzoic acid **1**.³⁶ To introduce the different amide moieties in the last step, esterification was performed to obtain ester **2**. For the synthesis of target compounds **23**, **24**, and **30–32**, the diethylamide moiety **3** was formed using HBTU as the coupling agent. In the next step, nucleophilic substitution with various amines afforded compounds **4–8**. Reduction of the nitro group was achieved using tin(II) to obtain *o*-phenylenediamines **9–13** (Scheme 1).

Scheme 1. Synthesis of *o*-Phenylene Diamine Precursors 9–13^a



^aConditions: (i) H_2SO_4 , EtOH, reflux, 24 h; (ii) HNEt_2 , $(\text{COCl})_2$, NEt_3 , DMF, 0 °C to rt, 5 h; (iii) NHR^2 , NEt_3 , EtOH, rt, 3 h; (iv) $\text{SnCl}_2 \cdot 2\text{H}_2\text{O}$, EtOH, reflux, 6 h.

To obtain benzimidazoles with various amide moieties and spacer lengths, diamines **9**, **12**, and **13** were coupled with

2-(4-ethoxyphenyl)acetic acid to afford compounds **14–16**. Cyclization was achieved in glacial acetic acid, and benzimidazoles **17–19** were obtained in quantitative yields. Ester **17** was hydrolyzed under basic conditions and then coupled with various amines using HBTU as a coupling agent. After purification, amides **20a–e** were obtained in high yields. For various spacer lengths, hydroxy compounds **18** and **19** were treated in an Appel-like reaction with phosphorus tribromide to obtain the bromo compounds **21** and **22**. In the last step, bromine was substituted with piperidine under basic conditions to afford compounds **23** and **24** (Scheme 2).

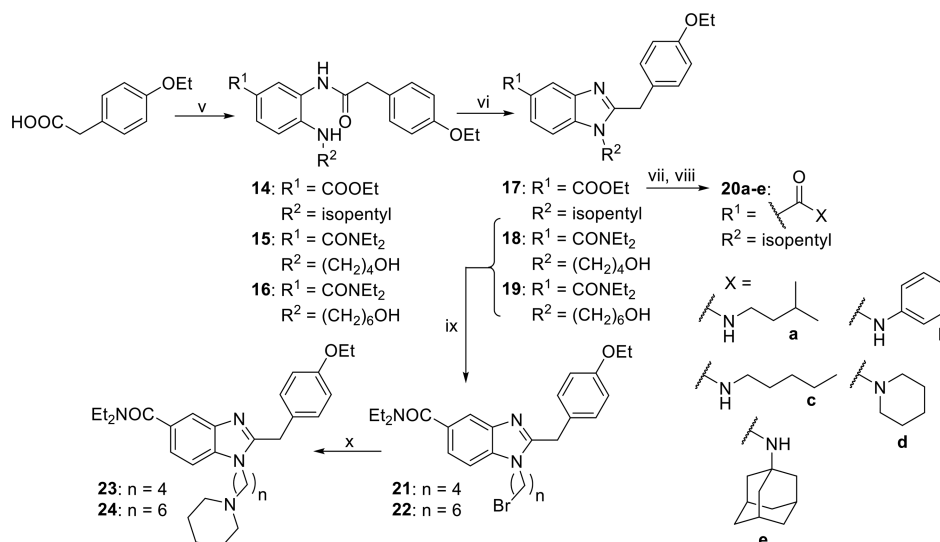
The synthesis of 2-amino benzimidazoles was performed as previously reported.³⁶ Upon reaction of benzylic and anilinic amines **25a–c** with carbon disulfide, isothiocyanates **26a–c** were obtained.⁴⁶ Thiourea derivatives **27–29** were afforded by reacting the respective isothiocyanates with *o*-phenylenediamine **10** or **11**. Cyclization was carried out using EDCI as a coupling reagent, and 2-amino benzimidazoles **30–32** were obtained (Scheme 3).

For the introduction of electron-withdrawing/donating functions at position 5 of the benzimidazole core, a different synthetic approach was applied. Starting from 1-chloro-2,4-dinitrobenzene **33**, nucleophilic substitution with isopentylamine led to compound **34** in quantitative yields. Selective reduction of the 2-nitro moiety to obtain *o*-phenylenediamine **35** was carried out according to Freitag et al.⁴⁷ using sodium sulfide as a reducing agent. Amide coupling and cyclization were carried out as described above. 5-Nitro benzimidazole **37** was reduced by tin(II) to afford 5-amino benzimidazole **38**. In the final step, HBTU-mediated amide coupling with benzoic acid afforded compound **39** (Scheme 4).

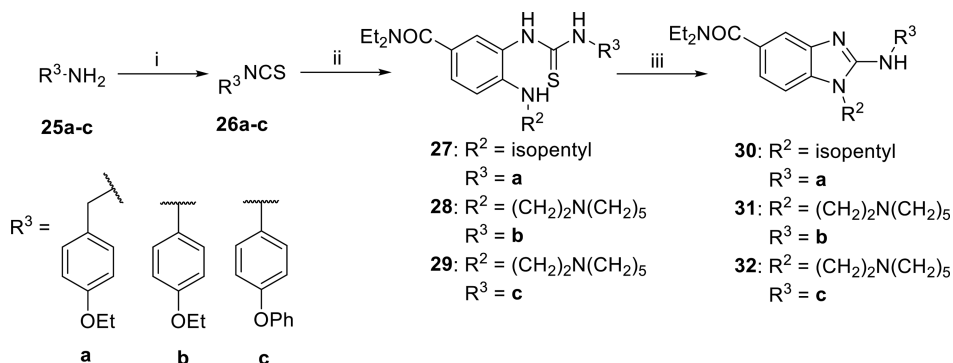
Pharmacological Profile of Dual-Acting Compounds.

All target compounds were tested for affinity to hCB_1R and hCB_2R in radioligand binding studies (HEK cells stably expressing hCB_2R ; CHO cells stably expressing hCB_1R). Inhibition of AChE (*ee*AChE, E.C.3.1.1.7, from electric eels and *hAChE*, E.C.3.1.1.7, from humans) and BChE (*hBChE*, E.C.3.1.1.8, from humans) was evaluated in the colorimetric Ellman's assay (Table 1). Sequence alignment had shown that the isoform *ee*AChE exhibits a very high sequence homology to the human enzyme (88% sequence identity)⁴⁸ (Table 1).

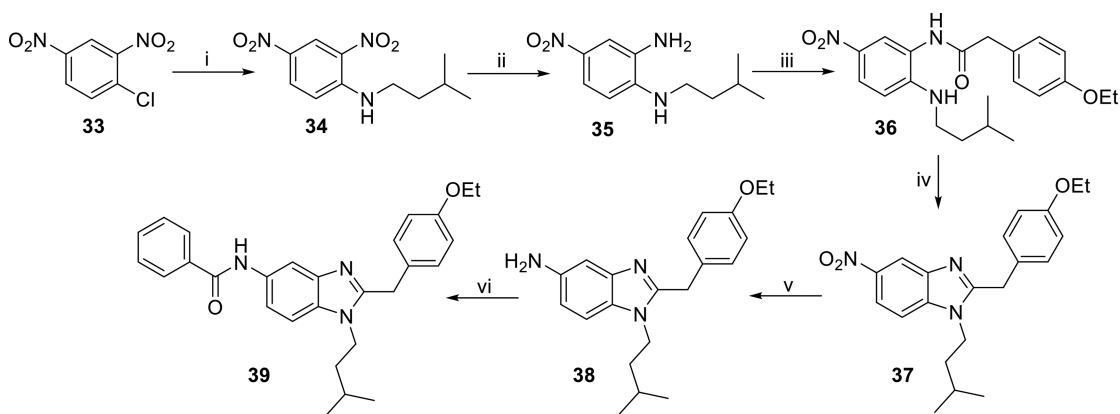
Scheme 2. Synthesis of Benzimidazoles with Different Amide Moieties or Spacer Lengths^a



^aConditions: (v) *o*-phenylene diamine **9**, **12**, or **13**, HBTU, NEt_3 , DMF, rt, 24 h; (vi) AcOH, reflux, 2 h; (vii) LiOH, THF/ H_2O , rt, 24 h; (viii) primary and secondary amines **a–e**, HBTU, NEt_3 , DMF, rt, 24 h; (ix) PBr_3 , CH_2Cl_2 , 0 °C to rt, 12 h; (x) piperidine, K_2CO_3 , DMF, 70 °C, 12 h.

Scheme 3. Synthesis of 2-Amino Benzimidazoles^a

^aConditions: (i) CS₂, NEt₃, Boc₂O, THF, 0 °C to rt, 12 h; (ii) *o*-phenylene diamine **10** or **11**, THF, rt, 6 h; (iii) EDCl·HCl, NEt₃, THF, reflux, 5 h.

Scheme 4. Synthesis of Benzimidazoles with Electron-Withdrawing/Donating Substituents at Position 5^a

^aConditions: (i) isopentylamine, NEt₃, EtOH, rt, 24 h; (ii) Na₂S·H₂O, NaHCO₃, MeOH/H₂O, reflux, 4 h; (iii) 2-(4-ethoxyphenyl)acetic, HBTU, NEt₃, DMF, rt, 12 h; (iv) AcOH, reflux, 6 h; (v) SnCl₂·2H₂O, EtOH, reflux, 6 h; (vi) benzoic acid, HBTU, NEt₃, DMF, rt, 6 h.

In the first set of compounds, we kept the benzimidazole scaffold of lead compound **A** and introduced different amide moieties at position 5 of the benzimidazole core (**20a–d**). While **20c**, with a straight *N*-alkyl chain, shows a low micromolar affinity toward *h*CB₂R and a micromolar inhibition of BChE, compound **20a**, with a branched *N*-alkyl chain, shows a micromolar inhibition of BChE as well as a submicromolar affinity toward *h*CB₂R (**20a**, $K_i(hCB_2R) = 763.3$ nM and $IC_{50}(hBChE) = 1.6$ μ M; **20c**, $K_i(hCB_2R) = 1.9$ μ M and $IC_{50}(hBChE) = 5.2$ μ M; **Table 1**). When we replaced the straight/branched *N*-alkyl chains with a 1-piperidinyl amide (**20d**), the activity at BChE did not change, but the affinity for *h*CB₂R could be increased (**20d**, $K_i(hCB_2R) = 384.5$ nM and $IC_{50}(hBChE) = 5.7$ μ M; **Table 1**). It is furthermore remarkable that the introduction of a 1-piperidinyl amide (**20d**), which is similar to AstraZeneca's benzimidazole **A**, resulted in some, albeit moderate, regain in affinity toward *h*CB₁R ($K_i(hCB_1R) = 17.0$ μ M; **Table 1**). The introduction of a sterically demanding 1-adamantyl amide scaffold (**20e**), a typical CB pharmacophore, resulted in a complete loss of activity at both ChEs. The affinity at *h*CB₂R still was in the micromolar range (**20e**, $K_i(hCB_2R) = 4.7$ μ M; **Table 1**), which suggests a tolerance of *h*CB₂R concerning bulky and nonpolar substituents at position 5 of the benzimidazole core. Lastly, we introduced an aniline amide (**20b**), which kept micromolar activity at BChE but led to an approximately 10-fold decreased affinity at *h*CB₂R compared to other investigated amides (**20a–e**) (**20b**, $K_i(hCB_2R) = 14.4$ μ M and $IC_{50}(hBChE) = 1.2$ μ M; **Table 1**). We also introduced a “flipped” amide, where the amine moiety is directly attached to

the benzimidazole (**39**). Compound **39** is a structural isomer of **20b** and surprisingly shows a different pharmacological profile. While **20b** shows a one-digit micromolar activity at BChE and two-digit affinity at *h*CB₂R (**Table 1**), **39** completely lost inhibitory activity at BChE, but the affinity toward *h*CB₂R is increased compared to compound **20b** (**39**, $K_i(hCB_2R) = 4.3$ μ M; **20b**, $K_i(hCB_2R) = 14.4$ μ M; **Table 1**).

With another set of compounds, we investigated the influence of electron-withdrawing/donating substituents at position 5 of the benzimidazole core, which was otherwise not altered (**37** and **38**). Our assumption was based on our previous results from computational studies³⁶ that an electron-withdrawing substituent is crucial for any affinity/activity at both *h*CB₂R and BChE. We could confirm this by completely losing activity at BChE and dramatically decreasing affinity at *h*CB₂R when we introduced an amino moiety (**38**). Moreover, an electron-withdrawing nitro substituent (**37**) achieved a submicromolar affinity at *h*CB₂R, but again it completely lost the ability to inhibit BChE (**37**, $K_i(hCB_2R) = 961.8$ nM; **Table 1**).

For a third set, we synthesized a set of “combination” compounds using scaffolds from our lead compounds **B**, **C**, and **D** and combining them in several 2-amino benzimidazoles (**31** and **32**). With this, we obtained **32**, a combination of the *para*-phenoxy phenyl moiety from **C** and ethylene piperidinyl from **D**, and **31**, which combine the *para*-ethoxy phenyl moiety of **B** with the ethylene piperidinyl moiety of **D**. Both compounds failed to show the desired pharmacological profile though. While affinity at *h*CB₂R decreased compared to the lead compounds **B–D**

Table 1. Results of the Biological Evaluation of the Inhibitory Effect of AChE/BChE and Radioligand Binding Studies at hCB_1R/hCB_2R

No.	X	R ¹	R ²	R ³	<i>h</i> BChE IC ₅₀ (pIC ₅₀ ± SD) or % Inhibition	AChE ^{c, d} IC ₅₀ (pIC ₅₀ ± SD) or % Inhibition	<i>h</i> CB ₂ R ^a K _i (pIC ₅₀ ± SD) or [³ H]CP55,950 displ. at 10 μM	<i>h</i> CB ₁ R ^b K _i (pIC ₅₀ ± SD) or [³ H]CP55,950 displ. at 10 μM
Tacrine					9.1 nM (8.0 ± 0.0)	18.5 nM ^c (7.7 ± 0.0)	n.d.	n.d.
Rimonabant					n.d.	n.d.	4.0%	143.0 nM (6.8 ± 0.1) 25.0 nM ⁴⁹
SR-144,528					n.d.	n.d.	19.7 nM (7.7 ± 0.1) 5.6 nM ⁵⁰	687.0 nM (6.1 ± 0.1) 254.0 nM ⁵⁰
A	CH ₂	NEt ₂			2 % at 10 μM	6 % ^c at 100 μM	36.7 nM ³⁶ (7.4 ± 0.1)	24 % ³⁶
B	NH	NEt ₂			3 % at 10 μM	13 % ^c at 10 μM	1.9 μM ³⁶ (5.7 ± 0.1)	13 % ³⁶
C	NH	NEt ₂			0 % at 10 μM	3 % ^c at 10 μM	426.0 nM ³⁶ (6.3 ± 0.2)	45 % ³⁶
D	CH ₂	NEt ₂			36.8 μM (4.4 ± 0.1)	12 % ^c at 10 μM	188.0 nM ³⁶ (6.7 ± 0.1)	14 % ³⁶
20a	CH ₂				1.6 μM (5.8 ± 0.1)	3 % ^d at 25 μM 11 % ^c at 10 μM	763.6 nM (6.1 ± 0.1)	37 %
20b	CH ₂				1.2 μM (5.9 ± 0.1)	2 % ^d at 10 μM 5 % ^c at 10 μM	14.4 μM (4.8 ± 0.2)	18 %
20c	CH ₂				5.2 μM (5.3 ± 0.1)	9 % ^d at 10 μM 6 % ^c at 10 μM	1.9 μM (5.7 ± 0.5)	39 %
20d	CH ₂				5.7 μM (5.2 ± 0.1)	8 % ^d at 10 μM 2 % ^c at 10 μM	384.5 nM (6.4 ± 0.4)	17.0 μM (4.8 ± 0.2)
20e	CH ₂				1 % at 10 μM	5 % ^d at 10 μM	4.7 μM (5.3 ± 0.4)	31 %
23	CH ₂	NEt ₂			2.7 μM (5.6 ± 0.1)	20.5 μM ^d (4.7 ± 0.2) 60.1 μM ^c (4.2 ± 0.2)	4.8 μM (5.3 ± 0.2)	2 %

(**31**, $K_i(hCB_2R) = 10.4 \mu M$; **32**, $K_i(hCB_2R) = 8.9 \mu M$), both compounds completely lost inhibitory activity at BChE. Nevertheless, both compounds are still selective hCB_2R ligands. Compound **30**

was developed by using the 2-amino benzimidazole scaffold from lead compound **B** and changing the *para*-ethoxy phenyl to a *para*-ethoxy benzyl moiety. With the additional methylene

Table 1. continued

No.	X	R ¹	R ²	R ³	<i>h</i> BChE IC ₅₀ (pIC ₅₀ ± SD) or % Inhibition	AChE ^{c, d} IC ₅₀ (pIC ₅₀ ± SD) or % Inhibition	<i>h</i> CB ₂ R ^a K _i (pIC ₅₀ ± SD) or [³ H]CP55,950 displ. at 10 μM	<i>h</i> CB ₁ R ^b K _i (pIC ₅₀ ± SD) or [³ H]CP55,950 displ. at 10 μM
24	CH ₂	NEt ₂			8.2 μM (5.1 ± 0.1)	11.9 μM ^d (4.9 ± 0.1) 20.0 μM ^c (4.7 ± 0.1)	1.0 μM (5.9 ± 0.1)	4 %
30	NH	NEt ₂			4 % at 50 μM	7 % ^d at 50 μM	353.4 nM (6.4 ± 0.1)	21 %
31	NH	NEt ₂			53.4 μM (4.3 ± 0.1)	18 % ^d at 100 μM 3 % ^c at 10 μM	10.4 μM (4.9 ± 0.2)	17 %
32	NH	NEt ₂			4 % at 25 μM	3 % ^d at 25 μM	8.9 μM (5.1 ± 0.2)	37 %
37	CH ₂	NO ₂			12 % at 50 μM	14 % ^d at 50 μM	961.8 nM (6.0 ± 0.2)	41 %
38	CH ₂	NH ₂			39 % at 100 μM	15 % ^d at 100 μM	21.0 μM (4.7 ± 0.1)	27 %
39	CH ₂				25 % at 10 μM	2 % ^d at 10 μM	4.3 μM (5.4 ± 0.4)	36 %

^aScreened on membranes of HEK cells stably expressing *h*CB₂R using 10 μM of the compound; values are mean values from at least 2 independent experiments performed in triplicates. *K_i* value was determined when displacement of [³H] CP 55,940 was >50%, mean values of at least 2 independent experiments performed in triplicates. ^bScreened on membranes of CHO cells stably expressing *h*CB₁R using 10 μM of the compound; values are mean values from at least 2 independent experiments performed in triplicates. *K_i* value was determined when displacement of [³H] CP 55,940 was >50%, mean values of at least 2 independent experiments. ^cValues are means of at least three determinations. AChE from human erythrocytes. n.d. = not determined ^dValues are means of at least three determinations. AChE from electric eel. Also included in this table, see references 36, 49, and 50.

group, a higher degree of freedom is achieved and the conjugated system is interrupted, which may increase basicity and thereby interaction with BChE. Compared to lead compound **B**, affinity toward *h*CB₂R increased; selectivity was kept (**30**, *K_i*(*h*CB₂R) = 353.4 nM), but again inhibition of both ChEs was lost.

On the basis of our previous computational studies, which indicated a binding cavity in the oxyanion hole of the BChE and the *N*¹-alkyl chain pointing toward it,³⁶ we changed the length of the ethylene piperidinyl moiety of our lead structure **D**. We synthesized *N*¹-substituted benzimidazoles with a butylene (**23**) and a hexylene spacer (**24**) with the aim to increase lipophilicity and interactions between the side chain and the oxyanion hole of the BChE. Compared to the structurally similar lead compound **D** with an ethylene spacer, both compounds **23** and **24** show an approximately 10-fold decreased affinity toward *h*CB₂R (**23**, *K_i*(*h*CB₂R) = 4.8 μM; **24**, *K_i*(*h*CB₂R) = 1.0 μM; Table 1), with an improved selectivity over *h*CB₁R. Regarding BChE, both compounds indeed showed a low micromolar activity at BChE (**23**, IC₅₀(*h*BChE) = 2.7 μM; **24**, IC₅₀(*h*BChE) = 8.2 μM; Table 1) but lose selectivity over AChE with longer alkylene spacers

(**23**, IC₅₀(*ee*AChE) = 20.5 μM; **24**, IC₅₀(*ee*AChE) = 11.9 μM; Table 1). When tested at the *h*AChE, both compounds showed a similar inhibitory activity (**23**, IC₅₀(*h*AChE) = 60.1 μM; **24**, IC₅₀(*h*AChE) = 20.0 μM; Table 1).

Since lead compounds **A–D** were previously only tested at the *eq*BChE and *ee*AChE (Figure 1), we also investigated activity at both human enzymes, *h*BChE and *h*AChE. Surprisingly, lead compounds **A–D**, which showed a (sub)micromolar activity at *eq*BChE, completely lost significant activity at *h*BChE. In contrast, values for *h*AChE were very similar to the *ee*AChE (Figure 1 and Table 1). We recommend using the human enzyme whenever possible, which is in the literature rarely done in the development of BChE inhibitors, probably due to its high price.^{27b} Some heterocyclic templates can show pronounced differences in inhibitory activities between species, so for each template, we recommend at least to test representative compounds at *h*BChE to check whether interspecies-dependent BChE inhibition occurs.^{27c}

We were able to successfully develop a set of second-generation benzimidazole/2-aminobenzimidazole compounds, which nearly all show good selectivity for both *h*CB₂R and *h*BChE

with affinity/activity in the micromolar to submicromolar range. Furthermore, our best compounds show a well-balanced activity profile at both targets. A balanced profile is one of the main difficulties in designing merged dual-active compounds.

For a better comparison of all compounds and investigating/describing SARs, we correlated pK_i values from hCB_2R and pIC_{50} values from $hBChE$ in Figure 3. Interpretation is greatly

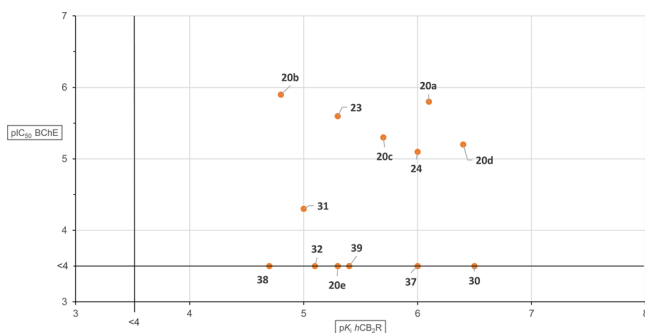


Figure 3. Plot of IC_{50} values for $hBChE$ inhibition against pK_i values of hCB_2R affinity. Compounds with no significant affinity for one of the targets are placed on the black lines.

simplified by the fact that the majority of compounds still show a high selectivity over both hCB_1R and $AChE$.

Computational Studies, Construction of the Active-State Model of the hCB_2R , and Docking of Compounds

20a and 20d. Computationally driven multitarget drug discovery has emerged recently as a subfield of computational drug design, and it uses fragment-based approaches to identify multitarget hits in silico or deals with optimizing multitarget hits, e.g., by application of molecular dynamics (MD) [ref 51 and references cited herein].

Within a previous study, an active state model of the hCB_2R was constructed based on the crystal structure of the active human β_2R adrenergic receptor ($h\beta_2R$).³⁶ Since a crystal structure of the hCB_1R in complex with the agonist AM11542 ((6aR,10aR)-3-(8-bromanyl-2-methyl-octan-2-yl)-6,6,9-trimethyl-6a,7,10,10a-tetrahydrobenzo[*c*]chromen-1-ol) was published (PDB ID: 5XRA),⁵² a new homology model of the hCB_2R based on this crystal structure was constructed because the homology between the hCB_2R and the hCB_1R is considerably higher than between the hCB_2R and the $h\beta_2R$. For the alignment of the amino acid sequences between the hCB_1R and the hCB_2R (Figure 4), the most conserved amino acid of each transmembrane (TM) domain according to Ballesteros and Weinstein⁵³ (marked by an asterisk) was used as reference.

For homology modeling of the hCB_2R , the software package SYBYL 7.0 (Tripos Inc.) was used. The flavodoxin of the hCB_1R crystal was deleted. The first 18 amino acids of the N-terminus and the last 44 amino acids of the C-terminus were not included in the hCB_2R homology model because these parts are not solved in the crystal structure of the hCB_1R . All amino acids that were different between the sequence of the hCB_1R (inclusive

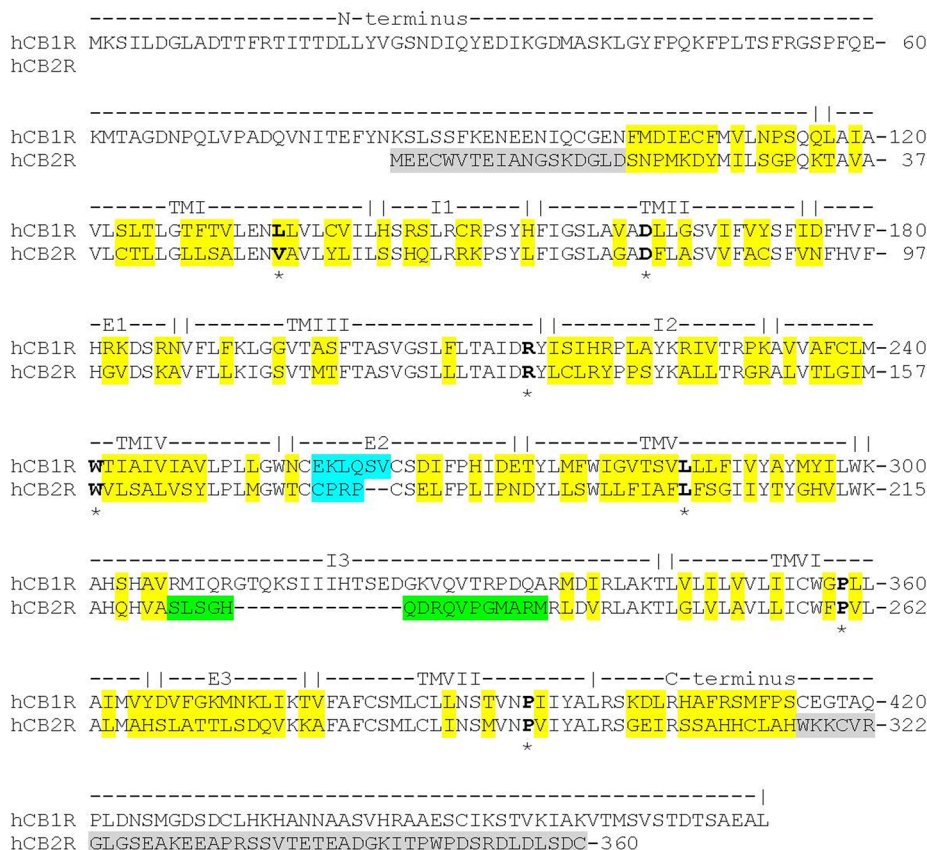


Figure 4. Amino acid sequence alignment of the hCB_1R (UniProtKB accession code: P21554) and the hCB_2R (UniProtKB accession code: P34972). Asterisk: highly conserved amino acids, according to the Ballesteros and Weinstein nomenclature. Yellow boxes: amino acids, different between hCB_1R and hCB_2R . Gray boxes: amino acids of the hCB_2R , not included in the homology model within the present work. Cyan boxes: part of the E2-loop, deleted in the hCB_1R template and inserted by "LoopSearch" according to the amino acid sequence of the hCB_2R . Green boxes: part of the I3-loop of the hCB_2R , inserted by "LoopSearch".

mutations in the X-ray structure) and the *hCB₂R* were mutated into the corresponding amino acid of the *hCB₂R*, except these parts of the extracellular loop E2 and the intracellular loop I3, marked in Figure 4: To model the E2-loop, the amino acids Glu258 (*hCB₁R*) to Val263 (*hCB₂R*) were deleted and the missing amino acids of the *hCB₂R* Cys175 to Pro178 were inserted, using the “LoopSearch” module of SYBYL 7.0 (Figure 4, cyan boxes). Furthermore, to model the I3-loop, the amino acids Ser222 to Met237 of the *hCB₂R* were inserted, using the “LoopSearch” module of SYBYL 7.0 (Figure 4, green boxes). Compounds **20a** and **20d** were docked manually in two different poses (mode 1 and mode 2), inspired by the AM11542-*hCB₁R*-crystal structure (5XRA), into the binding pocket of the *hCB₂R* (Figure 5).

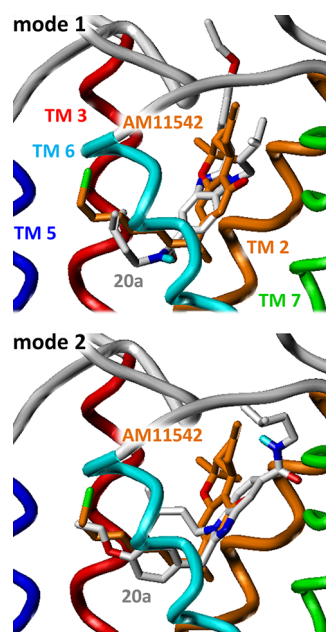


Figure 5. Docking poses (mode 1 and mode 2) of **20a** compared to the pose of compound AM11542 in the *hCB₁R*-crystal structure (5XRA).

Molecular Dynamics Simulations at the *hCB₂R*. The ligand–receptor complex, constructed with SYBYL 7.0, as described above was embedded in a POPC lipid bilayer. The parametrization for the ligands **20a** and **20d** was obtained from the PRODRG server (davapc1.bioch.dundee.ac.uk/prodrgr/). For the generation of the complete simulation box (6.9 nm × 6.9 nm × 9.2 nm) and subsequent molecular dynamics simulations, the software package GROMACS 4.0.2 (www.gromacs.org) was used. Intracellular and extracellular water molecules were added using the command “genbox”. To achieve electroneutrality, 5 sodium and 17 chloride ions were added using the command “genion”. After minimization of the simulation box, MD simulations (10 ns equilibration phase and 10 ns productive phase) were performed for the ligand-free *hCB₂R* and the ligand–*hCB₂R* complexes, as described previously.^{54,55}

Binding Mode of Compounds **20a and **20d** at the *hCB₂R*.** For compounds **20a** and **20d**, MD simulations for both binding modes 1 and 2 were performed. For **20a**, the short-range Coulomb and Lennard-Jones interactions amounted to ca. –19 kJ/mol and ca. –277 kJ/mol for mode 1 and ca. –44 kJ/mol and ca. –290 kJ/mol for mode 2. Similarly, for **20d**, the short-range Coulomb and Lennard-Jones interactions amounted to ca. –25 kJ/mol and ca. –246 kJ/mol for mode 1

and ca. –63 kJ/mol and ca. –260 kJ/mol for mode 2. Because mode 2 is the more stable one in both cases, subsequent data analysis was performed only on this mode. Since the orthosteric binding pocket of the *hCB₂R* is mainly formed by the aromatic amino acids Phe^{3.36}, Phe183 (E2-loop), Trp^{5.43}, and Trp^{6.48}, an aromatic moiety of the ligand in this region of the binding site should be preferred with respect to a more aliphatic one. Thus, for ligands containing an aromatic moiety in side chain R¹ and in side chain R³, e.g., **20b**, both modes should be considered.

The ligands **20a** and **20d** are stably embedded (mode 2) in the orthosteric binding pocket of the *hCB₂R* (Figure 6).

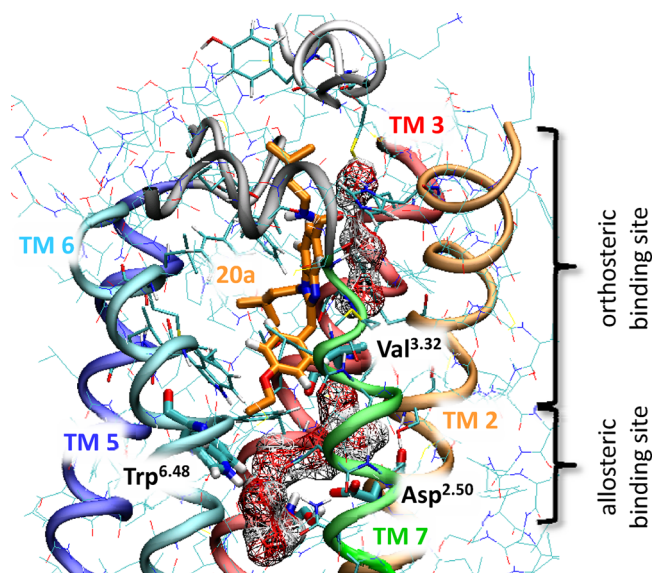


Figure 6. Orthosteric binding pocket of the *hCB₂R* with compound **20a** as well as internal water molecules and the allosteric binding site, as obtained by MD simulations.

For compound **20a**, the benzimidazole core interacts with Phe^{2.57}, Phe183 (E2-loop), and Phe^{7.35} (Figure 7a). The aliphatic side chain R¹ is embedded in a subpocket at the extracellular domains of the *hCB₂R*. The isopentyl moiety (R²) is well-embedded in a hydrophobic pocket, formed by the amino acids Ile^{3.29}, Val^{3.32}, Thr^{3.33} (methyl group), Phe^{3.36}, Phe183 (E2-loop), Ile186 (E2-loop), Leu^{5.40}, Trp^{5.43}, Leu^{5.44}, Val^{6.51}, and Met^{6.55} (Figure 7b). The 4-ethoxybenzyl moiety (R³) is embedded in a hydrophobic pocket, mainly formed by the amino acids Phe^{3.36}, Trp^{6.48}, Val^{6.51}, Met^{6.55}, and Leu^{7.41} (Figure 7c). During ~33% of the whole productive phase, a direct H-bond between the carbonyl oxygen of **20a** and the OH moiety of Ser^{7.39} was observed. Alternatively, the interaction between **20a** and the *hCB₂R* was stabilized by a water-mediated H-bond interaction between the CO moiety of **20a** and Ser^{7.39} or His^{2.65} (Figure 7d).

Furthermore, the MD simulations of the **20a**–*hCB₂R* complex revealed a well-established interaction network between the highly conserved Asn^{7.49}, Asn^{7.45}, Trp^{6.48}, Ser^{3.39}, Asp^{2.50}, and internal water molecules (Figure 8). A comparable water chain was also revealed by MD simulations for the histamine H₃ and H₄ receptor.⁵⁶ Thus, at the *hCB₂R*, the allosteric Asp^{2.50} binding site, which is described as the Na⁺ binding site for several GPCRs⁵⁷ is well-connected with the orthosteric ligand binding site. Because the highly conserved amino acids of the allosteric binding site may be involved in receptor activation, it may be speculated that ligands (e.g., agonists), bound to the orthosteric binding site, may transfer information for activation of the receptor

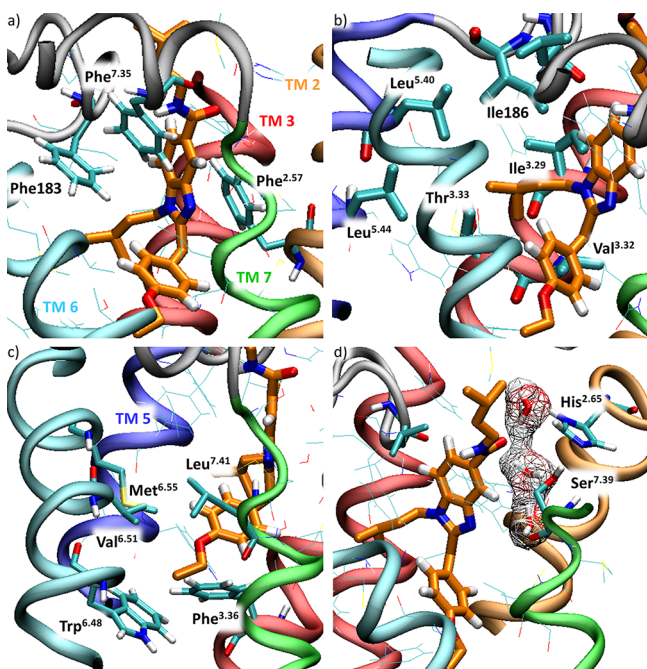


Figure 7. Interaction sites of the *hCB₂R* with (a) the benzimidazole core, (b) the isopentyl side chain (R^2), (c) the 4-ethoxy phenyl moiety (R^3), and (d) the carbonyl moiety (mediated by water molecules) of compound 20a.

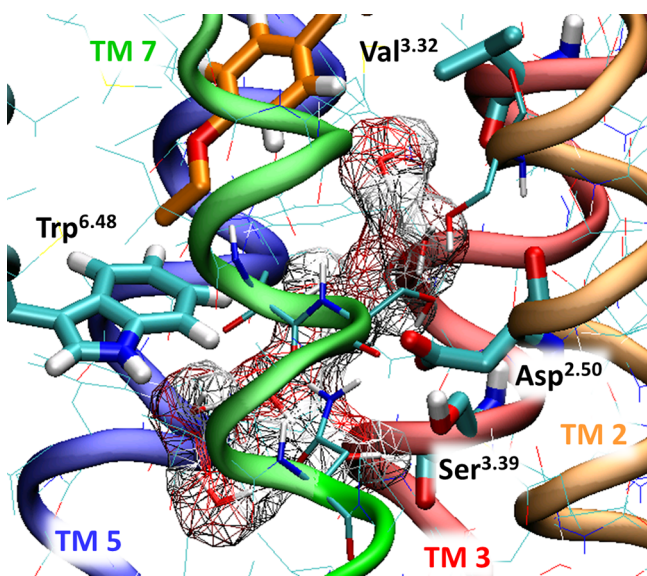


Figure 8. Interaction network between the *hCB₂R* and internal water molecules between the orthosteric ($\text{Val}^{3.32}$) and allosteric ($\text{Asp}^{2.50}$) binding site, obtained by MD simulations in the presence of 20a.

downstream not only by the highly conserved amino acids but also by the internal water molecules located in this region.

Compared to 20a, the MD simulations revealed different binding modes for 20d (Figure 9): For compound 20d, the benzimidazole core interacts with $\text{Phe}^{2.57}$, $\text{Phe}^{2.61}$, Phe^{183} (E2-loop), and $\text{Phe}^{7.35}$. The piperidine moiety R^1 is embedded in a subpocket at the extracellular domains of the *hCB₂R*, mainly formed by the amino acids $\text{Phe}^{2.61}$, Leu^{182} , $\text{Leu}^{6.54}$, and $\text{Lys}^{7.32}$ (aliphatic part). The isopentyl moiety (R^2) is well-embedded in a hydrophobic pocket, formed by the amino acids $\text{Val}^{2.56}$, $\text{Phe}^{3.25}$, $\text{Lys}^{3.28}$ (aliphatic part), and $\text{Ile}^{3.29}$. The 4-ethoxybenzyl moiety (R^3) is

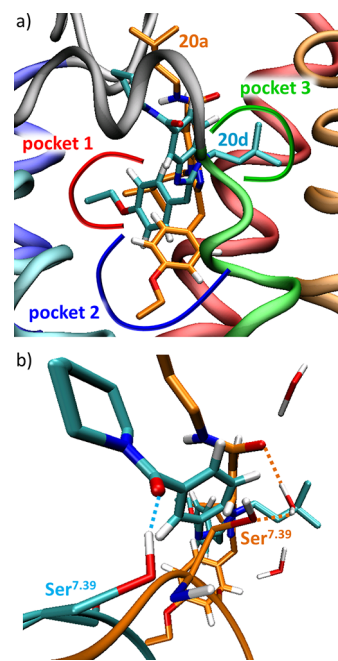


Figure 9. (a) Overlay of 20a and 20d in the binding pocket of the *hCB₂R*, obtained by MD simulations. (b) Differences in H-bond interactions between the *hCB₂R* and 20a or 20d.

embedded in a hydrophobic pocket, mainly formed by the amino acids $\text{Ile}^{3.29}$, $\text{Val}^{3.32}$, $\text{Thr}^{3.33}$ (methyl group), $\text{Phe}^{3.36}$, Phe^{183} (E2-loop), Ile^{186} (E2-loop), $\text{Leu}^{5.40}$, $\text{Trp}^{5.43}$, $\text{Leu}^{5.44}$, $\text{Val}^{6.51}$, and $\text{Met}^{6.55}$ (Figure 9a). During $\sim 95\%$ of the whole productive phase, a direct H-bond between the carbonyl oxygen and the OH moiety of $\text{Ser}^{7.39}$ was observed. However, in contrast to 20a, the H-bond to $\text{His}^{2.65}$ was not observed and there was no water-mediated interaction between the ligand and the receptor (Figure 9b). An overlay of 20a and 20d in the binding pocket of the *hCB₂R*, obtained by MD simulations, is presented in Figure 9: The moiety R^1 points for both ligands toward the extracellular region of the receptor. The isopentyl moiety (R^2) is located in pocket 1 in the case of 20a and in pocket 3 in the case of 20d. The 4-ethoxy phenyl moiety (R^3) is located in pocket 2 in the case of 20a and in pocket 1 in the case of 20d. Consequently, the benzimidazole core of 20d is twisted about 45° with respect to 20a.

Since pocket 1 ($\text{Ile}^{3.29}$, $\text{Val}^{3.32}$, $\text{Thr}^{3.33}$, $\text{Phe}^{3.36}$, Phe^{183} , Ile^{186} , $\text{Leu}^{5.40}$, $\text{Trp}^{5.43}$, $\text{Leu}^{5.44}$, $\text{Val}^{6.51}$ and $\text{Met}^{6.55}$) is formed by aromatic and aliphatic side chains, ligands comprising of one or more of these moieties may be able to establish more than one binding pose. In this context two orientations of ligand 20a (R^2 aliphatic) as well as 20d (R^3 aromatic/aliphatic) are to be considered. Furthermore, it can be speculated that an equilibrium between different binding poses may be established depending on the chemical nature of the moieties R^1 , R^2 and R^3 . Since the two ligands differ in R^1 , which points into the extracellular domain, this group may influence the equilibrium of different binding poses.

Determination of Efficacy at *hCB₂R*. CB_2Rs are coupled through $\text{G}_{i/o}$ proteins and negatively regulate adenylate cyclase, the enzyme that catalyzes the conversion of adenosine triphosphate (ATP) to cyclic adenosine monophosphate (cAMP).⁵⁸ One of the notable CB_2R biological responses is the regulation of intracellular cAMP levels. CB_2R agonists decrease cAMP levels and revert forskolin-stimulated cAMP production, while CB_2R antagonists/reverse agonists increase cAMP levels and enhance forskolin-stimulated cAMP production in cell lines.⁵⁹ So the

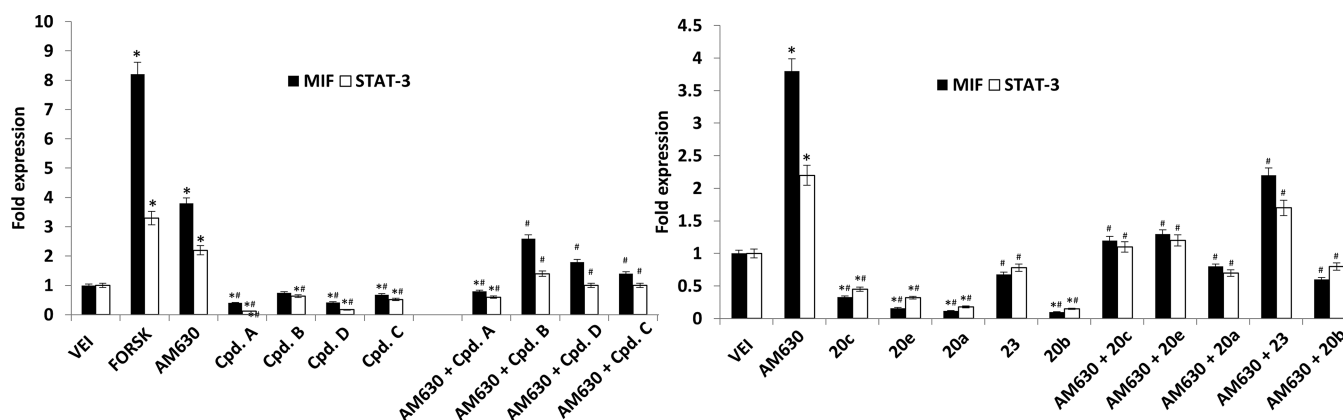


Figure 10. Test compounds (A–D, 20a–c, 20e, and 23) reduce MIF and STAT-3 gene expression. U266 cells were treated with test compounds (50 μ M), forskolin (10 μ M), or AM630 (25 μ M) for 2 h. In combination experiment (AM630 plus test compounds), U266 cells were preincubated with AM630 for 30 min before adding the test compounds. MIF and STAT-3 mRNA levels were determined by qRT-PCR. GAPDH was used for normalization. Data are expressed as relative fold with respect to vehicle-treated cells used as the control. Data are expressed as mean \pm SD * p < 0.01 vs untreated; # vs AM630.

detection of the cAMP concentration, for example, by ELISA, is a common method for the identification of CB₂R ligand activity. In addition, receptor-mediated changes in the intracellular cAMP concentration can be detected via changes in the expression level of particular genes, which are regulated by the transcription factor cAMP response-element binding (CREB) protein binding to upstream cAMP response elements (CREs).⁶⁰ Between potential cAMP-target genes, macrophage migration inhibitory factor (MIF), which is highly expressed in multiple myeloma, is under cAMP-induced expression, since a functional cAMP-responsive element (CRE) in the proximal region of the MIF promoter is detected.^{61,62} Signal transducer and activators of transcription (STAT-3) is another gene highly expressed in multiple myeloma cells, and its expression is also under CRE promoter control.^{63,64}

Before evaluating the CB₂R activity of the compounds, the nontoxic concentration of each compound was evaluated by an MTT assay, and the IC₅₀ values were determined. U266 myeloma cells were treated with different concentrations of each compound (up to 100 μ M) for 48 h, and the cell viability was calculated. As shown in Figure S1 of the Supporting Information, the compounds show different cytotoxic activity in U266 cells, with each IC₅₀ value over 40 μ M, calculated at 48 h post-treatment.

To evaluate the biological activity of the compounds (as agonist or antagonist/reverse agonist), a cAMP assay was applied. U266 cell lines were treated for 2 h with forskolin (10 μ M) as the cAMP-inducer, AM630 (25 μ M) as the CB₂R antagonist/reverse agonist or with test compounds (50 μ M) alone, and in combination with AM630, respectively. In combination treatment, U266 cells were pretreated with AM630 for 30 min and then treated with the single test compounds. In the cAMP assay, we found that forskolin increased the cAMP levels (as expected) and so did AM630 (by inhibiting CB₂R basal activity), compared to vehicle-treated cells (Figure S2 of the Supporting Information).

All of the test compounds decreased cAMP levels compared to vehicle, indicating that they are CB₂R agonists. To further confirm this data, test compounds were incubated in competition with AM630, and the results revealed that the compounds were able to revert AM630-increased cAMP levels (Figure S2 of the Supporting Information). By summarizing these results, we confirmed that test compounds A–D act, with different potency, as CB₂R agonists.

Since changes in the cAMP concentration can be detected via changes in expression level of specific genes regulated by the

CREB binding to upstream cAMP response elements (CREs), we selected two genes that are under cAMP-regulated transcription, the macrophage migration inhibitory factor (MIF) and the signal transducer and activator of transcription 3 (STAT-3). First, U266 cells were treated with forskolin to confirm that MIF and STAT-3 are under cAMP-induced transcription. As shown, both gene levels increase compared with vehicle-treated cells (Figure 10), confirming that this assay can show changes in the cAMP levels. Then, U266 cells were treated with test compounds A–D alone and in combination with AM630. The results show that AM630 increases the expression of MIF and STAT-3, confirming that AM630 increases the cAMP levels (Figure 10), as previously evidenced by cAMP ELISA, while all of our test compounds reduced MIF and STAT-3 expression levels compared with vehicle-treated cells and reduced AM630-induced MIF and STAT-3 when coincubating our test compounds and AM630 (Figure 10).

Herein, we confirmed that AM630 was able to increase cAMP production in U266 cells and that all compounds tested were able to reduce basal cAMP levels and to reverse the AM630-induced increase of cAMP concentration. An additional sensitive tool for evaluating variation in intracellular cAMP levels is the detection of CREB-induced gene expression.^{65,66} In this context, the transcription of two genes highly expressed in U266 cells, MIF and STAT-3, were found to be under CREB regulation.^{62,63} So, we applied a RT/PCR methodology to evaluate the MIF and STAT-3 gene expression levels in U266 cells. This experimental approach confirmed that AM630 as well as forskolin, by increasing the cAMP levels, induced MIF and STAT-3 expression, while test compounds reduced MIF and STAT-3 gene expression levels both when used alone or when combined with AM630. Since all of this data was strongly evidenced by cAMP ELISA and RT/PCR, we were able to characterize the agonist activity of test compounds and this data provides evidence that the entire set of test compounds acts as CB₂R agonists, further confirming the data obtained by the cAMP ELISA assay.

μ -Opioid Receptor Binding. As already described above, dual-acting compounds have been developed to be applied for a variety of different targets in various diseases. One example is merged/dual-acting μ -opioid (MOP) receptor agonists/neuronal nitric oxide synthase (nNOS) inhibitors for the treatment of pain. Such a set of compounds was designed by Renton et al. on the basis of several NOS inhibitors and etonitazene, a well-known

MOP receptor agonist developed in the 1960s.^{67,68} During the development of our own dual-acting compounds, we came across etonitazene, which shows strong structural similarities: an electron-withdrawing substituent at position 5 of the benzimidazole core (red), a 4-ethoxybenzyl moiety at position 2 (green), and a basic amine linked with an ethylene bridge to N^1 (blue), with the latter structural feature only shown by some of our compounds (Figure 11). On the basis of these observations,

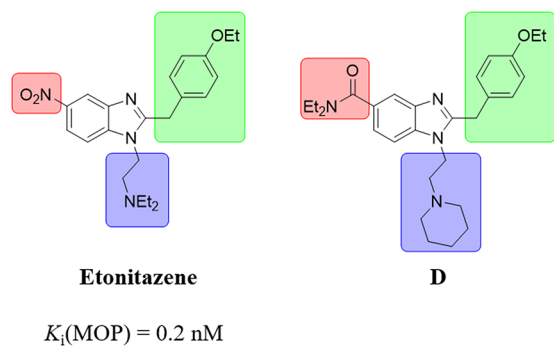


Figure 11. Structural similarities between etonitazene⁶⁸ and (exemplary) lead compound **D**: an electron-withdrawing substituent at position 5 of the benzimidazole (red), a 4-ethoxybenzyl moiety at position 2 (green), and a basic amine linked with an ethylene bridge to N^1 (blue).

we tested our lead compounds **A**, **B**, and **D** in a radioligand binding assay at the MOP receptor (HEK cells transiently transfected with the $h\text{MOP}$ receptor) to evaluate unwanted interactions with the MOP receptor and to avoid them in further compound development (Table 2).

Radioligand binding studies confirmed our assumptions. While compound **D**, with the highest structural analogy, shows a significant, albeit moderate, three-digit nanomolar binding to the MOP receptor (**D**, $K_i(\text{MOP}) = 556.0 \text{ nM}$; Table 2), lead compound **A** only shows a one-digit micromolar affinity (**A**, $K_i(\text{MOP}) = 6.7 \text{ }\mu\text{M}$; Table 2). This is probably due to the lack of a basic amine. Compound **B**, which does lack not only the basic amine but also the methylene unit between the benzimidazole core and the 4-ethoxy phenyl moiety, shows the lowest affinity at the MOP receptor (**B**, $K_i(\text{MOP}) = 53.6 \text{ }\mu\text{M}$; Table 2). Based on these observations for “designing out” the MOP affinity, a basic amine

attached over an alkylene linker to N^1 should advantageously be avoided and the methylene unit should be substituted by a 2-amino moiety. Substitution/removal of the electron-withdrawing amide function at position 5 should be avoided to keep affinity/activity at $h\text{CB}_2\text{R}$ and BChE as discussed above (cf. Table 1 and ref 36).

In Vivo Studies. Lead compounds **A** and **B** and compound **20a** were tested for their neuroprotectant and pro-cognitive effects in the in vivo mouse model of AD, in which neuroinflammation and cognitive deficits are induced by the intracerebroventricular injection of the oligomerized $A\beta_{25-35}$ peptide into the mouse brains.^{28,69,70}

Each compound was solubilized in DMSO/saline or DMSO/Tween-80/saline vehicle solutions (cf. Supporting Information for detailed description). Compounds were fully dissolved, and no precipitation was observed. Extended (in vitro) pharmacokinetic studies were not conducted since they are beyond the scope of this work.⁷¹

The prepared compounds were injected intraperitoneally between day 1 and 7. Animal status and weight were checked daily during the treatments. Vehicle solutions, compounds **A** and **B**, did not affect weight gains (+0.3 g/day on average). Compound **20a** decreased weight gain (+0.2 g/day at 0.3 mg/kg, +0.1 g/day at 1 mg/kg, and 0 g/day at 3 mg/kg) but did not provoke weight loss. No treatment induced behavioral alteration, prostration, signs of abdominal pain, or changes in the fur aspect, suggesting that high DMSO concentrations applied in some groups were well-tolerated. Moreover, since the injection period was limited and animals were used for behavioral observation 24 h after the last injection, vehicle-treated animals showed the performances expected for $\text{Sc.A}\beta^-$ or $A\beta_{25-35}$ -treated groups.^{69,70} The amyloid peptide was injected on day 1 and the behavioral examination performed between day 8 and 10. All animals were then sacrificed on day 11 and their brains stored at $-80 \text{ }^\circ\text{C}$ (Figure 12).

The spontaneous alternation performance, an index of spatial working memory, was tested on day 8 in the Y-maze test. Long-term memory response was measured on days 9 and 10 in a step-through passive avoidance test.

Repeated Treatment with Compounds **A**, **B**, and **20a**.

As described above, none of the treatments (ip for the compounds solubilized in DMSO/water or DMSO/Tween-80/water and ICV for peptides solubilized in water) affected the mouse body

Table 2. Biological Evaluation of Radioligand Binding Studies at the $h\text{MOP}$ Receptor

No.	X	R ¹	R ²	R ³	$K_i(h\text{MOP})^a$ ($\text{p}K_i \pm \text{SD}$)
Etonitazene					0.2 nM ⁶⁸
A	CH ₂	CONEt ₂			6.7 μM (5.2 \pm 0.1)
B	NH	CONEt ₂			53.6 μM (4.3 \pm 0.0)
D	CH ₂	CONEt ₂			556.0 nM (6.3 \pm 0.1)

^aScreened on membranes of HEK cells transiently transfected with the $h\text{MOP}$ receptor; values are mean values from at least 2 independent experiments performed in triplicates.

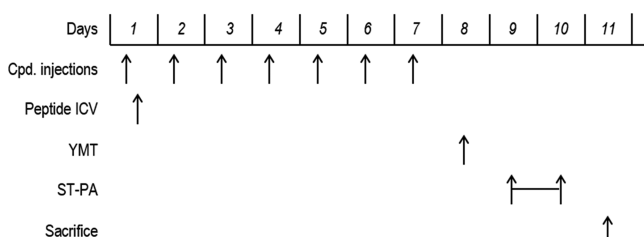


Figure 12. Protocol followed. Abbreviations key: Cpd, compound; ICV, intracerebroventricular injection; YMT, spontaneous alternation test in the Y-maze; ST-PA, step-through passive avoidance test.

weight, suggesting a good tolerability. Animals gained about 2.1 g during the 7 day treatment period.

Spontaneous Alternation Performances. CB₂ agonist **A** attenuated, significantly but partially, the Aβ_{25–35}-induced alternation deficit at the highest dose tested, 3 mg/kg (Figure 13a).

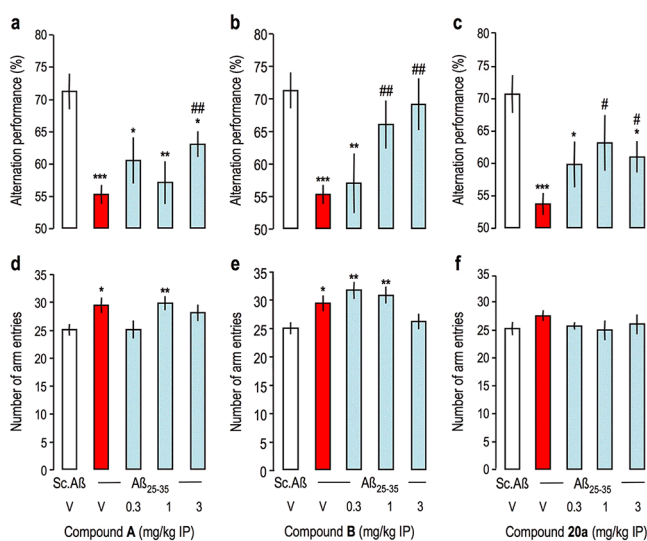


Figure 13. Effect of test compounds **A**, **B**, and **20a** on Aβ_{25–35}-induced spontaneous alternation deficits in mice. Animals received Aβ_{25–35} or Sc.Aβ peptide (9 nmol ICV) on day 1 and the test compounds (0.3 mg/kg ip) or vehicle solution (V, DMSO 20% in saline or DMSO 20%, Tween-80 2% in saline) od between days 1–7. Alternation performance was tested on day 8. Data shown mean ± SEM. ANOVA: F_(4,54) = 6.55, *p* < 0.001, *n* = 9–14 per group in part a; F_(4,54) = 5.43, *p* < 0.001, *n* = 8–14 per group in part b; F_(4,57) = 4.05, *p* < 0.01, *n* = 9–14 per group in part c; F_(4,54) = 2.72, *p* < 0.05 in part d; F_(4,54) = 4.70, *p* < 0.01 in part e; F_(4,57) = 0.59, *p* > 0.05 in part f. * *p* < 0.05, ** *p* < 0.01, *** *p* < 0.001 vs (Sc.Aβ+V)-treated group; ## *p* < 0.01, ### *p* < 0.001 vs (Aβ_{25–35}+V)-treated group; Dunnett's test.

Dual-acting compounds **B** and **20a** showed significant preventions at 1 and 3 mg/kg (Figure 13b,c). Note that the Aβ_{25–35} treatment slightly, but significantly for compounds **A** and **B** (Figure 13c,d), increased locomotion, measured in terms of number of arms entered during the session, in these experiments. This is not routinely observed but remains pertinent considering the model. Slight variations with compounds **A** and **B** were noted (Figure 13c,d).

Passive Avoidance Test. For the long-term memory response, CB₂ agonist **A** failed to show any prevention of the step-through latency deficit induced by Aβ_{25–35}, at all doses tested (Figure 14a). Dual-acting compound **B** showed significant prevention of the latency diminution at the highest dose tested,

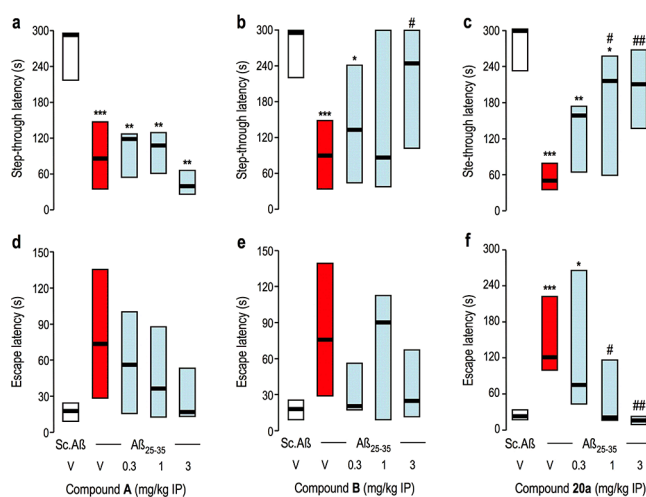


Figure 14. Effect of test compounds **A**, **B**, and **20a** on Aβ_{25–35}-induced passive avoidance deficits in mice. Animals received Aβ_{25–35} or Sc.Aβ peptide (9 nmol ICV) on day 1 and the test compounds (0.3 mg/kg ip) or vehicle solution (V, DMSO 20% in saline or DMSO 20%, Tween-80 2% in saline) od between days 1–7. Training was performed on day 9 and retention measured on day 10. Data show median and interquartile range. Kruskal–Wallis ANOVA: H = 19.0, *p* < 0.001, *n* = 9–14 per group in part a; H = 15.0, *p* < 0.01, *n* = 8–14 per group in part b; H = 21.1, *p* < 0.001, *n* = 11–14 in part c; H = 6.89, *p* > 0.05 in part d; H = 6.34, *p* > 0.05 in part e; H = 19.7, *p* < 0.001 in part f. * *p* < 0.05, ** *p* < 0.01, *** *p* < 0.001 vs (Sc.Aβ+V)-treated group; # *p* < 0.05, ## *p* < 0.01 vs (Aβ_{25–35}+V)-treated group; Dunn's test.

3 mg/kg (Figure 14b). Compound **20a** dose-dependently attenuated the step-through latency deficit induced by Aβ_{25–35} with significant effects at 1 and 3 mg/kg (Figure 14c).

Escape latency was also measured. For compounds **A** and **B**, the Kruskal–Wallis ANOVA did not lead to significant effects (Figure 14d,e), but tendencies could be noted. The Aβ_{25–35} treatment led to an increase in escape latency, and several groups treated with the compounds, particularly at the highest doses, showed a trend of a reduction of the latency close to the (Sc.Aβ/V) control group data (Figure 14d,e). For compound **20a**, the ANOVA was significant and the Aβ_{25–35}-induced increase was highly significant, while the two highest doses of **20a** significantly prevented the Aβ_{25–35}-induced increase (Figure 14f).

A protective activity for dual-acting compounds **B** and **20a** on the two behavioral responses analyzed at doses of 1–3 mg/kg was shown, and compound **20a** appeared as the most active with sustained prevention of Aβ_{25–35}-induced learning deficits in both tests at 1 mg/kg. Since compound **A** is a potent hCB₂R agonist, but weakly potent BChE inhibitor and compounds **B** and **20a** show balanced low micromolar activities at both targets, the in vivo studies prove cognition enhancement for such dual-acting compounds and, of course, also prove penetration of the blood–brain barrier. Obviously, the solubilization conditions used here remain first-attempt choices and will be improved in future studies. However, a correct bioavailability was expected for a small dual-acting compound with a much lower molecular weight compared to conventional covalently connected hybrid molecules. The compounds described herein are “true” hybrids in a way that these molecules merge the respective pharmacophores for two targets, whereas compounds termed “hybrid molecules” in the literature in the vast majority of cases covalently connect two distinct molecules that act at two different targets and therefore have a high molecular weight.^{34,35}

DISCUSSION AND CONCLUSION

Taken together, a compound library based on benzimidazoles and 2-aminobenzimidazoles was synthesized and SARs were investigated with respect to the hCB_1R and hCB_2R affinity and the AChE and hBChE inhibition, respectively. Generally, the compounds show excellent selectivity over both hCB_1R and AChE, and several compounds show well-balanced affinities at the two desired targets in the low micromolar range. Molecular docking and dynamics studies were performed applying for the first time a homology model of the hCB_2 based on the recently published crystal structure of the hCB_1 receptor bound to an agonist in the orthosteric binding site. While compound **20a** binds, as expected, to the orthosteric binding site, a stable amino acid and water interaction network was observed which extends into the allosteric binding site. Nitro-benzimidazoles can show a significant potency at the MOP receptor, and MOP affinities of dual-acting compounds could be designed out, e.g., by removing the basic nitrogen atom in the alkyl chain. Furthermore, it was proven for the first time by a cAMP assay as well as by two cAMP response elements (MIF and STAT-3) that the compounds act as agonists at the hCB_2R and might therefore exhibit antineuroinflammatory effects in vivo also. In an in vivo study with mice showing neuroinflammation and cognition deficits after $A\beta_{25-35}$ ICV administration, the ability and superiority of a well-balanced dual-acting compound compared to a high-affinity hCB_2R agonist with moderate BChE inhibition in improving cognition at dosages from 1 to 3 mg/kg were demonstrated. This shows that it is possible to design small molecules that act specifically at two very different targets like a GPCR and an enzyme with a high selectivity and a good potency in the same concentration range to yield compounds with a pronounced in vivo activity. The development methods like compound design and application of computational methods shown in this work will hopefully provide support in related drug development efforts for dual-acting compounds.

EXPERIMENTAL SECTION

General Information. All reagents were used without further purification and bought from common commercial suppliers. For anhydrous reaction conditions, THF was dried prior to use by refluxing over sodium slices for at least 2 days under an argon atmosphere. Thin-layer chromatography was performed on silica gel 60 (alumina foils with fluorescent indicator 254 nm). For detection, iodine vapor and UV light (254 and 366 nm) were used. For column chromatography, silica gel 60 (particle size 0.040–0.063 mm) was used. Nuclear magnetic resonance spectra were recorded with a Bruker AV-400 NMR instrument (Bruker, Karlsruhe, Germany) in $CDCl_3$, and chemical shifts are expressed in ppm relative to $CDCl_3$ (7.26 ppm for 1H and 77.16 ppm for ^{13}C).⁷² Purity was determined by HPLC (Shimadzu Products), containing a DGU-20A3R degassing unit, a LC20AB liquid chromatograph, and a SPD-20A UV/vis detector. UV detection was measured at 254 nm. Mass spectra were obtained by a LCMS 2020 (Shimadzu Products). As a stationary phase, a Synergi 4U fusion-RP (150 mm \times 4.6 mm) column was used, and as a mobile phase, a gradient of MeOH/water with 0.1% formic acid was used. Parameters: A = water, B = MeOH, $V(B)/(V(A) + V(B))$ = from 5% to 90% over 10 min, $V(B)/(V(A) + V(B))$ = 90% for 5 min, $V(B)/(V(A) + V(B))$ = from 90% to 5% over 3 min. The method was performed with a flow rate of 1.0 mL/min. Compounds were only used for biological evaluation if the purity was $\geq 95\%$.

General Procedure for the Synthesis of Target Compounds 20a–e. The respective ester compound **17** (1 equiv) was dissolved in a THF/water mixture (2:1), and LiOH (2 equiv) was added. The mixture was refluxed for 12 h. THF was evaporated, and the aqueous residue was acidified with 2 M aqueous HCl (pH = 4). The organic phase was separated with EtOAc and washed with water and brine. After the

residue was dried over Na_2SO_4 , the solvent was removed in vacuo and the product was used without further purification. The respective acid (1 equiv) was dissolved in DMF, and NEt_3 (1.5 equiv), HBTU (1.1 equiv), and the appropriate amine (1 equiv) were added in one portion. The mixture was stirred overnight at room temperature. Then, EtOAc and an aqueous saturated $NaHCO_3$ solution were added. The organic layer was washed several times with water and brine and dried over anhydrous Na_2SO_4 . The solvent was removed in vacuo, and the product was purified by column chromatography.

2-(4-Ethoxybenzyl)-N,1-diisopentyl-1H-benzo[d]imidazole-5-carboxamide (20a). **20a** was obtained as a light yellow solid (0.26 mmol, 0.11 g, 79%). 1H NMR (400 MHz, $CDCl_3$): δ = 8.08 (d, J = 1.2 Hz, 1H), 7.76 (dd, J = 8.4, 1.5 Hz, 1H), 7.23 (d, J = 8.5 Hz, 1H), 7.10 (d, J = 8.4 Hz, 2H), 6.78 (d, J = 8.5 Hz, 2H), 6.41 (s, 1H), 4.21 (s, 2H), 3.99–3.90 (m, 4H), 3.46 (dd, J = 13.8, 6.5 Hz, 2H), 1.71–1.61 (m, 1H), 1.56–1.45 (m, 3H), 1.34 (t, J = 7.0 Hz, 5H), 0.92 (d, J = 6.6 Hz, 6H), 0.86 (d, J = 6.6 Hz, 6H) ppm. ^{13}C NMR (101 MHz, $CDCl_3$): δ = 167.96, 158.05, 154.83, 141.97, 137.29, 129.47, 129.05, 127.68, 122.05, 117.78, 114.86, 109.29, 63.46, 42.67, 38.56, 38.43, 38.05, 33.69, 26.11, 25.98, 22.49, 22.31, 14.75 ppm. ESI: m/z calcd for $C_{27}H_{37}N_3O_2$ [$M + H$]⁺, 436.29; found, 436.35. HPLC purity: 98% (retention time = 11.03 min).

2-(4-Ethoxybenzyl)-1-isopentyl-N-phenyl-1H-benzo[d]imidazole-5-carboxamide (20b). **20b** was obtained as a light yellow solid (0.21 mmol, 92.0 mg, 64%). 1H NMR (400 MHz, $CDCl_3$): δ = 8.71–8.75 (m, 1H), 8.23 (s, 1H), 7.79–7.81 (m, 1H), 7.65–7.66 (d, J = 7.7 Hz, 2H), 7.18–7.25 (m, 3H), 6.97–7.03 (m, 3H), 6.68–6.70 (m, 2H), 4.12 (s, 2H), 3.84–3.90 (m, 4H), 1.18–1.30 (m, 6H), 0.79–0.81 (d, J = 6.6 Hz, 6H) ppm. ^{13}C NMR (101 MHz, $CDCl_3$): δ = 166.40, 158.20, 155.00, 141.04, 138.74, 137.33, 129.61, 129.01, 127.31, 124.18, 122.82, 120.36, 118.06, 114.96, 109.78, 63.57, 42.93, 38.06, 33.52, 26.24, 22.40, 14.86 ppm. ESI: m/z calcd for $C_{28}H_{31}N_3O_2$ [$M + H$]⁺, 442.24; found, 442.15. HPLC purity: 96% (retention time = 10.69 min).

2-(4-Ethoxybenzyl)-N-hexyl-1-isopentyl-1H-benzo[d]imidazole-5-carboxamide (20c). **20c** was obtained as a light yellow solid (0.15 mmol, 68.0 mg, 45%). 1H NMR (400 MHz, $CDCl_3$): δ = 8.03 (s, 1H), 7.80–7.82 (m, 1H), 7.30–7.33 (d, J = 8.5 Hz, 1H), 7.08–7.10 (d, J = 8.6 Hz, 2H), 6.75–6.77 (m, 2H), 6.46 (m, 1H), 4.25 (s, 2H), 4.00–4.04 (m, 2H), 3.90–3.96 (q, J = 7.0 Hz, 2H), 3.41–3.46 (m, 2H), 1.36–1.61 (m, 14H), 0.89–0.91 (m, 9H) ppm. ^{13}C NMR (101 MHz, $CDCl_3$): δ = 167.91, 158.46, 154.92, 140.02, 136.83, 130.12, 129.85, 127.02, 122.99, 117.06, 115.18, 110.11, 63.72, 43.25, 40.51, 38.17, 33.40, 31.77, 29.85, 26.93, 26.39, 22.82, 22.54, 14.99, 14.26 ppm. ESI: m/z calcd for $C_{28}H_{39}N_3O_2$ [$M + H$]⁺, 450.30; found, 450.25. HPLC purity: 99% (retention time = 11.23 min).

2-(4-Ethoxybenzyl)-1-isopentyl-1H-benzo[d]imidazol-5-yl)-(piperidin-1-yl)methanone (20d). **20d** was obtained as a light yellow solid (0.15 mmol, 68.0 mg, 45%). 1H NMR (400 MHz, $CDCl_3$): δ = 7.72 (s, 1H), 7.27–7.30 (m, 1H), 7.20–7.23 (d, J = 9.2 Hz, 1H), 7.07–7.10 (d, J = 8.7, 2H), 6.74–6.76 (m, 2H), 5.95 (s, 1H), 4.22 (s, 2H), 3.91–3.92 (m, 2H), 3.41–3.58 (br, 2H), 1.44–1.61 (m, 7H), 1.29–1.32 (m, 5H), 0.82–0.83 (d, J = 6.6 Hz, 6H) ppm. ^{13}C NMR (101 MHz, $CDCl_3$): δ = 170.73, 158.22, 154.33, 135.65, 130.75, 129.63, 127.52, 122.29, 117.87, 115.02, 109.77, 63.58, 42.85, 38.12, 33.58, 26.21, 24.75, 22.42, 14.87 ppm. ESI: m/z calcd for $C_{27}H_{35}N_3O_2$ [$M + H$]⁺, 434.27; found, 434.15. HPLC purity: 98% (retention time = 10.35 min).

N-((3*s*,5*s*,7*s*)-Adamantan-1-yl)-2-(4-ethoxybenzyl)-1-isopentyl-1H-benzo[d]imidazole-5-carboxamide (20e). **20e** was obtained as a light yellow solid (0.23 mmol, 113.0 mg, 70%). 1H NMR (400 MHz, $CDCl_3$): δ = 7.98 (s, 1H), 7.74–7.76 (d, J = 8.7 Hz, 1H), 7.30–7.33 (d, J = 8.7 Hz, 1H), 7.10–7.12 (m, 2H), 6.77–6.80 (m, 2H), 5.95 (s, 1H), 4.25 (s, 2H), 4.02–4.06 (m, 2H), 3.92–3.98 (d, J = 7.0 Hz, 2H), 2.14 (m, 9H), 1.72 (m, 6H), 1.54–1.61 (m, 1H), 1.35–1.39 (t, J = 7.0 Hz, 3H), 0.89–0.91 (d, J = 7.1 Hz, 6H) ppm. ^{13}C NMR (101 MHz, $CDCl_3$): δ = 167.19, 158.34, 154.87, 140.19, 131.68, 129.76, 127.10, 122.52, 117.11, 115.10, 109.92, 63.64, 52.53, 43.13, 41.83, 38.12, 36.57, 33.37, 29.70, 26.29, 22.48, 14.93 ppm. ESI: m/z calcd for $C_{32}H_{41}N_3O_2$ [$M + H$]⁺, 500.32; found, 500.25. HPLC purity: 99% (retention time = 11.77 min).

General Procedure for the Synthesis of Target Compounds 23 and 24. The respective bromine compound **21** or **22** (1 equiv) was

dissolved in DMF, and piperidine (2.5 equiv), Na₂CO₃ (3 equiv), and a catalytic amount of NaI were added. The mixture was stirred at 70 °C for 12 h. After the reaction has finished, water was added and the organics were extracted with dichloromethane. The organic phase was washed several times with water and afterward dried over Na₂SO₄. The solvent was removed in vacuo, and the crude product was afterward purified by column chromatography using dichloromethane/methanol/NH₃, aq 25% (15:1:0.1), as the eluent system.

2-(4-Ethoxybenzyl)-N,N-diethyl-1-(4-(piperidin-1-yl)butyl)-1H-benzod[imidazole-5-carboxamide (23). 23 was obtained as a light yellow oil (0.12 mmol, 58.0 mg, 46%). ¹H NMR (400 MHz, CDCl₃): δ = 8.00 (s, 1H), 7.74 (t, J = 0.8 Hz, 1H), 7.29 (d, J = 0.8 Hz, 1H), 7.15 (m, 2H), 6.82 (m, 2H), 4.25 (s, 2H), 3.96–4.03 (m, 4H), 3.30–3.61 (m, 4H), 2.52 (s, 3H), 2.36 (t, J = 7.2 Hz, 2H), 1.67–1.73 (m, 2H), 1.48–1.54 (m, 4H), 1.37 (t, J = 7.2 Hz, 3H), 1.13–1.27 (m, 10H) ppm. ¹³C NMR (101 MHz, CDCl₃): δ = 171.90, 158.16, 154.57, 142.17, 135.89, 131.29, 129.66, 128.08, 121.50, 117.70, 115.01, 109.72, 63.62, 57.74, 54.00, 43.88, 33.87, 27.28, 24.62, 23.58, 22.93, 14.94 ppm. ESI: *m/z* calcd for C₃₀H₄₂N₄O₂ [M + H]⁺, 491.34; found, 491.25. HPLC purity: 97% (retention time = 6.78 min).

2-(4-Ethoxybenzyl)-N,N-diethyl-1-(6-(piperidin-1-yl)hexyl)-1H-benzod[imidazole-5-carboxamide (24). 24 was obtained as a light yellow oil (0.26 mmol, 0.13 g, 70%). ¹H NMR (400 MHz, CDCl₃): δ = 7.98 (s, 1H), 7.72 (m, 1H), 7.25–7.26 (m, 1H), 7.11 (m, 2H), 6.79 (m, 2H), 4.22 (s, 4H), 3.93–3.99 (m, 4H), 3.27–3.59 (m, 4H), 2.41 (s, 3H), 2.28 (t, J = 8 Hz, 2H), 1.58–1.65 (m, 4H), 1.50–1.53 (m, 2H), 1.39–1.47 (m, 3H), 1.35 (t, J = 7.2 Hz, 3H), 1.20 (m, 9H) ppm. ¹³C NMR (101 MHz, CDCl₃): δ = 171.88, 158.09, 154.55, 142.18, 135.98, 131.09, 129.52, 128.05, 121.34, 117.63, 114.91, 109.64, 63.54, 59.02, 54.44, 44.16, 33.87, 29.50, 27.25, 26.83, 26.26, 25.48, 24.15, 14.88 ppm. ESI: *m/z* calcd for C₃₂H₄₆N₄O₂ [M + H]⁺, 519.37; found, 519.13. HPLC purity: 96% (retention time = 7.06 min).

General Procedure for the Synthesis of Target Compounds 30–32. The respective thiourea compound 27, 28, or 29 (1 equiv) was dissolved in anhydrous THF, and NEt₃ (1.5 equiv) and EDCI-HCl (2.5 equiv) were added. The mixture was refluxed for 3–5 h. Afterward, EtOAc was added, and the organic layer was washed with brine. The crude product was purified by column chromatography.

2-((4-Ethoxybenzyl)amino)-N,N-diethyl-1-isopentyl-1H-benzod[imidazole-5-carboxamide (30). The crude product was purified by column chromatography using petroleum ether and EtOAc (1:10) as eluent system. 30 was obtained as a light brown solid (0.71 mmol, 0.31 g, 38%). ¹H NMR (400 MHz, CDCl₃): δ = 7.42 (d, J = 1.0 Hz, 1H), 7.33–7.28 (m, 2H), 7.04 (dd, J = 8.0, 1.5 Hz, 1H), 6.97 (d, J = 8.0 Hz, 1H), 6.87–6.82 (m, 2H), 4.61 (d, J = 5.3 Hz, 2H), 4.00 (q, J = 7.0 Hz, 2H), 3.79 (dd, J = 16.4, 9.0 Hz, 1H), 3.43 (d, J = 3.8 Hz, 4H), 1.61–1.49 (m, 3H), 1.39 (t, J = 7.0 Hz, 3H), 1.21–1.09 (m, 6H), 0.91 (d, J = 6.2 Hz, 6H) ppm. ¹³C NMR (101 MHz, CDCl₃): δ = 13.79, 15.10, 23.03, 25.79, 37.93, 42.33, 47.91, 64.02, 114.72, 115.46, 119.32, 121.03, 129.99, 133.41, 134.45, 141.67, 151.22, 155.09, 172.78 ppm. ESI: *m/z* calcd for C₂₆H₃₆N₄O₂ [M + H]⁺, 437.28; found, 437.25. HPLC purity: 97% (retention time = 8.53 min).

2-((4-Ethoxyphenyl)amino)-N,N-diethyl-1-(2-(piperidin-1-yl)ethyl)-1H-benzod[imidazole-5-carboxamide (31). The crude product was purified by column chromatography using dichloromethane/methanol/NH₃, aq 25% (50:1:0.1), as the eluent system. 31 was obtained as a light yellow solid (0.56 mmol, 0.26 g, 85%). ¹H NMR (400 MHz, CDCl₃): δ = 7.52–7.43 (m, 3H), 7.05 (dt, J = 5.9, 3.0 Hz, 1H), 6.96 (d, J = 8.1 Hz, 1H), 6.88–6.81 (m, 2H), 3.97 (dt, J = 14.0, 4.9 Hz, 4H), 3.51–3.32 (m, 4H), 2.67 (dd, J = 5.4, 3.0 Hz, 2H), 2.51 (s, 4H), 1.68–1.59 (m, 4H), 1.54–1.42 (m, 2H), 1.38–1.32 (m, 3H), 1.23–1.02 (m, 6H) ppm. ¹³C NMR (101 MHz, CDCl₃): δ = 172.23, 154.35, 153.75, 142.04, 134.81, 133.71, 130.28, 120.74, 118.80, 115.22, 114.89, 106.63, 63.77, 55.27, 53.48, 43.24, 41.56, 25.84, 23.75, 14.91, 13.85 ppm. ESI: *m/z* calcd for C₂₇H₃₇N₅O₂ [M + H]⁺, 464.29; found, 464.15. HPLC purity: 96% (retention time = 6.18 min).

N,N-Diethyl-2-((4-phenoxyphenyl)amino)-1-(2-(piperidin-1-yl)ethyl)-1H-benzod[imidazole-5-carboxamide (32). The crude product was purified by column chromatography using dichloromethane/methanol/NH₃, aq 25% (50:1:0.1), as the eluent system. 32 was

obtained as a light brown solid (0.82 mmol, 0.42 g, 61%). ¹H NMR (400 MHz, CDCl₃): δ = 7.59–7.51 (m, 2H), 7.43 (d, J = 1.1 Hz, 1H), 7.25–7.16 (m, 2H), 7.03 (dt, J = 8.7, 4.3 Hz, 1H), 6.99–6.86 (m, 6H), 3.98–3.90 (m, 2H), 3.46–3.22 (m, 4H), 2.67–2.61 (m, 2H), 2.49 (s, 4H), 1.65–1.55 (m, 4H), 1.50–1.41 (m, 2H), 1.14–0.98 (m, 6H) ppm. ¹³C NMR (101 MHz, CDCl₃): δ = 172.22, 158.17, 153.12, 151.41, 141.87, 136.50, 134.66, 130.44, 129.60, 122.61, 120.29, 120.24, 119.07, 118.02, 115.06, 106.84, 59.92, 55.35, 41.60, 31.62, 25.84, 23.73, 13.88 ppm. ESI: *m/z* calcd for C₃₁H₃₇N₅O₂ [M + H]⁺, 512.29; found, 512.20. HPLC purity: 97% (retention time = 7.79 min).

N-(2-(4-Ethoxybenzyl)-1-isopentyl-1H-benzod[imidazol-5-yl]-benzamide (39). Benzoic acid (1 equiv) was dissolved in DMF, and NEt₃ (1.5 equiv), HBTU (1.1 equiv), and amine 38 (1 equiv) were added in one portion. The mixture was stirred overnight at room temperature. EtOAc and a saturated aqueous NaHCO₃ solution were added. The organic layer was washed several times with water and brine and dried over anhydrous Na₂SO₄. The solvent was removed in vacuo, and the product was purified by column chromatography using petroleum ether and EtOAc (1:2) as the eluent system. 39 was obtained as a colorless solid (0.42 mmol, 0.19 g, 64%). ¹H NMR (400 MHz, CDCl₃): δ = 8.08–7.95 (m, 4H), 7.56–7.42 (m, 3H), 7.29 (d, J = 9.3 Hz, 1H), 7.22–7.15 (m, 2H), 6.82 (dd, J = 8.6, 4.4 Hz, 2H), 4.43 (s, 2H), 4.08–4.01 (m, 2H), 4.01–3.93 (m, 2H), 1.62–1.50 (m, 1H), 1.41–1.32 (m, 5H), 0.89 (d, J = 6.6 Hz, 6H) ppm. ¹³C NMR (101 MHz, CDCl₃): δ = 165.98, 158.21, 150.89, 134.89, 131.75, 129.82, 129.61, 128.70, 127.33, 123.31, 114.98, 110.59, 109.88, 63.51, 42.97, 37.93, 33.09, 26.15, 22.33, 14.77 ppm. ESI: *m/z* calcd for C₂₈H₃₁N₃O₂ [M + H]⁺, 442.24; found, 442.10. HPLC purity: 99% (retention time = 9.27 min).

■ ASSOCIATED CONTENT

Supporting Information

The Supporting Information is available free of charge on the ACS Publications website at DOI: 10.1021/acs.jmedchem.7b01760.

Experimental and spectral data of compounds, detailed information about the measurement of inhibition of AChE and BChE, radioligand binding studies on the hCB₁R, hCB₂R, and hMOP receptors, efficacy on hCB₂R, information on cell culture and cell lines, statistics, animals, biochemical and histological procedures, and statistics of behavioral studies (PDF)

Molecular formula strings (CSV)

Crystal structure of the human CB1 receptor (PDB)

Accession Codes

PDB code for the crystal structure of the human CB1 receptor in complex with agonist AM11542 is 5XRA.⁵² This crystal structure was used for the generation of the homology model for computational studies of the human CB2 receptor in complex with compound 20a or 20d.

■ AUTHOR INFORMATION

Corresponding Author

*E-mail: michael.decker@uni-wuerzburg.de. Tel: 0049-931-31-89676.

ORCID

Michael Decker: 0000-0002-6773-6245

Author Contributions

The manuscript was written through contributions of all authors. All authors have given approval to the final version of the manuscript.

Funding

M. Decker gratefully acknowledges the German Science Foundation (Deutsche Forschungsgemeinschaft) for financial support (DFG DE1546/6-3). M. Decker and T. Maurice acknowledge support from Campus France (PHC Procope), and the German

Academic Exchange Service (DAAD), the latter providing funds from the Federal Ministry of Education and Research (BMBF). The Elite Network of Bavaria (Elitenetzwerk Bayern) awarded M. Hoffmann and J. Möller PhD positions within the International Doctoral Program "Receptor Dynamics". A travel grant by the Alzheimer Forschung Initiative e.V. for D. Dolles to present this work at the ACS spring meeting in San Francisco 2017 is gratefully acknowledged.

Notes

The authors declare no competing financial interest.

ACKNOWLEDGMENTS

We thank O. Lockridge (University of Nebraska Medical Center) for providing human BChE. Cell lines stably expressing hCB₁R and hCB₂R were kindly provided by AbbVie (Chicago, IL, USA). We thank S. Kachler and Professor K.-N. Klotz (Institute of Pharmacology and Toxicology, University of Würzburg) for the technical support and workspace for radioligand binding studies.

ABBREVIATIONS USED

A β , amyloid β ; ACh, acetylcholine; AChE, acetylcholinesterase; AD, Alzheimer's disease; ANOVA, analysis of variance; APP, amyloid precursor protein; ATP, adenosine triphosphate; BChE, butyrylcholinesterase; cAMP, cyclic adenosine monophosphate; CHO, Chinese hamster ovary; CNS, central nervous system; Cpd, compound; CRE, cAMP response element; CREB, cAMP response-element binding protein; EDCI, 1-ethyl-3-(3-(dimethylamino)propyl)carbodiimide; ELISA, enzyme-linked immunosorbent assay; EtOAc, ethyl acetate; GAPDH, glyceraldehyde 3-phosphate dehydrogenase; GPCR, G-protein coupled receptor; HBTU, 2-(1H-benzotriazol-1-yl)-1,1,3,3-tetramethyluronium hexafluorophosphate; hCB_{1/2}R, human cannabinoid receptor subtype 1/2; HEK, human embryonic kidney; h β ₂R, human β ₂R adrenergic receptor; ICV, intracerebroventricular; ip, intraperitoneal; MD, molecular dynamics; MIF, macrophage migration inhibitory factor; MOP, μ -opioid; MTT, 3-(4,5-dimethylthiazol-2-yl)-2,5-diphenyltetrazolium bromide; n.d., not determined; NMDA, N-methyl-D-aspartate receptor; nNOS, neuronal nitric oxide synthase; od, oculus dextrus; ROS, reactive oxygen species; (q)RT/PCR, (quantitative) reverse transcription polymerase chain reaction; SAR, structure-activity relationship; Sc.A β , scrambled amyloid β ; STAT-3, signal transducer and activator of transcription; ST-PA, step-through passive avoidance; TM, transmembrane; V or VEL, vehicle; YMT, Y-maze test.

REFERENCES

- (1) Prince, M.; Comas-Herrera, A.; Knapp, M.; Guerchet, M., Karagiannidou, M. *World Alzheimer Report 2016; Improving healthcare for people living with dementia; Coverage, quality and costs now and in the future*; Alzheimer's Disease International (ADI): London, 2016.
- (2) Zemek, F.; Drtinova, L.; Nepovimova, E.; Sepsova, V.; Korabecny, J.; Klimes, J.; Kuca, K. Outcomes of Alzheimer's disease therapy with acetylcholinesterase inhibitors and memantine. *Expert Opin. Drug Saf.* **2014**, *6*, 759–774.
- (3) Ballard, C.; Gauthier, S.; Corbett, A.; Brayne, C.; Aarsland, D.; Jones, E. Alzheimer's disease. *Lancet* **2011**, *377*, 1019–1031.
- (4) Duyckaerts, C.; Dickson, D. Neuropathology of Alzheimer's disease and its variants. In *Neurodegeneration: The Molecular Pathology of Dementia and Movement Disorders*; Dickson, D., Weller, R., Eds.; Wiley-Blackwell: Oxford, 2011; Vol. 2, pp 62–91.

- (5) Ferrer, I. Defining Alzheimer as a common age-related neurodegenerative process not inevitably leading to dementia. *Prog. Neurobiol.* **2012**, *97*, 38–51.

- (6) Wyss-Coray, T. Inflammation in Alzheimer disease: driving force, bystander or beneficial response? *Nat. Med.* **2006**, *12*, 1005–1015.

- (7) Perry, V. H.; Nicoll, J. A. R.; Holmes, C. Microglia in neurodegenerative disease. *Nat. Rev. Neurol.* **2010**, *6*, 193–201.

- (8) Matsuda, L. A.; Lolait, S. J.; Brownstein, M. J.; Young, A. C.; Bonner, T. I. Structure of cannabinoid receptor and functional expression of the cloned cDNA. *Nature* **1990**, *346*, 561–564.

- (9) Chiurchiù, V.; Battistini, L.; Maccarrone, M. Endocannabinoid signaling in innate and adaptive immunity. *Immunology* **2015**, *144*, 352–364.

- (10) Van Sickle, M. D.; Duncan, M.; Kingsley, P. J.; Mouihate, A.; Urbani, P.; Mackie, K.; Stella, N.; Makriyannis, A.; Piomelli, D.; Davison, J. S.; Marnett, L. J.; Di Marzo, V.; Pittmann, Q. J.; Patel, K. D.; Sharkey, K. A. Identification and functional characterization of brainstem cannabinoid CB₂ receptors. *Science* **2005**, *310*, 329–332.

- (11) Núñez, E.; Benito, C.; Pazos, M. R.; Barbachano, A.; Fajardo, O.; González, S.; Tolón, R. M.; Romero, J. Cannabinoid CB₂ receptors are expressed by perivascular microglial cells in the human brain: an immunohistochemical study. *Synapse* **2004**, *53*, 208–213.

- (12) Grünblatt, E.; Zander, N.; Bartl, J.; Jie, L.; Monoranu, C. M.; Arzberger, T.; Ravid, R.; Roggendorf, W.; Gerlach, M.; Riederer, P. Comparison analysis of gene expression patterns between sporadic Alzheimer's and Parkinson's disease. *J. Alzheimer's Dis.* **2007**, *12*, 291–311.

- (13) Solas, M.; Francis, P. T.; Franco, R.; Ramirez, M. J. CB₂ receptor and amyloid pathology in frontal cortex of Alzheimer's disease patients. *Neurobiol. Aging* **2013**, *34*, 805–808.

- (14) Fernández-Ruiz, J.; Romero, J.; Velasco, G.; Tolón, R. M.; Ramos, J. A.; Guzmán, M. Cannabinoid CB₂ receptor: a new target for controlling neural cell survival? *Trends Pharmacol. Sci.* **2007**, *28*, 39–45.

- (15) Molina-Holgado, F.; Molina-Holgado, E.; Guaza, C.; Rothwell, N. J. Role of CB₁ and CB₂ receptors in the inhibitory effects of cannabinoids on liposaccharide-induced nitric oxide release in astrocyte cultures. *J. Neurosci. Res.* **2002**, *67*, 829–836.

- (16) Sheng, W. S.; Hu, S.; Min, X.; Cabral, G. A.; Lokensgard, J. R.; Peterson, P. K. Synthetic cannabinoid WIN55,212–2 inhibits generation of inflammatory mediators by IL-1 β -stimulated human astrocytes. *Glia* **2005**, *49*, 211–219.

- (17) Ehrhart, J.; Obregon, D.; Mori, T.; Hou, H.; Sun, N.; Bai, Y.; Klein, T.; Fernandez, F.; Tan, J.; Shytle, R. D. Stimulation of cannabinoid receptor 2 (CB₂) suppresses microglial activation. *J. Neuroinflammation* **2005**, *2*, 29.

- (18) Wu, J.; Bie, B.; Yang, H.; Xu, J. J.; Brown, D. L.; Naguib, M. Activation of the CB₂ receptor system reverses amyloid-induced memory deficiency. *Neurobiol. Aging* **2013**, *34*, 791–804.

- (19) Martin-Moreno, A. M.; Brera, B.; Spuch, C.; Carro, E.; Garcia-Garcia, L.; Delgado, M.; Pozo, M. A.; Innamorato, N. G.; Cuadrado, A.; de Ceballos, M. L. Prolonged oral cannabinoid administration prevents neuroinflammation, lowers β -amyloid levels and improves cognitive performance in Tg APP 2576 mice. *J. Neuroinflammation* **2012**, *9*, 8–12.

- (20) Koppel, J.; Vingtdoux, V.; Marambaud, P.; d'Abramo, C.; Jimenez, H.; Stauber, M.; Friedman, R.; Davies, P. CB₂ receptor deficiency increases amyloid pathology and alters tau processing in a transgenic mouse model of Alzheimer's disease. *Mol. Med.* **2014**, *19*, 357–364.

- (21) Bisogno, T.; Oddi, S.; Piccoli, A.; Fazio, D.; Maccarrone, M. Type-2 cannabinoid receptors in neurodegeneration. *Pharmacol. Res.* **2016**, *111*, 721–730.

- (22) Davies, P.; Maloney, A. J. Selective loss of central cholinergic neurons in Alzheimer's disease. *Lancet* **1976**, *308*, 1403.

- (23) Nordberg, A.; Ballard, C.; Bullock, R.; Darreh-Shori, T.; Somogyi, M. A Review of butyrylcholinesterase as a therapeutic target in the treatment of Alzheimer's disease. *Prim. Care Companion CNS Disord.* **2013**, *15*, 2.

- (24) Darvesh, S.; Hopkins, D. A.; Geula, C. Neurobiology of butyrylcholinesterase. *Nat. Rev. Neurosci.* **2003**, *4*, 131–138.

- (25) Mesulam, M. M.; Geula, C. Butyrylcholinesterase reactivity differentiates the amyloid plaques of aging from those of dementia. *Ann. Neurol.* **1994**, *36*, 722–727.
- (26) Guillozet, A. L.; Smiley, J. F.; Mash, D. C.; Mesulam, M. M. Butyrylcholinesterase in the life cycle of amyloid plaques. *Ann. Neurol.* **1997**, *42*, 909–918.
- (27) (a) Greig, N. H.; Utsuki, T.; Ingram, D. K.; Wang, Y.; Pepeu, G.; Scali, C.; Yu, Q.-S.; Mamczarz, J.; Holloway, H. W.; Giordano, T.; Chen, D.; Furukawa, K.; Sambamurti, K.; Brossi, A.; Lahiri, D. K. Selective butyrylcholinesterase inhibition elevates brain acetylcholine, augments learning and lowers Alzheimer β -amyloid peptide in rodent. *Proc. Natl. Acad. Sci. U. S. A.* **2005**, *102*, 17213–17218. (b) Li, Q.; Yang, H.; Chen, Y.; Sun, H. Recent progress in the identification of selective butyrylcholinesterase inhibitors for Alzheimer's disease. *Eur. J. Med. Chem.* **2017**, *132*, 294–309. (c) Sawatzky, E.; Wehle, S.; Kling, B.; Wendrich, J.; Bringmann, G.; Sotriffer, C. A.; Heilmann, J.; Decker, M. Discovery of highly selective and nanomolar carbamate-based butyrylcholinesterase inhibitors by rational investigation into their inhibition mode. *J. Med. Chem.* **2016**, *59*, 2067–2082.
- (28) Maurice, T.; Strehaiano, M.; Siméon, N.; Bertrand, C.; Chatonnet, A. Learning performances and vulnerability to amyloid toxicity in the butyrylcholinesterase knockout mouse. *Behav. Brain Res.* **2016**, *296*, 351–360.
- (29) Kosak, U.; Brus, B.; Knez, D.; Sink, R.; Zakelj, S.; Trontelj, J.; Pisljar, A.; Slenc, J.; Gobec, M.; Zivin, M.; Tratnjek, L.; Perse, M.; Salat, K.; Podkova, A.; Filippek, B.; Nachon, F.; Brazzolotto, X.; Wieckowska, A.; Malawska, B.; Stojan, J.; Mlinaric Rascan, I.; Kos, J.; Coquelle, N.; Colletier, J.-P.; Gobec, S. Development of an *in-vivo* active reversible butyrylcholinesterase inhibitor. *Sci. Rep.* **2016**, *6*, 39495–39510.
- (30) Darvesh, S.; Hopkins, D. A.; Geula, C. Neurobiology of butyrylcholinesterase. *Nat. Rev. Neurosci.* **2003**, *4*, 131–138.
- (31) Wright, C. I.; Geula, C.; Mesulam, M.-M. Neurological cholinesterases in the normal brain and in Alzheimer's disease: relationship to plaques, tangles, and patterns of selective vulnerability. *Ann. Neurol.* **1993**, *34*, 373–384.
- (32) Morphy, R.; Rankovic, Z. Designed multiple ligands. An emerging drug discovery paradigm. *J. Med. Chem.* **2005**, *48*, 6523–6543.
- (33) (a) Nepovimova, E.; Uliassi, E.; Korabecny, J.; Pena-Altamira, L. E.; Samez, S.; Pesaresi, A.; Garcia, G. E.; Bartolini, M.; Andrisano, V.; Bergamini, C.; Fato, R.; Lamba, D.; Roberti, M.; Kuca, K.; Monti, B.; Bolognesi, M. L. Multitarget drug design strategy: quinone–tacrine hybrids designed To block amyloid- β aggregation and to exert anticholinesterase and antioxidant effects. *J. Med. Chem.* **2014**, *57*, 8576–8589. (b) Nepovimova, E.; Korabecny, J.; Dolezal, R.; Babkova, K.; Ondrejicek, A.; Jun, D.; Sepsova, V.; Horova, A.; Hrabinova, M.; Soukup, O.; Bukum, N.; Jost, P.; Muckova, L.; Kassa, J.; Malinak, D.; Andrs, M.; Kuca, K. Tacrine–Trolox Hybrids: A novel class of centrally active, nonhepatotoxic multi-target-directed ligands exerting anticholinesterase and antioxidant activities with low *in vivo* toxicity. *J. Med. Chem.* **2015**, *58*, 8985–9003. (c) Spilovska, K.; Korabecny, J.; Nepovimova, E.; Dolezal, R.; Mezeiova, E.; Soukup, O.; Kuca, K. Multitarget tacrine hybrids with neuroprotective properties to confront Alzheimer's disease. *Curr. Top. Med. Chem.* **2017**, *17*, 1006–1026.
- (34) Nimczick, M.; Decker, M. New approaches in the design and development of cannabinoid receptor ligands: multifunctional and bivalent compounds. *ChemMedChem* **2015**, *10*, 773–786.
- (35) Dolles, D.; Decker, M. Dual-acting compounds acting as receptor ligands and enzyme inhibitors. In *Design of Hybrid Molecules for Drug Development*; Decker, M., Ed.; Elsevier: Oxford, 2017; pp 137–165.
- (36) Dolles, D.; Nimczick, M.; Scheiner, M.; Ramler, J.; Stadtmüller, P.; Sawatzky, E.; Drakopoulos, A.; Sotriffer, C.; Wittmann, H.-J.; Strasser, A.; Decker, M. Aminobenzimidazoles and structural isomers as templates for dual-acting butyrylcholinesterase inhibitors and hCB₂R ligands to combat neurodegenerative disorders. *ChemMedChem* **2016**, *11*, 1270–1283.
- (37) Le Naour, M.; Akgün, E.; Yekkirala, A.; Lunzer, M. M.; Powers, M. D.; Kalyuzhny, A. E.; Portoghese, P. S. Bivalent ligands that target μ opioid (MOP) and cannabinoid 1 (CB₁) receptors are potent analgesics devoid of tolerance. *J. Med. Chem.* **2013**, *56*, 5505–5513.
- (38) Perrey, D. A.; Gilmour, B. P.; Thomas, B. F.; Zhang, Y. Toward the development of bivalent ligand probes of cannabinoid CB₁ and orexin OX₁ receptor heterodimers. *ACS Med. Chem. Lett.* **2014**, *5*, 634–638.
- (39) Lange, J. H. M.; Coolen, H. K. A.; Van der Neut, M. A. W.; Borst, A. J. M.; Stork, B.; Verveer, P. C.; Kruse, C. G. Design, synthesis, biological properties, and molecular modeling investigations of novel tacrine derivatives with a combination of acetylcholinesterase inhibition and cannabinoid CB₁ receptor antagonism. *J. Med. Chem.* **2010**, *53*, 1338–1346.
- (40) Montanari, S.; Scalvini, L.; Bartolini, M.; Belluti, F.; Gobbi, S.; Andrisano, V.; Ligresti, A.; Di Marzo, V.; Rivara, S.; Mor, M.; Bisi, A.; Rampa, A. Fatty acid amide hydrolase (FAAH), acetylcholinesterase (AChE), and butyrylcholinesterase (BuChE): networked targets for the development of carbamates as potential anti-Alzheimer's disease agents. *J. Med. Chem.* **2016**, *59*, 6387–6406.
- (41) Lipinski, C. A.; Lombardo, F.; Dominy, B. W.; Feeney, P. J. Experimental and computational approaches to estimate solubility and permeability in drug discovery and development settings. *Adv. Drug Delivery Rev.* **1997**, *23*, 3–25.
- (42) Stöbel, A.; Schlenk, M.; Hinz, S.; Küppers, P.; Heer, J.; Gütschow, M.; Müller, C. E. Dual Targeting of adenosine A_{2A} receptors and monoamine oxidase B by 4H-3,1-benzothiazin-4-ones. *J. Med. Chem.* **2013**, *56*, 4580–4596.
- (43) (a) Darras, F. H.; Pockes, S.; Huang, G.; Wehle, S.; Strasser, A.; Wittmann, H.-J.; Nimczick, M.; Sotriffer, C. A.; Decker, M. Synthesis, biological evaluation, and computational studies of tri- and tetracyclic nitrogen-bridgehead compounds as potent dual-acting AChE inhibitors and hH₃ receptor antagonists. *ACS Chem. Neurosci.* **2014**, *5*, 225–242. (b) Khan, N.; Saad, A.; Nurulain, S. M.; Darras, F. H.; Decker, M.; Sadek, B. The dual-acting H₃ receptor antagonist and AChE inhibitor UW-MD-71 dose-dependently enhances memory retrieval and reverses dizocilpine-induced memory impairments in Rats. *Behav. Brain Res.* **2016**, *297*, 155–164. (c) Sadek, B.; Khan, N.; Darras, F. H.; Pockes, S.; Decker, M. The dual-acting AChE inhibitor and H₃ receptor antagonist UW-MD-72 reverses amnesia induced by scopolamine or dizocilpine in passive avoidance paradigm in rats. *Physiol. Behav.* **2016**, *165*, 383–391.
- (44) (a) Pagé, D.; Balau, E.; Boisvert, L.; Liu, Z.; Milburn, C.; Tremblay, M.; Wei, Z.; Woo, S.; Luo, X.; Cheng, Y.-X.; Yang, H.; Srivastava, S.; Zhou, F.; Brown, W.; Tomaszewski, M.; Walpole, C.; Hodzic, L.; St-Onge, S.; Godbout, C.; Salois, D.; Payza, K. Novel benzimidazole derivatives as selective CB₂ agonists. *Bioorg. Med. Chem. Lett.* **2008**, *18*, 3695–3700. (b) Cheng, Y.-X.; Tomaszewski, M.; Walpole, C.; Yang, H. Novel Compounds. WO 02/085866 A1, October 31, 2002.
- (45) González-Naranjo, P.; Pérez-Macias, N.; Campillo, N. E.; Pérez, C.; Arán, V. J.; Girón, R.; Sánchez-Robles, E.; Martín, M. I.; Gómez-Canas, M.; García-Arencibia, M.; Fernández-Ruiz, J.; Páez, J. A. Cannabinoid agonists showing BuChE inhibition as potential therapeutic agents for Alzheimer's disease. *Eur. J. Med. Chem.* **2014**, *73*, 56–72.
- (46) Munch, H.; Hansen, J. S.; Pittelkow, M.; Christensen, J. B.; Boas, U. A new efficient synthesis of isothiocyanates from amines using di-*tert*-butyl dicarbonate. *Tetrahedron Lett.* **2008**, *49*, 3117–3119.
- (47) Freitag, M.; Schemies, J.; Larsen, T.; El Gaghlab, K.; Schulz, F.; Rumpf, T.; Jung, M.; Link, A. Synthesis and biological activity of splitomicin analogs targeted at human NAD⁺-dependent histone deacetylases (sirtuins). *Bioorg. Med. Chem.* **2011**, *19*, 3669–3677.
- (48) Darras, F. H.; Wehle, S.; Huang, G.; Sotriffer, C. A.; Decker, M. Amine substitution of quinazolinones leads to selective nanomolar AChE inhibitors with 'inverted' binding mode. *Bioorg. Med. Chem.* **2014**, *22*, 4867–4881.
- (49) Lange, J. H. M.; van Stuijvenberg, H. H.; Coolen, H. K. A. C.; Adolfs, T. J. P.; McCreary, A. C.; Keizer, H. G.; Wals, H. C.; Veerman, W.; Borst, A. J. M.; de Looft, W.; Verveer, C.; Kruse, C. G. Bioisosteric replacements of the pyrazole moiety of rimonabant: synthesis, biological properties, and molecular modeling investigations of thiazoles, triazoles, and imidazoles as potent and selective CB₁ cannabinoid receptor antagonists. *J. Med. Chem.* **2005**, *48*, 1823–1838.

- (50) Yao, B. B.; Hsieh, G. C.; Frost, J. M.; Fan, Y.; Garrison, T. R.; Daza, A. V.; Grayson, G. K.; Zhu, C. Z.; Pai, M.; Chandran, P.; Salyers, A. K.; Wensink, E. J.; Honore, P.; Sullivan, J. P.; Dart, M. J.; Meyer, M. D. *In vitro* and *in vivo* characterization of A-796260: a selective cannabinoid CB₂ receptor agonist exhibiting analgesic activity in rodent pain models. *Br. J. Pharmacol.* **2008**, *153*, 390–401.
- (51) Bottegoni, G.; Cavalli, A. Computational Methods in Multitarget Drug Discovery. In *Design of Hybrid Molecules for Drug Development*; Decker, M., Ed.; Elsevier: Oxford, 2017; pp 239–258.
- (52) Hua, T.; Vemuri, K.; Nikas, S. P.; Laprairie, R. B.; Wu, Y.; Qu, L.; Pu, M.; Korde, A.; Jiang, S.; Ho, J. H.; Han, G. W.; Ding, K.; Li, X.; Liu, H.; Hanson, M. A.; Zhao, S.; Bohn, L. M.; Makriyannis, A.; Stevens, R. C.; Liu, Z. J. Crystal structures of agonist-bound human cannabinoid receptor CB1. *Nature* **2017**, *547*, 468–471.
- (53) Ballesteros, J. A.; Weinstein, H. Integrated methods for the construction of three-dimensional models and computational probing of structure-function relations in G protein-coupled receptors. *Methods Neurosci.* **1995**, *25*, 366–428.
- (54) Igel, P.; Geyer, R.; Strasser, A.; Dove, S.; Seifert, R.; Buschauer, A. Synthesis and structure-activity relationships of cyanoguanidine-type and structurally related histamine H₄ receptor agonists. *J. Med. Chem.* **2009**, *52*, 6297–6313.
- (55) Strasser, A.; Striegl, B.; Wittmann, H.-J.; Seifert, R. Pharmacological profile of histaprodifens at four recombinant H₁-receptor species isoforms. *J. Pharmacol. Exp. Ther.* **2007**, *324*, 60–71.
- (56) Wittmann, H.-J.; Seifert, R.; Strasser, A. Sodium binding to hH_{3R} and hH_{4R} - a molecular modeling study. *J. Mol. Model.* **2014**, *20*, 2394–2404.
- (57) Strasser, A.; Wittmann, H.-J.; Schneider, E. H.; Seifert, R. Modulation of GPCRs by monovalent cations and anions. *Naunyn-Schmiedeberg's Arch. Pharmacol.* **2015**, *388*, 363–380.
- (58) Howlett, A. C.; Barth, F.; Bonner, T. I.; Cabral, G.; Casellas, P.; Devane, W. A.; Felder, C. C.; Herkenham, M.; Mackie, K.; Martin, B. R.; Mechoulam, R.; Pertwee, R. G. International Union of Pharmacology. XXVII. Classification of cannabinoid receptors. *Pharmacol. Rev.* **2002**, *54*, 161–202.
- (59) Ross, R. A.; Brockie, H. C.; Stevenson, L. A.; Murphy, V. L.; Templeton, F.; Makriyannis, A.; Pertwee, R. G. Agonist-inverse agonist characterization at CB₁ and CB₂ cannabinoid receptors of L759633, L759656 and AM630. *Br. J. Pharmacol.* **1999**, *126*, 665–672.
- (60) Williams, C. cAMP detection methods in HTS: selecting the best from the rest. *Nat. Rev. Drug Discovery* **2004**, *3*, 125–135.
- (61) Zheng, Y.; Wang, Q.; Li, T.; Qian, J.; Lu, Y.; Li, Y.; Bi, E.; Reu, F.; Qin, Y.; Drazba, J.; Hsi, E.; Yang, J.; Cai, Z.; Yi, Q. Role of myeloma-derived MIF in myeloma cell adhesion to bone marrow and chemotherapy response. *J. Natl. Cancer Inst.* **2016**, *108* (11), djw131.
- (62) Waeber, G.; Thompson, N.; Chautard, T.; Steinmann, M.; Nicod, P.; Pralong, F. P.; Calandra, T.; Gaillard, R. C. Transcriptional activation of the macrophage migration-inhibitory factor gene by the corticotropin-releasing factor is mediated by the cyclic adenosine 3',5'-monophosphate responsive element-binding protein CREB in pituitary cells. *Mol. Endocrinol.* **1998**, *12*, 698–705.
- (63) Alas, S.; Bonavida, B. Inhibition of constitutive STAT3 activity sensitizes resistant non-Hodgkin's lymphoma and multiple myeloma to chemotherapeutic drug-mediated apoptosis. *Clin. Cancer Res.* **2003**, *9*, 316–326.
- (64) Kato, K.; Nomoto, M.; Izumi, H.; Ise, T.; Nakano, S.; Niho, Y.; Kohno, K. Structure and functional analysis of the human STAT3 gene promoter: alteration of chromatin structure as a possible mechanism for the upregulation in cisplatin-resistant cells. *Biochim. Biophys. Acta, Gene Struct. Expression* **2000**, *1493*, 91–100.
- (65) Hill, S. J.; Baker, J. G.; Rees, S. Reporter-gene systems for the study of G-protein-coupled receptors. *Curr. Opin. Pharmacol.* **2001**, *1*, 526–532.
- (66) Wood, K. V. Marker proteins for gene expression. *Curr. Opin. Biotechnol.* **1995**, *6*, 50–58.
- (67) Renton, P.; Green, B.; Maddaford, S.; Rakhit, S.; Andrews, J. S. NOPiats: Novel dual action neuronal nitric oxide synthase inhibitors with μ -opioid agonist activity. *ACS Med. Chem. Lett.* **2012**, *3*, 227–231.
- (68) Hunger, A.; Kebrle, J.; Rossi, A.; Hoffmann, K. Benzimidazol-Derivate und verwandte Heterocyclus III. Synthese von 1-Aminoalkyl-2-benzyl-nitro-benzimidazolen. *Helv. Chim. Acta* **1960**, *43*, 1032–1046.
- (69) Maurice, T.; Lockhart, B. P.; Privat, A. Amnesia induced in mice by centrally administered β -amyloid peptides involves cholinergic dysfunction. *Brain Res.* **1996**, *706*, 181–193.
- (70) Lahmy, V.; Meunier, J.; Malmström, S.; Naert, G.; Givalois, L.; Kim, S. H.; Villard, V.; Vamvakides, A.; Maurice, T. Blockade of Tau hyperphosphorylation and A β 1–42 generation by the aminotetrahydrofuran derivative ANAVEX2–73, a mixed muscarinic and σ 1 receptor agonist, in a nontransgenic mouse model of Alzheimer's disease. *Neuropsychopharmacology* **2013**, *38*, 1706–1723.
- (71) Huang, G.; Drakopoulos, A.; Saedtler, M.; Zou, H.; Meinel, L.; Heilmann, J.; Decker, M. Cytotoxic properties of the alkaloid rutaecarpine and its oligocyclic derivatives and chemical modifications to enhance water-solubility. *Bioorg. Med. Chem. Lett.* **2017**, *27*, 4937–4941.
- (72) Gottlieb, H. E.; Kotlyar, V.; Nudelman, A. NMR chemical shifts of common laboratory solvents as trace impurities. *J. Org. Chem.* **1997**, *62*, 7512–7515.

Supporting Information

Structure-Activity Relationships and Computational Investigations into the Development of Potent and Balanced Dual-Acting Butyrylcholinesterase Inhibitors and Human Cannabinoid Receptor Subtype 2 Ligands with Pro-Cognitive *in vivo* Profile

Dominik Dolles, Matthias Hoffmann, Sandra Gunesch, Oliviero Marinelli, Jan Möller, Giorgio Santoni, Arnaud Chatonnet, Martin J. Lohse, Hans-Joachim Wittmann, Andrea Strasser, Massimo Nabissi, Tangui Maurice, Michael Decker

Chemistry	2
General Informations.....	2
Synthesis.....	3
Biological Evaluation.....	29
Inhibition of AChE and BChE	29
Radioligand Binding Studies on <i>hCB</i> ₂ R and <i>hCB</i> ₁ R.....	30
Radioligand Binding Studies on <i>hMOP</i> Receptor.....	32
Determination of Efficacy	34
<i>in vivo</i> Studies	39
References	43

Chemistry

General Informations

All reagents were used without further purification and bought from common commercial suppliers. For anhydrous reaction conditions, THF was dried prior to use by refluxing over sodium slices for at least two days under argon atmosphere.

Thin layer chromatography was performed on silica gel 60 (alumina foils with fluorescent indicator 254 nm). For detection iodine vapor and UV light (254 nm and 366 nm) were used. For column chromatography, silica gel 60 (particle size of 0.040 mm – 0.063 mm) was used.

Nuclear magnetic resonance spectra were recorded with a Bruker AV-400 NMR instrument (Bruker, Karlsruhe, Germany) in CDCl₃ and chemical shifts are expressed in ppm relative to CDCl₃ (7.26 ppm for ¹H and 77.16 ppm for ¹³C).¹

Purity was determined by HPLC (Shimadzu Products), containing a DGU-20A3R degassing unit, a LC20AB liquid chromatograph and a SPD-20A UV/Vis detector. UV detection was measured at 254 nm. Mass spectra were obtained by a LCMS 2020 (Shimadzu Products). As stationary phase a Synergi 4U fusion-RP (150 * 4.6 mm) column and as mobile phase a gradient of MeOH / water with 0.1% formic acid was used. Parameters: A: water, B: MeOH, V(B)/(V(A)+V(B)) = 5% to 90% over 10 min, V(B)/(V(A)+V(B)) = 90% for 5 min, V(B)/(V(A)+V(B)) = 90% to 5% over 3 min. The method was performed with a flow rate of 1.0 mL/min. Compounds were only used for biological evaluation if purity was ≥95%.

Synthesis

General procedure I for amide formation (for compounds 14 – 16, 20a – e, 36 and 39)

The respective acid (1 eq.) was dissolved in DMF and NEt_3 (1.5 eq.), HBTU (1.1 eq.) and the appropriate amine (1 eq.) were added in one portion. The mixture was stirred overnight at room temperature. Then, EtOAc and a sat. NaHCO_3 solution were added. The organic layer was washed several times with water and brine and dried over anhydrous Na_2SO_4 . The solvent was removed *in vacuo* and product was purified by column chromatography.

General procedure II for aryl halogen substitution (for compounds 4 – 8 and 34)

The respective halogenated aryl compound (1 eq.) was dissolved in EtOH and NEt_3 (1.5 eq.) and the appropriate amine (1.1 eq.) were added. The mixture was stirred overnight at 50 °C. Afterwards, the solvent was removed *in vacuo* and the residue taken up in EtOAc. The organic layer was washed with brine, dried over anhydrous Na_2SO_4 and the solvent removed *in vacuo*. Product was used without further purification.

General procedure III for the reduction of the nitro moiety (for compounds 9 – 13 and 38)

The respective nitro compound (1 eq.) was dissolved in EtOH and $\text{SnCl}_2 \cdot 2 \text{H}_2\text{O}$ (6.2 eq.) added. The mixture was refluxed overnight under argon atmosphere. After cooling to 0 °C, the mixture was basified (pH = 10) with 1 M NaOH_{aq} until precipitation. The precipitate was filtered off by suction and the solution concentrated *in vacuo*. The residue was suspended in water and extracted with CH_2Cl_2 . The organic layer was dried over anhydrous Na_2SO_4 and the solvent was removed *in vacuo*. Product was used without further purification.

General procedure IV for the cyclisation of the benzimidazole derivatives (for compounds 17 – 19 and 37)

The respective acetamide compound (1 eq.) was dissolved in glacial acetic acid, and the mixture refluxed for 1.5 h. The solution was then concentrated *in vacuo*, basified (pH = 10) with NH_{3, aq.} (25%) and extracted with CH₂Cl₂. The organic layer was dried over anhydrous Na₂SO₄, the solvent removed *in vacuo* and the pure product obtained after column chromatography.

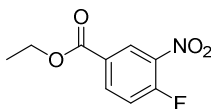
General procedure V for the formation of the isothiocyanates² (for compounds 26a – c)

The respective amine (1 eq.) and NEt₃ (1.2 eq.) were dissolved in anhydrous THF and cooled down to 0 °C. CS₂ (10 eq.) was added dropwise over a period of 20 minutes and the mixture stirred overnight at room temperature. The mixture was again cooled down to 0 °C and a solution of Boc₂O (1 eq.) and DMAP (cat.) in anhydrous THF added dropwise. The reaction was stirred for further 2 h. The solvent was removed *in vacuo* and Et₂O added until precipitation. The precipitate was filtered off and the filtrate was concentrated *in vacuo*. The crude product was purified by column chromatography if necessary.

General procedure VI for the formation of thiourea derivatives (for compounds 27 – 29)

The respective diamino compound (1 eq.) was dissolved in anhydrous THF and the appropriate isothiocyanate (1.0 eq. to 1.1 eq.) added. The mixture was stirred for 3 h to 7 h at room temperature. Afterwards, EtOAc was added and the organic layer washed with brine. The crude product was purified by column chromatography.

Synthesis of ethyl 4-fluoro-3-nitrobenzoate (2)



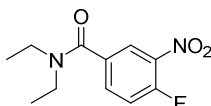
2

4-Fluoro-3-nitrobenzoic acid (5.4 mmol, 1.0 g) was dissolved in ethanol (20 mL) and a catalytic amount of concentrated sulfuric acid was added. The mixture was refluxed for 12 h. After the reaction has finished, solvent was removed *in vacuo* and the crude residue was taken up in EtOAc. The organic phase was washed with water and a saturated aqueous NaHCO₃ solution. After the organic phase was dried with Na₂SO₄, solvent was removed *in vacuo*, which afforded the product as a white solid (4.29 mmol, 0.91 g, 79%)

¹H NMR (400 MHz, CDCl₃): δ = 8.88 – 8.85 (m, 1H), 8.31 (s, 1H), 8.07 – 8.03 (m, 1H), 4.35 (q, J = 7.1 Hz, 2H), 1.38 (t, J = 7.1 Hz, 3H) ppm.

¹³C NMR (101 MHz, CDCl₃): δ = 165.34, 147.86, 136.51, 131.32, 129.61, 117.51, 113.58, 61.12, 14.53 ppm.

Synthesis of *N,N*-diethyl-4-fluoro-3-nitrobenzamide (3)



3

4-Fluoro-3-nitrobenzoic acid (8.1 mmol, 1.5 g) was dissolved in dichloromethane and a catalytic amount of DMF was added. The mixture was cooled down to 0 °C, oxalyl chloride (121.5 mmol, 10.4 mL) was added portionwise and stirred for 1.5 h at room temperature. Dichloromethane and oxalyl chloride were then removed *in vacuo*. The remaining residue was

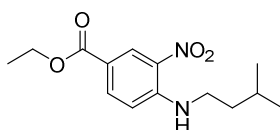
dissolved in dichloromethane, cooled down to 0 °C and a mixture of NEt₃ (24.37 mmol, 3.37 mL) and HNEt₂ (8.91 mmol, 0.93 mL) in dichloromethane was added dropwise. The mixture was stirred for 3 h at room temperature, washed with brine and dried over anhydrous Na₂SO₄. Dichloromethane was removed *in vacuo* to obtain the crude product, which was then purified by column chromatography using petroleum ether and ethyl acetate (1:1) as eluent system. **3** was obtained as an orange oil (6.22 mmol, 1.50 g, 77 %).

¹H NMR (400 MHz, CDCl₃): δ = 8.03 (d, *J* = 2.0, 4.8 Hz, 1H), 7.61 – 7.64 (m, 1H), 7.29 (dd, *J* = 1.6, 8.8 Hz, 1H), 3.34 (d, *J* = 10 Hz, 4H), 1.08-1.21 (m, 6H) ppm.

¹³C NMR (101 MHz, CDCl₃): δ = 167.47, 156.77, 154.11, 136.86, 133.81, 124.42, 118.81, 43.44, 13.99 ppm.

ESI: *m/z* calcd for C₁₁H₁₃FN₂O₃ [M+H]⁺: 241.10; found: 241.10.

Synthesis of ethyl 4-(isopentylamino)-3-nitrobenzoate (**4**)



4

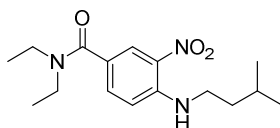
The reaction was carried out according to general procedure II using ethyl 4-fluoro-3-nitrobenzoate **2** (4.29 mmol, 0.91 g), isopentylamine (4.29 mmol, 0.5 mL) and NEt₃ (6.44 mmol, 0.89 mL). **4** was obtained as a yellow oil (4.25 mmol, 1.19 g, 99%).

¹H NMR (400 MHz, CDCl₃): δ = 8.88 – 8.85 (m, 1H), 8.31 (s, 1H), 8.07 – 8.03 (m, 1H), 6.88 – 6.83 (m, 1H), 4.35 (q, *J* = 7.1 Hz, 2H), 3.39 – 3.33 (m, 2H), 1.83 – 1.72 (m, 1H), 1.65 (q, *J* = 14.5, 7.1 Hz, 2H), 1.38 (t, *J* = 7.1 Hz, 3H), 0.99 (d, *J* = 6.8 Hz, 6H) ppm.

^{13}C NMR (101 MHz, CDCl_3): δ = 165.34, 147.86, 136.51, 131.32, 129.61, 117.51, 113.58, 61.12, 41.63, 37.79, 26.11, 22.57, 14.53 ppm.

ESI: m/z calcd for $\text{C}_{14}\text{H}_{20}\text{N}_2\text{O}_4$ $[\text{M}+\text{H}]^+$: 281.15; found: 281.00.

Synthesis of *N,N*-diethyl-4-(isopentylamino)-3-nitrobenzamide (**5**)



5

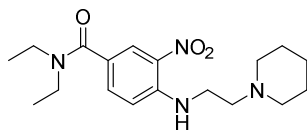
The reaction was carried out according to general procedure II using *N,N*-diethyl-4-fluoro-3-nitrobenzamide **3** (4.9 mmol, 1.2 g), isopentylamine (4.9 mmol, 0.6 mL) and NEt_3 (7.4 mmol, 1.0 mL). **5** was obtained as a yellow oil (4.8 mmol, 1.5 g, 95 %).

^1H NMR (400 MHz, CDCl_3): δ = 8.19 (d, J = 2.0 Hz, 1 H), 8.07 (br, NH), 7.48 (dd, J = 8.8, 2.0 Hz, 1 H), 6.81 (d, J = 8.8 Hz, 1 H), 3.37 (q, J = 6.8 Hz, 4 H), 3.27 (t, J = 7.2 Hz, 2 H), 1.67 – 1.71 (m, 1 H), 1.56 (q, J = 7.1 Hz, 2 H), 1.14 (t, J = 7.0 Hz, 6 H), 0.91 (d, J = 6.8 Hz, 6 H) ppm.

^{13}C NMR (101 MHz, CDCl_3): δ = 169.50, 146.02, 135.22, 130.61, 125.68, 123.18, 113.96, 41.95, 41.37, 37.71, 25.95, 22.44, 13.55 ppm.

ESI: m/z calcd for $\text{C}_{16}\text{H}_{25}\text{N}_3\text{O}_3$ $[\text{M}+\text{H}]^+$: 308.20; found: 308.00.

Synthesis of *N,N*-diethyl-3-nitro-4-((2-(piperidin-1-yl)ethyl)amino)benzamide (**6**)



6

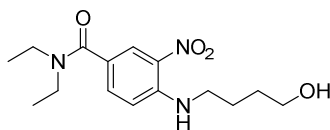
The reaction was carried out according to general procedure II using *N,N*-diethyl-4-fluoro-3-nitrobenzamide **3** (5.4 mmol, 1.3 g), commercially available 2-(piperidin-1-yl)ethan-1-amine (5.4 mmol, 0.8 mL) and NEt₃ (8.1 mmol, 1.2 mL). **6** was obtained as yellow oil (5.3 mmol, 1.6 g, 98%)

¹H NMR (400 MHz, CDCl₃): δ = 8.61 (s, 1H), 8.21 (s, 1H), 7.48 (d, *J* = 8.8 Hz, 1H), 6.80 (d, *J* = 8.9 Hz, 1H), 3.45 – 3.28 (m, 6H), 2.61 (t, *J* = 6.1 Hz, 2H), 2.40 (s, 4H), 1.60 – 1.53 (m, 4H), 1.45 – 1.36 (m, 2H), 1.15 (t, *J* = 7.0 Hz, 6H) ppm.

¹³C NMR (101 MHz, CDCl₃): δ = 169.44, 145.74, 134.94, 130.72, 125.56, 123.28, 114.27, 56.12, 54.15, 39.89, 38.55, 36.41, 25.99, 24.36 ppm.

ESI: *m/z* calcd for C₁₈H₂₈N₄O₃ [M+H]⁺: 349.22; found: 349.30.

Synthesis of *N,N*-diethyl-4-((4-hydroxybutyl)amino)-3-nitrobenzamide (**7**)



7

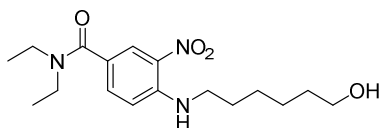
The reaction was carried out according to general procedure II using *N,N*-diethyl-4-fluoro-3-nitrobenzamide **3** (1.16 mmol, 0.28 g) and 4-amino-1-butanol (1.39 mmol, 0.12 g). **7** was obtained as a dark orange oil (1.16 mmol, 0.36 g, > 99%).

¹H NMR (400 MHz, CDCl₃): δ = 8.27 (d, J = 2.0 Hz, 1H), 8.20 (br, 1H), 7.56 (dd, J = 2.0, 6.8 Hz, 1H), 6.89 (d, J = 8.8 Hz, 1H), 3.73 (t, J = 6.0 Hz, 2H), 3.48 (s, 1H), 3.37-3.47 (m, 6H), 1.82-1.89 (m, 2H), 1.69-1.76 (m, 2H), 1.22 (t, J = 7.2 Hz, 6H) ppm.

¹³C NMR (101 MHz, CDCl₃): δ = 169.57, 146.07, 135.38, 130.75, 125.80, 123.70, 114.10, 62.39, 43.09, 30.06, 25.59 ppm.

ESI: m/z calcd for C₁₅H₂₃N₃O₄ [M+H]⁺: 310.18; found: 310.05.

Synthesis of *N,N*-diethyl-4-((6-hydroxyhexyl)amino)-3-nitrobenzamide (**8**)



8

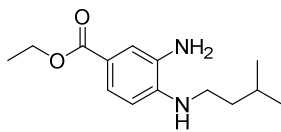
The reaction was carried out according to general procedure II using *N,N*-diethyl-4-fluoro-3-nitrobenzamide **3** (1.54 mmol, 0.37 g), 6-amino-1-hexanol (1.85 mmol, 0.22 g) and NEt₃ (2.3 mmol, 0.3 mL). **8** was obtained as a dark orange oil (1.38 mmol, 0.47 g, 89%).

¹H NMR (400 MHz, CDCl₃): δ = 8.27 (s, 1 H), 8.17 (br, NH), 7.55 (dd, J = 2.0, 6.8 Hz, 1 H), 6.87 (d, J = 8.8 Hz, 1 H), 3.66 (t, J = 6.4 Hz, 2 H), 3.32-3.47 (m, 6 H), 2.05 (d, J = 9.6 Hz, 1 H), 1.72-1.79 (m, 2 H), 1.57-1.63 (m, 2 H), 1.44-1.49 (m, 4 H), 1.21 (t, J = 7.2 Hz, 6 H) ppm.

¹³C NMR (101 MHz, CDCl₃): δ = 172.13, 149.27, 136.78, 132.12, 125.80, 123.23, 115.11, 61.67, 43.07, 32.31, 30.12, 27.66, 25.63 ppm.

ESI: m/z calcd for C₁₇H₂₇N₃O₄ [M+H]⁺: 338.21; found: 338.10.

Synthesis of ethyl 3-amino-4-(isopentylamino)benzoate (**9**)

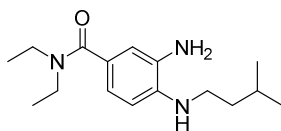


9

The reaction was carried out according to general procedure III using ethyl 4-(isopentylamino)-3-nitrobenzoate **4** (4.0 mmol, 1.13 g) and SnCl₂·2 H₂O (20.2 mmol, 4.6 g). **9** was obtained as a light yellow oil (4.0 mmol, 1.0 g, > 99%) and immediately used for the next reaction step.

ESI: *m/z* calcd for C₁₄H₂₂N₂O₂ [M+H]⁺: 251.18; found: 251.05.

Synthesis of 3-amino-*N,N*-diethyl-4-(isopentylamino)benzamide (**10**)

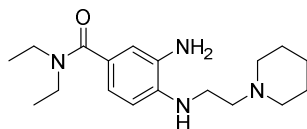


10

The reaction was carried out according to general procedure III using *N,N*-diethyl-4-(isopentylamino)-3-nitrobenzamide **5** (1.09 mmol, 0.34 g) and SnCl₂·2 H₂O (5.45 mmol, 1.22 g). **10** was obtained as colourless oil (0.84 mmol, 0.23 g, 77%) and immediately used for the next reaction step.

ESI: *m/z* calcd for C₁₆H₂₇N₃O [M+H]⁺: 278.22; found: 278.15.

Synthesis of 3-amino-*N,N*-diethyl-4-((2-(piperidin-1-yl)ethyl)amino)benzamide (**11**)

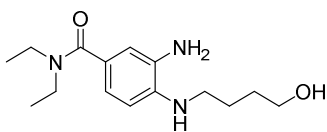


11

The reaction was carried out according to general procedure III using *N,N*-diethyl-3-nitro-4-((2-(piperidin-1-yl)ethyl)amino)benzamide **6** (2.90 mmol, 1.01 g) and SnCl₂·2 H₂O (17.4 mmol, 3.9 g). **11** was obtained as a light yellow oil (2.86 mmol, 0.91 g, 98%) and immediately used for the next reaction step.

ESI: *m/z* calcd for C₁₈H₃₀N₄O [M+H]⁺: 319.24; found: 319.45.

Synthesis of 3-amino-*N,N*-diethyl-4-((4-hydroxybutyl)amino)benzamide (**12**)

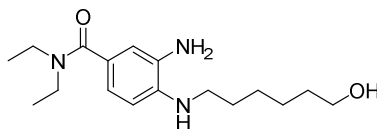


12

The reaction was carried out according to general procedure III using *N,N*-diethyl-4-((4-hydroxybutyl)amino)-3-nitrobenzamide **7** (1.16 mmol, 0.36 g) and SnCl₂·2 H₂O (6.96 mmol, 1.57 g). **12** was obtained as a pale yellow oil (1.16 mmol, 0.32 g, > 99%) and immediately used for the next reaction step.

ESI: *m/z* calcd for C₁₅H₂₅N₃O₂ [M+H]⁺: 280.20; found: 280.15.

Synthesis of 3-amino-*N,N*-diethyl-4-((6-hydroxyhexyl)amino)benzamide (**13**)

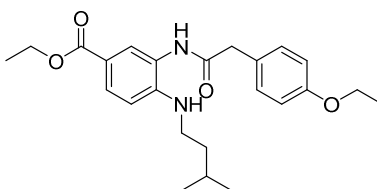


13

The reaction was carried out according to general procedure III using *N,N*-diethyl-4-((4-hydroxyhexyl)amino)-3-nitrobenzamide **8** (1.38 mmol, 0.47 g) and SnCl₂·2 H₂O (8.28 mmol, 1.87 g). **13** was obtained as a pale yellow oil (1.32 mmol, 0.41 g, 96%) and immediately used for the next reaction step.

ESI: *m/z* calcd for C₁₇H₂₉N₃O₂ [M+H]⁺: 308.23; found: 308.15.

Synthesis of ethyl 3-(2-(4-ethoxyphenyl)acetamido)-4-(isopentylamino)benzoate (**14**)



14

The reaction was carried out according to general procedure I using ethyl 3-amino-4-(isopentylamino)benzoate **9** (4.0 mmol, 1.0 g) and 2-(4-ethoxyphenyl)acetic acid (4.0 mmol, 0.6 g). The crude product was purified by column chromatography using petroleum ether and EtOAc (1:1) as eluent system. **14** was obtained as light brown oil (2.18 mmol, 0.90 g, 60%).

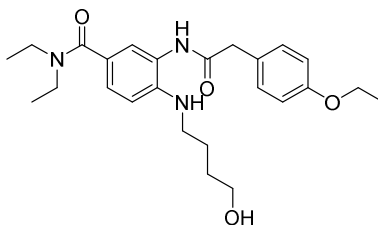
¹H NMR (400 MHz, CDCl₃): δ = 7.86 – 7.82 (m, 1H), 7.73 – 7.71 (m, 1H), 7.32 – 7.29 (m, 2H), 6.97 – 6.94 (m, 2H), 6.65 (d, *J* = 8.7 Hz, 1H), 4.32 (q, *J* = 7.1 Hz, 2H), 4.17 (q, *J* = 7.1

Hz, 2H), 3.74 (s, 2H), 3.14 – 3.08 (m, 2H), 1.70 – 1.65 (m, 1H), 1.50 – 1.40 (m, 5H), 1.37 (t, $J = 7.1$ Hz, 3H), 0.96 (d, $J = 6.6$ Hz, 6H) ppm.

^{13}C NMR (101 MHz, CDCl_3): $\delta = 170.98, 166.57, 158.77, 147.35, 130.61, 130.25, 127.97, 126.60, 121.68, 118.58, 115.51, 110.82, 63.67, 60.51, 41.77, 38.75, 38.29, 26.11, 22.68, 14.94, 14.57$ ppm.

ESI: m/z calcd for $\text{C}_{24}\text{H}_{32}\text{N}_2\text{O}_4$ $[\text{M}+\text{H}]^+$: 413.24; found: 413.10.

Synthesis of 3-(2-(4-ethoxyphenyl)acetamido)-*N,N*-diethyl-4-((4-hydroxybutyl)amino)-benzamide (15)



15

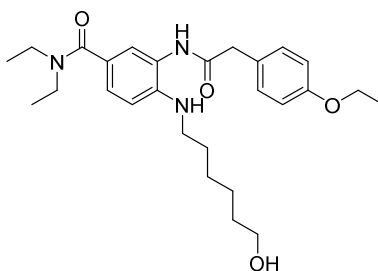
The reaction was carried out according to general procedure I using 3-amino-*N,N*-diethyl-4-((4-hydroxybutyl)amino)benzamide **12** (1.16 mmol, 0.32 g) and 2-(4-ethoxyphenyl)acetic acid (1.16 mmol, 0.21 g). The crude product was purified by column chromatography using petroleum ether and EtOAc (1:2) as eluent system. **15** was obtained as light brown oil (0.49 mmol, 0.22 g, 43%).

^1H NMR (400 MHz, CDCl_3): $\delta = 7.88$ (s, 1H), 7.32 - 7.43 (m, 2H), 7.15 (d, $J = 8.8$ Hz, 2H), 6.83 (d, $J = 8.4$ Hz, 2H), 4.73 (s, 2H), 4.05 - 4.21 (m, 4H), 3.34 - 3.66 (m, 4H), 3.28 (t, $J = 6.8$, 2H), 1.51 - 1.81 (m, 4H), 1.39 (t, $J = 7.2$ Hz, 3H), 1.19 - 1.29 (m, 6H) ppm.

^{13}C NMR (101 MHz, CDCl_3): δ = 171.84, 155.18, 149.51, 142.00, 135.86, 131.43, 130.48, 129.59, 127.90, 121.70, 117.76, 115.19, 114.66, 109.59, 61.67, 59.46, 43.42, 32.56, 31.95, 29.82, 28.16, 14.94, 14.32 ppm.

ESI: m/z calcd for $\text{C}_{25}\text{H}_{35}\text{N}_3\text{O}_4$ $[\text{M}+\text{H}]^+$: 442.26; found: 442.30.

Synthesis of 3-(2-(4-ethoxyphenyl)acetamido)-*N,N*-diethyl-4-((6-hydroxyhexyl)amino)-benzamide (16)



16

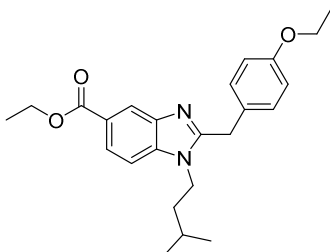
The reaction was carried out according to general procedure I using 3-amino-*N,N*-diethyl-4-((4-hydroxyhexyl)amino)benzamide **13** (1.32 mmol, 0.41 g) and 2-(4-ethoxyphenyl)acetic acid (1.32 mmol, 0.23 g). The crude product was purified by column chromatography using petroleum ether and EtOAc (1:2) as eluent system. **16** was obtained as yellow oil (0.69 mmol, 0.32 g, 53%).

^1H NMR (400 MHz, CDCl_3): δ = 7.88 (s, 1H), 7.27 - 7.39 (m, 2H), 7.16 (d, J = 8.8 Hz, 2H), 6.86 (d, J = 8.4 Hz, 2H), 4.89 (s, 2H), 3.93 - 4.05 (m, 4H), 3.34 - 3.66 (m, 4H), 3.28 (t, J = 6.8, 2H), 1.51 - 1.81 (m, 6H), 1.39 (m, 5H), 1.18 - 1.27 (m, 6H) ppm.

^{13}C NMR (101 MHz, CDCl_3): δ = 171.84, 151.11, 149.31, 142.12, 135.86, 131.43, 130.61, 129.47, 127.90, 121.70, 117.76, 115.08, 114.66, 109.60, 60.44, 43.43, 33.95, 32.56, 30.33, 29.82, 28.16, 27.57, 14.94, 14.34 ppm.

ESI: m/z calcd for $C_{27}H_{39}N_3O_4$ $[M+H]^+$: 470.29; found: 470.30.

Synthesis of ethyl 2-(4-ethoxybenzyl)-1-isopentyl-1H-benzo[d]imidazole-5-carboxylate (**17**)



17

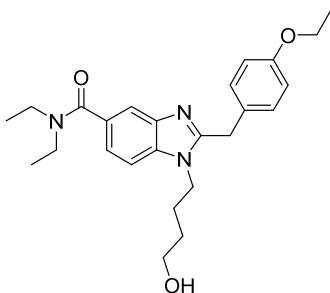
The reaction was carried out according to general procedure IV using ethyl 3-(2-(4-ethoxyphenyl)acetamido)-4-(isopentylamino)benzoate **14** (2.18 mmol, 0.90 g). **17** was obtained as light brown oil (2.08 mmol, 0.82 g, 95%) and was used for the next reaction step without purification.

¹H NMR (400 MHz, $CDCl_3$): δ = 8.44 (s, 1H), 7.95 – 7.91 (m, 1H), 7.21 (d, J = 8.4 Hz, 1H), 7.10 (d, J = 8.8 Hz, 2H), 6.78 (d, J = 8.8 Hz, 2H), 4.35 (q, J = 7.1 Hz, 2H), 4.20 (s, 2H), 3.96 – 3.89 (m, 4H), 1.56 – 1.46 (m, 1H), 1.39 – 1.28 (m, 8H), 0.85 (d, J = 6.8 Hz, 6H) ppm.

¹³C NMR (101 MHz, $CDCl_3$): δ = 167.17, 158.05, 155.08, 142.21, 138.53, 129.49, 127.69, 124.35, 123.82, 121.71, 114.86, 108.88, 63.44, 60.71, 42.67, 38.04, 33.77, 26.11, 22.31, 14.76, 14.37 ppm.

ESI: m/z calcd for $C_{24}H_{20}N_2O_3$ $[M+H]^+$: 395.23; found: 395.15.

Synthesis of 2-(4-ethoxybenzyl)-*N,N*-diethyl-1-(4-hydroxybutyl)-1*H*-benzo[*d*]imidazole-5-carboxamide (**18**)



18

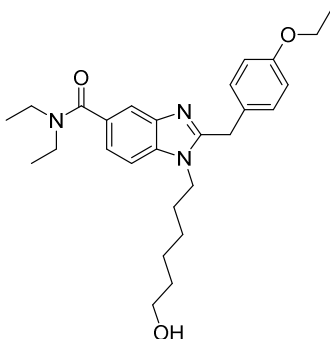
The reaction was carried out according to general procedure IV using 3-(2-(4-ethoxyphenyl)acetamido)-*N,N*-diethyl-4-((4-hydroxybutyl)amino)-benzamide **15** (0.40 mmol, 0.24 g). The crude product was purified by column chromatography using petroleum ether and EtOAc (1:2) as eluent system. **18** was obtained as light brown oil (0.35 mmol, 0.15 g, 88%).

¹H NMR (400 MHz, CDCl₃): δ = 7.76 (s, 1H), 7.27 - 7.33 (m, 2H), 7.15 (d, J = 8.8 Hz, 2H), 6.83 (d, J = 8.4 Hz, 2H), 4.27 (s, 2H), 3.93 - 4.05 (m, 4H), 3.34 - 3.66 (m, 4H), 3.28 (t, J = 6.8, 2H), 1.51 - 1.81 (m, 4H), 1.39 (t, J = 7.2 Hz, 3H), 1.18 - 1.27 (m, 6H) ppm.

¹³C NMR (101 MHz, CDCl₃): δ = 171.84, 158.28, 154.51, 142.04, 136.86, 131.43, 130.48, 129.59, 127.90, 121.70, 117.76, 115.08, 114.66, 109.60, 63.64, 60.46, 42.43, 33.96, 32.56, 29.82, 28.16, 14.94, 14.34 ppm.

ESI: m/z calcd for C₂₅H₃₃N₃O₃ [M+H]⁺: 424.26; found: 424.30.

Synthesis of 2-(4-ethoxybenzyl)-*N,N*-diethyl-1-(4-hydroxyhexyl)-1*H*-benzo[*d*]imidazole-5-carboxamide (19)



19

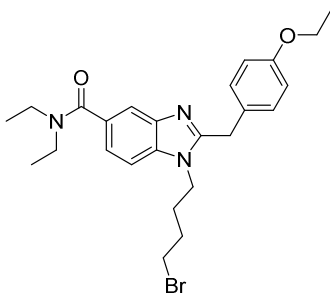
The reaction was carried out according to general procedure IV using 3-(2-(4-ethoxyphenyl)acetamido)-*N,N*-diethyl-4-((6-hydroxyhexyl)amino)-benzamide **16** (0.79 mmol, 0.48 g). The crude product was purified by column chromatography using petroleum ether and EtOAc (1:2) as eluent system. **19** was obtained as light brown oil (0.55 mmol, 0.25 g, 70%).

¹H NMR (400 MHz, CDCl₃): δ = 7.76 (s, 1H), 7.27 - 7.33 (m, 2H), 7.15 (d, J = 8.8 Hz, 2H), 6.83 (d, J = 8.4 Hz, 2H), 4.27 (s, 2H), 3.93 - 4.05 (m, 4H), 3.34 - 3.66 (m, 4H), 3.28 (t, J = 6.8, 2H), 1.51 - 1.81 (m, 6H), 1.39 (m, 5H), 1.18 - 1.27 (m, 6H) ppm.

¹³C NMR (101 MHz, CDCl₃): δ = 171.84, 158.28, 154.51, 142.00, 135.86, 131.43, 130.61, 130.48, 129.59, 127.90, 121.70, 117.76, 115.19, 115.08, 114.66, 109.60, 63.64, 43.42, 33.95, 32.56, 30.33, 29.82, 28.16, 27.57, 14.94, 14.22 ppm.

ESI: m/z calcd for C₂₇H₃₇N₃O₃ [M+H]⁺: 452.29; found: 452.32.

Synthesis of 1-(4-bromobutyl)-2-(4-ethoxybenzyl)-*N,N*-diethyl-1*H*-benzo[*d*]imidazole-5-carboxamide (**21**)



21

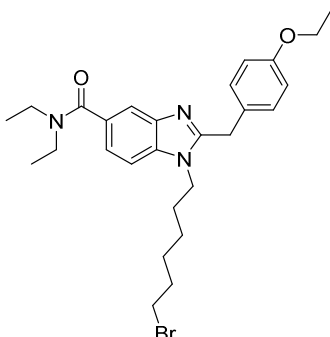
Hydroxy compound **18** (0.40 mmol, 0.17 g) was dissolved in dichloromethane, cooled to 0 °C and phosphorous tribromide (1.00 mmol, 90.0 μ L) was added. The mixture was stirred for 10 min at 0 °C and was then allowed to warm to room temperature and stirred for further 12 h. After the reaction has finished, the mixture was quenched with water and neutralized with a saturated aqueous NaHCO₃ solution. The organics were extracted with dichloromethane and afterwards dried over Na₂SO₄. The solvent was removed *in vacuo* and the bromine compound **21** was obtained without further purification (0.39 mmol, 189.7 mg, 98%).

¹H NMR (400 MHz, CDCl₃): δ = 7.76 (s, 1H), 7.27-7.33 (m, 2H), 7.15 (d, *J* = 8.8 Hz, 2H), 6.83 (d, *J* = 8.4 Hz, 2H), 4.27 (s, 2H), 3.93-4.05 (m, 4H), 3.70 (t, *J* = 6.8, 2H), 3.34-3.66 (m, 4H), 1.51-1.81 (m, 4H), 1.39 (t, *J* = 7.2 Hz, 3H), 1.18-1.27 (m, 6H) ppm.

¹³C NMR (101 MHz, CDCl₃): δ = 170.67, 158.28, 154.51, 142.09, 135.86, 131.43, 130.61, 130.48, 129.59, 127.90, 121.70, 117.76, 115.19, 115.08, 114.66, 109.60, 63.64, 43.42, 33.95, 32.56, 29.82, 28.16, 14.94, 14.34 ppm.

ESI: *m/z* calcd for C₂₅H₃₂BrN₃O₂ [M+H]⁺: 485.17, 487,17; found: 486.18, 488.15.

Synthesis of 1-(6-bromohexyl)-2-(4-ethoxybenzyl)-*N,N*-diethyl-1*H*-benzo[*d*]imidazole-5-carboxamide (**22**)



22

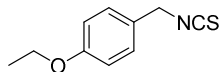
Hydroxy compound **19** (1.31 mmol, 0.59 g) was dissolved in dichloromethane, cooled to 0 °C and phosphorous tribromide (3.30 mmol, 0.31 mL) was added. The mixture was stirred for 10 min at 0 °C and was then allowed to warm to room temperature and stirred for further 12 h. After the reaction has finished, the mixture was quenched with water and neutralized with a saturated aqueous NaHCO₃ solution. The organics were extracted with dichloromethane and afterwards dried over Na₂SO₄. The solvent was removed *in vacuo* and the bromine compound **22** was obtained without further purification (1.21 mmol, 0.62 g, 92%).

¹H NMR (400 MHz, CDCl₃): δ = 7.76 (s, 1H), 7.27 - 7.33 (m, 2H), 7.15 (d, *J* = 8.8 Hz, 2H), 6.83 (d, *J* = 8.4 Hz, 2H), 4.27 (s, 2H), 3.93 - 4.05 (m, 4H), 3.34 - 3.76 (m, 4H), 3.28 (t, *J* = 6.8, 2H), 1.51 - 1.86 (m, 6H), 1.40 (m, 5H), 1.18 - 1.27 (m, 6H) ppm.

¹³C NMR (101 MHz, CDCl₃): δ = 171.84, 158.28, 154.51, 141.88, 135.86, 131.43, 130.61, 130.48, 129.59, 127.90, 121.70, 117.76, 115.19, 115.08, 114.66, 109.60, 63.64, 43.42, 33.95, 32.56, 30.33, 29.82, 28.16, 27.57, 14.94, 14.34 ppm.

ESI: *m/z* calcd for C₂₇H₃₆BrN₃O₂ [M+H]⁺: 513.20, 515.20; found: 514.22, 516.24.

Synthesis of 1-ethoxy-4-(isothiocyanatomethyl)benzene (**26a**)



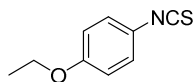
26a

The synthesis was carried out according to general procedure V using (4-ethoxyphenyl)methanamine (4.63 mmol, 0.67 mL), carbon disulfide (46.4 mmol, 2.8 mL), NEt₃ (5.56 mmol, 0.77 mL) and Boc₂O (4.63 mmol, 1.01 g). The crude product was purified by column chromatography using petroleum ether and EtOAc (10:1) as eluent system. **26a** was obtained as a colorless liquid (4.14 mmol, 0.81 g, 89%)

¹H NMR (400 MHz, CDCl₃): δ = 7.25 – 7.20 (m, 2H), 6.94 – 6.88 (m, 2H), 4.61 (s, 2H), 4.03 (q, J = 7.0 Hz, 2H), 1.43 (t, J = 7.0 Hz, 3H) ppm.

¹³C NMR (101 MHz, CDCl₃): δ = 159.04, 131.87, 128.42, 126.21, 114.87, 63.58, 48.33, 14.85 ppm.

Synthesis of 1-ethoxy-4-isothiocyanatobenzene (**26b**)



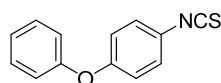
26b

The synthesis was carried out according to general procedure V using *p*-phenetidine (7.28 mmol, 0.94 mL), carbon disulfide (72.8 mmol, 4.4 mL), NEt₃ (8.74 mmol, 1.2 mL) and Boc₂O (7.28 mmol, 1.58 g). **26b** was obtained as a light brown solid (6.14 mmol, 1.10 g, 84%)

¹H NMR (400 MHz, CDCl₃): δ = 7.15 (m, 2H), 6.84 (m, 2H), 4.02 (q, *J* = 8.4 Hz, 2H), 1.41 (t, *J* = 6.8 Hz, 3H) ppm.

¹³C NMR (101 MHz, CDCl₃): δ = 158.15, 127.10, 116.36, 115.46, 64.01, 14.84 ppm.

Synthesis of 1-isothiocyanato-4-phenoxybenzene (**26c**)



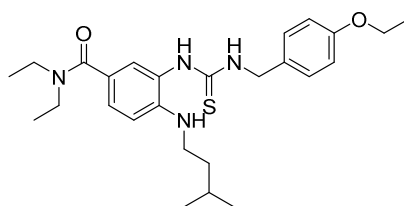
26c

The synthesis was carried out according to general procedure V using *p*-phenoxy aniline (5.4 mmol, 1.0 g), carbon disulfide (54.0 mmol, 3.3 mL), NEt₃ (6.5 mmol, 0.9 mL) and Boc₂O (5.4 mmol, 1.2 g). The crude product was purified by column chromatography using only petroleum ether as eluent system. **26c** was obtained as a colorless liquid (4.1 mmol, 0.93 g, 76%)

¹H NMR (400 MHz, CDCl₃): δ = 6.93 – 6.98 (m, 2H), 7.00 – 7.05 (m, 2H), 7.14 – 7.21 (m, 3H), 7.34 – 7.41 (m, 2H) ppm.

¹³C NMR (101 MHz, CDCl₃): δ = 119.27, 119.42, 124.13, 125.87, 127.16, 130.01, 135.02, 156.30, 156.58 ppm.

Synthesis of 3-(3-(4-ethoxybenzyl)thioureido)-*N,N*-diethyl-4-(isopentylamino)benzamide (**27**)



27

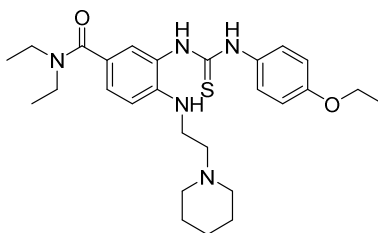
The reaction was carried out according to general procedure VI using o-phenylene diamine **10** (2.96 mmol, 0.82 g) and isothiocyanate **26a** (2.96 mmol, 0.57 g). The crude product was purified by column chromatography using dichloromethane:methanol:NH₃, aq. 25% (20:1:0.1) as eluent system. **27** was obtained as light yellow oil (1.85 mmol, 0.85 g, 61%).

¹H NMR (400 MHz, CDCl₃): δ = 7.23 – 7.12 (m, 4H), 6.88 – 6.82 (m, 2H), 6.82 – 6.77 (m, 1H), 4.71 (d, *J* = 5.3 Hz, 2H), 3.31 (dd, *J* = 13.8, 6.8 Hz, 4H), 3.05 – 2.97 (m, 2H), 1.64 (m, 1H), 1.37 (td, *J* = 6.7, 1.9 Hz, 5H), 1.08 (t, *J* = 7.0 Hz, 6H), 0.91 (d, *J* = 6.6 Hz, 6H) ppm.

¹³C NMR (101 MHz, CDCl₃): δ = 182.40, 171.34, 158.99, 158.40, 146.10, 129.15, 128.37, 127.80, 126.16, 114.84, 114.55, 110.32, 63.54, 63.43, 48.29, 41.55, 38.17, 26.05, 22.61, 14.85, 14.79 ppm.

ESI: *m/z* calcd for C₂₆H₃₈N₄O₂S [M+H]⁺: 471.27; found: 471.15.

Synthesis of 3-(3-(4-ethoxyphenyl)thioureido)-*N,N*-diethyl-4-((2-(piperidin-1-yl)ethyl)amino)benzamide (**28**)



28

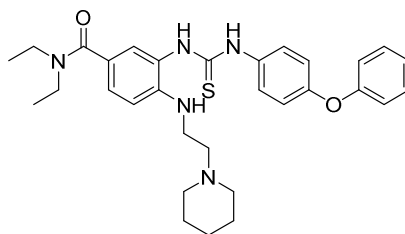
The reaction was carried out according to general procedure VI using o-phenylene diamine **11** (2.86 mmol, 0.91 g) and isothiocyanate **26b** (2.86 mmol, 0.51 g). The crude product was purified by column chromatography using dichloromethane:methanol:NH₃, aq. 25% (20:1:0.1) as eluent system. **28** was obtained as light yellow oil (0.66 mmol, 0.33 g, 23%).

¹H NMR (400 MHz, CDCl₃): δ = 7.30 (d, J = 8.8 Hz, 2H), 7.18 (s, 1H), 6.82 (d, J = 8.9 Hz, 2H), 6.80 – 6.76 (m, 1H), 6.56 (d, J = 8.9 Hz, 1H), 3.96 (t, J = 5.7 Hz, 2H), 3.40 (d, J = 6.7 Hz, 4H), 3.13 (s, 2H), 2.56 (dd, J = 11.6, 5.4 Hz, 2H), 2.39 (s, 4H), 1.53 (m, 6H), 1.41 – 1.30 (m, 3H), 1.13 (t, J = 7.0 Hz, 6H) ppm.

¹³C NMR (101 MHz, CDCl₃): δ = 206.72, 181.86, 171.24, 157.09, 145.79, 128.43, 127.89, 126.89, 116.83, 114.72, 114.31, 110.81, 63.64, 56.94, 54.29, 53.50, 43.26, 38.58, 30.88, 25.86, 24.29, 14.79, 14.17 ppm.

ESI: m/z calcd for C₂₇H₃₉N₅O₂S [M+H]⁺: 498.28; found: 498.15.

Synthesis of *N,N*-diethyl-3-(3-(4-phenoxyphenyl)thioureido)-4-((2-(piperidin-1-yl)ethyl)amino)benzamide (**29**)



29

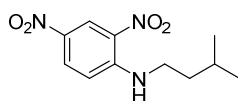
The reaction was carried out according to general procedure VI using *o*-phenylene diamine **11** (2.60 mmol, 0.83 g) and isothiocyanate **26c** (2.60 mmol, 0.59 g). The crude product was purified by column chromatography using dichloromethane:methanol:NH₃, aq. 25% (20:1:0.1) as eluent system. **29** was obtained as light yellow oil (1.34 mmol, 0.73 g, 51%).

¹H NMR (400 MHz, CDCl₃): δ = 7.48 (d, J = 8.7 Hz, 1H), 7.37 – 6.52 (m, 11H), 3.66 – 3.11 (m, 6H), 2.63 (m, 2H), 2.55 – 2.30 (m, 4H), 1.62 – 1.48 (m, 4H), 1.45 – 1.37 (m, 2H), 1.23 – 1.12 (m, 6H) ppm.

^{13}C NMR (101 MHz, CDCl_3): δ = 181.78, 171.26, 169.58, 157.06, 154.87, 145.92, 129.75, 129.71, 127.92, 126.27, 123.37, 123.30, 118.96, 118.92, 118.88, 118.61, 56.98, 54.32, 43.27, 39.83, 31.61, 25.87, 24.27, 13.88 ppm.

ESI: m/z calcd for $\text{C}_{31}\text{H}_{39}\text{N}_5\text{O}_2\text{S}$ $[\text{M}+\text{H}]^+$: 546.28; found: 546.15.

Synthesis of *N*-isopentyl-2,4-dinitroaniline (**34**)



34

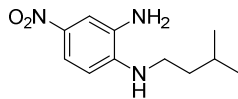
The reaction was carried out according to general procedure II using 1-chloro-2,4-dinitrobenzene **33** (7.40 mmol, 1.50 g), isopentylamine (8.20 mmol, 0.95 mL) and NEt_3 (11.1 mmol, 1.52 mL). **34** was obtained as a yellow solid (7.26 mmol, 1.84 g, 98%).

^1H NMR (CDCl_3 , 400 MHz): δ = 9.11 (d, J = 2.6 Hz, 1H), 8.52 (s, 1H), 8.26 (dd, J = 9.5, 2.6 Hz, 1H), 6.94 – 6.91 (m, 1H), 3.46 – 3.38 (m, 2H), 1.84 – 1.64 (m, 3H), 1.00 (d, J = 6.5 Hz, 6H) ppm.

^{13}C NMR (CDCl_3 , 101 MHz): δ = 148.38, 135.92, 130.34, 130.27, 124.35, 113.90, 41.89, 37.48, 25.96, 22.38 ppm.

ESI: m/z calcd for $\text{C}_{11}\text{H}_{15}\text{N}_3\text{O}_4$ $[\text{M}+\text{H}]^+$: 254.11; found: 254.00.

Synthesis of *N*¹-isopentyl-4-nitrobenzene-1,2-diamine (**35**)



35

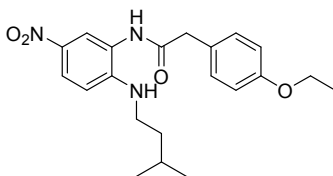
The reaction was carried out according to Freitag *et al.*³ by dissolving dinitro compound **34** (1.97 mmol, 0.50 g) in methanol. The solution was refluxed and a mixture of Na₂S·H₂O (60%) (19.7 mmol, 3.16 g) and NaHCO₃ (19.7 mmol, 1.65 g) in water was added dropwise over a period of 1 h. The reaction was refluxed for further 4 h. After the reaction has cooled down to room temperature, methanol was evaporated and residue was taken up in EtOAc. The organics were extracted with EtOAc (3 times) and the combined organic phase was washed twice with water. The organic phase was dried over Na₂SO₄ and the solvent was removed in vacuo. The crude product was purified by column chromatography using petroleum ether and EtOAc (2:1) as eluent system. **35** was obtained as a red solid (1.38 mmol, 0.31 g, 70%).

¹H NMR (CDCl₃, 400 MHz): δ = 7.84 (dd, *J* = 8.9, 2.2 Hz, 1H), 7.66 (d, *J* = 2.4 Hz, 1H), 6.56 (d, *J* = 8.9 Hz, 1H), 3.23 (t, *J* = 6.4 Hz, 2H), 1.79 – 1.68 (m, 1H), 1.59 (dd, *J* = 14.7, 7.1 Hz, 2H), 0.97 (d, *J* = 6.6 Hz, 6H) ppm.

¹³C NMR (CDCl₃, 101 MHz): δ = 145.09, 138.01, 131.14, 119.76, 112.96, 108.38, 41.94, 38.07, 26.04, 22.53 ppm.

ESI: *m/z* calcd for C₁₁H₁₇N₃O₂ [M+H]⁺: 224.13; found: 224.00.

Synthesis of 2-(4-ethoxyphenyl)-N-(2-(isopentylamino)-5-nitrophenyl)acetamide (36)



36

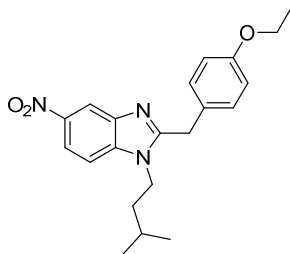
The reaction was carried out according to general procedure I using *o*-phenylene diamine **35** (4.61 mmol, 1.04 g) and 2-(4-ethoxyphenyl)acetic acid (5.07 mmol, 0.91 g). **36** was obtained as brown oil (4.52 mmol, 1.73 g, 98%).

¹H NMR (400 MHz, CDCl₃): δ = 8.03 – 7.91 (m, 2H), 7.28 (d, J = 8.4 Hz, 2H), 6.94 – 6.88 (m, J = 7.5 Hz, 2H), 6.56 (d, J = 9.1 Hz, 1H), 4.02 (dt, J = 11.9, 6.0 Hz, 2H), 3.72 (s, 2H), 3.15 – 3.06 (m, 2H), 1.67 – 1.58 (m, J = 13.3, 6.7 Hz, 1H), 1.45 – 1.38 (m, 5H), 0.93 (d, J = 6.6 Hz, 6H) ppm.

¹³C NMR (101 MHz, CDCl₃): δ = 171.27, 158.68, 148.68, 137.03, 130.39, 126.33, 124.69, 122.72, 121.36, 115.48, 115.34, 63.53, 43.17, 41.73, 38.63, 25.91, 22.46, 14.80 ppm.

ESI: m/z calcd for C₂₁H₂₇N₃O₄ [M+H]⁺: 386.20; found: 386.00.

Synthesis of 2-(4-ethoxybenzyl)-1-isopentyl-5-nitro-1*H*-benzo[*d*]imidazole (37)



37

The reaction was carried out according to general procedure IV using amide **36** (4.52 mmol, 1.73 g). The crude product was purified by column chromatography using petroleum ether and EtOAc (3:1) as eluent system. **37** was obtained as a colorless solid (2.78 mmol, 1.02 g, 62%).

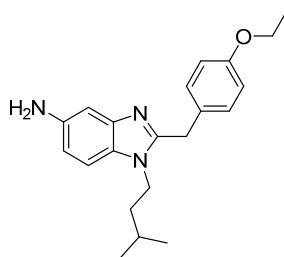
¹H NMR (CDCl₃, 400 MHz): δ = 8.65 (d, J = 2.1 Hz, 1H), 8.18 (dd, J = 8.9, 2.1 Hz, 1H), 7.31 (d, J = 8.9 Hz, 1H), 7.15 (d, J = 8.6 Hz, 2H), 6.87 – 6.80 (m, 2H), 4.29 (s, 2H), 4.09 – 3.94 (m, 4H), 1.65 – 1.51 (m, 1H), 1.45 – 1.33 (m, 5H), 0.91 (d, J = 6.6 Hz, 6H) ppm.

¹³C NMR (CDCl₃, 101 MHz): δ = 158.29, 157.11, 143.57, 141.47, 139.35, 129.57, 126.88, 118.35, 116.02, 115.04, 109.22, 63.53, 43.09, 38.08, 33.80, 26.17, 22.31, 14.77 ppm.

ESI: m/z calcd for C₂₁H₂₅N₃O₃ [M+H]⁺: 368.19; found: 368.10.

HPLC purity: 99% (Retention time: 11.66 min).

Synthesis of 2-(4-ethoxybenzyl)-1-isopentyl-1*H*-benzo[*d*]imidazol-5-amine (**38**)



38

The reaction was carried out according to general procedure III using nitro compound **37** (1.44 mmol, 0.53 g) and SnCl₂·2 H₂O (7.21 mmol, 1.63 g). The crude product was purified by column chromatography using only EtOAc as eluent system. **38** was obtained as a light yellow oil (1.33 mmol, 0.45 g, 93%).

¹H NMR (400 MHz, CDCl₃): δ = 7.01 (d, *J* = 8.5 Hz, 2H), 6.92 (d, *J* = 14.1 Hz, 1H), 6.90 – 6.84 (m, 1H), 6.67 (d, *J* = 8.5 Hz, 2H), 6.53 – 6.47 (m, 1H), 4.02 (s, 2H), 3.86 – 3.75 (m, 2H), 3.75 – 3.65 (m, 4H), 1.44 – 1.32 (m, 1H), 1.21 (t, *J* = 7.0 Hz, 4H), 1.16 – 1.08 (m, 2H), 0.73 (d, *J* = 6.7 Hz, 6H) ppm.

¹³C NMR (101 MHz, CDCl₃): δ = 169.90, 156.80, 151.86, 142.71, 141.18, 128.43, 127.50, 113.66, 111.10, 108.51, 103.35, 62.32, 41.27, 37.02, 32.61, 25.01, 21.30, 13.72 ppm.

ESI: *m/z* calcd for C₂₁H₂₇N₃O [M+H]⁺: 338.22; found: 338.05.

HPLC purity: 98% (Retention time: 7.89 min).

Biological Evaluation

Inhibition of AChE and BChE

AChE (E.C. 3.1.1.7, from electric eel or humans) and BChE (E.C. 3.1.1.8, from equine) were purchased from Sigma-Aldrich. BChE (E.C. 3.1.1.8, from humans) was kindly provided by Oksana Lockridge from the University of Nebraska, Medical Center. DTNB (Ellman's reagent), ATC and BTC iodides were obtained from Fluka Analytical, tacrine hydrochloride was purchased from Sigma-Aldrich.

The stock solutions of the test compounds were prepared in ethanol (33.3 mM) and diluted to the desired concentrations. For the testing 50 μ L DTNB and 50 μ L enzyme were added to 1.5 mL of the buffer. After 50 μ L of the test compound was added, the mixture was incubated for 4.5 min. Afterwards, 10 μ L ATC or BTC were added and the mixture was allowed to incubate for further 2.5 min. Enzyme activity was then observed via UV ($\lambda = 412$ nm).

Radioligand Binding Studies on *hCB₂R* and *hCB₁R*

SR-144,528 (inverse agonist for *hCB₂R*) was bought from Santa Cruz Biotechnology Inc.; unlabeled CP-55,940 (unspecific agonist for *hCB₂R* and *hCB₁R*) was bought from Sigma-Aldrich Life Science; radioactive labeled [³H]CP-55,940 was bought from Hartmann Analytic GmbH; Rimonabant (inverse agonist for *hCB₁R*) was obtained by an in-house synthesis.

Cells were a kindly gift from AbbVie Laboratories (Chicago, U. S. A.). Human embryonic kidney cells (HEK) stably expressing the *hCB₂R* were grown in Dulbecco's modified Eagle's medium containing high glucose supplemented with 8 % fetal calve serum and 25 µg/ml zeocin in a 37 °C incubator in the presence of 5% CO₂. Chinese hamster ovary cells (CHO) stably expressing the *hCB₁R* were grown in Ham's F-12 Nutrient Mix supplemented with 8 fetal calve serum and 400 µg/ml geneticin in a 37 °C incubator in the presence of 5% CO₂. Cells were splitted twice a week.

Cells (either HEK cells stably expressing *hCB₂R* or CHO cells stably expressing *hCB₁R*) were harvested and homogenized in Tris-EDTA buffer (50 mM Tris-HCl pH = 7.4; 1 mM MgCl₂ · 6 H₂O; 1 mM EDTA) using an ultra turax for 2x 15 s bursts. The suspensions were centrifuged for 10 min at 1 408 g at 4 °C. The pellets were discarded and the supernatant was centrifuged at 140 657 g for 50 min at 4 °C. The final membrane pellet was homogenized in binding buffer (50 mM Tris-HCl pH = 7.4; 5 mM MgCl₂ · 6 H₂O; 2.5 mM EDTA), shock frosted with liquid nitrogen and stored at -80°C until use.

Saturation assays were done similar to Murkherjee *et al.*⁴ to determine the K_D-value of the membrane samples. Saturation assays were done with 8 concentrations of [³H]CP-55,940 ranging from 0.088 nM to 4.4 nM. Reactions were started by adding 8 µg membrane per well of a 96 well Multiscreen filter plate (Millipore) containing the radioligand in assay buffer (50 mM Tris-HCl, pH = 7.4; 5 mM MgCl₂ · 6 H₂O; 2.5 mM EDTA; 2 mg/ml BSA). After 3 h incubation at room temperature the reaction was stopped by vacuum filtration and each well

was washed 4 times with cold binding buffer (50 mM Tris-HCl, pH = 7.4; 5 mM MgCl₂ · 6 H₂O; 2.5 mM EDTA). The filter plate was dried at 40 °C. Activity was counted in a Micro Beta Trilux-Counter (Wallac) using IRGA Safe plus-scintillation cocktail (Perkin Elmer). Competition assays were done with 5-11 concentrations of replacing ligands (0.1 nM – 0.4 mM) and 0.44 nM [³H]CP-55,940. Non-specific binding was determined using 10 μM compound **1** for hCB₂R and 10 μM rimonabant for hCB₁R.

To determine the EC₅₀ values, statistical evaluations and sigmoidal dose-response curve fittings were performed with GraphPad Prism 5 software for Windows (Version 5.01, August 7, 2007).

K_i values was determined when displacement of [³H]CP 55,940 was higher than 60% at 100 μM test compound concentration. According to the Cheng-Prusoff equation:

$$K_i = \frac{EC_{50}}{1 + \frac{[L^*]}{K_D}}$$

with [L*] as radioligand concentration (0.44 nM), the K_i value was calculated of at least two individual experiments.

K_D values and standard errors were for hCB₂R K_D(hCB₂R) = 4.31 ± 2.10 and for hCB₁R

K_D(hCB₁R) = 2.24 ± 1.15.

Radioligand Binding Studies on *h*MOP Receptor

Cell Culture:

All experiments were performed with transiently transfected HEK 293-TSA cells (Sigma, Munich, Germany). Cells were cultured in DMEM (Dulbecco's modified Eagle's medium) (PAN Biotech, Aidenbach, Germany), supplemented with 4,5 g/L Glucose, 2 mM L-Glutamin 10% FCS (Biochrome), 100 units/mL penicillin and 0,1 mg/mL streptomycin, at 37 °C, 5% CO₂. To split cells, growth medium was removed by aspiration and cells were washed once with 5 ml of phosphate-buffered saline (Sigma), followed by trypsinization for 1-2 minutes in 1.5 ml of Trypsin 0.05% / EDTA 0.02% (PAN biotech) solution.

Transfection of Cells:

The day before transfection 90% confluent 15 cm cell-culture dishes were split 1:8. On day of transfection the medium was exchanged and 20 mL fresh DMEM was added. Transfections were set up using 10 µg empty Vector (pcDNA 3.0) mixed with 10 µg pcDNA3.0 encoding for the human μ -opioid receptor wildtype in 450 µL milliQ water. Afterwards 50 µL of 2.5 M CaCl₂ solution was added and mixed well. To this Mixture 500 µL of 2x BBS-buffer (pH = 6.95) were added, vortexed and incubated for 20 minutes at 25 °C. Then the mixture was added dropwise on the dishes with fresh medium. Cells were then kept for 48 hours in cell-culture before harvesting.

Membrane Preparation:

Transfected HEK 293-TSA Cells from eight 15 cm dishes were grown until 90% confluence and harvested in buffer solution (5 mM TRIS, 2 mM EDTA, pH = 7.4) using a cell scratcher. Cells were pelleted by 10 minutes centrifugation at 800g. The pellet was resuspended in 15 mL phosphate-buffered saline containing 20 mM HEPES and 10 mM

EDTA at pH 7.4. The following steps were all carried out at 4 °C. The resuspended cells were homogenized with two 15-second bursts of an Ultra-Turrax Homogenizer (TP 18-10, IKA, Staufen, Germany) and afterwards transferred to centrifuge tubes. After 10 minutes centrifugation at 3200 rpm and 4 °C (JA-17 rotor, Beckman Coulter GmbH, Krefeld, Germany) the supernatant was transferred to ultracentrifuge-tubes. Ultracentrifugation was done at 37000 rpm and 4 °C for 40 minutes (70 Ti rotor, Beckman Coulter GmbH, Krefeld, Germany). The pellet was resuspended in buffer (50 mM Tris, 100 mM NaCl, 3 mM MgCl₂, pH = 7.4) and the ultracentrifugation and resuspension steps were repeated once. The resulting suspension was homogenized to ensure homogenous dispersion. The product was transferred in aliquots and frozen using liquid nitrogen. Aliquots were stored at -80°C. Protein concentration was measured using a BCA-kit (Pierce BCA Protein Assay Kit, Life Technologies GmbH, Darmstadt, Germany). Receptor-concentration was measured as B_{max} by [³H]-Diprenorphine saturation-binding.

Heterologous Competition Radio-Ligand Binding:

A mixture of cell-membranes (adjusted protein-amount which represents 15 pM receptor-concentration) and 0.28 nM [³H]-Diprenorphine (3H-DPN, PerkinElmer, Rodgau, Germany) was incubated with varying concentrations of the analyzed compounds in a binding buffer (50 mM Tris, 100 mM NaCl, 3 mM MgCl₂, pH = 7.4). Unspecific binding was determined with 10 µM concentration of naloxone (Tocris Bioscience, Bristol, UK). Binding reactions were incubated for 4 h at 25 °C assuring constant agitation. Free radioligand was separated from bound radioligand by fast filtration and washing with 4 °C binding buffer on a 96-well filtermat (GF/C –Filtermat A, PerkinElmer, Rodgau, Germany) using a 96-well Harvester (MachIII, Tomtec Inc. , Hamden, USA). Radioligand activity was measured by scintillation

counting with aid of a melt-on scintillator (MeltiLex, PerkinElmer, Rodgau, Germany). Competition binding data were fit to a one-site K_i model using GraphPad PRISM 7.0.

Determination of Efficacy

Materials and Methods

Cell culture

U266 MM cell line was purchased from ATCC (LGC Standards, Milan, IT). Cell authentication was performed by IST (Genova, Italy). Cell line was cultured in RPMI1640 medium (Lonza, Milan, IT) supplemented with 10% foetal bovine serum (FBS), 2 mM L-glutamine, 100 IU/ml penicillin, 100 µg/ml ampicillin/streptomycin, 1 mM sodium pyruvate and growth at 37°C with 5% CO₂ and 95% humidity.

Compounds

AM630 and forskolin (Tocris Bioscience, Bristol, UK) were dissolved in DMSO at 25 mM concentration. Test compounds were dissolved at 50 mM concentration in DMSO. All compounds were aliquoted and used one time after defrosting.

MTT assay

U266 cell line (4×10^4 cells/ml) were seeded in 96-well plates, in final volume of 100 µl/well. After one day of incubation, compounds or vehicles were added at different concentration. Six replicates were used for each treatment. At the indicated time point, cell viability was assessed by adding 0.8 mg/ml of 3-[4,5-dimethylthiazol-2-yl]-2,5 diphenyl tetrazolium bromide (MTT) (Sigma Aldrich) to the media. After 3 h, the plates were centrifuged, the supernatant was removed, and the pellet was solubilized with 100 µl/well DMSO. The absorbance of the samples against a background control (medium alone) was measured at 570 nm using an ELISA reader microliter plate (BioTek Instruments, Winooski,

VT, USA). In some experiments, one hour of pre-incubation with forskolin or AM630 was performed. Each sample was evaluated in six wells and in two independent experiments.

cAMP assay

1 x 10⁶/ml U266 cells were plated in 24 wells plate and treated with the appropriate compounds for 2 hours. After treatment, the cells were processed for detection of cAMP levels, using the cAMP assay kit (Enzo Life Sciences, Farmingdale, NY, USA) according to the manufacturer's protocol. The concentration of cAMP was calculated by measuring the absorbance at 450 nm with an ELISA reader. Each compound was evaluated in duplicated and in two independent assay. cAMP levels were represent as pmol/mg of protein.

RNA extraction and RT/PCR

At the appropriate incubation times, total RNA from treated and vehicle U266 cell was extracted using the RNeasy MiniKit (Qiagen), and cDNA was synthesized using the High-Capacity cDNA Archive Kit (Applied Biosystems, Foster City, PA) according to the manufacturer's instructions.

Quantitative real-time polymerase chain reactions (qRT-PCR) for MIF, STAT-3 and GAPDH were performed using the iQ5 Multicolor Real-Time PCR Detection System (Bio-Rad, Hercules, CA). PCR reaction was performed with SYBRGreen qPCR mastermix (Qiagen) using 500 ng of cDNA for reaction, following the amplification protocol indicated by the manufacture's instruction. All samples were assayed in triplicates in the same plate and GAPDH levels were used to normalize mRNA contents, and target gene levels were calculated by the $2^{-\Delta\Delta C_t}$ method. cDNA from forskolin-treated cells was used as CREB-induced MIF and STAT-3 positive control. cDNA from cells treated with test compound A were used for CB₂ agonist MIF and STAT-3 gene expression control. cDNA from AM630-

treated cells was used for antagonist/inverse agonist CB₂ MIF and STAT-3 expression control. Each sample was evaluated in triplicate and in three different experiments.

Statistical analysis

The statistical significance for MTT and RT/PCR assay was determined by analysis of variance (ANOVA). The calculation of IC₅₀ was performed by non-lin fit of log-dose vs response, using Prism 5.01 (Graph Pad) software. cAMP concentration was calculated utilizing a 4 parameter logistic (4PL) curve fitting program.

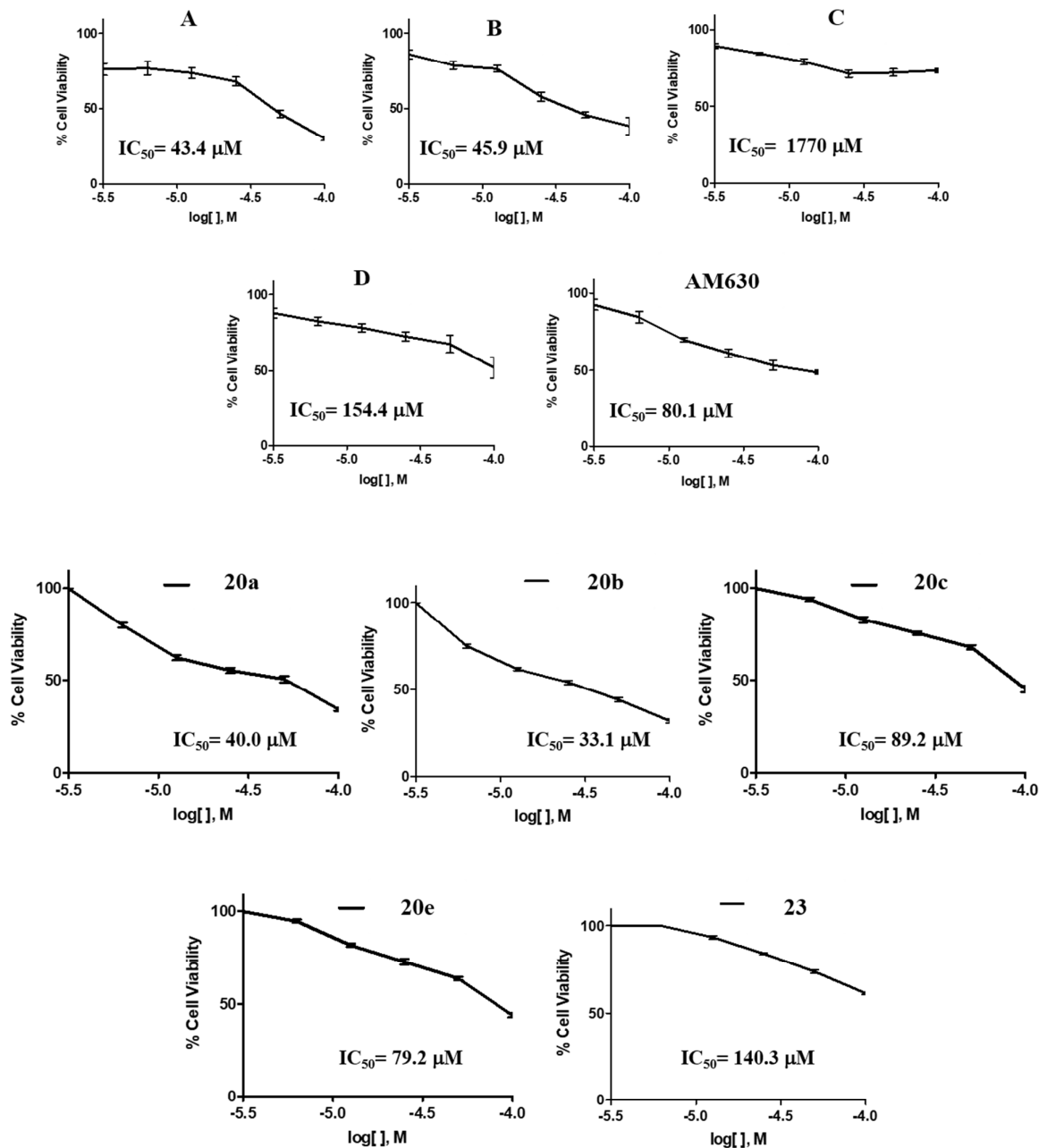


Figure S1. Test compounds (A-D, 20a-c, 20e and 23) effect on U266 cell viability. U266 cells were treated with different doses of test compounds or AM630 (from 0 to 100 μM) and cell viability was evaluated at 72 h post-treatments, by MTT assay. Data shown are expressed as mean ± S.D. of three independent experiments. IC₅₀ of test compounds and AM630 are indicated. Each compound was tested in six wells/experiments.

Sample	cAMP (pmol/mg) ± S.D.
VEHICLE	16,2 ± 0.15
FORSKOLIN	67.4 ± 3.4*
AM630	22.3 ± 1.8*
A	8.6 ± 0.4*
B	10.4 ± 0.8*
C	12.6 ± 0.6*
D	10.2 ± 1.0*
AM630 + A	9.6 ± 0.5*#
AM630 + B	12.4 ± 0.9*#
AM630 + C	16.3 ± 0.8*#
AM630 + D	15.3 ± 1.1*#

Figure S2. The effect of test compounds on AM630-induced stimulation of cAMP production in U266 cells. 4 x 10⁴ U266 cells were plated in 24 well plates and treated for 24 hours with the appropriate compound. In combination treatments, U266 cells were pre-incubated with 25 μM AM630 for 30 minutes before adding test compounds. U266 cell lines were treated with forskolin (10 μM), AM630 (25 μM), test compounds (50 μM). cAMP concentration was represented as picograms for mg of protein (pg/mg). * indicate any values that are significantly different from vehicle treated cells (**P < 0.01), #° indicate any values that are significantly different from AM630 treated cells (**P < 0.01). Values represent the mean ± S.D. (n= 4) calculated from two wells/treatment and in two independent experiments.

in vivo Studies

Aim of the study

To test 3 compounds **A**, **B** and **20a** as protectant drugs in the *in vivo* mouse model of Alzheimer's disease induced by *intracerebroventricular* (i.c.v.) injection of oligomerized A β ₂₅₋₃₅ peptide.

Each compound was injected *intraperitoneally* (i.p.) o.d. between day 1 and 7, as summarized in Figure 12 (see manuscript). The peptide was injected on day 1 and behavioural examination performed between day 8 and 10. All animals were then sacrificed on day 11 and their brain stored at -80°C awaiting further biochemical analyses.

Methods

Animals

Male Swiss mice, 6 weeks old and weighing 30-35 g, from JANVIER (Saint Berthevin, France), were kept for housing and experiments took place within the animal facility building of the University of Montpellier (CECEMA, Office of Veterinary Services agreement # B-34-172-23). Animals were housed in groups with access to food and water ad libitum, except during behavioral experiments. They were kept in a temperature and humidity controlled animal facility on a 12 h/12 h light/dark cycle (lights off at 07:00 pm). All animal procedures were conducted in strict adherence to the European Union directive of September 22, 2010 (2010/63/UE).

Drugs preparation

Compounds were weighed, solubilized in pure DMSO and a stock solution at 1 mg/ml was prepared in DMSO/saline or DMSO/Tween-80/saline. The percentage of DMSO in saline were 20% for compound **A**, 60% for compound **B** and 20% for compound **20a** after a

presolubilization in Tween-80 (10% final; Sigma-Aldrich). The stock solution, corresponding to a dose of 5 mg/ml if injected, could be kept at +4°C for a couple of days and dilutions (0.6 x, 0.2 x, 0.06 x) were prepared from it. Vehicle solutions used for control groups were DMSO 20% in saline for compounds **A** and **B** and DMSO 20%, Tween-80 3% in saline for compound **20a**.

Amyloid peptides preparation and injection

Mice were anesthetized with isoflurane 2.5% and were injected i.c.v. with A β ₂₅₋₃₅ peptide (9 nmol/mouse) or Sc.A β peptide (9 nmol/mouse), in a final volume of 3 μ l/mouse, according to the previously described method.⁵⁻¹⁰ Homogeneous oligomeric preparation of A β ₂₅₋₃₅ peptide was performed by incubation 4 days at 37 °C according to Maurice *et al.*⁵ The Sc.A β peptide solution was also incubated but does not oligomerize.⁵⁻¹¹

Spontaneous alternation performances

On day 8, all animals were tested for spontaneous alternation performance in the Y-maze, an index of spatial working memory. The Y-maze is made of grey polyvinylchloride. Each arm is 40 cm long, 13 cm high, 3 cm wide at the bottom, 10 cm wide at the top, and converging at an equal angle. Each mouse will be placed at the end of one arm and allowed to move freely through the maze during an 8 min session. The series of arm entries, including possible returns into the same arm, was checked visually. An alternation was defined as entries into all three arms on consecutive occasions. The number of maximum alternations is therefore the total number of arm entries minus two and the percentage of alternation was calculated as (actual alternations / maximum alternations) x 100. Parameters included the percentage of alternation (memory index) and total number of arm entries (exploration index).^{5-7, 9, 10} Animals that shown an extreme behavior (Alternation percentage < 20% or >

90% or number of arm entries < 10 were discarded from the calculation. In this study, no animal was discarded accordingly (0% attrition).

Passive avoidance test

On days 9 and 10, a passive avoidance test was performed. The apparatus is a two-compartment (15 x 20 x 15 cm high) box with one compartment illuminated with white polyvinylchloride walls and the other darkened with black polyvinylchloride walls and a grid floor. A guillotine door separates each compartment. A 60 W lamp positioned 40 cm above the apparatus lights up the white compartment during the experiment. Scrambled foot shocks (0.3 mA for 3 s) were delivered to the grid floor using a shock generator scrambler (Lafayette Instruments, Lafayette, USA). The guillotine door was initially closed during the training session. During the training session, on day 9, each mouse was placed into the white compartment. After 5 s, the door was raised. When the mouse entered the darkened compartment and placed all its paws on the grid floor, the door was closed and the foot shock delivered for 3 s. The step-through latency, that is, the latency spent to enter the darkened compartment, and the number of vocalizations was recorded. The retention test was carried out 24 h after training, on day 10. Each mouse was placed again into the white compartment. After 5 s, the door was raised. The step-through and escape latencies (corresponding to the re-exit from the darkened compartment) were recorded up to 300 s. Animals that show all latencies during the training and retention session lower than 10 s are considered as failing to respond to the procedure and were discarded from the calculations. In this study, no animal was discarded accordingly.

Sacrifice and Brain sampling

On day 11, all animals were sacrificed, their brains dissected out to isolate the hippocampus and cortex. Samples were frozen in liquid nitrogen and stored at -80°C awaiting further analysis.

Statistical analyses

All values, except passive avoidance latencies, were expressed as mean \pm S.E.M. Statistical analyses were performed on the different conditions using one-way ANOVA (F value), followed by the Dunnett's post-hoc multiple comparison test. Passive avoidance latencies do not follow a Gaussian distribution, since upper cut-off times are set. They were therefore analyzed using a Kruskal-Wallis non-parametric ANOVA (H value), followed by a Dunn's multiple comparison test. $p < 0.05$ was considered as statistically significant.

References

[1] Gottlieb, H. E.; Kotlyar, V.; Nudelman, A. NMR Chemical Shifts of Common Laboratory Solvents as Trace Impurities. *J. Org. Chem.* **1997**, *62*, 7512 – 7515.

[2] Munch, H.; Hansen, J. S.; Pittelkow, M.; Christensen, J. B.; Boas, U. A. A new efficient synthesis of isothiocyanates from amines using di-*tert*-butyl dicarbonate. *Tetrahedron Lett.* **2008**, *49*, 3117 – 3119.

[3] Freitag, M.; Schemies, J.; Larsen, T.; El Gaghlab, K.; Schulz, F.; Rumpf, T.; Jung, M.; Link, A. Synthesis and biological activity of splitomicin analogs targeted at human NAD⁺-dependent histone deacetylases (sirtuins). *Bioorg. Med. Chem.* **2011**, *19*, 3669 – 3677.

[4] Murkherjee, S.; Adams, M.; Whiteaker, K.; Daza, A.; Kage, K.; Cassar, S.; Meyer, M.; Yao, B. B. Species comparison and pharmacological characterization of rat and human CB₂ cannabinoid receptors. *Eur. J. Pharmacol.* **2004**, *505*, 1 – 9.

[5] Maurice, T.; Lockhart, B. P.; Privat, A. Amnesia induced in mice by centrally administered β -amyloid peptides involves cholinergic dysfunction. *Brain Res.* **1996**, *706*, 181 – 193.

[6] Maurice, T.; Su, T. P.; Privat, A. Sigma₁ (σ_1) receptor agonists and neurosteroids attenuate β_{25-35} -amyloid peptide-induced amnesia in mice through a common mechanism. *Neuroscience* **1998**, *83*, 413 – 428.

[7] Meunier, J.; Ieni, J.; Maurice, T. The anti-amnesic and neuroprotective effects of donepezil against amyloid β_{25-35} peptide-induced toxicity in mice involve an interaction with the σ_1 receptor. *Br. J. Pharmacol.* **2006**, *149*, 998 – 1012.

[8] Meunier, J.; Villard, V.; Givalois, L.; Maurice, T. The γ -secretase inhibitor 2-[(1R)-1-[(4-chlorophenyl)sulfonyl](2,5-difluorophenyl)amino]ethyl-5-fluorobenzenebutanoic acid

(BMS-299897) alleviates A β ₁₋₄₂ seeding and short-term memory deficits in the A β ₂₅₋₃₅ mouse model of Alzheimer's disease. *Eur. J. Pharmacol.* **2013**, *698*, 193 – 199.

[9] Villard, V.; Espallergues, J.; Keller, E.; Alkam, T.; Nitta, A.; Yamada, K.; Nabeshima, T.; Vamvakides, A.; Maurice, T. Anti-amnesic and neuroprotective effects of the aminotetrahydrofuran derivative ANAVEX1-41 against amyloid beta(25-35)-induced toxicity in mice. *Neuropsychopharmacology* **2009**, *34*, 1552 – 1566.

[10] Villard, V.; Espallergues, J.; Keller, E.; Vamvakides, A.; Maurice, T. Anti-amnesic and neuroprotective potentials of the mixed muscarinic receptor/sigma₁ (σ_1) ligand ANAVEX2-73, a novel aminotetrahydrofuran derivative. *J. Psychopharmacol.* **2011**, *25*, 1101 – 1117.

[11] Zussy, C.; Brureau, A.; Delair, B.; Marchal, S.; Keller, E.; Ixart, G.; Naert, G.; Meunier, J.; Chevallier, N.; Maurice, T.; Givalois, L. Time-course and regional analyses of the physiopathological changes induced after cerebral injection of an amyloid- β fragment in rats. *Am. J. Pathol.* **2011**, *179*, 315 – 334.

Appendix IV

Dolles, D.; Strasser, A.; Wittmann, H.-J.; Marinelli, O.; Nabissi, M.; Pertwee, R. G.; Decker, M. The First Photochromic Affinity Switch for the Human Cannabinoid Receptor 2. *Adv. Therap.* **2018**, DOI: 10.1002/adtp.201700032.

Copyright (2018) Wiley-VCH Verlag GmbH & Co. KGaA, Weinheim. Reproduced with permission.

<http://onlinelibrary.wiley.com/doi/10.1002/adtp.201700032/abstract>

The First Photochromic Affinity Switch for the Human Cannabinoid Receptor 2

Dominik Dolles, Andrea Strasser, Hans-Joachim Wittmann, Oliviero Marinelli, Massimo Nabissi, Roger G. Pertwee, and Michael Decker*

The *hCB₂R* plays an important role in the immune system and is centrally expressed in microglia. The *hCB₂R* activated by agonists hold great therapeutic potential, e.g., in neuroinflammation. It is currently not yet elucidated how pathophysiological processes are mediated by the *hCB₂R*. Here, photochromic affinity switches based on a drugable benzimidazole core through azologization and computational studies are developed. Structure-activity relationships (SARs) lead to compounds with high selectivity over *hCB₁R* that can be reversibly switched to a higher affinity *cis*-form proved on the receptor level by radioligand binding studies and translating into an affinity change in a functional GTP γ S assay. cAMP ELISA and the change in expression level of two genes regulated by CREB proves that the compounds act as partial agonists.

agonist SR141716A (rimonabant) had been approved as a drug for obesity in European countries, albeit its putative risk of psychiatric problems led to its suspension from the market in 2008. Far less is known about the *hCB₂R* and its role in the healthy, but especially in the diseased human body. It was first recognized as the “peripheral” CBR,^[2] since *hCB₂R*s are localized in the immune system and modulate immune cell migration and cytokine release.^[3] More recently, it was shown that the *hCB₂R* is located in the central nervous system also, mainly expressed in microglial cells.

Pronounced overexpression of *CB₂R* and fatty acid amide hydrolase is observed in

neuroinflammatory processes in the brain and specifically in microglia cells that surround β -amyloid plaques.^[4] The expression level correlates well with $A\beta_{42}$ -level and plaque formation, although not directly with cognitive status, indicating that pathogenic processes lead to *hCB₂R* overexpression.^[5] Due to the expression of *hCB₂R* in activated microglia and the possibility of reduction of cell activation by *hCB₂R* agonists, therapeutic application of such compounds is promising. It was shown in several in vitro-assays that *hCB₂R* agonists and partial agonists reduce both the number of activated microglia cells surrounding $A\beta$ plaques and the level of pro-inflammatory cytokines. It is currently not yet elucidated how exactly these effects are mediated by the *hCB₂R*, in which sequence (patho)physiologic activation takes place and which time-scale is underlying these processes.^[6]

Both *hCBR* subtypes are activated to the same extent by endocannabinoids and classical phytocannabinoids like Δ^9 -THC,^[7] which also activates GPR18, GPR55, peroxisome proliferator-activated receptor gamma nuclear receptor, and Transient Receptor Potential Ankyrin 1 (TRPA1) and Transient Receptor Potential Vannilloid-type 2 (TRPV2) cation channels at $>1 \mu\text{M}$.^[8]

In the last years “photopharmacology” has rapidly emerged and found remarkable application for the control of biological functions by light with the unprecedented spatio-temporal solution that was made possible by chemical photoswitches that are incorporated into biologically active molecules. The underlying principle is the fast and reversible change of their chemical structure to yield photoisomers with a structural and polarity change that can exhibit different binding to a biological target.^[9–11] Azobenzenes and diarylethenes are currently the most widely applied and the most versatile templates, with regard to chemical and photochemical stability, stability in biological media, the “orthogonality” or lack of interference with

1. Introduction

Human cannabinoid receptors (*hCBRs*) consist of two subtypes of G-protein coupled receptors (GPCRs), *hCB₁R*, and *hCB₂R*. *CB₁R*s are found in the central nervous system.^[1] The identification of (-)-trans- Δ^9 -tetrahydrocannabinol (Δ^9 -THC) as a phytocannabinoid initiated drug development efforts targeting the endocannabinoid system. As a result, the *hCB₁R*-selective inverse

D. Dolles, Prof. M. Decker
Pharmaceutical and Medicinal Chemistry
Institute of Pharmacy and Food Chemistry
Julius Maximilian University of Würzburg
Würzburg, Germany
E-mail: Michael.Decker@uni-wuerzburg.de

Dr. A. Strasser, Dr. H.-J. Wittmann
Pharmaceutical and Medicinal Chemistry II
Institute of Pharmacy
University of Regensburg
Regensburg, Germany

O. Marinelli, Dr. M. Nabissi
School of Pharmacy
Department of Experimental Medicine
University of Camerino
Camerino, Italy

Prof. R. G. Pertwee
School of Medicine, Medical Sciences and Nutrition
Institute of Medical Sciences
University of Aberdeen
Aberdeen, Scotland, UK

 The ORCID identification number(s) for the author(s) of this article can be found under <https://doi.org/10.1002/adtp.201700032>

DOI: 10.1002/adtp.201700032

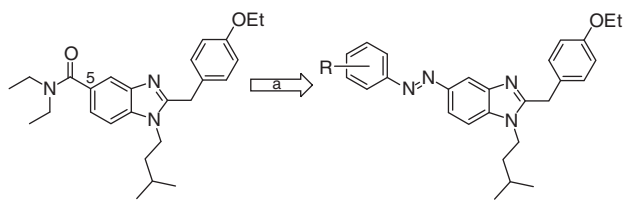


Figure 1. Azologization approach to obtain 5-substituted benzimidazole azobenzenes.

the assay readout of the biological system, and especially their medicinal chemical compatibility for small and biologically active molecules.^[9–13] Remarkably and surprisingly, GPCRs, next to enzymes the most important drug targets, have only been addressed very recently with photoswitchable tool compounds. Targets have been the metabotropic glutamate receptors,^[14,15] the class B glucagon-like peptide-1 receptor,^[16,17] the adenosine, the dopamine and μ -opioid receptor,^[18–20] and the muscarinic acetylcholine receptor.^[9] At the same time of the preparation of this manuscript, Westphal et al. described photoswitchable THC-derivatives, two of which act as CB₁R agonists, as shown by coupling with an inwardly-rectifying potassium channel and forskolin-stimulated cAMP production.^[21] Both ligands act in the nanomolar range and one influences efficacy as well as affinity.

Herein, we describe the design of benzimidazole-based photo-switches by “azologization” that change specifically affinity at the hCB₂R upon irradiation.^[13,22] We describe their synthesis, photochemical characterization, radioligand binding studies, GTPyS data with regard to affinity and efficacy, and computational studies. In contrast to the above work describing THC-derivatives, our compounds (a) are highly selective for the hCB₂R over the hCB₁R, (b) show higher affinity when “switched on” (to the *cis*-form), which is of considerable importance when using such GPCR ligands as molecular tool compounds for investigating receptor-activation kinetics,^[9] and (c) lack a concomitant change in efficacy. Therefore a single pharmacological compound property (here affinity over efficacy) can be investigated at a given time.

2. Chemistry

Based on our work on hCB₂R ligands^[24] and on structure-activity relationship (SAR) results obtained by AstraZeneca,^[25] we investigated a reasonable position, where a (substituted) azobenzene could be introduced. In the manner described by Trauner and colleagues,^[12] the azologization approach was applied and as suggested by computational studies the diethylamide side chain at position 5 was replaced by an azobenzene with different substitution patterns (**Figure 1**).

For the introduction of the (substituted) azobenzenes at position 5 of the benzimidazole core, synthesis started from commercially available 1-chloro-2,4-dinitrobenzene **1** (**Scheme 1**). In the first step, a nucleophilic aromatic substitution with isopentylamine was performed to obtain **2** in quantitative yields. Selective one-sided reduction of the 2-nitro moiety to obtain N¹-isopentyl-4-nitrobenzene-1,2-diamine **3** was carried out according to Freitag et al.^[26] using sodium sulfide as reducing agent. *o*-Phenylene diamine **3** was then reacted with 2-(4-ethoxyphenyl)acetic acid us-

ing HBTU. For cyclization, amide **4** was refluxed in glacial acetic acid and 5-nitro benzimidazole **5** was obtained. The nitro moiety was then reduced by using tin(II) to yield 5-amino benzimidazole **6**. For the azo-coupling, the respective (substituted) anilines **7a–i** were first partially oxidized to the nitroso moiety **8a–i** using oxone^[19] and then coupled with the 5-amino benzimidazole **6** in a Mills reaction under acidic conditions. The resulting (substituted) 5-azobenzene benzimidazoles **9a–i** were obtained in moderate to good yields.

3. Photophysical Properties

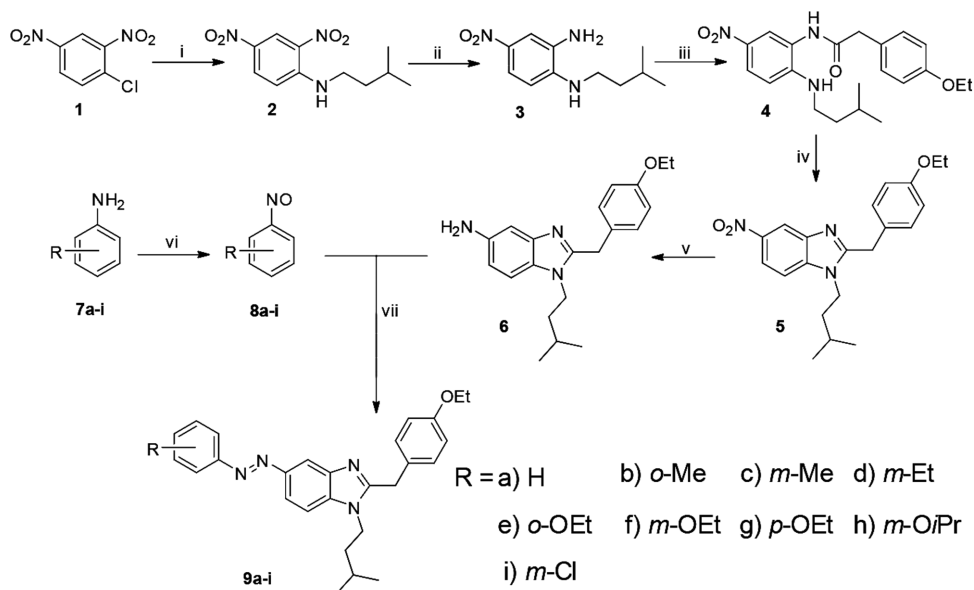
Photochromic behavior of compounds **9a–i** was investigated by UV-spectroscopy using a 50 μ M solution in ethanol. All compounds measured show a clear photochromic behavior with π – π^* and n – π^* transitions at absorption maxima of around 325 nm and 430 nm, respectively. All compounds can be stably switched from the *trans*-state to the *cis*-state by using UV light ($\lambda = 366$ nm) and vice versa by day light. This process can be repeated for many cycles. All compounds show long thermal stability at room temperature (>3 h) (**Figure 2**). In addition, *trans:cis* ratios were also quantified for all compounds by HPLC (cf. Supporting Information Table S1). Under daylight all compounds remain to $\approx 85\%$ in the *trans*-form. Using UV ($\lambda = 366$ nm) all compounds can almost quantitatively be switched to the *cis*-forms.

4. Pharmacological Evaluation and Computational Studies

All target compounds were tested for their affinity to both hCB₁R and hCB₂R in radioligand binding studies. The aim was not to obtain compounds with high affinity towards hCB₂R with selectivity over the hCB₁R, but also to effectively increase this affinity upon irradiation with UV-light (“switching-on”).

All compounds tested show high affinity towards hCB₂R in the two-digit or low three-digit nanomolar range. The *cis*-isomers show increased affinity compared to the *trans*-isomer. The most pronounced effect was obtained by the introduction of a substituent and altering its position. The unsubstituted **9a-trans** shows high affinity towards hCB₂R and selectivity over hCB₁R. After irradiation, affinity of **9a-cis** towards hCB₂R does not change significantly ($K_i(hCB_2R) = 28.9$ nM), but selectivity is greatly decreased (hCB₁R displ. of radioligand at 10 μ M = 84%). The two ortho-substituted compounds **9b-trans** and **9e-trans** show high affinity towards hCB₂R, but only show a slight affinity change when irradiated with UV-light. *para*-Substitution does not only decrease affinity towards hCB₂R, but affects affinity (**9g-trans**: $K_i(hCB_2R) = 152.4$ nM and **9g-cis**: $K_i(hCB_2R) = 129.5$ nM). The best results regarding affinity switch are obtained by *meta*-substitution (**Figure 6A**): **9c-trans** and **9f-trans** show three-digit nanomolar affinity towards hCB₂R, and affinity is strongly increased upon irradiation (**Table 1**).

Lastly, we introduced larger substituents to see, if steric hindrance further enhance affinity switch. *Meta*-substitution with ethyl (**9d**), isopropyl (**9h**), or chlorine (**9i**) still provide compounds with high affinity towards hCB₂R, but no significant change in affinity is observed.



Scheme 1. Synthesis of 5-azobenzene benzimidazoles: i) isopentylamine, NEt₃, EtOH, rt, 24 h; ii) Na₂S · H₂O, NaHCO₃, MeOH/H₂O, reflux, 4 h; iii) 2-(4-ethoxyphenyl)acetic, HBTU, NEt₃, DMF, rt, 12 h; iv) glacial acetic acid, reflux, 6 h; v) SnCl₂ · 2 H₂O, EtOH, reflux, 6 h; vi) oxone, CH₂Cl₂/H₂O, rt, 4 h; vii) acetic acid, CH₂Cl₂, rt, 24 h.

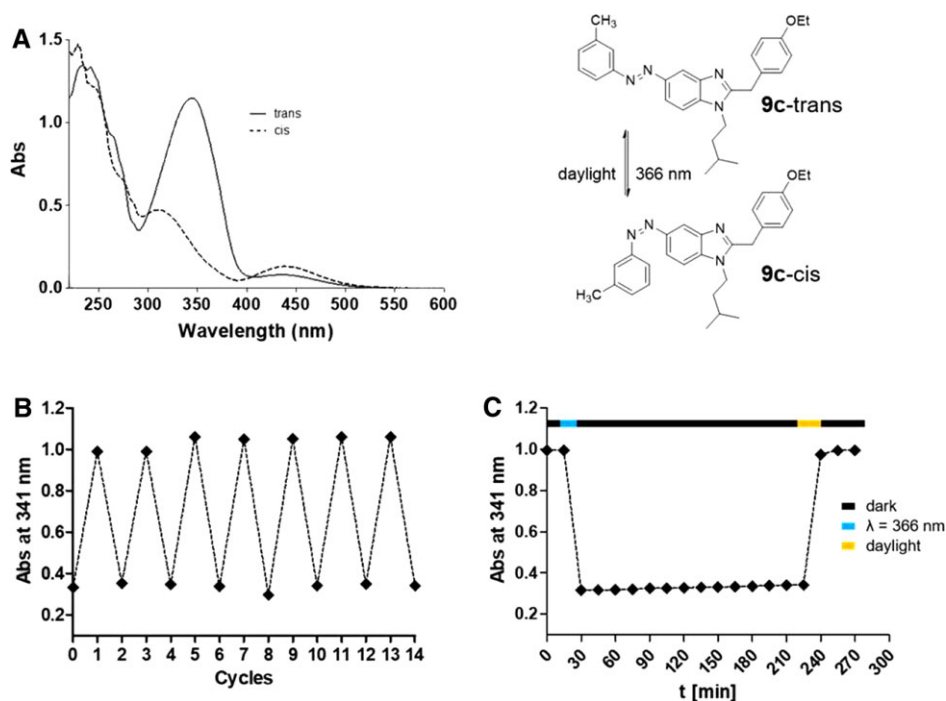


Figure 2. A) UV spectrum of **9c** (*trans*: solid line; *cis*: dotted line), B) switching cycles of **9c**, C) thermal stability at room temperature of **9c** over a period of >3 h.

Compounds **9c-trans** and **9c-cis** were docked in two different orientations into the homology model of the hCB₂R. Within mode I, the ethoxyphenyl moiety of both compounds was docked into the orthosteric binding site mainly formed by the amino acids Val^{3.32}, Thr^{3.33}, Phe^{3.36}, Phe183 (E2-loop), Leu^{5.40}, Trp^{5.43}, Leu^{5.44}, Trp^{6.48}, Val^{6.51}, Met^{6.55}, and Leu^{7.41}. For this mode (data not shown), the experimentally determined affinities at the hCB₂R in dependence of the substitution pattern at the azoben-

zene moiety could not be explained. For mode II, both compounds were docked with the (substituted) azobenzene moiety in the orthosteric binding pocket. Data suggest that the *m*-CH₃ azobenzene moiety of **9c-trans** is located in an aromatic side pocket formed by the amino acids Phe^{3.36}, Trp^{5.43}, and Trp^{6.48}, while the *m*-CH₃ azobenzene moiety of **9c-cis** is embedded in an aromatic side pocket, mainly formed by the amino acids Phe183 (E2-loop), Tyr^{5.39}, and Trp^{5.43} (Figure 3).

Table 1. Results of radioligand binding studies at *hCB₁R* and *hCB₂R*.

Compound	<i>hCB₂R</i> <i>K_i</i> (pIC ₅₀ ± SD) or [³ H]CP55,950 displ. at 10 μM	<i>hCB₁R</i> <i>K_i</i> (pIC ₅₀ ± SD) or [³ H]CP55,950 displ. at 10 μM
CP55,940	28.1 nM (7.5 ± 0.1)	20.2 nM (7.7 ± 0.1)
Rimonabant	4.0%	143.0 nM (6.8 ± 0.1)
9a-trans	39.7 nM (7.4 ± 0.1)	48%
9a-cis	28.9 nM (7.5 ± 0.1)	84%
9b-trans	41.8 nM (7.4 ± 0.2)	62%
9b-cis	16.3 nM (7.8 ± 0.2)	69%
9c-trans	147.6 nM (6.8 ± 0.1)	59%
9c-cis	17.7 nM (7.8 ± 0.1)	73%
9d-trans	122.8 nM (6.9 ± 0.1)	54%
9d-cis	32.4 nM (7.5 ± 0.1)	67%
9e-trans	41.5 nM (7.4 ± 0.1)	73%
9e-cis	25.7 nM (7.6 ± 0.2)	88%
9f-trans	194.5 nM (6.7 ± 0.1)	47%
9f-cis	35.5 nM (7.4 ± 0.1)	55%
9g-trans	152.4 nM (6.8 ± 0.1)	57%
9g-cis	129.5 nM (6.9 ± 0.2)	74%
9h-trans	392.5 nM (6.4 ± 0.1)	50%
9h-cis	82.6 nM (7.1 ± 0.1)	50%
9i-trans	88.9 nM (7.1 ± 0.1)	51%
9i-cis	41.8 nM (7.4 ± 0.2)	65%

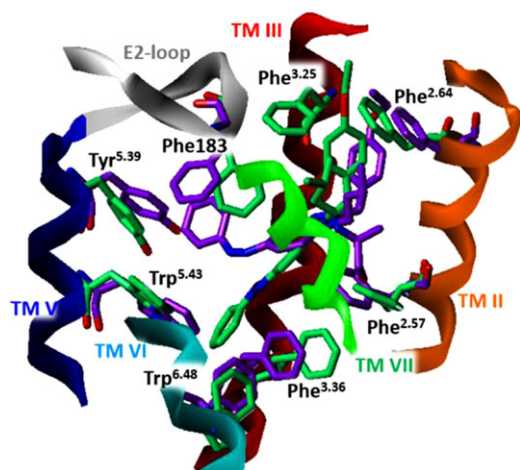


Figure 3. Overlay of the binding mode of **9c-trans** (green carbon atoms) and **9c-cis** (violet carbon atoms) in binding pocket of the *hCB₂R*, obtained by docking studies (For reasons of clarity only the core of **9** is shown).

For **9c-trans**, a slight steric clash of the *m*-CH₃ with Thr^{3.37} is observed (Figure 4), which explains its reduced affinity. In contrast, the *m*-CH₃ of **9c-cis** fits well into a small cavity, which is not occupied of **9a-cis**, which explains the slightly increased affinity of **9c-cis** compared to **9a-cis**. The same is true for other small side chains in the *m*-position, e.g. for **9d** and **9f**. The ethoxy moiety at *o*-position of **9e-trans** and **9e-cis** is well tolerated, because there is a small gap in the binding site, where the ethoxy moiety is able to bind (Figure 4). In contrast, a substituent in *p*-position is neither tolerated for the *trans* nor for the *cis* configuration, because, as

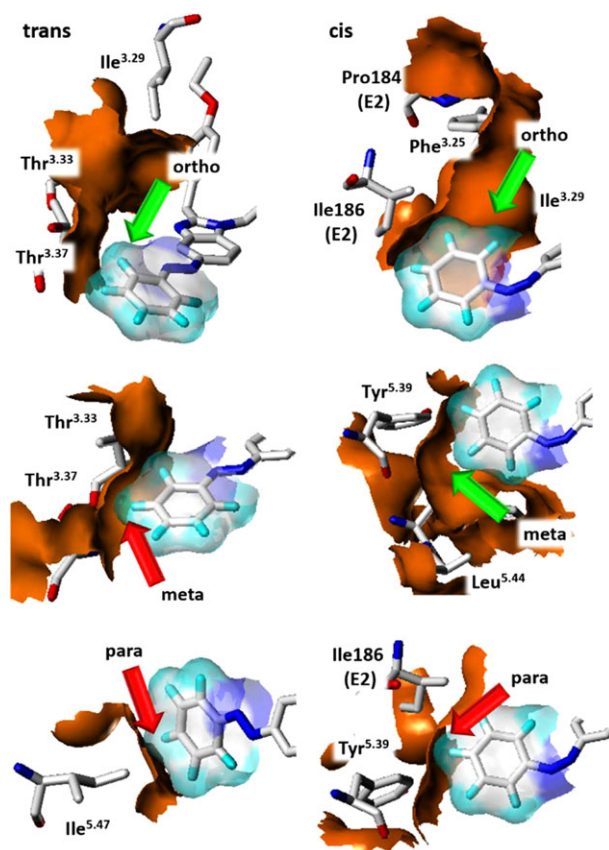


Figure 4. **9a-trans** (left) and **9a-cis** (right), docked into the binding pocket of the *hCB₂R*. Shown is the presence (green arrows) or absence (red arrows) of additional gaps for small substituents at the azobenzene moiety in *o*-, *m*-, and *p*-position.

shown for **9a**, there is no vacant gap in the binding pocket (Figure 4), which is in well accordance to the experimentally determined affinities (Table 1). Summarizing up, the present docking study shows well that in contrast to the *o*- and *p*-substitution, only small substituents in *m*-position lead to an affinity switch between described *trans*- and *cis*-configured azobenzene derivatives.

To investigate efficacy, representative unsubstituted compound **9a** (with no significant change in affinity upon irradiation) was checked in a cAMP ELISA assay and via changes in the expression level of two genes, which are regulated by the transcription factor cAMP response-element binding protein (CREB) binding to upstream cAMP response elements (CRE).^[27] Macrophage Migration Inhibitory Factor (MIF) and Signal Transducer and Activator of Transcription (STAT-3) were selected as genes, both are highly expressed in multiple myeloma cells under CREB promoter control. As shown in Figure 5, the compound behaves as a partial agonist antagonizing the effect of the standard CBR antagonist AM630. Partial agonism should antagonize the effect of a potent agonist like CP55,940 as measured in GTPγS studies.

Compound **9c** with the largest (i.e., eight- to ninefold, Figure 6A) difference in affinity upon irradiation and good selectivity over *hCB₁R* was subsequently investigated in GTPγS studies to check whether an affinity change is also reflected in an assay

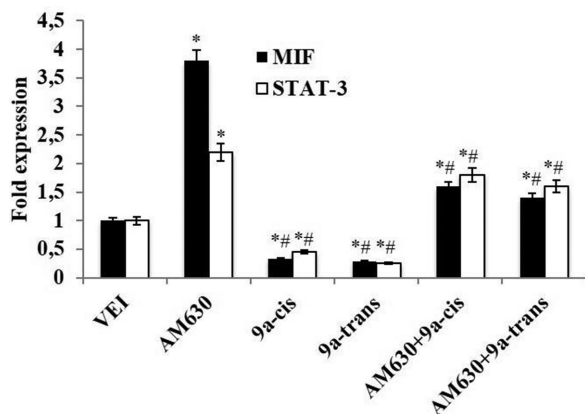


Figure 5. Compounds **9a-trans** and **9a-cis** reduce MIF and STAT-3 gene expression. U266 cells were treated with **9a-cis** or **9a-trans** (50 μ M), AM630 (25 μ M) for 2 h. In combination experiment (AM630 plus **9a-trans** or **9a-cis**), U266 cells were pre-incubated with AM630 for 30 min before adding **9a-trans** or **9a-cis**. MIF and STAT-3 mRNA levels were determined by qRT-PCR. GAPDH was used for normalization. Data are expressed as relative fold with respect to vehicle treated cells used as control. Data are expressed as mean \pm SD. * p < 0.01 versus untreated; # versus AM630.

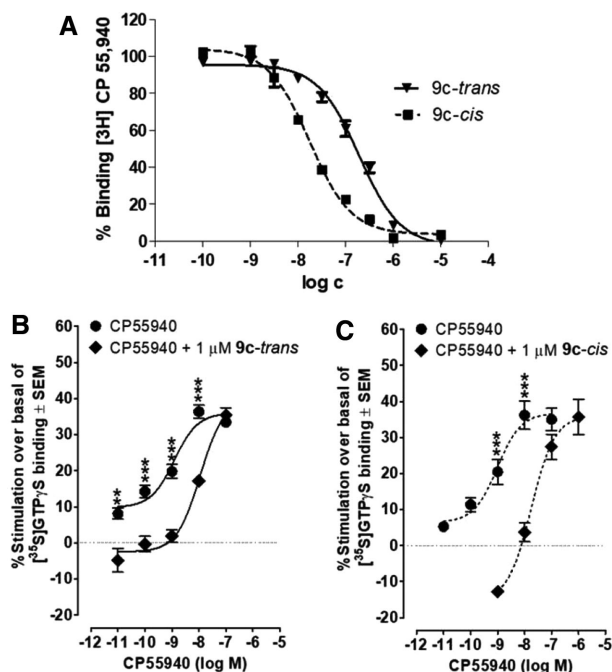


Figure 6. A) Radioligand binding data of **9c-trans** and **9c-cis**, B) GTP γ S results for CP55,940 and CP55,940 + 1 μ M **9c-trans**, C) GTP γ S results for CP55,940 and CP55,940 + 1 μ M **9c-cis**. Symbols represent mean values \pm SEM (n = 6). Mean EC₅₀, E_{min}, and E_{max} values for CP-55,940 determined in the presence or absence of **9c-trans** or **9c-cis**, together with the 95% confidence limits of these values, are listed in Table 2 of supporting information. The asterisks indicate that the mean response to a particular concentration of CP-55 940 in the presence of **9c-trans** or **9c-cis** is significantly different from the mean response to the same concentration of CP-55 940 in the absence of **9c-trans** or **9c-cis**, displayed in the same Figure (6B or 6C; ** p < 0.01; *** p < 0.001; Student's unpaired t -test).

which uses different experimental conditions and reflects intracellular signaling. As in the reporter gene assay for cAMP, no change in efficacy was observed upon irradiation (data not shown). Indeed, at a concentration of 1 μ M of **9c**, a twofold rightshift of the curve of the standard *h*CB₂R agonist CP55,940 can be observed (Figure 6B, C; for experimental details and data cf. Supporting Information), proving affinity switching behavior in a functional assay also.

Taken together, SARs led to the first nanomolar *h*CB₂R-selective affinity switch, with activation upon irradiation and no concomitant switch in efficacy, which might help to elucidate the yet unknown role of this GPCR, e.g., in neurodegenerative disorders.

5. Experimental Section

For experimental details: see Supporting Information.

Supporting Information

Supporting Information is available from the Wiley Online Library or from the author.

Acknowledgments

M.D. gratefully acknowledges financial support by the International Doctoral Program "Receptor Dynamics" funded within the framework of the Elite Network of Bavaria (ENB).

Conflict of Interest

The authors declare no conflict of interest.

Keywords

azobenzene, benzimidazole, CB₂, efficacy, photopharmacology

Received: December 20, 2017
Published online: February 7, 2018

- [1] R. G. Pertwee, *Br. J. Pharmacol.* **2006**, *147*, 163.
- [2] S. Galiège, S. Mary, J. Marchand, D. Dussossoy, D. Carriere, P. Carayon, M. Bouaboula, D. Shire, G. LeFur, P. Casellas, *Eur. J. Biochem.* **1995**, *232*, 54.
- [3] A. C. Howlett, M. E. Abood, in *Cannabinoid Pharmacology*, Vol. 80 (Eds: D. Kendall, S. P. H. Alexander), Elsevier, Cambridge, **2017**, p. 169.
- [4] C. Benito, E. Nunez, R. M. Tolon, E. J. Carrier, A. Rabano, C. J. Hillard, J. Romero, *J. Neurosci.* **2003**, *23*, 11136.
- [5] M. Solas, P. T. Francis, R. Franco, M. J. Ramirez, *Neurobiol. Aging* **2013**, *34*, 805.
- [6] E. Aso, I. Ferrer, *Front. Pharmacol.* **2014**, *5*, 37.
- [7] E. B. Russo, *Br. J. Pharmacol.* **2001**, *163*, 1344.

- [8] E. B. Russo, J. Marcu, in *Cannabinoid Pharmacology*, Vol. 80, (Ed.: D. Kendall, S. P. H. Alexander), Elsevier, Cambridge, **2017**, p. 67.
- [9] L. Agnetta, M. Kauk, M. C. A. Canizal, R. Messerer, U. Holzgrabe, C. Hoffmann, M. Decker, *Angew. Chem. Int. Ed.* **2017**, *56*, 7282; *Angew. Chem.* **2017**, *129*, 7388.
- [10] W. Szymanski, J. M. Beierle, H. A. Kistemaker, W. A. Velema, B. L. Feringa, *Chem. Rev.* **2013**, *113*, 6114.
- [11] W. A. Velema, W. Szymanski, B. L. Feringa, *J. Am. Chem. Soc.* **2014**, *136*, 2178.
- [12] J. Broichhagen, J. A. Frank, D. Trauner, *Acc. Chem. Res.* **2015**, *48*, 1947.
- [13] X. Chen, S. Wehle, N. Kuzmanovic, B. Merget, U. Holzgrabe, B. König, C. A. Sotriffer, M. Decker, *ACS Chem. Neurosci.* **2014**, *5*, 377.
- [14] J. Broichhagen, T. Podewin, H. Meyer-Berg, Y. von Ohlen, N. R. Johnston, B. J. Jones, S. R. Bloom, G. A. Rutter, A. Hoffmann-Röder, D. J. Hodson, D. Trauner, *Angew. Chem. Int. Ed.* **2015**, *54*, 15565.
- [15] J. Levitz, C. Pantoja, B. Gaub, H. Janovjak, A. Reiner, A. Hoagland, D. Schoppik, B. Kane, P. Stawski, A. F. Schier, D. Trauner, E. Y. Isacoff, *Nat. Neurosci.* **2013**, *16*, 507.
- [16] J. Broichhagen, N. R. Johnston, Y. von Ohlen, H. Meyer-Berg, B. J. Jones, S. R. Bloom, G. A. Rutter, D. Trauner, D. J. Hodson, *Angew. Chem. Int. Ed.* **2016**, *55*, 5865.
- [17] Z. B. Mehta, N. R. Johnston, M.-S. Nguyen-Tu, J. Broichhagen, P. Schultz, D. P. Larner, I. Leclerc, D. Trauner, G. A. Rutter, D. J. Hudson, *Sci. Rep.* **2017**, *7*, 291.
- [18] M. I. Bahamonde, J. Taura, S. Paoletta, A. A. Gakh, S. Chakraborty, J. Hernando, V. Fernandez-Duenas, K. A. Jacobson, P. Gorostiza, F. Ciruela, *Bioconjugate Chem.* **2014**, *25*, 1847.
- [19] M. Schönberger, D. Trauner, *Angew. Chem. Int. Ed.* **2014**, *53*, 3264.
- [20] D. Lachmann, C. Studte, B. Männel, H. Hübner, P. Gmeiner, B. König, *Chem. Eur. J.* **2017**, *23*, 13423.
- [21] M. V. Westphal, M. A. Schafroth, R. C. Sarott, M. A. Imhoff, C. P. Bold, P. Leippe, A. Dhopeshwarkar, J. M. Grandner, V. Katritch, K. Mackie, D. Trauner, E. M. Carreira, J. A. Frank, *J. Am. Chem. Soc.* **2017**, DOI: 10.1021/jacs.7b06456.
- [22] M. Nimczick, D. Pemp, F. H. Darras, X. Chen, J. Heilmann, M. Decker, *Bioorg. Med. Chem.* **2014**, *22*, 3938.
- [23] M. Nimczick, M. Decker, *ChemMedChem* **2015**, *10*, 773.
- [24] D. Dolles, M. Nimczick, M. Scheiner, J. Ramler, P. Stadtmüller, E. Sawatzky, A. Drakopoulos, C. Sotriffer, H.-J. Wittmann, A. Strasser, M. Decker, *ChemMedChem* **2016**, *11*, 1270.
- [25] D. Page, E. Balaux, L. Boisvert, Z. Liu, C. Milburn, M. Tremblay, Z. Wei, S. Woo, X. Luo, Y.-X. Cheng, H. Yang, S. Srivastava, F. Zhou, W. Brown, M. Tomaszewski, C. Walpole, L. Hodzic, S. St-Onge, C. Godbout, D. Salois, K. Payza, *Bioorg. Med. Chem.* **2008**, *18*, 3695.
- [26] M. Freitag, J. Schemies, T. Larsen, K. El Gaghlab, F. Schulz, T. Rumpf, M. Jung, A. Link, *Bioorg. Med. Chem.* **2011**, *19*, 3669.
- [27] C. Williams, *Nat. Rev. Drug Discov.* **2004**, *3*, 125.

Table of Content

Chemistry	2
Photophysical Properties	18
Pharmacological Evaluation.....	20
Radioligand Binding Studies	20
Determination of Efficacy	22
[³⁵ S]-GTP γ S binding assay	25
Computational Studies	28
References	29

Chemistry

General Information

All reagents were used without further purification and bought from common commercial suppliers.

Thin layer chromatography (TLC) was performed on silica gel 60 (alumina foils with fluorescent indicator 254 nm). For detection iodine vapor and UV light (254 nm and 366 nm) were used. For column chromatography, silica gel 60 (particle size of 0.040 mm – 0.063 mm) was used.

Nuclear magnetic resonance spectra were recorded with a Bruker AV-400 NMR instrument (Bruker, Karlsruhe, Germany) in CDCl₃ and chemical shifts are expressed in ppm relative to CDCl₃ (7.26 ppm for ¹H and 77.16 ppm for ¹³C).¹

The LCMS-system from Shimadzu Products, contained a DGU-20A3R degassing unit, a LC20AB liquid chromatograph and a SPD-20A UV/Vis detector. Mass spectra were obtained by a LCMS 2020. As stationary phase a Synergi 4U fusion-RP (150 * 4.6 mm) column and as mobile phase a gradient of MeOH / water with 0.1% trifluoroacetic acid was used. Parameters: A: water, B: MeOH, V(B)/(V(A)+V(B)) = 5 % to 90 % over 10 min, V(B)/(V(A)+V(B)) = 90 % for 5 min, V(B)/(V(A)+V(B)) = 90 % to 5 % over 3 min. Both methods were performed with a flow rate of 1.0 mL/min. UV detection was measured at 254 nm.

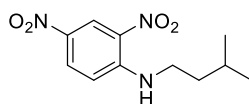
General procedure I for the partial oxidation of anilines (for compounds **8a-i**)

The respective aniline (1 eq.) was dissolved in CH₂Cl₂ and an aqueous solution of oxone (commercially available mixture of 2 KHSO₅·KHSO₄·K₂SO₄) (1 eq.) was added. The mixture was stirred at room temperature for 3 h to 5 h. The end of the reaction was indicated by TLC. The organic and the aqueous phase were separated and the aqueous phase was extracted with CH₂Cl₂. The combined organic phases were washed with aqueous HCl (5%) and brine and were afterwards dried over anhydrous Na₂SO₄. The solvent was removed *in vacuo* and the crude product was used immediately for the next reaction step.

General procedure II for the Mills reaction / azo-coupling (for compounds **9a-i**)

The respective aniline (1 eq.) was dissolved in a 1:1 mixture of CH₂Cl₂ and acetic acid. The respective nitroso compound (4-6 eq.) was added and the mixture was stirred at room temperature for 24 h. After the reaction has finished, water and CH₂Cl₂ was added and the phases were separated. The organic phase was dried over anhydrous Na₂SO₄ and the solvent was removed *in vacuo*. The crude product was purified by column chromatography if necessary.

Synthesis of *N*-isopentyl-2,4-dinitroaniline (**2**)



2

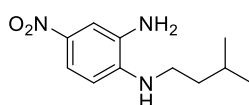
1-chloro-2,4-dinitrobenzene **1** (7.40 mmol, 1.50 g, 1 eq.) was dissolved in EtOH and NEt₃ (11.1 mmol, 1.52 mL, 1.5 eq.) and isopentylamine (8.20 mmol, 0.95 mL, 1.1 eq.) were added. The mixture was stirred overnight at 50 °C. Afterwards, the solvent was removed *in vacuo* and the residue taken up in EtOAc. The organic layer was washed with brine, dried over anhydrous Na₂SO₄ and the solvent removed *in vacuo*. Product was obtained as yellow solid used without further purification (7.26 mmol, 1.84 g, 98%).

¹H NMR (CDCl₃, 400 MHz): δ = 9.11 (d, *J* = 2.6 Hz, 1H), 8.52 (s, 1H), 8.26 (dd, *J* = 9.5, 2.6 Hz, 1H), 6.94 – 6.91 (m, 1H), 3.46 – 3.38 (m, 2H), 1.84 – 1.64 (m, 3H), 1.00 (d, *J* = 6.5 Hz, 6H) ppm.

¹³C NMR (CDCl₃, 101 MHz): δ = 148.38, 135.92, 130.34, 130.27, 124.35, 113.90, 41.89, 37.48, 25.96, 22.38 ppm.

ESI: *m/z* calcd for C₁₁H₁₅N₃O₄ [M+H]⁺: 254.11; found: 254.00.

Synthesis of *N*¹-isopentyl-4-nitrobenzene-1,2-diamine (**3**)



3

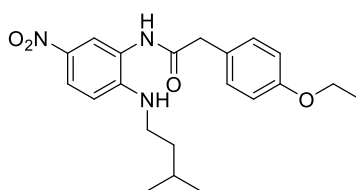
The dinitro compound **2** (1.97 mmol, 0.50 g) was dissolved in methanol. The solution was refluxed and a mixture of Na₂S·H₂O (60%) (19.7 mmol, 3.16 g) and NaHCO₃ (19.7 mmol, 1.65 g) in water was added dropwise over a period of 1 h. The reaction was refluxed for further 4 h. After the reaction has cooled down to room temperature, methanol was evaporated and residue was taken up in EtOAc. The organics were extracted with EtOAc (3 times) and the combined organic phase was washed twice with water. The organic phase was dried over Na₂SO₄ and the solvent was removed *in vacuo*. The crude product was purified by column chromatography using petroleum ether and EtOAc (2:1) as eluent system. **3** was obtained as a red solid (1.38 mmol, 0.31 g, 70%).

¹H NMR (CDCl₃, 400 MHz): δ = 7.84 (dd, J = 8.9, 2.2 Hz, 1H), 7.66 (d, J = 2.4 Hz, 1H), 6.56 (d, J = 8.9 Hz, 1H), 3.23 (t, J = 6.4 Hz, 2H), 1.79 – 1.68 (m, 1H), 1.59 (dd, J = 14.7, 7.1 Hz, 2H), 0.97 (d, J = 6.6 Hz, 6H) ppm.

¹³C NMR (CDCl₃, 101 MHz): δ = 145.09, 138.01, 131.14, 119.76, 112.96, 108.38, 41.94, 38.07, 26.04, 22.53 ppm.

ESI: m/z calcd for C₁₁H₁₇N₃O₂ [M+H]⁺: 224.13; found: 224.00.

Synthesis of 2-(4-ethoxyphenyl)-N-(2-(isopentylamino)-5-nitrophenyl)acetamide (4)



4

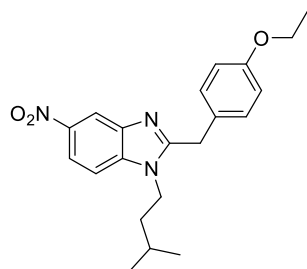
2-(4-ethoxyphenyl)acetic (5.07 mmol, 0.91 g, 1.1 eq.) was dissolved in DMF and NEt₃ (1.5 eq.), HBTU (1.1 eq.) and diamine **3** (4.61 mmol, 1.04 g, 1 eq.) were added in one portion. The mixture was stirred overnight at room temperature. Then, EtOAc and a sat. NaHCO₃ solution were added. The organic layer was washed several times with water and brine and dried over anhydrous Na₂SO₄. The solvent was removed *in vacuo* and product **4** was obtained as brown oil (4.52 mmol, 1.73 g, 98%).

¹H NMR (400 MHz, CDCl₃): δ = 8.03 – 7.91 (m, 2H), 7.28 (d, J = 8.4 Hz, 2H), 6.94 – 6.88 (m, J = 7.5 Hz, 2H), 6.56 (d, J = 9.1 Hz, 1H), 4.02 (dt, J = 11.9, 6.0 Hz, 2H), 3.72 (s, 2H), 3.15 – 3.06 (m, 2H), 1.67 – 1.58 (m, J = 13.3, 6.7 Hz, 1H), 1.45 – 1.38 (m, 5H), 0.93 (d, J = 6.6 Hz, 6H) ppm.

¹³C NMR (101 MHz, CDCl₃): δ = 171.27, 158.68, 148.68, 137.03, 130.39, 126.33, 124.69, 122.72, 121.36, 115.48, 115.34, 63.53, 43.17, 41.73, 38.63, 25.91, 22.46, 14.80 ppm.

ESI: m/z calcd for C₂₁H₂₇N₃O₄ [M+H]⁺: 386.20; found: 386.00.

Synthesis of 2-(4-ethoxybenzyl)-1-isopentyl-5-nitro-1H-benzo[d]imidazole (5)



5

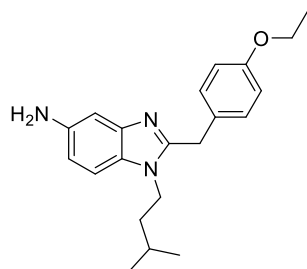
The respective acetamide **4** (4.52 mmol, 1.73 g, 1 eq.) was dissolved in glacial acetic acid, and the mixture refluxed for 1.5 h. The solution was then concentrated *in vacuo*, basified (pH = 10) with NH_{3,aq.} (25%) and extracted with CH₂Cl₂. The organic layer was dried over anhydrous Na₂SO₄, the solvent removed *in vacuo*. The crude product was purified by column chromatography using petroleum ether and EtOAc (3:1) as eluent system. **5** was obtained as a colorless solid (2.78 mmol, 1.02 g, 62%).

¹H NMR (CDCl₃, 400 MHz): δ = 8.65 (d, J = 2.1 Hz, 1H), 8.18 (dd, J = 8.9, 2.1 Hz, 1H), 7.31 (d, J = 8.9 Hz, 1H), 7.15 (d, J = 8.6 Hz, 2H), 6.87 – 6.80 (m, 2H), 4.29 (s, 2H), 4.09 – 3.94 (m, 4H), 1.65 – 1.51 (m, 1H), 1.45 – 1.33 (m, 5H), 0.91 (d, J = 6.6 Hz, 6H) ppm.

¹³C NMR (CDCl₃, 101 MHz): δ = 158.29, 157.11, 143.57, 141.47, 139.35, 129.57, 126.88, 118.35, 116.02, 115.04, 109.22, 63.53, 43.09, 38.08, 33.80, 26.17, 22.31, 14.77 ppm.

ESI: m/z calcd for C₂₁H₂₅N₃O₃ [M+H]⁺: 368.19; found: 368.10.

Synthesis of 2-(4-ethoxybenzyl)-1-isopentyl-1H-benzo[d]imidazol-5-amine (6)



6

The respective nitro compound **5** (1.44 mmol, 0.53 g, 1 eq.) was dissolved in EtOH and SnCl₂·2 H₂O (7.21 mmol, 1.63 g, 6.2 eq.) added. The mixture was refluxed overnight under argon

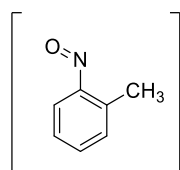
atmosphere. After cooling to 0 °C, the mixture was basified (pH = 10) with 1 M NaOH_{aq} until precipitation. The precipitate was filtered off by suction and the solution concentrated *in vacuo*. The residue was suspended in water and extracted with CH₂Cl₂. The organic layer was dried over anhydrous Na₂SO₄ and the solvent was removed *in vacuo*. Product **6** was obtained as a light yellow oil (1.33 mmol, 0.45 g, 93%) and used without further purification.

¹H NMR (400 MHz, CDCl₃): δ = 7.01 (d, *J* = 8.5 Hz, 2H), 6.92 (d, *J* = 14.1 Hz, 1H), 6.90 – 6.84 (m, 1H), 6.67 (d, *J* = 8.5 Hz, 2H), 6.53 – 6.47 (m, 1H), 4.02 (s, 2H), 3.86 – 3.75 (m, 2H), 3.75 – 3.65 (m, 4H), 1.44 – 1.32 (m, 1H), 1.21 (t, *J* = 7.0 Hz, 4H), 1.16 – 1.08 (m, 2H), 0.73 (d, *J* = 6.7 Hz, 6H) ppm.

¹³C NMR (101 MHz, CDCl₃): δ = 169.90, 156.80, 151.86, 142.71, 141.18, 128.43, 127.50, 113.66, 111.10, 108.51, 103.35, 62.32, 41.27, 37.02, 32.61, 25.01, 21.30, 13.72 ppm.

ESI: *m/z* calcd for C₂₁H₂₇N₃O [M+H]⁺: 338.22; found: 338.05.

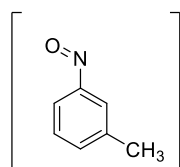
Synthesis of 1-methyl-2-nitrosobenzene (**8b**)



8b

The reaction was carried out according to general procedure I using *o*-toluidine (3.79 mmol, 0.41 mL) and oxone (3.79 mmol, 1.16 g). The crude product was immediately used without further purification for the next reaction step (3.79 mmol, 0.46 g, > 99%).

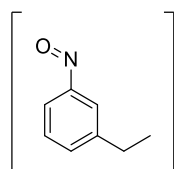
Synthesis of 1-methyl-3-nitrosobenzene (**8c**)



8c

The reaction was carried out according to general procedure I using *m*-toluidine (2.13 mmol, 0.23 mL) and oxone (2.13 mmol, 0.65 g). The crude product was immediately used without further purification for the next reaction step (2.13 mmol, 0.26 g, > 99%).

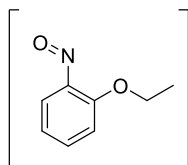
Synthesis of 1-ethyl-3-nitrosobenzene (8d)



8d

The reaction was carried out according to general procedure I using 3-ethyl aniline (4.43 mmol, 0.55 mL) and oxone (4.43 mmol, 1.36 g). The crude product was immediately used without further purification for the next reaction step (4.43 mmol, 0.59 g, > 99%).

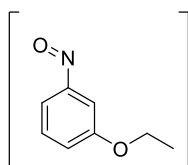
Synthesis of 1-ethoxy-2-nitrosobenzene (8e)



8e

The reaction was carried out according to general procedure I using *o*-phenetidine (1.65 mmol, 0.22 mL) and oxone (1.65 mmol, 0.51 g). The crude product was immediately used without further purification for the next reaction step (1.65 mmol, 0.25 g, > 99%).

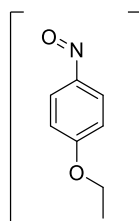
Synthesis of 1-ethoxy-3-nitrosobenzene (8f)



8f

The reaction was carried out according to general procedure I using *m*-phenetidine (3.91 mmol, 0.52 mL) and oxone (3.91 mmol, 1.20 g). The crude product was immediately used without further purification for the next reaction step (3.91 mmol, 0.59 g, > 99%).

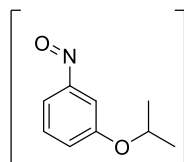
Synthesis of 1-ethoxy-4-nitrosobenzene (8g)



8g

The reaction was carried out according to general procedure I using *p*-phenetidine (1.42 mmol, 0.18 mL) and oxone (1.42 mmol, 0.44 g). The crude product was immediately used without further purification for the next reaction step (1.42 mmol, 0.21 g, > 99%).

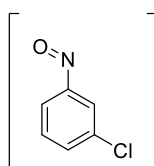
Synthesis of 1-isopropoxy-3-nitrosobenzene (8h)



8h

The reaction was carried out according to general procedure I using 3-isopropyl aniline (4.43 mmol, 0.65 mL) and oxone (4.43 mmol, 1.36 g). The crude product was immediately used without further purification for the next reaction step (4.43 mmol, 0.73 g, > 99%).

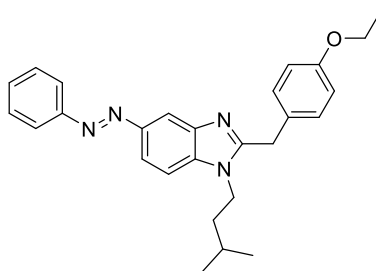
Synthesis of 1-chloro-3-nitrosobenzene (8i)



8i

The reaction was carried out according to general procedure I using 3-chloroaniline (1.78 mmol, 0.19 mL) and oxone (1.78 mmol, 0.55 g). The crude product was immediately used without further purification for the next reaction step (1.78 mmol, 0.27 g, > 99%).

Synthesis of 2-(4-ethoxybenzyl)-1-isopentyl-5-(phenyldiazenyl)-1*H*-benzo[*d*]imidazole (**9a**)



9a

The reaction was carried out according to general procedure II using amine **6** (0.51 mmol, 0.17 g) and nitroso benzene (3.03 mmol, 0.33 g). The crude product was purified by column chromatography using petroleum ether and EtOAc (2:1) as eluent system. The pure product was obtained as bright orange solid (0.34 mmol, 0.15 g, 67%).

¹H NMR (400 MHz, CDCl₃): δ = 8.30 (dd, J = 7.1, 1.9 Hz, 1H), 7.90 – 7.84 (m, 3H), 7.48 – 7.34 (m, 3H), 7.26 (d, J = 8.7 Hz, 1H), 7.14 – 7.08 (m, 2H), 6.79 – 6.73 (m, 2H), 4.25 (s, 2H), 3.92 (ddd, J = 12.1, 8.9, 5.2 Hz, 4H), 1.55 – 1.48 (m, 1H), 1.38 – 1.28 (m, 5H), 0.85 – 0.83 (d, J = 6.7 Hz, 6H) ppm.

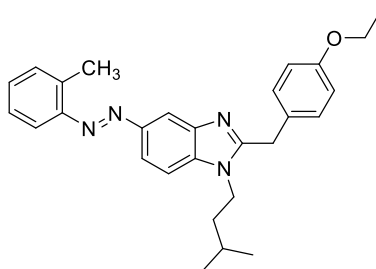
¹³C NMR (101 MHz, CDCl₃): δ = 158.18, 154.82, 152.73, 149.03, 141.48, 136.94, 130.54, 129.60, 129.05, 127.33, 122.75, 117.22, 115.80, 114.98, 109.62, 63.52, 42.91, 38.09, 33.56, 26.19, 22.35, 14.79 ppm.

ESI: m/z calcd for C₂₇H₃₀N₄O [M+H]⁺: 426.56; found: 427.20.

HPLC purity: > 99%

trans:cis ratio: 88:12 (Retention time (trans): 12.4 min; Retention time (cis): 10.7 min).

Synthesis of 2-(4-ethoxybenzyl)-1-isopentyl-5-(o-tolyldiazenyl)-1H-benzo[d]imidazole (9b)



9b

The reaction was carried out according to general procedure II using amine **6** (0.63 mmol, 0.21 g) and nitroso compound **8b** (3.79 mmol, 0.46 g). The crude product was purified by column chromatography using petroleum ether and EtOAc (3:1) as eluent system. The pure product was obtained as dark orange solid (0.17 mmol, 75 mg, 27%).

¹H NMR (400 MHz, CDCl₃): δ = 8.38 (d, J = 1.6 Hz, 1H), 7.94 (dd, J = 8.6, 1.8 Hz, 1H), 7.68 (d, J = 7.7 Hz, 1H), 7.36 – 7.24 (m, 4H), 7.21 – 7.15 (m, 2H), 6.87 – 6.81 (m, 2H), 4.28 (s, 2H), 4.04 – 3.94 (m, 4H), 2.73 (s, 3H), 1.64 – 1.51 (m, 1H), 1.41 (dt, J = 18.1, 6.9 Hz, 5H), 0.91 (d, J = 6.6 Hz, 6H) ppm.

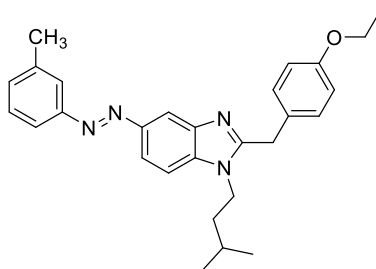
¹³C NMR (101 MHz, CDCl₃): δ = 157.07, 153.98, 149.76, 148.27, 141.48, 136.70, 136.20, 130.13, 129.33, 128.52, 126.66, 125.37, 116.85, 114.42, 114.17, 113.89, 108.33, 62.46, 41.75, 37.10, 32.79, 25.13, 21.33, 16.50, 13.76 ppm.

ESI: m/z calcd for C₂₈H₃₂N₄O [M+H]⁺: 440.59; found: 441.25.

HPLC purity: > 99%

trans:cis ratio: 87:13 (Retention time (trans): 12.6 min; Retention time (cis): 10.8 min).

Synthesis of 2-(4-ethoxybenzyl)-1-isopentyl-5-(m-tolyldiazenyl)-1H-benzo[d]imidazole (9c)



9c

The reaction was carried out according to general procedure II using amine **6** (0.36 mmol, 0.12 g) and nitroso compound **8c** (2.13 mmol, 0.26 g). The crude product was purified by column chromatography using petroleum ether and EtOAc (2:1) as eluent system. The pure product was obtained as dark orange solid (0.29 mmol, 0.13 g, 81%).

¹H NMR (400 MHz, CDCl₃): δ = 8.37 (d, J = 1.6 Hz, 1H), 7.92 (dd, J = 8.7, 1.8 Hz, 1H), 7.77 – 7.72 (m, 2H), 7.43 – 7.36 (m, 1H), 7.33 – 7.28 (m, 1H), 7.28 – 7.24 (m, 1H), 7.20 – 7.15 (m, 2H), 6.86 – 6.81 (m, 2H), 4.29 (s, 2H), 4.02 – 3.95 (m, 4H), 2.46 (s, 3H), 1.63 – 1.51 (m, 1H), 1.43 – 1.35 (m, 5H), 0.90 (d, J = 6.6 Hz, 6H) ppm.

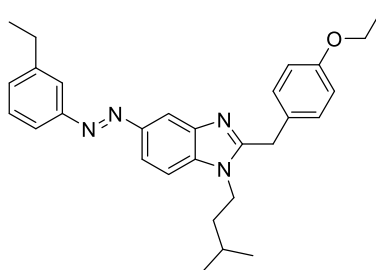
¹³C NMR (101 MHz, CDCl₃): δ = 157.09, 153.85, 151.81, 147.89, 141.16, 137.87, 136.14, 130.23, 128.53, 127.82, 126.55, 121.75, 119.33, 115.79, 115.06, 113.90, 108.46, 62.46, 41.79, 37.07, 32.71, 25.14, 21.32, 20.36, 13.76 ppm.

ESI: m/z calcd for C₂₈H₃₂N₄O [M+H]⁺: 440.59; found: 441.30.

HPLC purity: > 99%

trans:cis ratio: 94:6 (Retention time (trans): 12.8 min; Retention time (cis): 10.8 min).

Synthesis of 2-(4-ethoxybenzyl)-5-((3-ethylphenyl)diazenyl)-1-isopentyl-1H-benzo[d]imidazole (**9d**)



9d

The reaction was carried out according to general procedure II using amine **6** (0.74 mmol, 0.25 g) and nitroso compound **8d** (4.43 mmol, 0.59 g). The crude product was purified by column chromatography using petroleum ether and EtOAc (2:1) as eluent system. The pure product was obtained as orange oil (0.60 mmol, 0.27 g, 81%).

¹H NMR (400 MHz, CDCl₃): δ = 8.41 (d, J = 1.6 Hz, 1H), 7.95 (dd, J = 8.7, 1.7 Hz, 1H), 7.83 – 7.76 (m, 2H), 7.44 (t, J = 7.7 Hz, 1H), 7.33 (t, J = 8.6 Hz, 2H), 7.18 (d, J = 8.6 Hz, 2H), 6.85

(d, $J = 5.7$ Hz, 2H), 4.35 (s, 2H), 4.05 – 3.96 (m, 4H), 2.78 (q, $J = 7.6$ Hz, 2H), 1.64 – 1.54 (m, 1H), 1.43 – 1.31 (m, 8H), 0.91 (d, $J = 6.6$ Hz, 6H) ppm.

^{13}C NMR (101 MHz, CDCl_3): $\delta = 176.46, 158.15, 154.99, 152.86, 149.11, 145.30, 140.94, 136.55, 130.28, 129.59, 128.94, 127.28, 121.92, 120.44, 117.41, 114.98, 109.70, 63.50, 42.86, 37.96, 28.80, 26.17, 22.30, 21.01, 15.51, 14.75$ ppm.

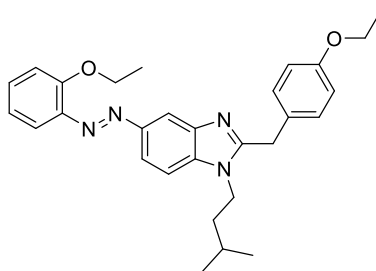
ESI: m/z calcd. for $\text{C}_{29}\text{H}_{34}\text{N}_4\text{O}$ $[\text{M}+\text{H}]^+$: 455.62; found: 455.20.

HPLC purity: 97%

trans:cis ratio: 92:8 (Retention time (trans): 11.9 min; Retention time (cis): 10.6 min).

Synthesis of 2-(4-ethoxybenzyl)-5-((2-ethoxyphenyl)diazenyl)-1-isopentyl-1H-benzo[d]

Imidazole (9e)



9e

The reaction was carried out according to general procedure II using amine **6** (0.41 mmol, 0.14 g) and nitroso compound **8e** (1.65 mmol, 0.25 g). The crude product was purified by column chromatography using petroleum ether and EtOAc (3:1) as eluent system. The pure product was obtained as dark orange oil (0.10 mmol, 47 mg, 24%).

^1H NMR (400 MHz, CDCl_3): $\delta = 8.38$ (s, 1H), 7.95 (d, $J = 8.7$ Hz, 1H), 7.71 (dd, $J = 8.0, 1.7$ Hz, 1H), 7.42 – 7.29 (m, 2H), 7.18 (d, $J = 8.2$ Hz, 2H), 7.12 – 7.05 (m, 1H), 7.05 – 6.97 (m, 1H), 6.84 (d, $J = 8.6$ Hz, 2H), 4.34 – 4.23 (m, 4H), 4.04 – 3.95 (m, 4H), 1.62 – 1.49 (m, 4H), 1.45 – 1.36 (m, 5H), 0.91 (d, $J = 6.6$ Hz, 6H) ppm.

^{13}C NMR (101 MHz, CDCl_3): $\delta = 158.14, 156.34, 154.77, 149.58, 142.74, 131.80, 129.58, 127.56, 120.94, 117.61, 117.07, 115.72, 114.96, 114.80, 109.46, 65.48, 63.51, 42.86, 38.10, 33.68, 26.19, 22.35, 15.00, 14.79$ ppm.

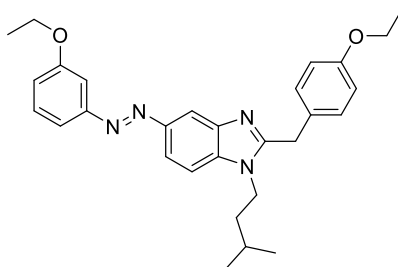
ESI: m/z calcd for $\text{C}_{29}\text{H}_{34}\text{N}_4\text{O}_2$ $[\text{M}+\text{H}]^+$: 470.62; found: 471.20.

HPLC purity: 98%

trans:cis ratio: 85:15 (Retention time (trans): 11.5 min; Retention time (cis): 10.5 min).

Synthesis of 2-(4-ethoxybenzyl)-5-((3-ethoxyphenyl)diazenyl)-1-isopentyl-1H-benzo[d]

Imidazole (9f)



9f

The reaction was carried out according to general procedure II using amine **6** (0.65 mmol, 0.22 g) and nitroso compound **8f** (3.91 mmol, 0.59 g). The crude product was purified by column chromatography using petroleum ether and EtOAc (2:1) as eluent system. The pure product was obtained as dark orange solid (0.57 mmol, 0.27 g, 88%).

¹H NMR (400 MHz, CDCl₃): δ = 8.37 (d, J = 1.6 Hz, 1H), 7.91 (dd, J = 8.7, 1.7 Hz, 1H), 7.60 – 7.53 (m, 1H), 7.50 – 7.44 (m, 1H), 7.40 (t, J = 8.0 Hz, 1H), 7.30 (d, J = 8.7 Hz, 1H), 7.21 – 7.12 (m, 2H), 7.03 – 6.97 (m, 1H), 6.88 – 6.79 (m, 2H), 4.28 (s, 2H), 4.13 (q, J = 7.0 Hz, 2H), 3.98 (q, J = 7.0 Hz, 4H), 1.61 – 1.50 (m, 1H), 1.45 (t, J = 7.0 Hz, 3H), 1.42 – 1.34 (m, 5H), 0.90 (d, J = 6.7 Hz, 6H) ppm.

¹³C NMR (101 MHz, CDCl₃): δ = 173.11, 158.65, 157.07, 153.98, 152.94, 147.73, 141.21, 136.21, 128.52, 126.57, 116.64, 115.83, 115.76, 115.15, 113.89, 108.46, 105.33, 62.66, 41.76, 37.05, 32.63, 28.66, 25.12, 23.02, 21.31, 13.79 ppm.

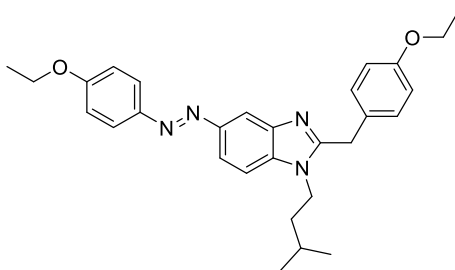
ESI: m/z calcd for C₂₉H₃₄N₄O₂ [M+H]⁺: 470.62; found: 471.25.

HPLC purity: 99%

trans:cis ratio: 95:5 (Retention time (trans): 12.6 min; Retention time (cis): 10.8 min).

Synthesis of 2-(4-ethoxybenzyl)-5-((4-ethoxyphenyl)diazenyl)-1-isopentyl-1H-benzo[d]

Imidazole (9g)



9g

The reaction was carried out according to general procedure II using amine **6** (0.24 mmol, 80 mg) and nitroso compound **8g** (1.42 mmol, 0.21 g). The crude product was purified by column chromatography using petroleum ether and EtOAc (1:1) as eluent system. The pure product was obtained as dark orange solid (0.076 mmol, 36 mg, 32%).

¹H NMR (400 MHz, CDCl₃): δ = 8.33 (d, J = 1.1 Hz, 1H), 7.97 – 7.88 (m, 3H), 7.34 (d, J = 8.7 Hz, 1H), 7.20 (d, J = 8.5 Hz, 2H), 7.05 – 6.96 (m, 2H), 6.86 – 6.79 (m, 2H), 4.36 (s, 2H), 4.12 (q, J = 7.0 Hz, 2H), 4.06 – 3.94 (m, 4H), 1.64 – 1.53 (m, 1H), 1.49 – 1.43 (m, 3H), 1.43 – 1.34 (m, 5H), 0.91 (d, J = 6.6 Hz, 6H) ppm.

¹³C NMR (101 MHz, CDCl₃): δ = 160.25, 157.23, 153.34, 148.36, 145.87, 135.01, 128.63, 125.98, 123.63, 118.74, 116.57, 114.00, 113.67, 113.56, 108.72, 62.80, 42.00, 36.99, 32.27, 28.68, 25.17, 22.87, 21.32, 13.76 ppm.

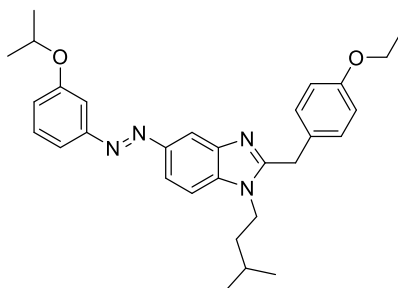
ESI: m/z calcd for C₂₉H₃₄N₄O₂ [M+H]⁺: 470.62; found: 471.20.

HPLC purity: 96%

trans:cis ratio: 88:12 (Retention time (trans): 12.2 min; Retention time (cis): 10.7 min).

Synthesis of 2-(4-ethoxybenzyl)-1-isopentyl-5-((3-isopropoxyphenyl)diazenyl)-1H-benzo[d]

Imidazole (9h)



9h

The reaction was carried out according to general procedure II using amine **6** (0.74 mmol, 0.25 g) and nitroso compound **8h** (4.43 mmol, 0.73 g). The crude product was purified by column chromatography using petroleum ether and EtOAc (2:1) as eluent system. The pure product was obtained as orange oil (0.17 mmol, 86.0 mg, 32%).

¹H NMR (400 MHz, CDCl₃): δ = 8.30 (d, J = 1.5 Hz, 1H), 7.85 (dd, J = 8.7, 1.7 Hz, 1H), 7.49 – 7.42 (m, 1H), 7.42 – 7.39 (m, 1H), 7.36 – 7.30 (m, 1H), 7.26 (d, J = 8.7 Hz, 1H), 7.10 (d, J = 8.6 Hz, 2H), 6.95 – 6.90 (m, 1H), 6.76 (d, J = 8.7 Hz, 2H), 4.66 – 4.58 (m, 1H), 4.26 (s, 2H), 3.96 – 3.88 (m, 4H), 1.56 – 1.45 (m, 1H), 1.35 – 1.29 (m, 11H), 0.84 (d, J = 6.6 Hz, 6H) ppm.

¹³C NMR (101 MHz, CDCl₃): δ = 175.53, 160.01, 154.73, 151.99, 148.89, 146.30, 140.94, 137.03, 131.10, 129.39, 127.94, 126.32, 121.92, 119.45, 118.52, 114.98, 109.70, 66.36, 64.86, 42.86, 37.96, 32.91, 26.17, 21.30, 21.01, 14.75 ppm.

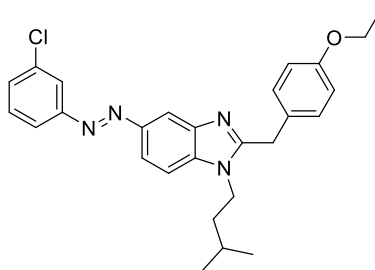
ESI: m/z calcd for C₃₀H₃₆N₄O [M+H]⁺: 485.64; found: 485.20.

HPLC purity: 96%

trans:cis ratio: 93:7 (Retention time (trans): 12.1 min; Retention time (cis): 10.7 min).

Synthesis of 5-((3-chlorophenyl)diazenyl)-2-(4-ethoxybenzyl)-1-isopentyl-1H-benzo[d]

Imidazole (9i)



9i

The reaction was carried out according to general procedure II using amine **6** (0.29 mmol, 0.10 g) and nitroso compound **8i** (1.78 mmol, 0.25 g). The crude product was purified by column chromatography using petroleum ether and EtOAc (2:1) as eluent system. The pure product was obtained as orange solid (0.20 mmol, 93 mg, 70%).

¹H NMR (400 MHz, CDCl₃): δ = 8.37 (d, J = 8.0 Hz, 1H), 7.96 – 7.88 (m, 2H), 7.83 (d, J = 7.5 Hz, 1H), 7.48 – 7.37 (m, 2H), 7.33 (d, J = 8.7 Hz, 1H), 7.18 (d, J = 8.4 Hz, 2H), 6.83 (d, J = 8.5 Hz, 2H), 4.30 (s, 2H), 4.04 – 3.95 (m, 4H), 1.64 – 1.51 (m, 1H), 1.44 – 1.34 (m, 5H), 0.91 (d, J = 6.6 Hz, 6H) ppm.

¹³C NMR (101 MHz, CDCl₃): δ = 158.19, 155.09, 153.56, 148.65, 141.89, 137.47, 135.05, 130.17, 130.08, 129.59, 127.35, 122.22, 121.71, 117.28, 116.20, 114.98, 109.67, 63.51, 42.92, 38.10, 33.67, 26.19, 22.35, 14.79 ppm.

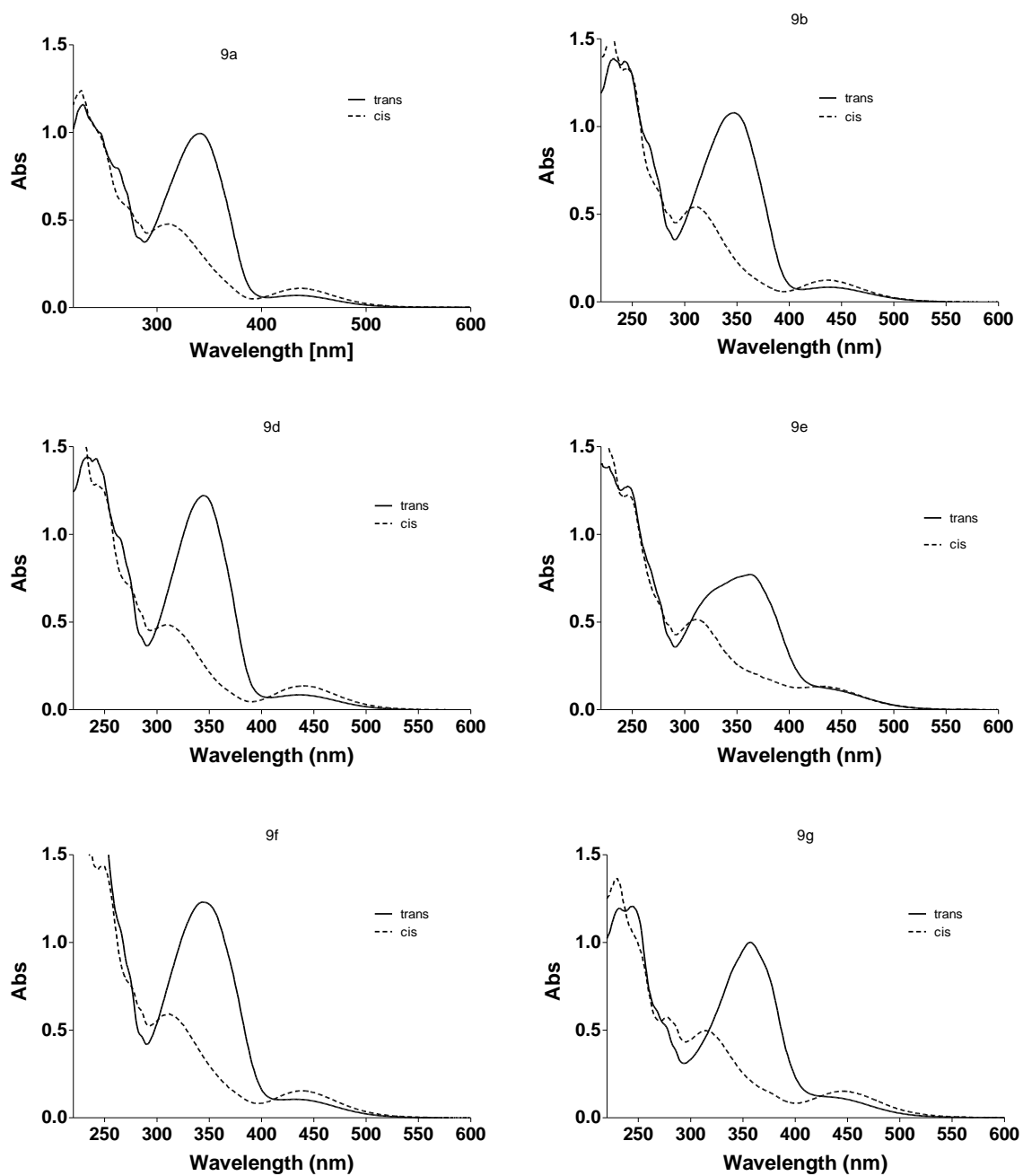
ESI: m/z calcd for C₂₇H₂₉ClN₄O [M+H]⁺: 460.20, 462.20; found: 461.20, 463.10.

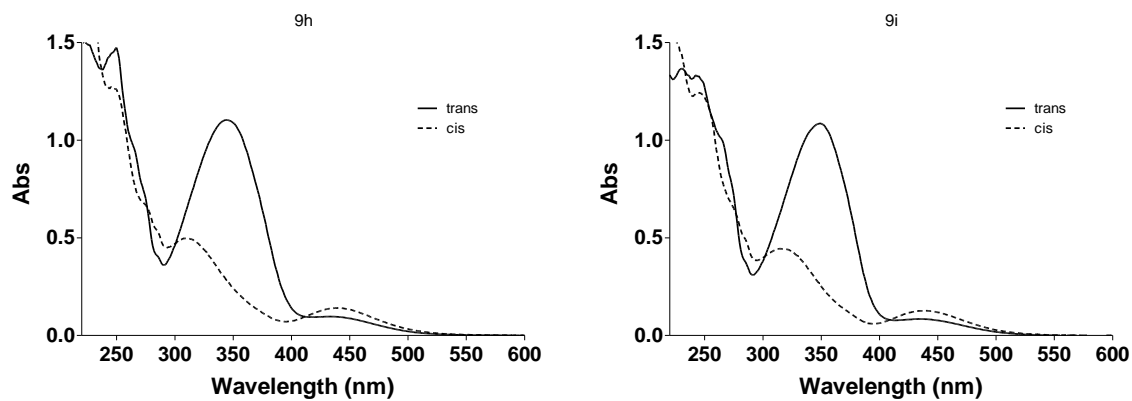
HPLC purity: > 99%

trans:cis ratio: 95:5 (Retention time (trans): 13.9 min; Retention time (cis): 11.0 min).

Photophysical Properties

UV spectra were obtained from 50 μM solution of the respective compound dissolved in ethanol:





A UV spectrum of compound 9c can be found in the manuscript (Figure 2).

Switching cycles and thermal stability is shown in the manuscript (Figure 2) and applies to all compounds tested because of their high structural similarity.

Table 1. *trans:cis* ratios of test compounds at daylight and after irradiation with UV light ($\lambda = 366$ nm)

Compound	daylight		366 nm	
	<i>trans</i>	<i>cis</i>	<i>trans</i>	<i>cis</i>
9a	88	12	10	90
9b	87	13	7	93
9c	94	6	6	94
9d	92	8	8	92
9e	85	15	5	95
9f	95	5	4	96
9g	88	12	7	93
9h	93	7	6	94
9i	95	5	8	92

Pharmacological Evaluation

Radioligand Binding Studies

Unlabeled CP55,940 (unspecific agonist for *hCB₂R* and *hCB₁R*) was bought from Sigma-Aldrich Life Science; radioactive labeled [³H]CP55,940 was bought from Hartmann Analytic GmbH; Rimonabant (inverse agonist for *hCB₁R*) was obtained by an in-house synthesis.

Cells were a kindly gift from AbbVie Laboratories (Chicago, U. S. A.). Human embryonic kidney cells (HEK) stably expressing the *hCB₂R* were grown in Dulbecco's modified Eagle's medium containing high glucose supplemented with 8 % fetal calve serum and 25 µg/ml zeocin in a 37 °C incubator in the presence of 5% CO₂. Chinese hamster ovary cells (CHO) stably expressing the *hCB₁R* were grown in Ham's F-12 Nutrient Mix supplemented with 8 fetal calve serum and 400 µg/ml geneticin in a 37 °C incubator in the presence of 5% CO₂. Cells were splitted twice a week.

Cells (either HEK cells stably expressing *hCB₂R* or CHO cells stably expressing *hCB₁R*) were harvested and homogenized in Tris-EDTA buffer (50 mM Tris-HCl pH = 7.4; 1 mM MgCl₂ · 6 H₂O; 1 mM EDTA) using an ultra turax for 2x 15 s bursts. The suspensions were centrifuged for 10 min at 1 408 g at 4 °C. The pellets were discarded and the supernatant was centrifuged at 140 657 g for 50 min at 4 °C. The final membrane pellet was homogenized in binding buffer (50 mM Tris-HCl pH = 7.4; 5 mM MgCl₂ · 6 H₂O; 2.5 mM EDTA), shock frosted with liquid nitrogen and stored at -80°C until use.

Saturation assays were done similar to Murkherjee *et al.*² to determine the *K_D*-value of the membrane samples. Saturation assays were done with 8 concentrations of [³H]CP55,940 ranging from 0.088 nM to 4.4 nM. Reactions were started by adding 8 µg membrane per well of a 96 well Multiscreen filter plate (Millipore) containing the radioligand in assay buffer (50 mM Tris-HCl, pH = 7.4; 5 mM MgCl₂ · 6 H₂O; 2.5 mM EDTA; 2 mg/ml BSA). After 3 h incubation at room temperature the reaction was stopped by vacuum filtration and each well was washed 4 times with cold binding buffer (50 mM Tris-HCl, pH = 7.4; 5 mM MgCl₂ · 6 H₂O; 2.5 mM EDTA). The filter plate was dried at 40 °C. Activity was counted in a Micro Beta Trilux-Counter (Wallac) using IRGA Safe plus-scintillation cocktail (Perkin Elmer). Competition assays were done with 5-11 concentrations of replacing ligands (0.1 nM – 0.4 mM) and 0.44 nM [³H]CP55,940.

To determine the EC₅₀ values, statistical evaluations and sigmoidal dose-response curve fittings were performed with GraphPad Prism 5 software for Windows (Version 5.01, August 7, 2007).

K_i values was determined when displacement of [^3H]CP 55,940 was higher than 60% at 100 μM test compound concentration. According to the Cheng-Prusoff equation:

$$K_i = \frac{EC_{50}}{1 + \frac{[L^*]}{K_D}}$$

with $[L^*]$ as radioligand concentration (0.44 nM), the K_i value was calculated of at least two individual experiments. K_D values and standard errors were for $h\text{CB}_2\text{R}$ $K_D(h\text{CB}_2\text{R}) = 4.31 \pm 2.10$ and for $h\text{CB}_1\text{R}$ $K_D(h\text{CB}_1\text{R}) = 2.24 \pm 1.15$.

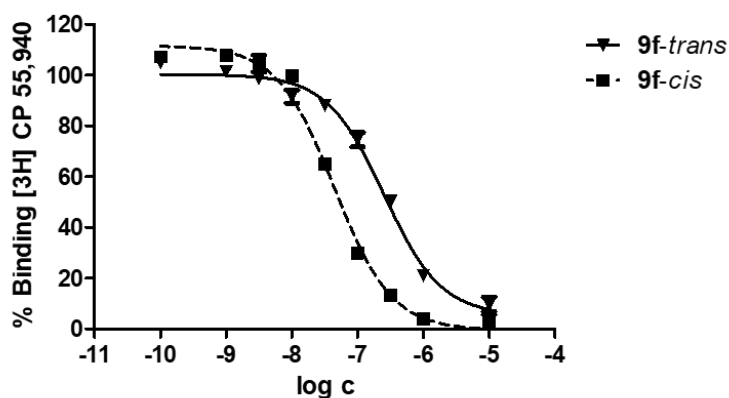


Figure 1. Radioligand binding data of 9f-trans (straight line) and 9f-cis (dotted line).

Determination of Efficacy

Materials and Methods

Cell culture

U266 MM cell line was purchased from ATCC (LGC Standards, Milan, IT). Cell authentication was performed by IST (Genova, Italy). Cell line was cultured in RPMI1640 medium (Lonza, Milan, IT) supplemented with 10% foetal bovine serum (FBS), 2 mM L-glutamine, 100 IU/ml penicillin, 100 µg/ml ampicillin/streptomycin, 1 mM sodium pyruvate and growth at 37°C with 5% CO₂ and 95% humidity.

Compounds

AM630 and forskolin (Tocris Bioscience, Bristol, UK) were dissolved in DMSO at 25 mM concentration. Test compounds were dissolved at 50 mM concentration in DMSO. All compounds were aliquoted and used one time after defrosting.

MTT assay

U266 cell line (4 x 10⁶ cells/ml) were seeded in 96-well plates, in final volume of 100 µl/well. After one day of incubation, compounds or vehicles were added at different concentration. Six replicates were used for each treatment. At the indicated time point, cell viability was assessed by adding 0.8 mg/ml of 3-[4,5-dimethylthiazol-2-yl]-2,5 diphenyl tetrazolium bromide (MTT) (Sigma Aldrich) to the media. After 3 h, the plates were centrifuged, the supernatant was removed, and the pellet was solubilized with 100 µl/well DMSO. The absorbance of the samples against a background control (medium alone) was measured at 570 nm using an ELISA reader microliter plate (BioTek Instruments, Winooski, VT, USA). In some experiments, one hour of pre-incubation with forskolin or AM630 was performed. Each sample was evaluated in six wells and in two independent experiments.

cAMP assay

1 x 10⁶/ml U266 cells were plated in 24 wells plate and treated with the appropriate compounds for 2 hours. After treatment, the cells were processed for detection of cAMP levels, using the cAMP assay kit (Enzo Life Sciences, Farmingdale, NY, USA) according to the manufacturer's protocol. The concentration of cAMP was calculated by measuring the absorbance at 450 nm with an ELISA reader. Each compound was evaluated in duplicated and in two independent assay. cAMP levels were represent as pmol/mg of protein.

RNA extraction and RT/PCR

At the appropriate incubation times, total RNA from treated and vehicle U266 cell was extracted using the RNeasy MiniKit (Qiagen), and cDNA was synthesized using the High-Capacity cDNA Archive Kit (Applied Biosystems, Foster City, PA) according to the manufacturer's instructions.

Quantitative real-time polymerase chain reactions (qRT-PCR) for MIF, STAT-3 and GAPDH were performed using the iQ5 Multicolor Real-Time PCR Detection System (Bio-Rad, Hercules, CA). PCR reaction was performed with SYBRGreen qPCR mastermix (Qiagen) using 500 ng of cDNA for reaction, following the amplification protocol indicated by the manufacturer's instruction. All samples were assayed in triplicates in the same plate and GAPDH levels were used to normalize mRNA contents, and target gene levels were calculated by the $2^{-\Delta\Delta C_t}$ method. cDNA from forskolin-treated cells was used as CREB-induced MIF and STAT-3 positive control. cDNA from cells treated with test compound **A** were used for CB₂ agonist MIF and STAT-3 gene expression control. cDNA from AM630-treated cells was used for antagonist/inverse agonist CB₂ MIF and STAT-3 expression control. Each sample was evaluated in triplicate and in three different experiments.

Statistical analysis

The statistical significance for MTT and RT/PCR assay was determined by analysis of variance (ANOVA). The calculation of IC₅₀ was performed by non-lin fit of log-dose vs response, using Prism 5.01 (Graph Pad) software. cAMP concentration was calculated utilizing a 4 parameter logistic (4PL) curve fitting program.

Treatments	cAMP (pmol/mg) ± S.D.
VEHICLE	16,2 ± 0.15
FORSKOLIN	67.4 ± 3.4*
AM630	22.3 ± 1.8*
MD 132 cis	10.2 ± 0.7*
MD 132 trans	10.4 ± 1.1*
AM630 + MD 132 cis	12.3 ± 0.9*#
AM630 + MD 132 trans	12.7 ± 1.1*#

Figure 2. The effect of **9a-trans** and **9a-cis** on AM630-induced stimulation of cAMP production in U266 cells. 4×10^4 U266 cells were plated in 24 well plates and treated for 24 hours with compounds **9a-trans** and **9a-cis**. In combination treatments, U266 cells were pre-incubated with 25 μ M AM630 for 30 minutes before adding **9a-trans** or **9a-cis**. U266 cell lines were treated with Forsk (10 μ M), AM630 (25 μ M), **9a-trans** or **9a-cis** (50 μ M). cAMP concentration was represented as pictograms for mg of protein (pg/mg). * indicate any values that are significantly different from vehicle treated cells (** $P < 0.01$), # indicate any values that are significantly different from AM630 treated cells (** $P < 0.01$). Values represent the mean \pm S.D. ($n = 4$) calculated from two wells/treatment and in two independent experiments.

[³⁵S]-GTPγS binding assay

CHO cells

Chinese hamster ovary (CHO) cells stably transfected with cDNA encoding human cannabinoid CB₂ receptors ($B_{\max} = 215 \text{ pmol}\cdot\text{mg}^{-1}$) were purchased from PerkinElmer Life Sciences Inc. (Boston, MA, USA). They were maintained at 37°C in 5% CO₂ in Dulbecco's modified Eagles's medium nutrient mixture F-12 HAM, supplemented with 1 mM L-glutamine, 10% fetal bovine serum, 0.6% penicillin–streptomycin and 400 μg·mL⁻¹ G418. These *hCB₂* CHO cells were passaged twice weekly using PBS-EDTA buffer (1 mM EDTA in PBS solution).

Membrane and whole-cell preparation.

[³⁵S]GTPγS assays were performed with *hCB₂* CHO cell membranes, prepared as described by Ross *et al.*^[3]. For membrane preparation, cells were removed from flasks by scraping, centrifuged at 489 x *g* and then frozen as a pellet at -20°C until required. Before use in a [³⁵S]GTPγS assay, cells were defrosted and diluted in GTPγS binding buffer.

[³⁵S]-GTPγS binding assay

The method used for measuring agonist-stimulated binding of [³⁵S]GTPγS was based on a previously described protocol.^[4] The assays were carried out with GTPγS binding buffer (50 mM Tris-HCl, 50 mM Tris-base, 5 mM MgCl₂, 1 mM EDTA, 100 mM NaCl, 1 mM dithiothreitol, 0.1% BSA) in the presence of [³⁵S]GTPγS (0.1 nM) and GDP (30 mM) in a final volume of 500 μL. Binding was initiated by the addition of [³⁵S]GTPγS to deep well blocks. Nonspecific binding was measured in the presence of 30 μM GTPγS. All assays were performed at 30°C for 60 min before termination by addition of ice-cold Tris binding buffer and vacuum filtration using a 24-well sampling manifold (Brandel Cell Harvester) and Brandel GF/B filters that had been soaked in wash buffer at 4°C for at least 24 h (Brandel Inc, Gaithersburg, MD, USA). The radioactivity was quantified by liquid scintillation spectrometry. In all these assays we used a protein concentration of 50 μg per well of membranes obtained from *hCB₂* CHO cells. [³⁵S]GTPγS (1250 Ci·mmol⁻¹) was obtained from PerkinElmer Life Sciences Inc. (Boston, MA, USA), GTPγS from Roche Diagnostic (Indianapolis, IN, USA) and GDP from Sigma-Aldrich.

Some [³⁵S]GTPγS assays were performed with samples of **9c-cis** that had been switched from **9c-trans** by exposing the *trans*-isomer to UV light (365 nm) for 10 minutes in the presence of

red light but not of daylight or of any other kind of light. All additions to deep well blocks were made in the presence of red light only, after which the blocks were kept in total darkness (under aluminium foil), apart from brief exposures to red light.

Analysis of data

Values have been expressed as means and variability as SEM or as 95% confidence limits. Mean EC₅₀, mean minimal effect (E_{min}) and mean maximal effect (E_{max}) values, and SEM or 95% confidence limits of these values, have been calculated by nonlinear regression analysis using the equation for a sigmoid concentration-response curve (GraphPad Prism. P values < 0.05 were considered significant.

Table 2. Effects of 1 μM **9c** on the mean EC_{50} , E_{\min} and E_{\max} values of CP55,940 for its stimulation of [^{35}S]GTP γS binding to membranes obtained from Chinese hamster ovary (CHO) cells stably transfected with human CB_2 cannabinoid receptors.

Treatment(s) in addition to CP55940	CP55940 parameters	Mean EC_{50} , E_{\min} and E_{\max} values of CP55940	95% confidence limits	n
Figure 6b data				
None	EC_{50} (nM)	1.22	0.56 & 2.66	6
None	E_{\min} (%)	9.84	6.45 & 13.22	
None	E_{\max} (%)	35.98	32.60 & 39.36	
1 μM 9c-trans	EC_{50} (nM)	10.99#	5.87 & 20.56	6
1 μM 9c-trans	E_{\min} (%)	-2.47*	-5.38 & 0.43	
1 μM 9c-trans	E_{\max} (%)	39.49	32.98 & 46.01	
Figure 6c data				
None	EC_{50} (nM)	0.98	0.36 & 2.64	6
None	E_{\min} (%)	6.44	1.47 & 11.40	
None	E_{\max} (%)	36.76	31.82 & 41.70	
1 μM 9c-cis	EC_{50} (nM)	17.74#	7.81 & 40.30	6
1 μM 9c-cis	E_{\min} (%)	-15.30*	-23.60 & -6.99	
1 μM 9c-cis	E_{\max} (%)	35.99	29.70 & 42.28	

Each symbol (# for EC_{50} and * for E_{\min}), indicates a significant difference ($P < 0.05$) (Figure 6b) between a mean EC_{50} or E_{\min} value of CP55,940 determined in normal light in the presence of 1 μM **9c-trans**, and a mean EC_{50} or E_{\min} value of CP55,940 determined in normal light in the absence of 1 μM **9c-trans**, or (Figure 6c) between a mean EC_{50} or E_{\min} value of CP55,940 determined in darkness or under red light in the presence of 1 μM **9c-cis**, and a mean EC_{50} or E_{\min} value of CP55,940 determined in darkness or under red light in the absence of 1 μM **9c-cis**. Significant differences are indicated by non-overlapping 95% confidence limits.

Computational Studies

For construction of a homology model of the *hCB*₂R, based on the crystal structure of the *hCB*₁R (pdb code: 5XRA)^[5], the software SYBYL 7.0 (Tripos Inc.) was used. The first 18 amino acids of the *N*-terminus and the last 44 amino acids of the *C*-terminus were not included into the homology model, because these parts are not present in the crystal structure. After deleting the flavodoxin, all amino acids, being different between the sequence of the *hCB*₁R-crystal and the *hCB*₂R were mutated into the corresponding amino acids of the *hCB*₂R. For modelling of the E2-loop, the amino acids Glu258 to Val263 of the *CB*₁R-crystal were deleted and the missing amino acids of the *hCB*₂R Cys179 to Pro182 were inserted, by applying the “LoopSearch” module of SYBYL. For modelling of the I3-loop the amino acids Ser222 to Met237 were also included using “LoopSearch”. The model was refined and energetically minimized, as described.^[6] The compounds **9c-trans** and **9c-cis** were docked, in two different poses into the binding pocket of the homology model, inspired by the AM11542-*hCB*₁R-crystal (pdb code: 5XRA).

References

- [1] H. E. Gottlieb, V. Kotlyar, A. Nudelman, *J. Org. Chem.* **1997**, *62*, 7512-7515.
- [2] S. Murkherjee, M. Adams, K. Whiteaker, A. Daza, K. Kage, S. Cassar, M. Meyer, B. B. Yao, *Eur. J. Pharmacol.* **2004**, *505*, 1-9.
- [3] R. A. Ross, H. C. Brockie, L. A. Stevenson, V. L. Murphy, F. Templeton, A. Makriyannis, R. G. Pertwee, *Br. J. Pharmacol.* **1999**, *126*, 665-672.
- [4] A. Thomas, L. A. Stevenson, K. N. Wease, M. R. Prince, G. Baillie, R. A. Ross, R. G. Pertwee, *Br. J. Pharmacol.* **2005**, *146*, 917-926.
- [5] T. Hua, K. Vemuri, S. P. Nikas, R. B. Laprairie, Y. Wu, L. Qu, M. Pu, A. Korde, S. Jiang, J. H. Ho, G. W. Han, K. Ding, X. Li, H. Liu, M. A. Hanson, S. Zhao, L. M. Bohn, A. Makriyannis, R. C. Stevens, Z. J. Liu, *Nature* **2017**, *547*, 468 – 471.
- [6] P. Igel, R. Geyer, A. Strasser, S. Dove, R. Seifert, A. Buschauer, *J. Med. Chem.* **2009**, *52*, 6297 – 6313.

